DEEP CRUSTAL STRUCTURE OF THE CENTRAL NORTH SEA

By

Richard John Hunter

Submitted for the degree of

Doctor of Philosophy

University of London

(Royal School of Mines)

April 1991

ACKNOWLEDGEMENTS

I would like to express my sincere thanks to Enterprise Oil PLC who have funded this research since its start in September 1987, and to my research supervisors Dr. Mike Warner and Dr. Anna Thomas-Betts for their very helpful advice over the past few years.

Thanks also go to: Dave Latin and Nicky White of Cambridge University for their advice on subsidence and melting, Dr R. Hipkin of the Grant Institute for his general advice, especially on filtering techniques, at a crucial stage in the work and Dr. M. Lee of the BGS (Keyworth) for providing the 3D gravity modelling program.

I would like to thank all my friends and colleagues of the Geophysics Group (Imperial College) for putting up with me and for providing perfectly reflective surfaces from which many an idea has been bounced. Thanks also to Simon Kelk for his mildly amusing windscreen wiper anecdote and for reminding me that you can't cough when it's raining. And thanks to Vic Reeves, Bob Mortimor, Audrey Hepburn (1958), David Lynch and Silvie Guillem for moments of inspiration during the writing of this thesis.

Last, but by no means least I would like to thank my family for all their support and particularly my parents to whom this work is dedicated.

ABSTRACT

The North Sea Basin has undergone a complex geological history culminating in two periods of rifting and extension in the Mesozoic. Although much is known of the structure of the upper-crust in the basin, comparatively little is known of the deep crustal structure. This is especially true in the 'triple-junction' area of the Central North Sea where there is a lack of deep seismic reflection data. The primary purpose of this research was to determine the extent of crustal thinning in this area. In the absence of deep seismic reflection data it was decided to estimate crustal thinning by analysing the gravity and magnetic fields.

A detailed qualitative analysis of the Bouguer anomaly data shows that the field is characterised by low-amplitude anomalies between −28 and 35 mGals. Seismic data shows that low-density sediments reach thicknesses of more than 6 km in parts of the basin which would give rise to large negative gravity anomalies. It follows that the basin must be compensated at depth by an excess mass. If an assumption of Airy-type isostatic compensation by varying the depth of the Moho is made, together with an assumption of a laterally and vertically homogeneous basement and upper-mantle, then the compensating mass (and therefore the depth to the Moho) can be modelled. The gravitational effect of the near-surface layers down to the Base-Cretaceous was calculated in 3D and removed from the Bouguer anomaly field. After low-pass filtering in the wavenumber domain, the remaining residual field was modelled using an automatic iterative forward modelling routine and several models for the depth to the Moho were made. The Moho is shown to shallow from 32 km in off-axis areas to approximately 15 km in the centre of the 'triple-junction'. The general shape of the Moho topography is determined by the principal structures in the area, the shallowest points being associated with the rift-axes. An analysis of the errors involved in the modelling technique shows that errors in the Moho depth are not in excess of +/−1.6 km. After a detailed analysis of the magnetic field in the area, refinements were made to these models by modelling the magnetic anomalies associated with relatively

high density bodies such as the basalts of the Piper-Forties Volcanic Province and the East Forties Basin Intrusion.

Crustal extension factors or 'Beta factors' (defined by the ratio of the thickness of unstretched crust to the thickness of the pre-rift crystalline basement) were estimated for every point in the study area using the models of Moho topography derived by modelling the regional gravity field. They reach maximum values of approximately 2.8 in the centre of the 'triple-junction'. The errors associated with the larger Beta factors are large (up to 0.5) however the results obtained are in good agreement with those obtained by previous workers who have estimated extension by subsidence analysis.

The McKenzie and Bickle (1988) technique has been used in the past to relate crustal extension with melting. The method accurately predicts the presence of the Piper-Forties Basalts and the East Forties Basin Intrusion in areas which are associated with large amounts of extension. The average thickness of melt predicted by this method (approx. 0.7 km) is also in reasonable agreement with the thicknesses derived from 2.5D modelling of the magnetic field (less than 1.2 km).

CONTENTS

1 INTRODUCTION 1

1.1 Background and Research aims 1
1.2 Study Area 2
1.3 Organisation 4

2 GEOLOGY AND STRUCTURAL EVOLUTION OF THE NORTH SEA BASIN 6

2.1 Introduction 6
2.2 Geological Evolution: A Brief Summary 6
2.3 Magmatism in the Central North Sea 15
2.3.1 Introduction 15
2.3.2 The Piper-Forties Volcanic Province 15
2.4 Principal Structures in the Study Area 20
2.5 The Nature of the Crystalline Basement 22

3 ANALYSIS OF THE GRAVITY DATA 23

3.1 Introduction 23
3.2 Gravity Data 24
3.2.1 Data Source 24
3.2.2 Processing 25
3.3 Qualitative Interpretation 26
3.3.1 Analysis of the Bouguer Anomaly Map 26
3.3.1.1 Northern Zone 28

3.3.1.2 Central Zone 29
3.3.1.3 Southern Zone 30
3.3.2 Enhanced Images 31
3.3.2.1 First Horizontal Derivative 31
3.3.2.2 Shaded Relief Images 33
3.4 3D Modelling Technique 38
3.4.1 Calculating the Field Due to Near-Surface Layers 39
3.4.1.1 Sedimentary Thicknesses 39
3.4.1.2 Densities Used in Modelling 41
3.4.1.3 Computing the Gravitational Effect 47
3.4.1.4 Results Obtained Using The Plouff Routine 50
3.4.2 Analysis of the Residual Field 57
3.4.2.1 Spectral Analysis 61
3.4.2.2 Filtered Data 63
3.4.3 Automatic Iterative Forward Modelling 65
3.5 Results 67
3.5.1 Results Obtained Using Unfiltered Residual Gravity 67
3.5.2 Results Obtained Using Filtered Residual Gravity After 50 Iterations 71
3.5.3 Results Obtained Using Filtered Residual Gravity After 20 Iterations 75
3.5.4 Quantification of Errors 79
3.5.4.1 Accuracy of the Original Survey 79
3.5.4.2 Accuracy of the Seismic Structure Maps 80
3.5.4.3 Accuracy of the Gridding Process 80
3.5.4.4 Accuracy of Density Estimates 81
3.4.4.5 Errors Due to the Three-Dimensional Modelling 82
3.5.4.6 Overall Estimation of Errors 82
3.6 Summary 82

4 ANALYSIS OF AEROMAGNETIC DATA 85

4.1 Introduction 85

4.2 Aeromagnetic Data 87
4.2.1 Survey Details 87
4.2.2 Processing 87
4.3 Regional Interpretation of Aeromagnetic Data 88
4.3.1 Qualitative Interpretation of the Aeromagnetic Map 88
4.3.1.1 Northern Zone 90
4.3.1.2 Central Zone 91
4.3.1.3 Southern Zone 92
4.3.2 First Horizontal Derivative 95
4.3.2.1 Northern Zone 95
4.3.2.2 Central Zone 97
4.3.2.3 Southern Zone 97
4.3.3 Shaded Relief Images 99
4.3.4 Second Vertical Derivative Image 105
4.3.5 Depth Estimates from Spectral Analysis 108
4.4 Quantitative Modelling 110
4.4.1 Modelling the Piper-Forties Volcanic Province 116
4.4.2 Comparison with Previous Work 121
4.4.3 Modelling the East Forties Basin Anomaly 121
4.5 Summary 124

5 COMBINING MAGNETIC AND GRAVITY MODELLING 126

5.1 Introduction 126
5.2 The Relationship Between the Gravity Moho and the Magnetic Field 128
5.3 Calculation the Pseudo-Gravitational Field 130
5.4 Calculating the Gravity Field From Magnetic Models 133
5.5 Results of 3D Modelling 143
5.6 Estimation of Errors 148
5.7 Summary 149

6 EXTENSION IN THE NORTH SEA BASIN 151

6.1 Introduction 151
6.2 Models for Lithospheric Extension 152
6.2.1 Introduction 152
6.2.2 Extension by Pure Shear 152
6.2.2.1 Uniform Stretching Models 152
6.2.2.2 Non-Uniform Depth Dependent Stretching 155
6.2.3 Extension by Simple Shear 156
6.3 Extension in the North Sea Basin: A Summary of Previous Work 160
6.3.1 Introduction 160
6.3.2 Measuring Extension on Faults 161
6.3.3 Measuring Crustal Thinning 161
6.3.4 Subsidence Analysis 171
6.3.4.1 Modelling Subsidence 172
6.3.4.2 Previous Work 179
6.4 Estimating Crustal Extension From 3D Gravity Modelling 189
6.4.1 Introduction 189
6.4.2 Crustal Thinning and Extension 189
6.4.3 Possible Errors 193
6.4.4 Comparison with Previous Work 196
6.5 The Relationship Between extension and Magmatism in the North Sea 202
6.5.1 Introduction 202
6.5.2 Summary of Method 203
6.5.2.1 Potential Temperature 203
6.5.2.2 Initial Mechanical Boundary Layer Thickness 206
6.5.2.3 Lithospheric Extension 207
6.5.3 Results 207
6.5.4 Magmatism and Decoupled Strain Rate Extension 209
6.6 Summary 212

7 CONCLUSIONS AND DISCUSSION 214

7.1 Conclusions 214
7.2 Discussion 218
7.2.1 Isostatic Equilibrium 218
7.2.2 Uniform Basement and Nature of the Moho 225
7.2.3 Control of North Sea Rifts by Caledonian Basement Structures 227
7.2.4 Further Work 218

REFERENCES 229

CHAPTER 1

INTRODUCTION

1.1 BACKGROUND AND RESEARCH AIMS

The North Sea Basin has undergone a complex geological history culminating in the formation of the North Sea rift system during three phases of extension in the Upper-Palaeozoic and Mesozoic. The rift system consists of three arms: the Central Graben, the Viking Graben and the Outer Moray Firth Basin, which meet in a 'triple-junction' in the Forties area. This 'triple-junction' is the dominant structural feature of the Central North Sea. Exploration for hydrocarbons in the area has resulted in a detailed knowledge of the structural, stratigraphic and sedimentological characteristics of the upper crust. However, relatively little is known of the structure of the lower crust in the area. What data there is comes either from regional gravity studies or analyses of deep seismic reflection or refraction profiles.

The 'triple-junction' area is characterised by exceptionally thick sedimentary sequences, especially in the graben axes where the Base-Zechstein has been measured as occurring at depths of greater than 7 km (Day et al, 1981). Such thick sequences seriously degrade the ability of the deep seismic reflection technique to image the lower crust (pers comm. M. Warner, Imperial College). Thus, although there are numerous deep seismic reflection profiles crossing the northern and southern parts of the basin there are none crossing the 'triple-junction' area of the Central North Sea.

The primary purpose of this research is to measure the amount of crustal thinning which has taken place due to lithospheric extension in this area. This is done by modelling the regional gravity field in three dimensions. The princip

behind this is simple. The Bouguer anomaly is considered to be the sum of the gravitational effects of the low density sedimentary basin infill and the gravitational effect of a high density compensating mass. The crystaline basement is assumed to be laterally and vertically homogeneous. The sedimentary effect can be calculated and removed from the Bouguer anomaly field. The result is a modified field which, after filtering, can be used to model the distribution of the compensating mass. This compensating mass is considered to be anomalously shallow, high-density, upper-mantle material. The final model therefore represents the depth to the Moho for every point in the study area. Once such a model of crustal thinning is produced, estimates of the amount of extension can be made by comparing the thickness of the basement in rifted areas with the thickness of unstretched crust. A secondary aim of the research is to compare these estimates with those obtained by other workers who have used subsidence analysis to quantify the amount of extension in the Central North Sea.

The modelling procedure involves a detailed analysis of both the Bouguer gravity and aeromagnetic data from the Central North Sea. A subsidiary aim of the research is to present qualitative interpretations of these data sets together with detailed 2.5 dimensional models of the magmatic areas in the region by modelling the principal aeromagnetic anomalies of the area.

1.2 STUDY AREA

This research involves two study areas (figure 1.1). The qualitative interpretations of both the Bouguer anomaly and aeromagnetic data sets involve a large area defined approximately by longitudes 2° E to 2° W and latitudes 57° to 59° N. Restrictions of the 3D modelling technique (3.4) mean that a reduced area had to be used for the models of crustal thinning. This revised study area consists of the eastern half of the area used for the qualitative interpretations and falls approximately between longitudes 0° and 2° E and latitudes 57° to 59° N. The digital grids used throughout this research are all based on the same rectangular

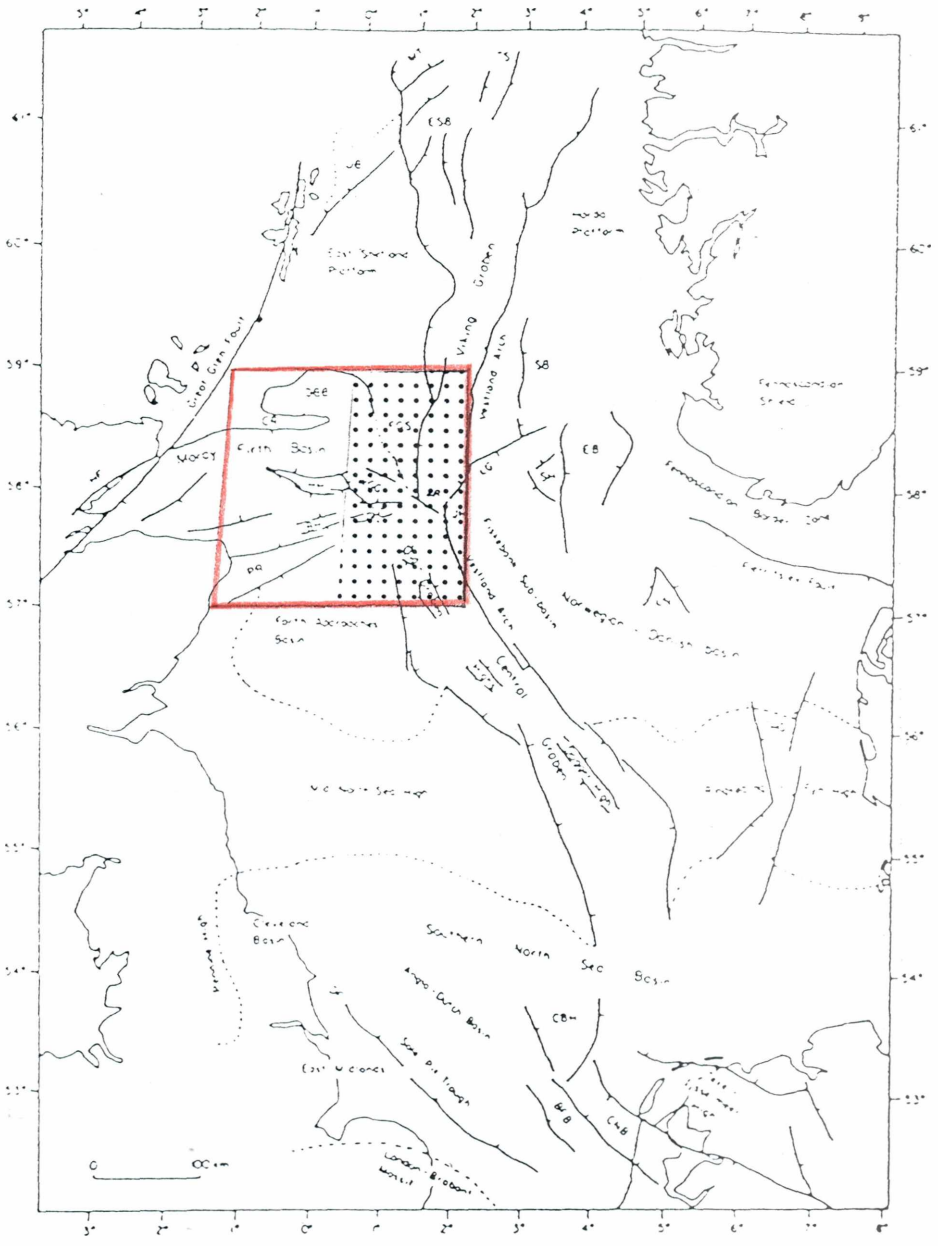


Fig. 6.1. Structural elements of the North Sea Basins.
Abbreviations:

AR	Andrew Ridge	ESB	East Shetland Basin	LN	Lista Nose
BFB	Broad Fourteens Basin	FGS	Fladen Ground Spur	MT	Magnus Trough
BH	Buchan Horst	GH	Glenn Horst	PR	Peterhead Ridge
CBH	Cleaver Bank High	HF	Helmsdale Fault	SB	Stord Basin
CNB	Central Netherlands Basin	HG	Horn Graben	SH	Sele High
CR	Caithness Ridge	HH	Halibut Horst	TS	Tampen Spur
DBB	Dutch Bank Basin	JH	Jaeren High	UB	Unst Basin
DF	Dowsing Fault	LG	Ling Graben	WGG	Witch Ground Graben
EB	Egersund Basin				

FIGURE 1.1 Map showing the principal structural elements of the North Sea Basin. Study area 1 (used in qualitative interpretations of the potential field data) is outlined in red. Study area 2 (used in 3D gravity modelling) is stippled. Adapted from Brown (1984).

UTM projection, the coordinates shown on all the images presented in chapters 3 to 7 are in units of kilometres.

1.3 ORGANISATION

This thesis is organised into seven chapters each dealing with a specific aspect of the research. In chapter 2 the structural and tectonic framework of the Central North Sea is outlined. The principal structures in the study area are discussed together with the nature of the sedimentary infill of the basin. A separate section deals specifically with the nature of magmatism in the Central North Sea. This chapter also includes a brief section on the nature of the crystalline basement in the Central North Sea.

Chapter 3 deals with the analysis of gravity data. The first part of the chapter outlines the nature of the data itself and how it is processed into a digital grid format. This is followed by a detailed qualitative interpretation of the gravity data for the study area in which the principal trends and anomalies are discussed. The largest part of the chapter involves a detailed description of the gravity modelling technique. This involves several stages each of which is dealt with in a separate section. Several results of the modelling are shown and the errors involved in the whole process are quantified.

The next chapter is an analysis of the aeromagnetic data. As in chapter 3, the nature of the data is outlined and a detailed qualitative interpretation of the data is discussed. The magnetic field associated with the study area is more complex than the equivalent Bouguer gravity field, thus the qualitative interpretation of the magnetic data is more detailed. Two areas which are characterised by having large positive magnetic anomalies are analysed in detail. These are the Piper-Forties Volcanic Province and the East Forties Basin. Several 2.5D models of the causative bodies of these anomalies are presented toward the end of this chapter.

Chapter 5 is a relatively short section of the thesis which explains how the magnetic models derived in the previous chapter can be used to modify and improve the models of the gravity Moho derived in chapter 3. The end result is a final model which can be used to quantify crustal thinning and from there, estimate the amount of extension which has occurred in the area.

The topic of extension is dealt with in chapter 6. Most of the chapter is devoted to a review of the major items of research which have attempted to quantify extension in the North Sea Basin, together with a discussion of the principal models by which the lithosphere might be extended. The models of the gravity Moho topography presented in chapter 5 are used to estimate crustal extension factors for the study area. These estimates are then compared and contrasted with similar estimates made by previous workers. An attempt is made to quantify the errors in the method and the geological implications of the results are discussed. The chapter also contains a brief discussion of the relationship between magmatism and extension in the Central North Sea.

The final chapter provides a summary of the main conclusions and observations made during this research. It also includes a discussion of some important points arising during the course of the work but which were not previously mentioned in any great detail. For instance, the degree to which local Airy isostasy can be applied to the study area. Some suggestions for future research are also made.

Several transparent overlays are included with this thesis. These may be used in conjunction with many of the images presented throughout the work. They include maps of the principal structures in both study areas, a qualitative interpretation of the magnetic data, estimates of extension made from a study of basement subsidence and a plot of the North Sea licensing blocks.

CHAPTER 2

GEOLOGY AND STRUCTURAL EVOLUTION OF THE NORTH SEA BASIN

2.1 INTRODUCTION

In this chapter the tectonic framework and geological history of the North Sea Basin are outlined. The area has had a long and complex geological history which has been the subject of a great deal of research by many authors; for more detailed studies the reader is referred to: Zeigler (1981,1982), Zeigler and Van Hoorn (1990), Glennie (1984) and Gibbs (1990).

Section 2.2 of this chapter summarises the geological evolution of the whole basin. Special emphasis is placed on the Mesozoic rifting episodes in which the North Sea graben system developed. The nature of magmatism in the Central North Sea is discussed in section 2.3, whilst in section 2.4 the principal geological structures of the study are outlined. The final section is a very brief discussion concerning the nature of the crystalline basement in the North Sea area.

2.2 GEOLOGICAL EVOLUTION: A BRIEF SUMMARY

The geometry of the North Sea Basin can be considered to be the result of plate movements involving tension, compression and strike-slip activity in different directions at different times in its developmental history. It is necessary to look back to the Pre-Cambrian to follow this development fully.

Figure 2.1 (after Glennie, 1984) shows cartoons of the relative plate

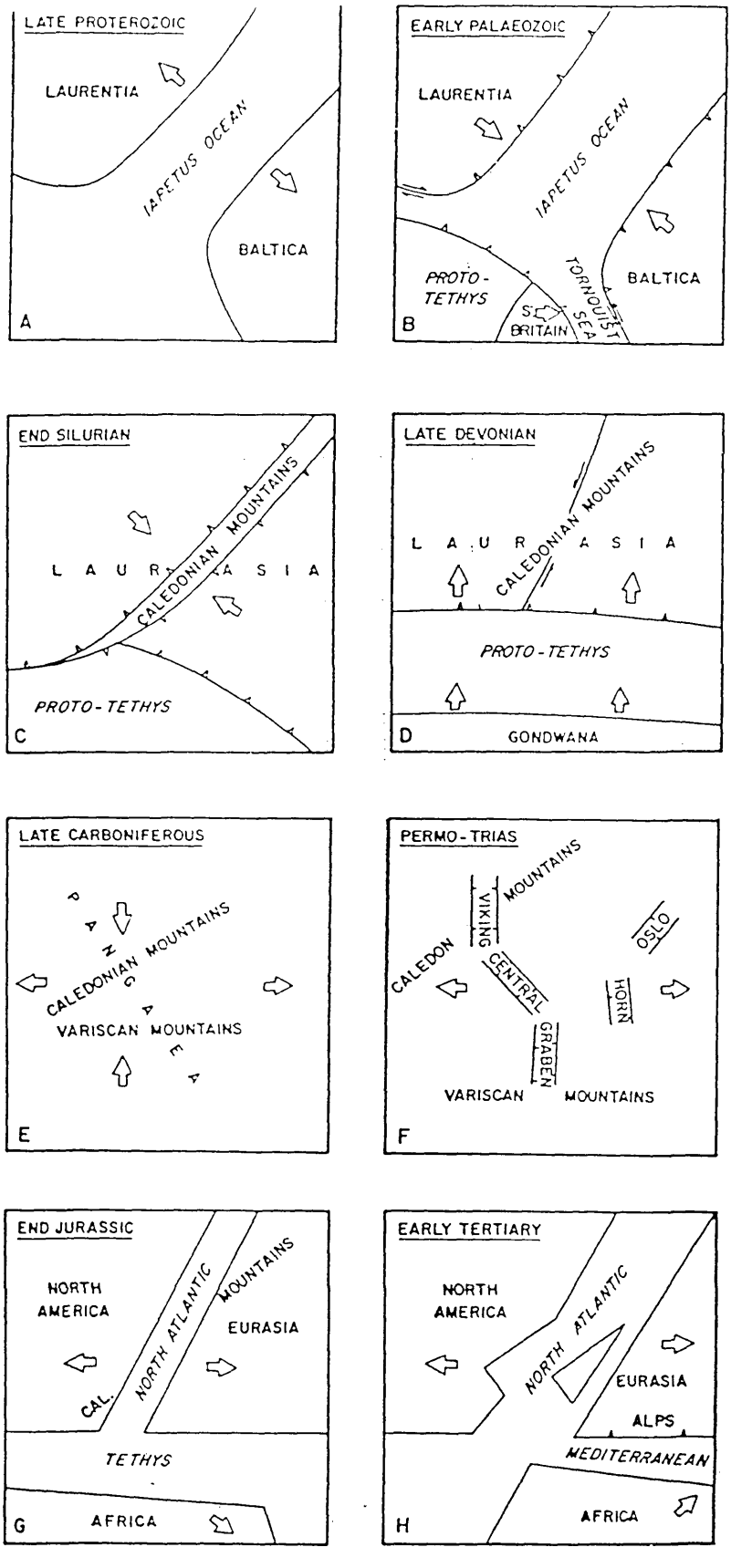


FIGURE 2.1 Cartoons of relative plate movements that affected the North Sea area since the late Proterozoic. After Glennie (1984).

movements that affected the North Sea area since the late-Proterozoic. During the late-Proterozoic to early-Palaeozoic the North Sea area comprised widely separated fragments in different parts of the Iapetus Ocean and Tornquist Sea together with their flanking areas (cartoons A and B on figure 2.1). Closure of the Iapetus during the early-Palaeozoic Caledonian orogeny led to intense metamorphism. Much of the crystalline basement underlying the North Sea Basin consolidated during this period. Figure 2.2 shows the late-Caledonian tectonic framework of north-west Europe (after Ziegler, 1981). The eastern part of the basin is underlain by a late Pre-Cambrian basement which forms the westernmost edge of the Fennoscandian shield. In the northern North Sea the Scottish-Norwegian Caledonides are characterised by a NE - SW structural grain (Ziegler and Van Hoorn, 1990 and Johnson and Dingwall, 1981) whereas the north German-Polish Caledonian fold belt is characterised by a N - S grain in the Central North Sea and a more NW - SE trend in the southern part of the basin.

The Devonian period is characterised by the post-orogenic collapse of the Caledonides. This was accompanied by major sinistral movements between the Laurentian-Greenland shield to the west and the Fennoscandian shield to the east (cartoon D on figure 2.1). By the end of the Devonian much of the Central and Southern North Sea areas had a thick cover of continental sandstone. Wrench movements ceased in the early-Carboniferous and the North Atlantic - Arctic areas became dominated by crustal extension. In the south, convergence between the Laurentian and Gondwana plates led to the onset of the Variscan orogeny, the main phase of which occurred in the late-Visean. Figure 2.3 (after Ziegler, 1981) shows a reconstruction of Westphalian palaeogeography. Carboniferous sediments in the Central and Norther North Sea are limited to small basinal areas such as the Moray Firth and the eastward extension of the Midland Valley. The Southern North Sea formed part of the Variscan foredeep into which thick sequences of sediments accumulated. By the end-Stephanian to early-Permian the whole of north-west Europe was transected by the late Variscan post-orogenic system of conjugate shear faults (Ziegler and Van Hoorn, 1990). Wrench movements on these faults triggered widespread intrusive and extrusive

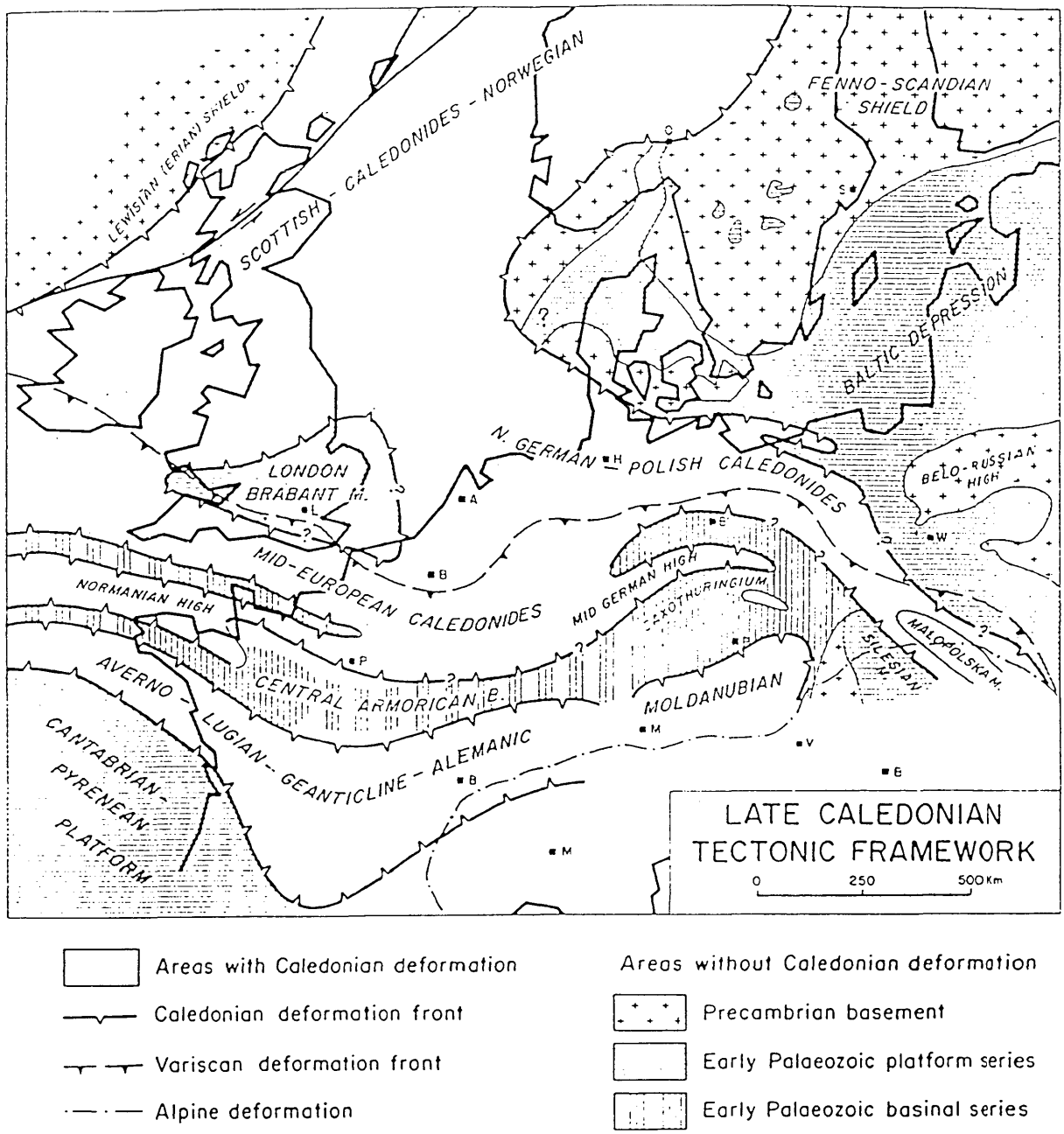


FIGURE 2.2 Late Caledonian tectonic framework of North-West Europe. After Ziegler (1981).

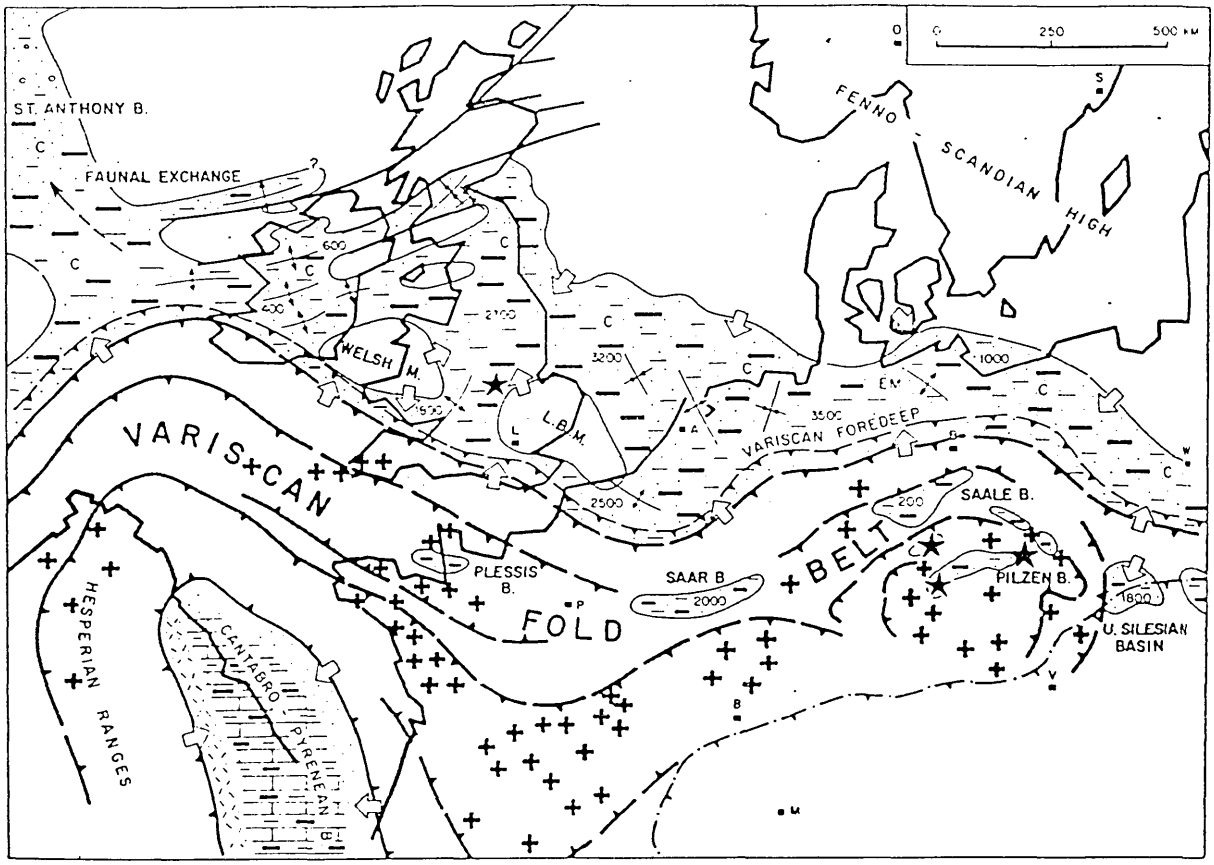


FIGURE 2.3 Westphalian palaeogeography of North-West Europe. After Ziegler (1981).

magmatism. Ziegler and Van Hoorn (1990), note that in the Central and Northern North Sea the configuration of Devonian and Carboniferous basins cannot be accurately resolved on the basis of seismic and well data. However, they also note that locally there is evidence of thick Devonian and/or Carboniferous rocks below the base Triassic or Base-Permian unconformity which might suggest that some crustal thinning had taken place.

By the end-Autanian, wrench faulting had ceased and the area became dominated by two E - W trending subsiding basins separated by the Mid North Sea High which had developed during the transition between the Carboniferous and the Permian (figure 2.4). Desert conditions existed and during the Rotliegendes thick sequences (greater than 1500 m) of aeolian sandstones and evaporites were deposited in the Southern Permian basin. The distribution of Rotliegendes sedimentation in the Northern Basin is incompletely known, although Ziegler (1982) and Glennie (1984,1986) believe thicknesses may reach 600 m.

The Zechstein Sea flooded both basins from the north at the transition to the late Permian. The Base-Zechstein is marked by the thin highly organic Kupferschiefer shale, indicating that both basins had subsided below mean sea-level prior to the transgressive episode. Repeated glacio-eustatic sea-level fluctuations governed the accumulation of five depositional cycles during the Zechstein. Each cycle ends in the development of thick sequences of gypsum (now anhydrite) followed by halite and potassic salts. The halite reached sufficient thicknesses over many parts of the basin to permit later diapirism.

The late Permian saw the onset of rifting propagated in the Norwegian-Greenland Sea area southward into the Faeroe-Rockall trough (Ziegler and Van Hoorn, 1990). There is little evidence of rifting actually governing Zechstein facies patterns in the North Sea area, however the two Permian basins continued to subside in response to a thermal event possibly induced by the late-Carboniferous wrench faulting (Glennie, 1984 and Pegrum 1984).

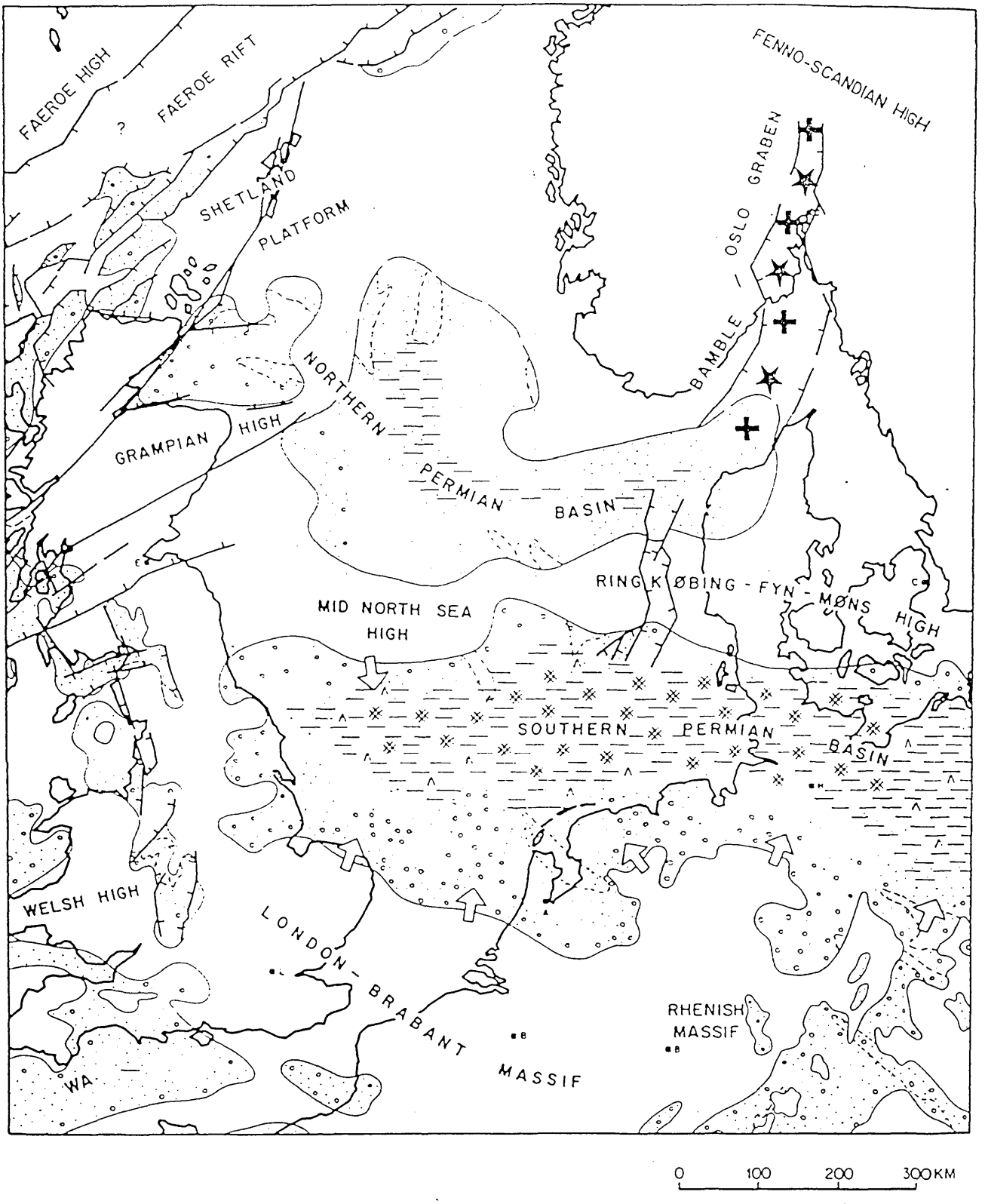


FIGURE 2.4 Rotliegende palaeogeography of the North Sea area. After Ziegler and Van Hoorn (1990).

In the Norwegian-Greenland Sea area rifting accelerated into the Triassic so that by the early-Triassic the whole of north-west Europe was subject to regional tensional stresses. This tensional phase saw the creation of the North Sea rift system (cartoon F on figure 2.1) which (according to Ziegler, 1981) were entirley new features. However, they may (in part) owe their location to the presence of major discontinuities in the Caledonian basement (see 7.3). Conformable Triassic sediments are dominantly red-beds including alluvial fan, fluvial, aeolian, sabkha, lacustrine and shallow marine facies with regional tectonism controlling sedimentation. Throughout the Triassic, the continually subsiding continental basins were filled with cyclical clastics reaching thicknesses of 2000 m in the Central Gaben area. However, the exact nature of the distribution of Triassic sediments is relatively poorly defined in the North Sea area.

The Rhaetic and Hettangian saw the establishment of marine conditions in the Southern and south-Central North Sea. In the north, continental sandstones built up in the subsiding Viking Graben. The Central Graben continued to subside during the lower-Jurassic however, much of the sedimentary sequences may have been removed due to erosion during the mid-Jurassic. The mid-Jurassic is characterised in the Central North Sea by a period of regional doming. Uplift of this dome lead to the erosion of some of the early-Jurassic sediments (Ziegler, 1981). The period is also associated with the development of a large volcanic province in the 'triple-junction' area of the basin. This is known as the Piper-Forties Volcanic Province (or just the Forties Volcanic Province) and is discussed in more detail in the next section of this chapter. By the end-Bajocian the dome was collapsing and sedimentation resumed in the Central Graben.

The mid-Jurassic to early-Cretaceous is dominated by a major period of extension in the North Sea. The precise timing, mode and amount of extension are the subjects of some controversy and are discussed at length in chapter 6. Barton and Wood (1984) believe that the main phase of extension took place in the mid-Jurassic although Ziegler (1982) considers the main phase to start in the mid-Jurassic but also envisages a second phase occurring in the late-Jurassic (late-

Kimmerian rifting pulse).

The rate of crustal extension diminished gradually after the late-Kimmerian (Ziegler and Van Hoorn, 1990). During the early-Cretaceous differential subsidence of the graben system was accompanied by the gradual infilling of deep-water shales and minor pelagic carbonates. These shales reach 1000 m in thickness in parts of the Viking Graben and 250 - 500 m in the Central Graben. By the end of the early-Cretaceous rifting had ceased and post-rift thermal subsidence was occurring over the whole area. A global rise in sea-level during the late-Cretaceous caused a progressive overstepping of the basin margins and a rapid decrease in clastic influx. Clear water conditions prevailed throughout the Upper-Cretaceous leading to the deposition of thick sequences of chalk (up to 2000 m in the Central Graben).

The early Cenozoic is characterised by an increase in igneous activity along the Faeroe - West-Shetland and mid-Norway rift zone. During this period north-west Europe as a whole became affected by the compressional tectonics of the Alpine orogeny. These stresses induced the inversion of Mesozoic grabens and troughs up to 1500 km north of the collision front (Ziegler, 1988). Apart from a final minor rifting pulse (the Laramide pulse) in which only major faults were re-activated (Ziegler and Louwerens, 1979) the rest of the Cenozoic is characterised by post-rift thermal subsidence and the formation of a broad saucer-shaped basin. In the rift-axis areas post-rift sediments reach thicknesses of up to 3.5 km. These sediments can be broadly divided into two groups; the deep-water sands (Central Graben) and fluxo-turbidites (Viking Graben) of the early Eocene and the deltaic sands and pelagic clays of Oligocene and younger epochs.

2.3 MAGMATISM IN THE CENTRAL NORTH SEA

2.3.1 Introduction

As outlined in 2.2 the North Sea Basin as a whole has undergone three principal phases of extension each of which are associated with magmatic activity. These are:

1) Palaeozoic Events. These occurred between the Carboniferous and early-Permian and resulted in a large magmatic province consisting mainly of alkali basalts (Dixon et al, 1981, Latin et al, 1990a) which stretched east-west from northern Britain to eastern Germany.

2) Mesozoic Events. These occurred during the Triassic and mid-Jurassic to early-Cretaceous. Since the amount of crustal extension which occurred during the Triassic event is likely to be relatively small (see chapter 6) the Triassic event was probably amagmatic. The mid-Jurassic phase however, is associated with four volcanic provinces: the Piper-Forties Province in the 'triple-junction' area, the 'Central North Sea' province in the central part of the Central Graben, the Egursund Basin province and the Netherlands Province (see figure 2.5, after Latin 1990).

3) Tertiary Events. These occurred on the northern edge of the basin and are associated with the final stages in the opening of the North Atlantic. These events produced very large volumes of flood basalts which form the Tertiary Igneous Province of north-west Britain. More detail can be found in Upton (1988).

2.3.2 The Piper-Forties Volcanic Province.

The only area of extensive magmatism found in the study area considered here is the Piper-Forties Volcanic Province. The province was first discovered in 1970

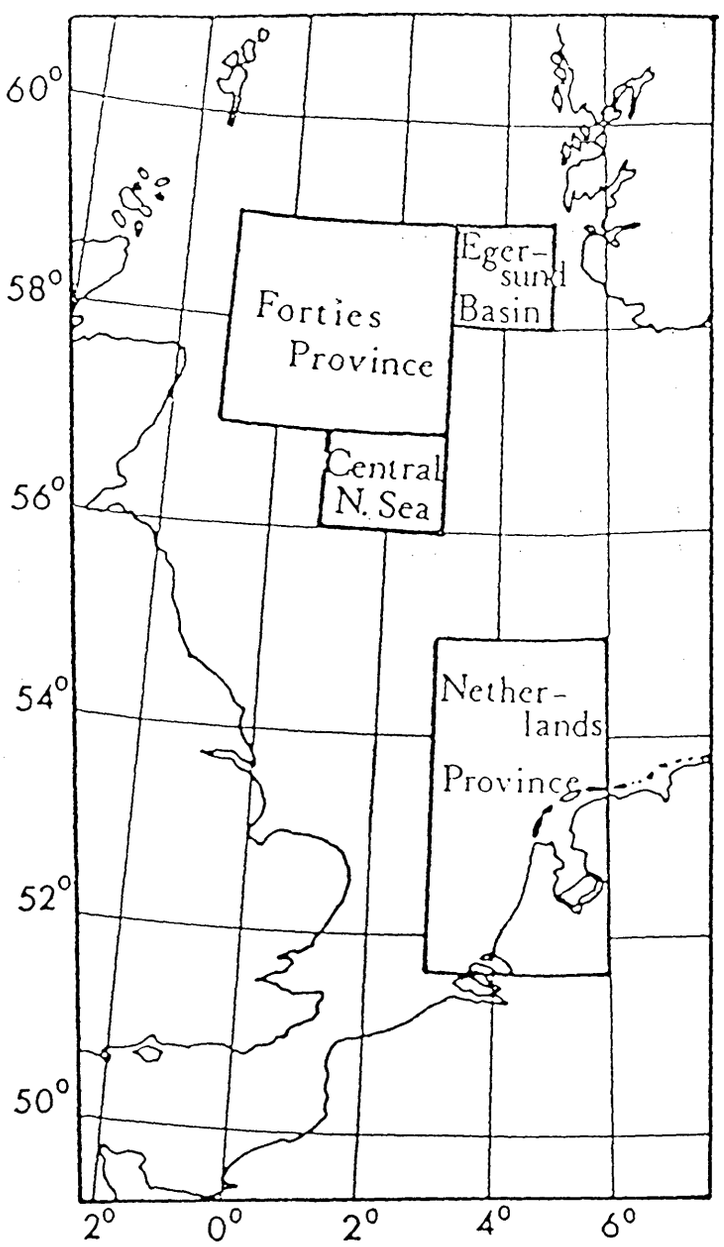


FIGURE 2.5 Sketch map showing the four main areas of Mesozoic igneous activity in the North Sea area. After Latin (1990).

during exploratory drilling in the area of the Forties oil field (Howitt et al, 1975). Figure 2.6 taken from Latin (1990) shows the location of wells which sample igneous rock in the 'triple-junction' area. The distribution of these wells define a roughly circular province of approximately 100 km in diameter centred on the southern side of the Witch Ground Graben. The area is also associated with a large positive magnetic anomaly. A detailed analysis of the magnetic field in the area is presented in chapter 4. This chapter also contains several models of the province which were made by modelling 2.5D magnetic profiles taken across the region.

The petrographic and mineralogical characteristics of the Piper-Forties Volcanic Province rocks have been described in detail in Fall (1980), Fall et al (1982) and Latin et al (1990a). For the purpose of this summary it is sufficient to note that the dominant rock-type is an extrusive, mildly undersaturated, porphyritic alkali basalt. Several individual flows can be recognised by the presence of fine-grained oxidised tops. Interbedded sediments indicate that they were erupted in a subaerial setting in a deltaic environment.

In terms of lithostratigraphy the province is termed the Rattray Volcanic Formation which forms part of the Fladen Group. (Andrews and Brown, 1987 and Harker et al, 1987). Harker et al (1987) report that although the interbedded sedimentary units are rarely fossiliferous the palynoflora indicate a mid-Jurassic (Bajocian/Bathonian) deltaic environment. The basalts lie unconformably on red-beds of inferred Triassic age (Howitt et al, 1975, Harker et al, 1987) and are overlain by 2-3 km of younger Mesozoic and Cenozoic sediments. Latin (1990) reports that in all the wells he studied from the area the sediments directly above the basalts were from the Piper Formation of the Upper-Oxfordian or from younger sequences. Radiometric ages of the basalts show wide variations even from rocks of the same area (Ritchie et al, 1988, Howitt et al, 1975). Latin et al (1990a) and Latin (1990) provide a review of all the radiometric ages available for the rocks of the province however, they can only conclude that there is no radiometric evidence that the basalts are any older than 150 - 160 Ma (Callovian).

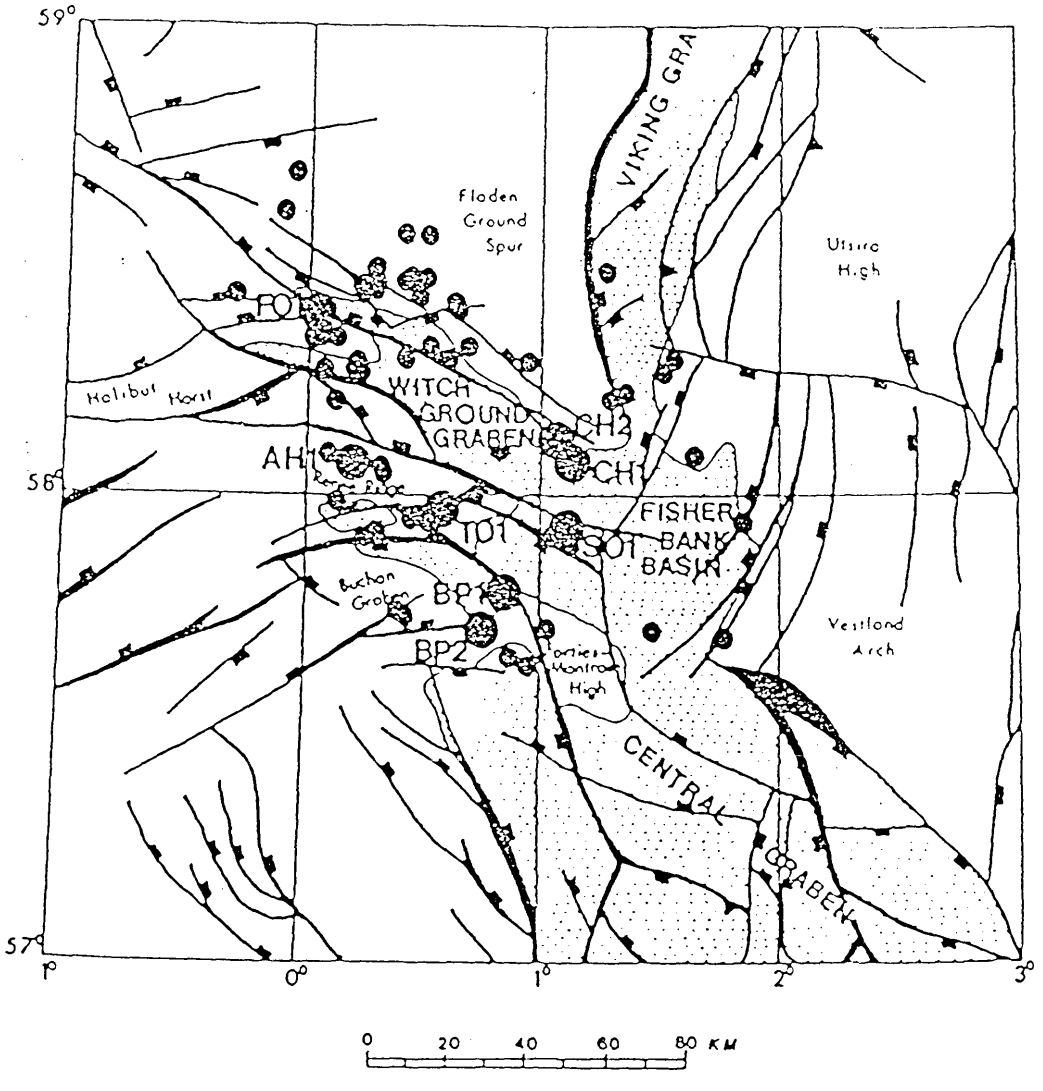


FIGURE 2.6 The main structural elements of the 'triple-junction' area and the location of wells (dark circles) which have penetrated igneous rocks. The dotted area indicates the main graben features as defined by the 3.0 second TWT contour at Base-Cretaceous level. After Latin (1990).

The total amount of igneous material in the province is still uncertain. The large thicknesses of sedimentary cover (2-3 km) means that wells penetrating the volcanics rarely reach their base. Ritchie et al (1988) report that the thickest sequence encountered by wells to dat is 1492 m recorded from well 21/3b-3 (Occidental). Volumes can be estimated by modelling the magnetic anomaly associated with the province. Woodhall and Knox (1979) integrated the evidence from well data, seismic and aeromagnetic surveys to produce an isopach map of the basalt. This is shown in chapter 4 (figure 4.19). Their model indicates a maximum thickness of 3-4 km in the Witch Ground Graben. Modelling of aeromagnetic data performed in this research and discussed in chapter 4 indicates thicknesses of up to 8 km in some places (possibly a vent site) but on average the overall thickness is less than 1.2 km.

A second centre of magmatic activity can be recognised from the aeromagnetic data. This occurs in the East Forties Basin (Fisher Bank Basin) and is interpreted as being a deep-seated mafic intrusion (possibly of Gabbro) occurring at depths of greater than 7 km (see chapter 4). The age of this body is completely unknown and it may not be at all related to the mid-Jurassic voclanics of the Forties Province.

In summary then, the Piper-Forties Volcanic province consists of an average thickness of less than 1.2 km of alkali basalts which were erupted sub-aerially into a deltaic environment. The time of emplacement was in the mid-Jurassic probably between the Bajocian and Callovian, which would mean that they were extruded relatively early in the Jurassic syn-rift sequence and predate the main upper-Jurassic extensional phase. The implications of the timing of magmatic activity are discussed in chapter 6.

2.4 PRINCIPAL STRUCTURES IN THE STUDY AREA.

Figure 2.7 shows the principal structures occurring in the study area (see also structural overlays 1 and 2). The area is dominated by the three arms of the North Sea rift system which probably first opened in the Triassic rifting event (see 2.2). In the north-east of the study area the southern end of the Viking Graben is the main structural feature. In the study area it is bound to the west by a large rotational normal fault. To the east (and just out of the study area) it is bound by the raised basement of the Utsira high. The southern end of the Viking Graben opens out into the East Forties Basin (a.k.a the Fisher bank Basin). This is an area of very thick sediments (the Base-Zechstein is mapped as occurring at depths of greater than 6.5 km in Day et al, 1981) and is also associated with a large mafic intrusion of unknown age (see chapter 4). South of the East Forties basin the dominant structural feature is the northern end of the Central Graben. In this area its trend is approximately N - S although further south it changes to a more NW - SE structural trend. At its northern end it is roughly twice as wide as the South Viking Graben. Again it is bound by major rotational faults and contains thick sequences of sediments. A series of locally prominent Palaeozoic basement horst structures (Mid-Graben Highs) divide the graben into a shallow western and a deeper eastern part. In the study area the northern most of these is known as the Forties-Montrose Ridge.

West of the East Forties Basin the third arm of the rift system (the Moray Firth Basin) becomes the most important structural feature. This is a more complex structure than the North Central or South Viking grabens and consists of two E - W trending grabens (the Witch Ground and Buchan Grabens) separated by the Renee Ridge and the Halibut Horst, an elongate E - W trending basement ridge. In the east of the area the Moray Firth Basin is bound to the north and south by the Wick Fault and the Banff fault respectively. North of the Wick fault in the north-west of the area the Caithness ridge is an elongate E - W trending basement high on the southern edge of the East Shetland Platform. The East Shetland Platform itself is a broad area of Palaeozoic basement which

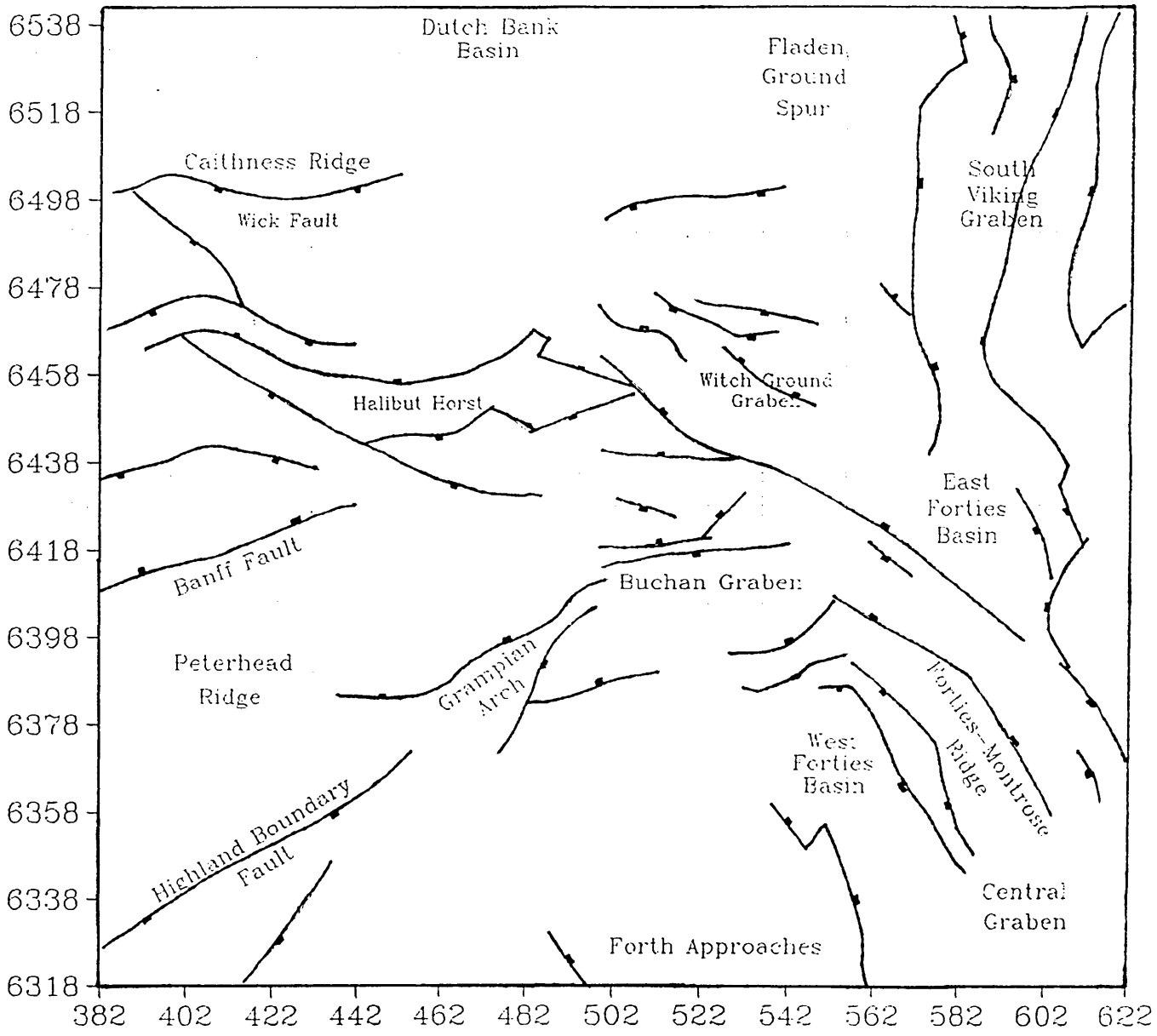


FIGURE 2.7 Principal structural elements of the study area (see figure 1.1). UTM projection, axes coordinates are in units of kilometres.

remained stable during the evolution of the graben system. In the northern part of the study area the platform is embayed by the Dutch Bank Basin (a.k.a Piper Embayment). A south-east extension of the East Shetland Platform known as the Fladen Ground Spur separates the southern end of the Viking Graben from the Moray Firth Basin.

The south-west of the study area is characterised by NE - SW trending linear features. These are Caledonian structures (one of which is an eastward extension of the Highland Boundary Fault) in an area of relatively shallow basement.

2.5 THE NATURE OF THE CRYSTALLINE BASEMENT.

In a study of several wells in the area Frost et al (1981) report that, as outlined in 2.2 and Ziegler and Van Hoorn (1990), much of the basement underlying the North Sea Basin was consolidated during the compressional tectonics of the Caledonian orogeny. Figure 2.2 shows the late Caledonian Tectonic front as interpreted by Ziegler (1981). Only the eastern part of the Central North Sea is underlain by an entirely Pre-Cambrian basement (part of the Fennoscandian shield). North of a line representing a north-eastern extension of the Highland Boundary Fault the crystalline basement consists of high-grade metamorphic rocks (e.g. amphibolite facies gneiss) and some deformed plutonic rocks that were probably first metamorphosed in the Grampian orogenic phase but which underwent retrogressive overprinting during the main phase of the Caledonian at around 440 - 450 Ma. South of this line the crystalline basement consists of lower grade metamorphic rocks (e.g. lower greenschist facies phylites) with radiometric ages of around 440 - 450 Ma, corresponding to the main deformational phase of the Caledonian orogeny. The dominant Caledonian trend in the study area is NE - SW to ENE - WSW. The influence of Caledonian features on the evolution of the basin is discussed in 7.2.3 and in Johnson and Dingwall (1981).

CHAPTER 3

ANALYSIS OF THE GRAVITY DATA

3.1 INTRODUCTION

This research is primarily concerned with quantifying crustal extension in the Central North Sea. One method of doing this is to measure crustal thickness within the rifted region and to compare this with similar measurements made in areas unaffected by rifting. Estimates of crustal thickness can be made by modelling the regional gravity field.

Section 3.2 of this chapter summarizes how gravity data is acquired and explains its subsequent processing into grid format.

A detailed qualitative interpretation of the Bouguer anomaly map for the area 2°W - 2°E, 57°N - 59°N is presented in section 3.3. Principal trends and anomalies are discussed and several images of the data enhanced by image processing techniques are included.

The full method for modelling the gravity field is explained in section 3.4. An assumption is made that the Bouguer anomaly field is the sum of the gravitational effects of near-surface layers (down to the Base-Cretaceous) and the effect of a compensating homogeneous upper-mantle body. If the crystalline basement is assumed to be both laterally and vertically homogeneous then the gravitational effect of the near-surface layers can be calculated and subtracted from the Bouguer anomaly data. The resultant field can then be modelled in three dimensions, the end result being a model representing the depth to the Moho for every point in the study area.

The technique for producing digital grids of all the near-surface layers is explained and a full description of the 3D forward modelling routine used to calculate their gravitational effects is presented. Before this calculation can take place an estimate of the density of each layer has to be made. The reasons for choosing the densities used are discussed and the results of the calculation for each layer is presented. Once the stripping process is complete the resultant field needs to be filtered as it contains a proportion of high frequency data inconsistent with deep sources. The digital filtering technique is outlined in full and the final result is discussed. This field provides an input to a 3D iterative forward modelling routine. A full explanation of the iterative process is presented at the end of this section.

The results of the 3D modelling are presented in section 3.5. Three different models are shown to demonstrate how altering certain modelling parameters (such as the numbers of iterations) affects the final model. The geological implications of these models are discussed later in chapter 6 which deals with the extensional history of the North Sea. Section 3.5 ends with a quantification of the errors involved in the modelling process. The final section (3.6) is a brief summary of the most important points outlined in this chapter.

3.2 GRAVITY DATA

3.2.1 Data Source

The Bouguer anomaly data used in this research was kindly provided by the British Geological Survey. Data between latitudes 58° and 59° N form part of a regional gravity survey covering the UK sector of the North Sea and was carried out in the summers of 1977 and 1978 by the Marine Geophysics Unit of the Institute of Geological Sciences (now BGS).

The data were recorded on a Lacoste and Romberg air-sea meter along ship

tracks with a separation of 12 to 15 km. Data spacing along each survey line ranges between 2 and 3 km. Data from the southern half of the study area come from an earlier survey where the coverage was not so dense. More detailed information about the data can be found in Tulley and Donato (1985).

The difficulty of recording in a marine environment means that survey accuracy is reduced from the typical land-based value of 0.1 mGal to between 1 and 2 mGal. In the case of this survey Tulley and Donato (1985) report an internal accuracy (based on the arithmetic mean of cross-tie errors) of better than 1 mGal.

Bouguer gravity anomalies are calculated using a density of 2.67 g cm^{-3} for the slab correction. Since the study area is entirely marine this simply consists of a replacement for the water layer.

3.2.2 Processing

The 3D modelling and image processing routines used in this research require input data to be in the form of digital grids. This section describes how track data provided by the BGS is converted into grid format.

Briggs (1974) suggested a method for machine contouring using a technique of minimum curvature. This was later developed by Swain (1976) into an iterative routine which automatically produces a best fit numerical surface to irregularly spaced data. Although the BGS Bouguer anomaly data is closely spaced along track lines (2-3 km), the lines themselves are more than 10 km apart. Also the density of coverage in the south of the study area is relatively poor compared with that in the north. Swain (1976) shows that the minimum curvature method is a useful technique for interpolating data which is either irregular and/or relatively widely spaced with respect to the grid interval chosen for the final numerical surface.

In order to enhance higher frequency features many of the image processing

and data display routines used in this research provide superior results when the input grid interval is small. However, a very large grid (produced by a very small grid spacing) renders these routines computationaly inefficient. For a region the size of the study area an acceptable grid spacing was found to be 2 km.

Swain's routine was adapted for use with the IBM PC by Duncan Cowan (Cowan Geodata Ltd). His program, BIGMINC, was used to convert the BGS Bouguer gravity data into a digital grid in the UTM projection. The minimum curvature technique ensures that energy from spuriously high frequency features introduced during the interpolation process is kept to a minimum. The resulting grid has a 2 km interval and consists of 121 by 113 data points.

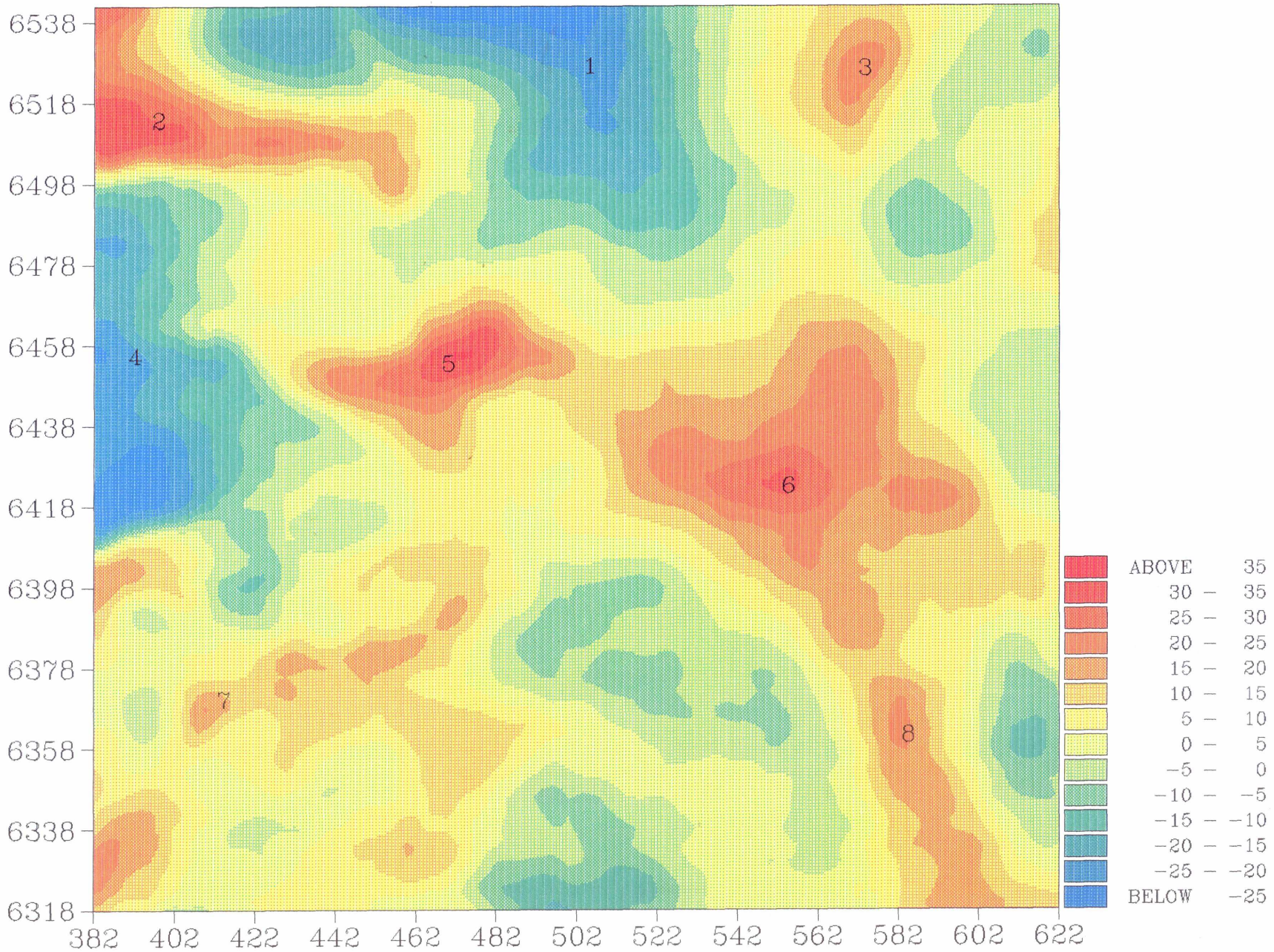
3.3 QUALITATIVE INTERPRETATION

Regional scale interpretations of the BGS Bouguer anomaly data set for the UK sector of the North Sea can be found in Donato and Tulley (1981) and Tulley and Donato (1985). A larger scale interpretation of the gravity data for the whole of the Northern and Central North Sea can be found in Hospers et al (1985). The following interpretation is made with reference to these earlier works although it is primarily based on the grids and images produced during this research.

3.3.1 Analysis of the Bouguer Anomaly Map

Figure 3.1 shows the gridded Bouguer anomaly data for the study area. It is presented in a rectangular UTM projection (central meridian at 0 degrees longitude). The coordinate axes are in units of kilometres. An obvious feature of the whole area is the relatively low amplitude of the anomalies, ranging between approximately −28 and +35 mGal. Day et al (1981) and Ziegler

FIGURE 3.1 Bouguer anomaly map for the study area. Units are in mGals. The map is in a rectangular UTM projection (central meridian 0 degrees longitude). Axes coordinates are in units of kilometres.


6538
6518
6498
6478
6458
6438
6418
6398
6378
6358
6338
6318
382
402
422
442
462
482
502
522
542
562
582
602
622
1
2
3
4
5
6
7
8
ABOVE 35
30 – 35
25 – 30
20 – 25
15 – 20
10 – 15
5 – 10
0 – 5
−5 – 0
−10 – −5
−15 – −10
−20 – −15
−25 – −20
BELOW −25

(1982) note that sedimentary sequences exist at depths in excess of 8 km in the 'triple-junction' area. Such thick sediments should lead to large negative Bouguer anomalies. It follows that since such large negative anomalies are not seen in the area there must be some compensating mass at depth. This assumption forms the basis of the modelling technique discussed later in this chapter.

The anomalies discussed here are numbered on figure 3.1. Structural overlay 1 can be used in conjunction with all the maps and images presented in this section. The study area has also been divided into 3 zones (marked on structural overlay 1). These zones are purely for ease of reference and bear no relation to any structural zoning within the area.

3.3.1.1 Northern Zone

This is dominated by a large scale gravity low (feature 1). In the study area the anomaly measures approximately 70 km N-S and 90 km E-W although this feature does continue northwards out of the study area for a further 70 km. At its centre point (on the northern edge of the area) the anomaly reaches a minimum of −28 mGal. The seismic structure maps of the North Sea produced by Day et al (1981) do not show sedimentary thicknesses below the Base- Cretaceous in areas north of approximately 58°N. The Base-Cretaceous itself is shown to be either absent or relatively shallow in this area. However, Tulley and Donato (1985) point out that this deep gravity low correlates with the location of thickened sediments assumed to be of a Permo-Triassic and/or Devonian age under a Tertiary cover.

The gravity signature of the Caithness ridge (feature 2) appears as a narrow E-W trending gravity high. The maximum Bouguer anomaly associated with this structure is 35 mGal although there is a secondary peak of some 25 mGal roughly 40 km to the east of the primary maximum. The whole feature measures approximately 105 km E-W by 60 km N-S. The southern edges of this feature are clearly marked by steep gravity gradients (3.3.2.1), generally indicative of a fault

bounded structure.

Feature 3 is a small isolated gravity high of approximately 25 mGal in the north east corner of the zone. It continues northwards out of the study area for a further 35 km to form a narrow NNE-SSW trending anomaly occurring at the southern end of the Viking Graben. Tulley and Donato (1985) have interpreted this feature as a basement ridge occurring on the faulted margin of the graben. Day et al (1981) show this ridge as having thin Cretaceous cover in places, its eastern edge being bound by a large N-S trending fault down-throwing 2.5 km to the east. This fault is clearly defined in the first horizontal derivative image (3.3.2.1).

3.3.1.2 Central Zone

The western section of this zone is dominated by a large gravity low (feature 4). This measures roughly 90 km N-S and reaches a low of -28 mGal in its southern part. It correlates with the thick sediments of the Outer Moray Firth Basin. It continues westwards out of the study area until it merges with a second gravity low associated with the Inner Moray Firth Basin. The feature is bounded to the north and south by steep gravity gradients (3.3.2.1). The northern margin correlates with the position of the Wick fault (separating the basin from the Caithness Ridge) whilst the southern margin correlates with the position of the Banff fault.

Feature 5 is an E-W trending gravity high which is associated with the Halibut Horst. The anomaly measures approximately 70 km N-S across its widest point, reaches a maximum of 35 mGal in the centre and is bound on all four sides by steep gravity gradients. The horst itself lies just to the east of the Outer Moray Firth Basin and is a fault bounded Devonian basement ridge. The maps of Day et al (1981) show it to have thin Cretaceous cover in places.

The Halibut Horst anomaly merges to the east into a broad gravity high

(feature 6). This feature measures more than 120 km E-W and 80 km N-S. At its central point the anomaly reaches a maximum of approximately 31 mGal. To the south it merges into a NNW-SSE trending gravity high (3.3.1.3). The anomaly falls in the centre of the 'triple-junction' area and has an associated complex magnetic anomaly (chapter 4) correlating with the position of the Piper-Forties Volcanic Province (2.3.2).

3.3.1.3 Southern Zone

The western side of this zone has a complex gravity signature. It consists of a series of low amplitude (less than 20 mGal) anomalies trending NE-SW. This is a typical Caledonian trend (Anderton et al, 1979, Johnson and Dingwall, 1981) and the anomalies (e.g. feature 7) correlate with fault bounded ridges in the Caledonian basement. The magnetic signature in this area (4.3.1.3) is even more complex indicating that the basement is relatively near to the surface.

Feature 8 in the east of this zone is a long, narrow NNW-SSE trending gravity high correlating with (and on the same trend as) the northern end of the Central Graben. In fact it correlates with a series of mid-Central Graben basement ridges and in particular with a structure known as the Forties-Montrose Ridge. The mid-point of the anomaly is marked by a small isolated high of 21 mGal. At this point the anomaly is approximately 40 km across. This feature broadens to the north (3.3.1.2) and to the south. The broad southern end of the anomaly occurs some 50 to 60 km south of the study area.

As mentioned earlier the thick sediments of the Central Graben cannot explain the presence of a positive anomaly in this area. It must be caused by a combination of the basement ridge structures and a much deeper compensating mass. Results of modelling this structure are shown later in this chapter.

3.3.2 Enhanced Images

A variety of numerical techniques can easily be applied to gridded data to enhance different qualities in the potential field. No new information should be created but previously masked effects can be brought out and interpreted much more readily. Two principal methods were applied to the gravity data set. The first involves finding the horizontal gradient whilst the second involves the production of shaded relief images.

3.3.2.1 First Horizontal Derivative

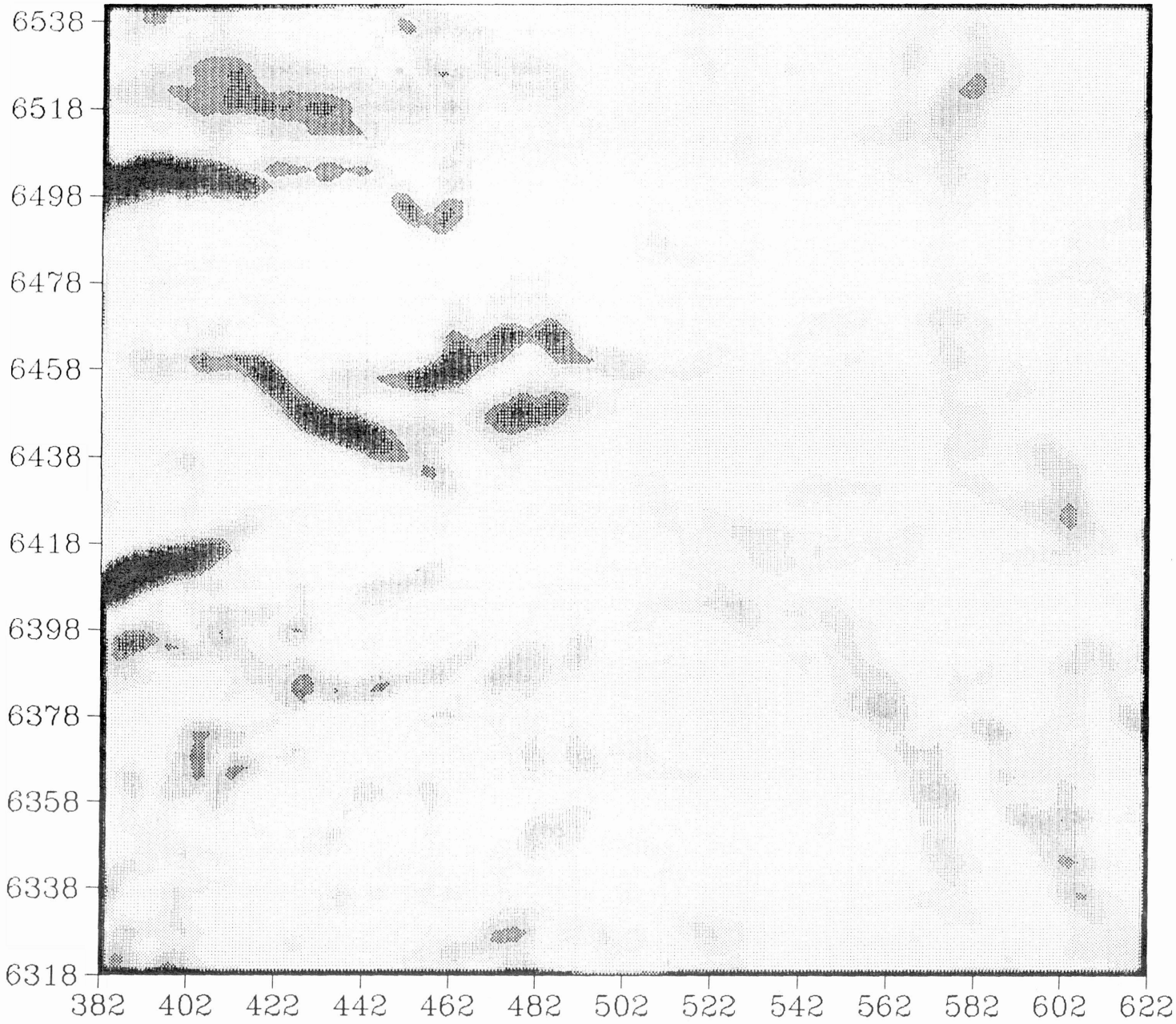
Horizontal derivatives have long been recognised as an effective means of enhancing anomalies due to contacts and discontinuities (Telford et al 1976, Parasnis, 1962).

The local gradient of the gravity field is calculated for all grid points using the potential field values of the grid points surrounding it. A 'slope' is calculated from each point in the grid. This is the absolute value of the maximum gradient presented by a nine point (3 by 3) array. The method brings out any change as a positive feature, making interpretation easier and avoiding the possibility of a positive gradient in one direction partially cancelling a negative change in another.

Figure 3.2 is a grey-scale representation of the first horizontal derivative of the gravity field. Since the initial data is very smooth the gradient field is relatively featureless. The darker lines represent increased gradient and should relate to steep geological contacts such as faults.

The overlay of primary structures (derived from seismics) shows clearly how well this technique works for marking the location of major discontinuities. The Wick fault in the north west of the area is clearly delineated as is the fault-bound

FIGURE 3.2 First horizontal derivative of Bouguer anomaly. Darker areas correspond to areas of increased local gradient in the gravity field and tend to pick out major geological contacts such as faults.


6538
6518
6498
6478
6458
6438
6418
6398
6378
6358
6338
6318
382
402
422
442
462
482
502
522
542
562
582
602
622

nature of the Halibut Horst in the centre of the area. The Banff fault at the southern end of the Outer Moray Firth Basin is also clearly shown. Other structures defined by this technique include the long N-S trending fault on the western flank of the South Viking Graben, the faults of the Peterhead ridge in the south-west of the area and the fault zone on the eastern side of the Forties-Montrose ridge.

This technique also seems to reveal several structures which are not included on the primary structure map. In the south-west corner of the study area a complex zone of cross-cutting SW-NE and NW-SE trending structures is revealed. This is also very apparent from the magnetic data (4.3.1.3). In the south-east, the eastern fault of the Forties-Montrose ridge is not picked out by the gradient but it does seem to indicate either another fault or an extension of this one to the south. There is also the possibility of a north-trending lineament within the Buchan Graben.

Care should be taken not to over-interpret these enhanced images. For instance, some of the N-S and E-W trending features are purely artifacts of the original gridding procedure.

3.3.2.2 Shaded Relief Images

The technique of shaded relief originates from aerial photography and remote sensing. Originally it was an attempt to produce an image of the topographical surface at any angle of illumination. In its application to potential fields, each field value (represented by a data point on a digital grid) is imagined to represent a small surface. The angles subtended by these 'surfaces' to an imaginary horizontal are determined by their relative value to the surrounding data points (Dods 1985). The calculated quantity is directionally proportional to the spatial angle between the illumination direction and the horizontal to the surface element under consideration which is proportional to the dot products of these directions (fig 3.3).

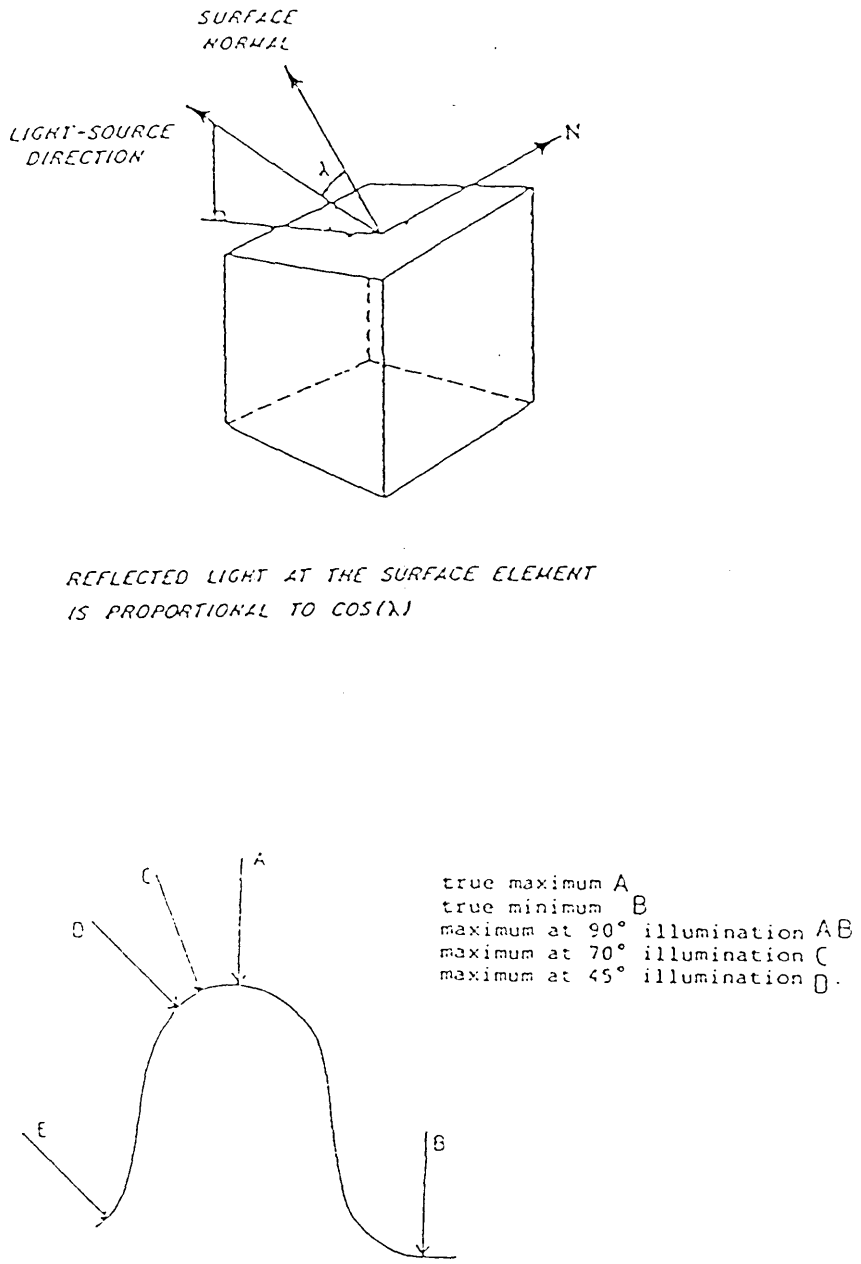


FIGURE 3.3 The principal behind shaded relief. The lower diagram demonstrates that maxima in the field will be displaced toward the direction of illumination.

The shaded relief images of the Bouguer gravity data presented here (figs 3.4 and 3.5) are somewhat degraded by the presence of N-S and E-W trending lines. As mentioned in the previous section these lineaments are an unfortunate product of the original gridding procedure and are not related to geological trends. Attempts to remove them using a Fourier filtering technique was largely unsuccessful. However, these lines do not mask the main trends which are fortunately SW-NE or NNW-SSE in this area.

Figure 3.4 shows the gravity field 'illuminated' at an incident angle of 45 degrees from the north-east. The relatively low amplitude of the field means that a scaling factor of 50 has to be applied to the data before the image is created. Features trending perpendicular to the source of illumination will be enhanced. The NNW-SSE trending gravity ridge in the south-east of the region is clearly picked out as are the southern and western edges of prominent features such as the Caithness Ridge and the Halibut Horst. More subtle features enhanced in this image include several north-west trending structures in the south-west corner of the area and a stronger lineament north of the Caithness ridge which seems to cut into the East-Shetland Platform.

Figure 3.5 is the gravity field illuminated at 45 degrees from the north-west. Again a scaling factor of 50 has been applied. This time NE-SW trending lineaments will be enhanced. As before the Caithness Ridge and Halibut Horst are very prominent. The south-west section is dominated by strong lineaments which are due to structures within the Caledonian basement. The Banff fault is clearly picked out as is the Peterhead Ridge and a structure which may be an eastern extension of the Highland Boundary Fault. An interesting point to note is the apparent continuation of these Caledonian trending features west of the 'triple-junction ' area. The Permo-Triassic NNW-SSE trend of the Central Graben seems to cut across these older features.

These shaded relief images should not be used to delineate the exact position of structural lineaments. The technique always displaces the highs and lows

FIGURE 3.4 Shaded relief image of Bouguer anomaly. The field is 'illuminated' from the north-east at an incident angle of 45 degrees.

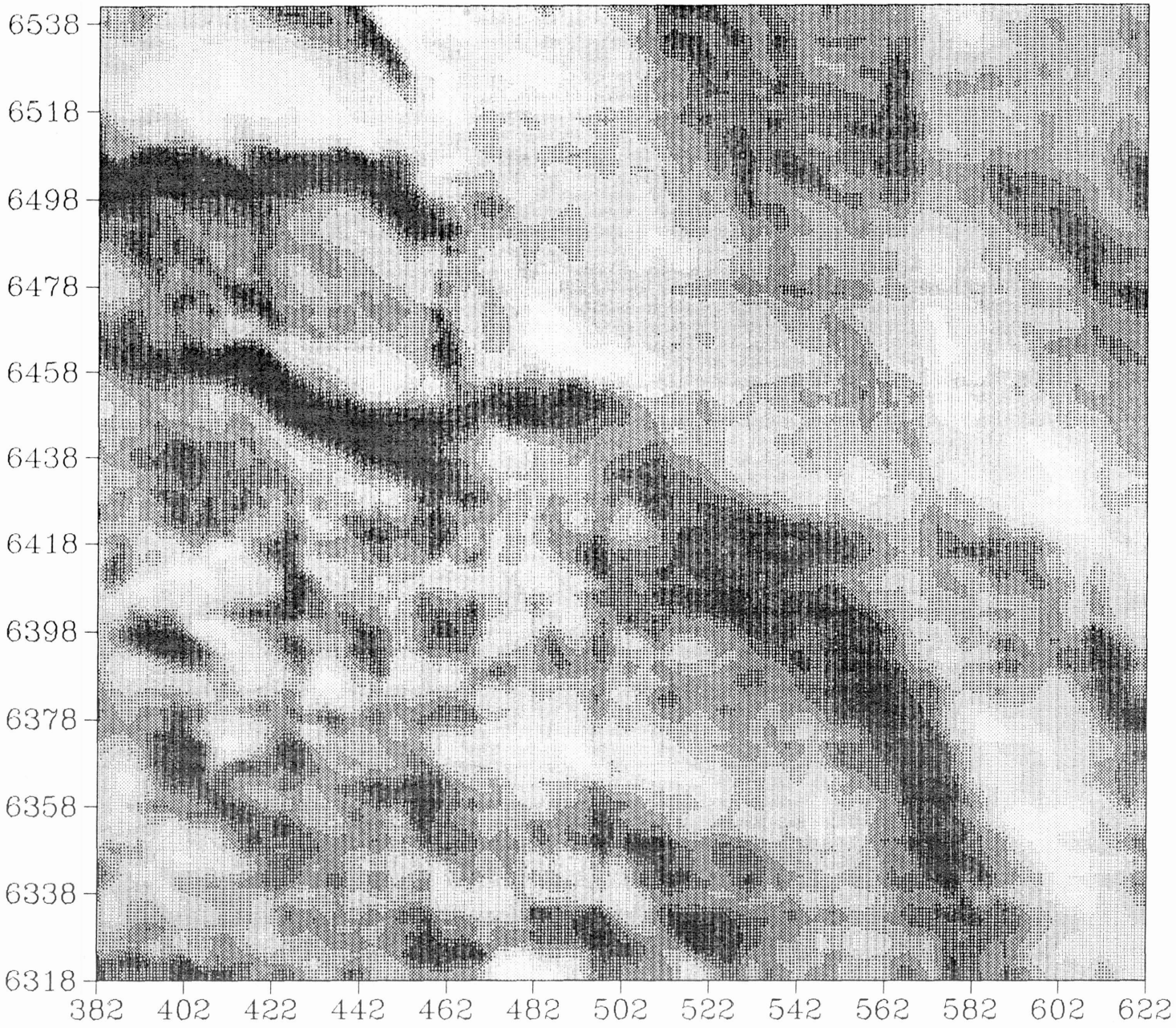
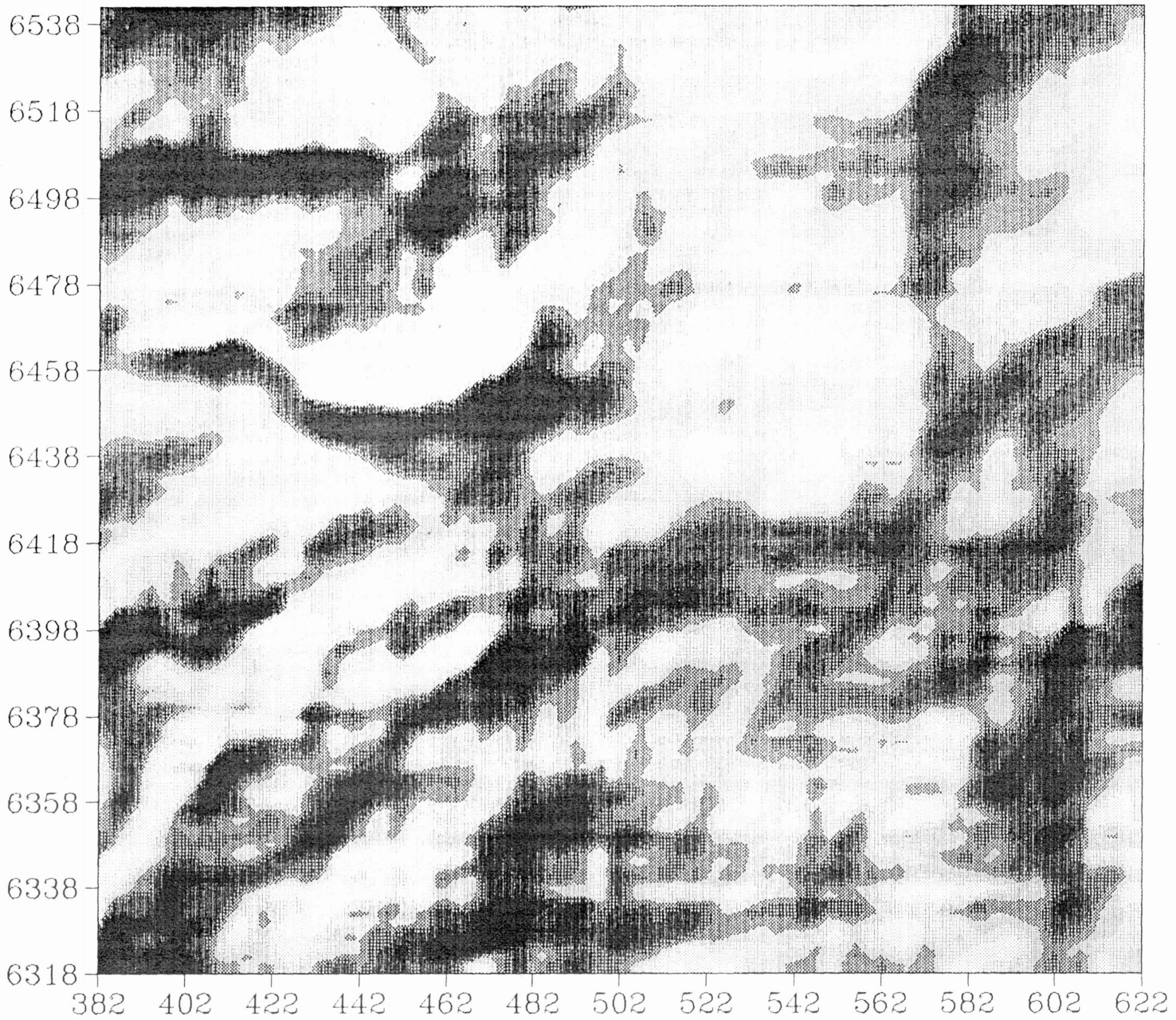

6538
6518
6498
6478
6458
6438
6418
6398
6378
6358
6338
6318
382
402
422
442
462
482
502
522
542
562
582
602
622

FIGURE 3.5 Shaded relief image of Bouguer anomaly. The field is 'illuminated' from the north-west at an incident angle of 45 degrees.


6538
6518
6498
6478
6458
6438
6418
6398
6378
6358
6338
6318
382
402
422
442
462
482
502
522
542
562
582
602
622

towards the illumination direction (fig 3.3). The magnitude of this displacement decreases with increasing angle of incidence. Structural trends are more correctly located using horizontal derivative methods (3.3.2.1).

3.4 3D MODELLING TECHNIQUE

As mentioned in 3.3 the Bouguer anomaly data for the study area ranges between approximately −28 and +35 mGal. Evidence from seismic and well data shows that sediments occur at depths of over 8 km in the graben areas (Ziegler 1982, Day et al 1981). Such low density sequences should yield large negative Bouguer anomalies. It follows that this effective mass deficiency must be compensated at depth by an excess mass. The distribution of this excess mass can be modelled in three dimensions.

The technique in principle is a simple one. The gravitational effect of each of the sedimentary layers is calculated in three dimensions. Their total effect is than removed from the Bouguer anomaly data for the study area. Variations in the resulting residual field are then assumed to be caused by relatively deep density contrasts. If a laterally and vertically homogeneous basement is assumed, then the sole density contrast occurring at depth will be that which occurs across the Moho. Thus, a 'Moho topography' can be modelled using this residual anomaly.

This method obviously involves several assumptions. The first of these is that crustal thinning in the North Sea is the direct result of lithospheric extension (see chapter 6) and that Airy-type isostatic compensation of low-density sedimentary basin infil, results in variations in the depth to Moho. The assumption that both the crystalline basement (here taken to be everything between the Base-Cretaceous and the Moho) and the upper-most mantle are laterally and vertically homogeneous in terms of density is therefore, of crucial importance to the technique. The geological implications of these assumptions are discussed later in this chapter and in chapters 6 and 7. This section outlines each stage in the

modelling technique.

3.4.1 Calculating the Field Due to Near-Surface Layers.

3.4.1.1 Sedimentary Thicknesses.

Information regarding sedimentary thicknesses for the study area comes from the regional seismic structure maps produced by Day et al (1981). These maps are based on data derived from both commercial seismic data and well logs and are reproduced on a scale of 1:2 500 000. Each map shows depths to the following horizons: Palaeocene Ash Marker, Top Cretaceous (including Dinantian Chalk), Base Cretaceous, Top Triassic, Top Bacton Group, Top Zechstein and Base Zechstein. Unfortunately coverage over the study area is only complete down to the Base Cretaceous.

In order to calculate the gravitational effect of each layer each map needs to be put into digital format in the same geographical projection as the Bouguer anomaly grid. Maps for the Top Palaeocene, Top Cretaceous and Base Cretaceous were digitised along contour lines and converted to UTM coordinates. Each data set was then converted to grid format using the minimum curvature technique discussed in 3.2.2.

West of zero degrees longitude the sedimentary sequence is complicated by geological structures such as the Halibut Horst and Caithness Ridge. The gridding procedure inevitably simplifies such features leading to inaccuracies in the resultant map. To keep errors to a minimum it was decided to reduce the study area for modelling to that half lying east of the meridian where the gross geological structure of the sediments is much more simple. This revised study area still includes the 'triple-junction' zone and several important structures such as the Forties-Montrose ridge and the Piper-Forties Volcanic Province.

It is important to note that the digital maps for each of the near-surface layers covers a larger area than the study area itself. This larger size is used to avoid an undesirable 'edge-effect' affecting data in the study area during the calculation of the near-surface gravity effect (3.4.1.3). Smoothing over structures such as the Halibut Horst during the gridding process will therefore have a minimal affect on the calculated gravity for the study area.

Figures 3.6 to 3.9 show the digitised sedimentary maps for the study area. Each map represents the depth (from sea-level) to that particular horizon.

The Top-Palaeocene depth map (fig 3.7) shows a smooth horizon deepening from less than 1 km in the north-west to over 3 km in the south-east at the deepest point. On a regional scale the Top-Palaeocene reaches a maximum depth of approximately 3.3 km in the centre of the basin (roughly 56.5°N, 3°E) which is just south-east of the study area.

The Top-Cretaceous map (fig 3.8) is also relatively smooth and shows a similar pattern to that of the Top-Palaeocene with a general deepening from the north-west to south-east. The depth varies between approximately 1.5 km in the north-east to almost 3.5 in the south-east. The structure is complicated west of the study area towards the Moray Firth Basin. There are several large faults cutting through the Top-Cretaceous such as those bounding the Halibut Horst where the Top-Cretaceous is absent.

The Base-Cretaceous map (fig 3.9) is more complex. Again there is a general deepening to the south-east (up to depths of 5 km) with the shallowest part in the north-east. Over the Fladen Ground Spur the Base-Cretaceous is absent. The complex nature of this map arises because the Base-Cretaceous marker is a diachronous unconformity. Several large faults occur in the study area at Base-Cretaceous level. They are not marked on the map but generally occur where the depth gradient is steep (the result of smoothing during the gridding process). Away from the study area the Base-Cretaceous is at its deepest in the centre of

the basin (greater than 5 km in places). To the west the Halibut Horst has only a thin Cretaceous cover and the Base-Cretaceous is totally absent from the Caithness Ridge. In the north the Base-Cretaceous is absent west of approximately zero degrees longitude but there is a dramatic deepening into the Viking Graben east of the meridian.

Digital bathymetric data was purchased from the National Geophysical Data Center, Colorado. Depth points are produced on magnetic tape for a worldwide grid at five minute intervals. The correct data points were extracted from this data base and re-gridded in a rectangular projection using the minimum curvature method. The resulting bathymetric map for the study area is shown in figure 3.6. The map is fairly smooth with bathymetric depths not exceeding 0.2 km for the study area.

3.4.1.2 Densities Used In Modelling

In order to calculate the gravitational effect of each of the near-surface layers an accurate estimation of their densities has to be made. The regional study made by Donato and Tulley (1981) includes estimates of densities made from formation density logs from several wells in the study area. In the absence of any other data collected on this scale it was decided to use these values in this research. The densities used are listed in table 3.1.

Table 3.1 Densities used in the Modelling Process

LAYER	DENSITY (g cm^{-3})	DENSITY CONTRAST (W.R.T. 2.75 g cm^{-3})
Sea Water	1.03	−0.08
Post Palaeocene	2.10	−0.65
Palaeocene	2.20	−0.55
Cretaceous	2.45	−0.30
Upper Mantle	3.25	0.50

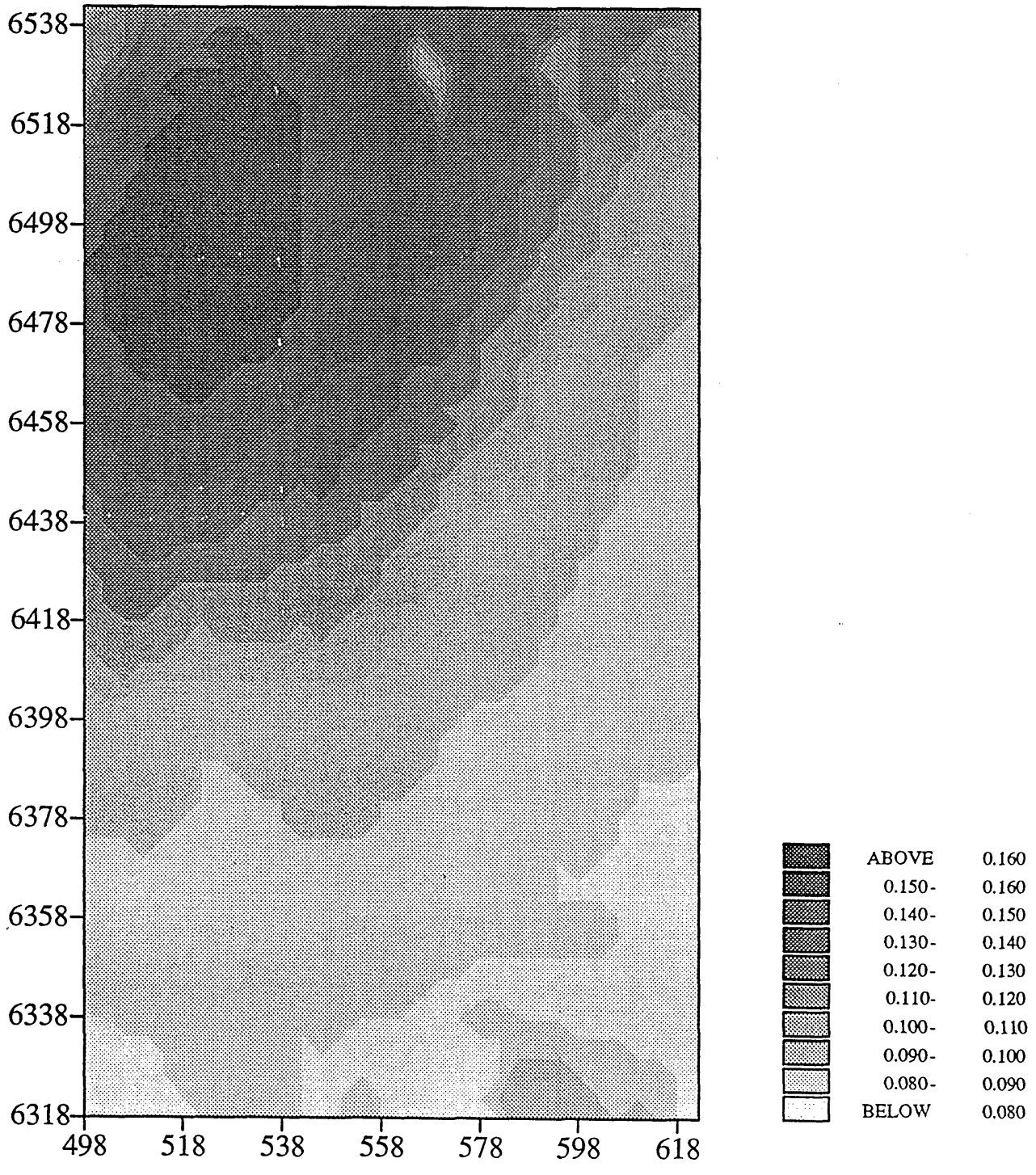


FIGURE 3.6 Bathymetric map for the study area. (From National Geophysical Data Center, Colorado). Units are in kilometres. The high frequency nature of the image is due to the 4 km grid spacing of the data set.

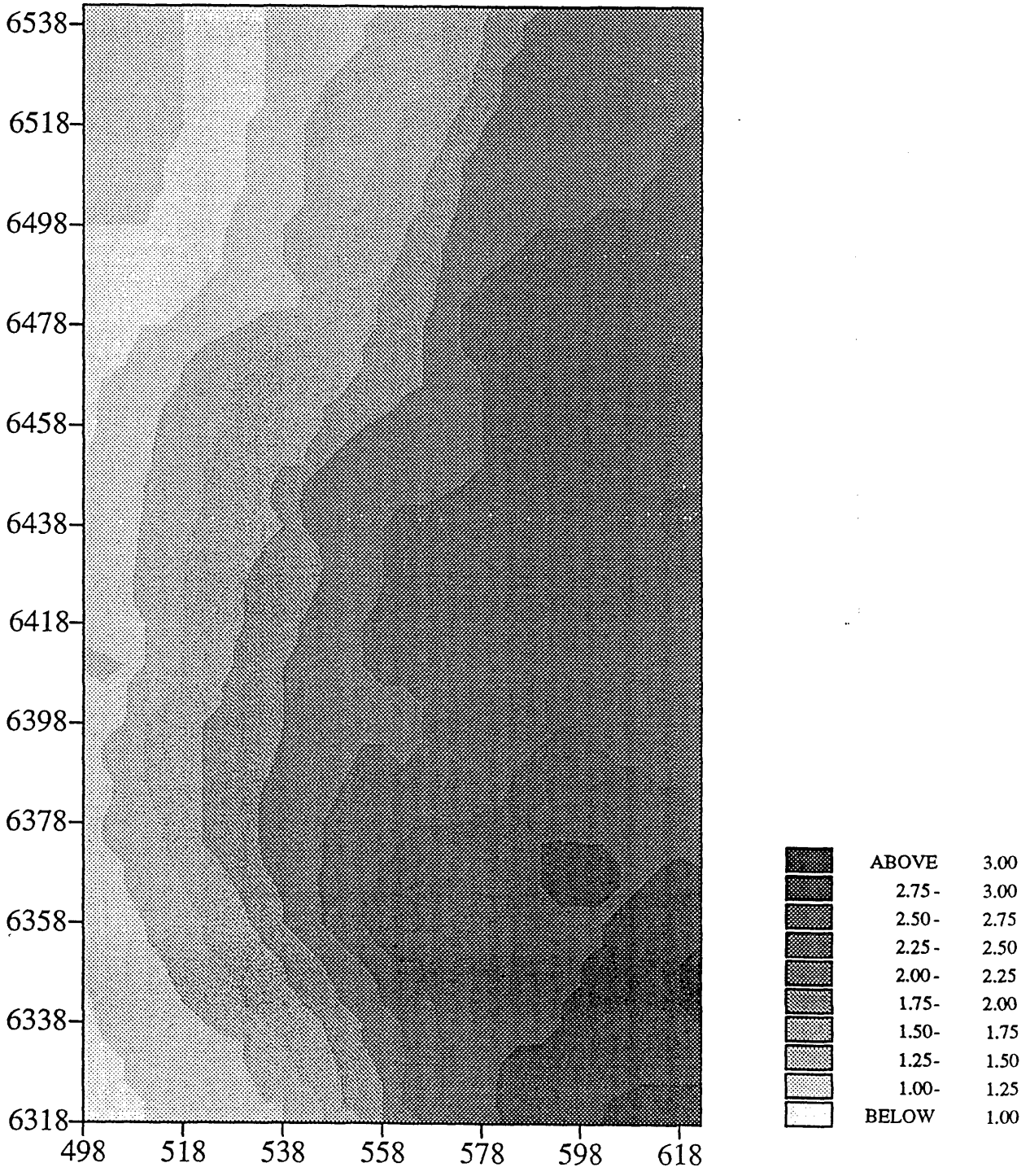


FIGURE 3.7 Depth to the Top Palaeocene. (From Day et al, 1981). Units are in kilometres. The high frequency nature of the image is due to the 4 km grid spacing of the data set.

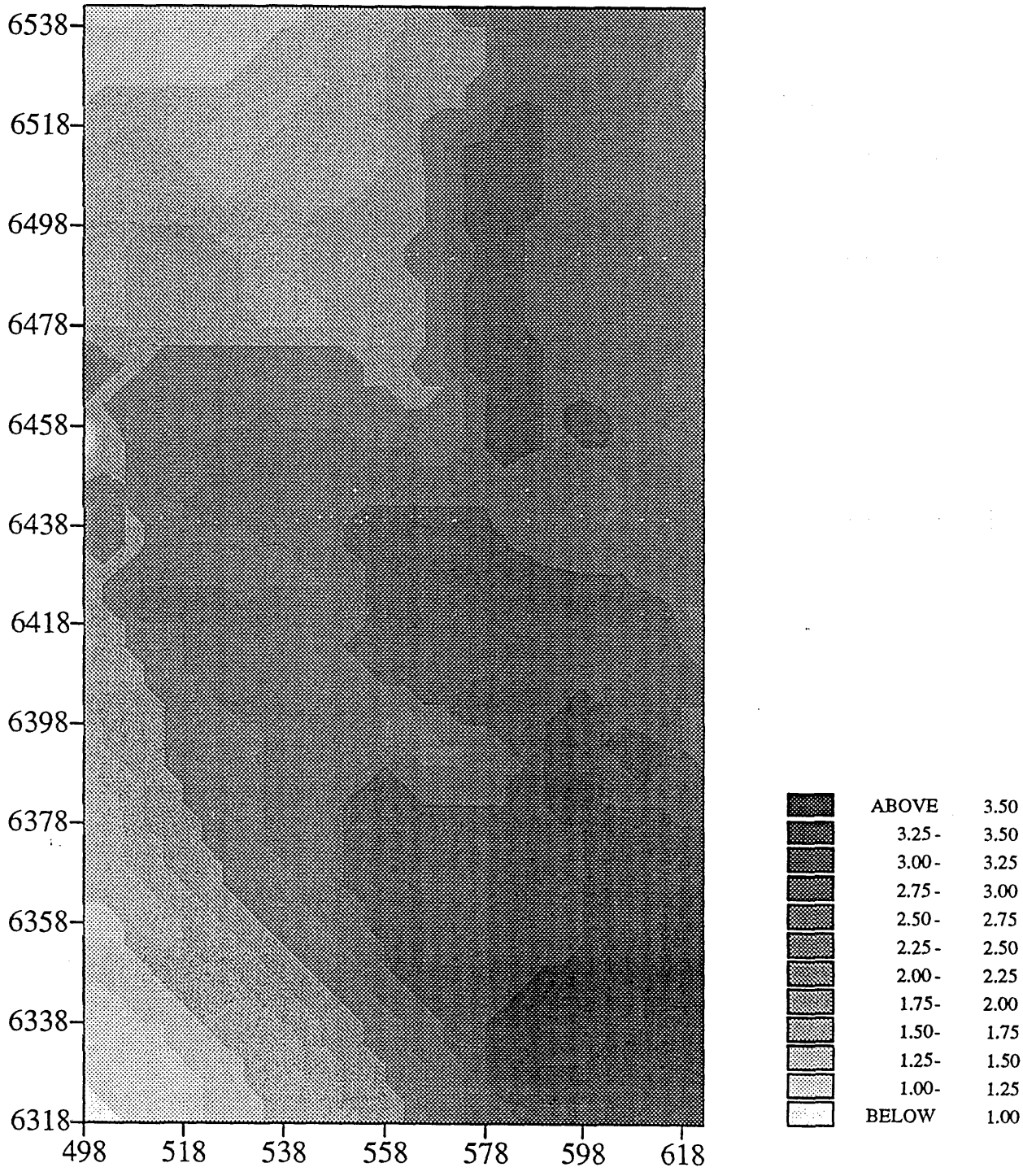


FIGURE 3.8 Depth to the Top Cretaceous. (From Day et al, 1981). Units are in kilometres. The high frequency nature of the image is due to the 4 km grid spacing of the data set.

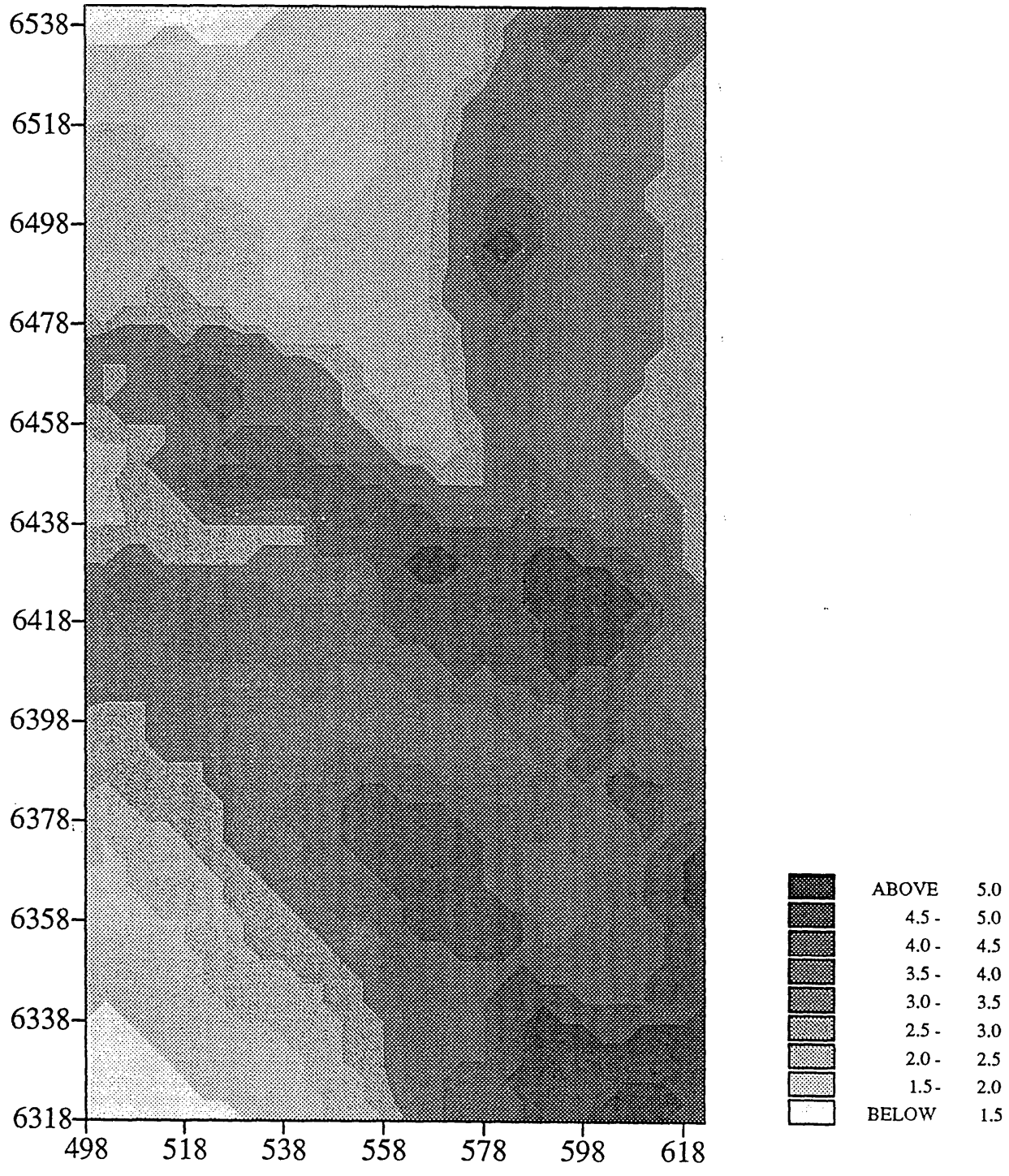


FIGURE 3.9 Depth to the Base Cretaceous. (From Day et al, 1981). Units are in kilometres. The high frequency nature of the image is due to the 4 km grid spacing of the data set.

The basement, here considered to be everything between the Base-Cretaceous and the Moho, is assumed to be laterally and vertically homogeneous with a density of 2.75 g cm^{-3}. This is consistent with granitic or anorthositic material.

Ringwood (1975) points out that possible upper mantle rocks can only have a limited composition the most likely being that of peridotite. This has a possible density range of between 2.78 and 3.37 g cm^{-3} (Telford et al 1976), however, the lower of these densities is probably associated with highly serpentinised Peridotite. In this case a value of 3.25 g cm^{-3}. was used (consistent with Donato and Tulley (1981)).

The density contrast shown in table 3.1 are the difference between the density of each layer and that of the basement. In the case of the water layer a density contrast of -0.08 g cm^{-3} was used. This is because the original BGS Bouguer gravity data already includes a correction for the water layer, effectively replacing it with material of density 2.67 g cm^{-3}. The difference between 2.67 and 2.75 g cm^{-3}. is -0.08 g cm^{-3}.

One of the problems associated with using densities derived from well data is that many of the wells used tend to sample rocks on the tips of fault blocks or at the edges of basins. Economic considerations mean that wells are rarely drilled below depths of a few kilometres. Since sediments will de-water and compact with depth their densities will increase correspondingly. It is likely, therefore, that densities derived from well data are not accurate for deep sequences towards the centre of the basin. Donato and Tulley (1981) do not provide information about the exact location of their wells, nor about sampling depths.

In an attempt to correct for this problem the 3D forward modelling routine allows for an increasing density with depth (3.4.1.3). A separate study was made using this technique rather than the fixed density method. The results of both methods are presented in 3.4.1.4.

3.4.1.3 Computing the Gravitational Effect.

The computer routine used to calculate the gravitational effect of the near-surface layers is an adaption of one originally developed by Plouff (1975). This routine allows the calculation of the vertical component of gravity anywhere inside, outside or on the surface of polygonal prisms. Each prism is defined by two parallel horizontal planes at the top and bottom linked by vertical sides. Any complex geological body can be defined by an assemblage of such prisms. In this case the two horizontal planes defining the top and bottom of the prisms are the digital grids representing the top and bottom of each near-surface layer. Each grid point is considered to be the centre of a prism whose length is equivalent to the grid spacing.

The formula for the gravity effect of a polygonal prism is based on the vertical integration of Talwani and Ewing's (1960) formula for the gravitational attraction of a horizontal polygonal lamina. The full derivation is given in Plouff (1975).

The program itself is designed to run on a VAX Station 3100. It has the ability of calculating the net gravitational effect of a body at any position offset from the location of that body. Thus, apart from the digital grids representing the upper and lower surfaces of each layer, the routine also requires as input the geographical position of each grid point and the required location of the output grid.

As mentioned in 3.4.1.1 the input depth grids have to cover a larger area than the study area itself. This is to avoid an edge effect affecting the calculated anomaly within the zone. In fact the depth grids cover an extra 48 km on all four sides of the study area (fig 3.10). To reduce computing time the grid spacing was increased from 2 km to 4 km. During a test procedure it was found that the increased grid spacing did not adversely affect the end result but reduced processing time dramatically.

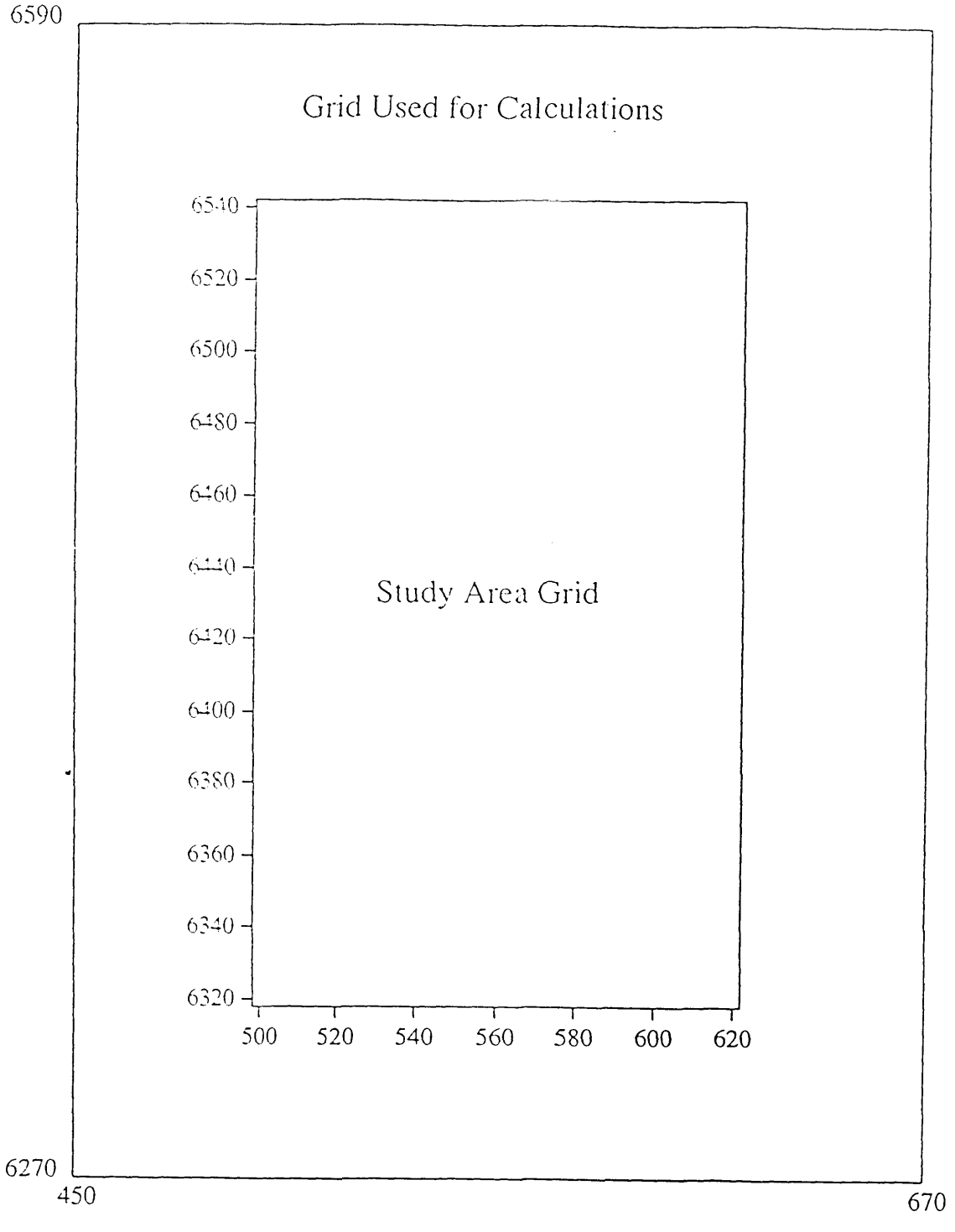


FIGURE 3.10 Grid dimensions. The outer block represents the full size of the grids used in the modelling. The inner block represents the study area. The difference in size avoids an undesirable edge-effect affecting data in the study area itself.

Before any real data was used the program was tested using simple shapes to represent the geological model. The results obtained where in very good agreement with those calculated by hand and those obtained using similar shapes calculated using previously tried and tested 2.5D modelling routines.

As mentioned in 3.4.1.2, the routine requires the input of a single density contrast for each layer. Alternatively it is able to calculate density contrasts on the basis of an increasing density with depth for a given rock type. Sclater and Christie (1980) noted that the density of a given sediment will increase with depth of burial due to de-watering and loss of porosity. They noted that the decay of porosity with depth of burial for certain generalised lithologies was an exponential function (see 6.3.4.1). Thus for simple lithologies such as sand, shale and chalk, theoretical compaction curves can be generated which predict the variation of density with increased depth of burial. In this case the calculation is made using compaction curves (pers. com. N. White) for the following dominant lithologies: sand, shale, chalk, basalt, salt, anhydrite, dolostone and limestone. Each sedimentary layer is divided into a pre-defined number of sub-layers with a calculation made for the centre point of each of these. In this study the post-Palaeocene layer was considered to dominated by a shale lithology, the Palaeocene to be dominantly sand and the Cretaceous layer to be principally chalk. The calculation was made for four sub-layers within each of these sequences. The results are discussed in the next section.

Perhaps the greatest source of error in this method is that such sweeping generalisation of rock-type, porosity, and permeability have to be made. The constant densities used by Donato and Tulley (1981) may be more inaccurate at large depths but they are at least derived from well data relating specifically to the rocks of each sequence.

3.4.1.4 Results Obtained Using the Plouff Routine

Figures 3.11 to 3.14 show the calculated gravitational effect for the water layer, the post-Palaeocene layer, the Palaeocene layer and the Cretaceous layer respectively. By far the greatest contribution to the total gravitational attraction of the near-surface layers comes from the post-Palaeocene layer. Values vary from −20 mGal in the north-west to −75 mGal in the south-east where the sediments are at their thickest.

The total effect of all four layers is shown in figure 3.15. Over the study area the anomalies vary between approximately −26 and −115 mGal. The largest anomaly is found in the south-east corner of the study area (i.e. towards the centre of the basin) however, a second large negative anomaly is centred over the East Forties Basin in the centre of the 'triple-junction' zone. Even though the post-Palaeocene layer contributes the most to the magnitude of the overall total, the smoothness of the field due to this layer means that the shape of the end result (figure 3.15) is largely governed by the field due to the Cretaceous layer (fig 3.14).

Figure 3.16 shows the difference between the original Bouguer anomaly data and the total effect of the near-surface layers. The low amplitude of the original data and the large negative contribution of the sediments means that this residual field is entirely positive. It follows the same trend as the three arms of the graben system. The largest anomalies of approximately 115 mGal occur at the centre of the 'triple-junction' and at the northern end of the Central Graben. Even before any modelling of the mass causing this residual field has taken place it is apparent that the distribution of this mass will follow more or less the same shape as the field.

In sections 3.4.1.2 and 3.4.1.3 it was mentioned that a complementary study was made using densities varying with depth for each of the sedimentary layers. Figure 3.17 shows the total effect of all the near-surface layers using this method

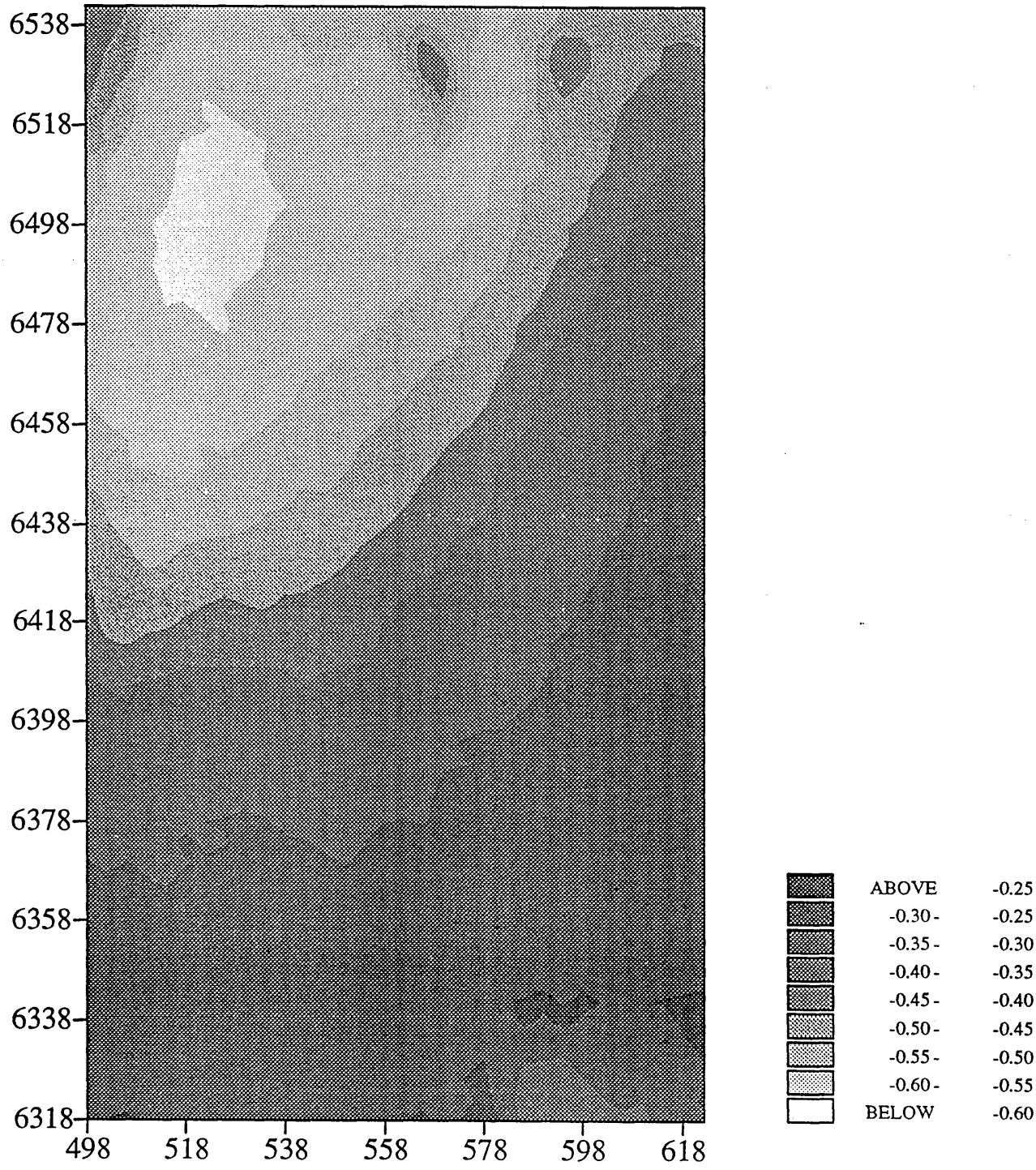


FIGURE 3.11 Calculated gravitational effect of the water layer (units in mGals).

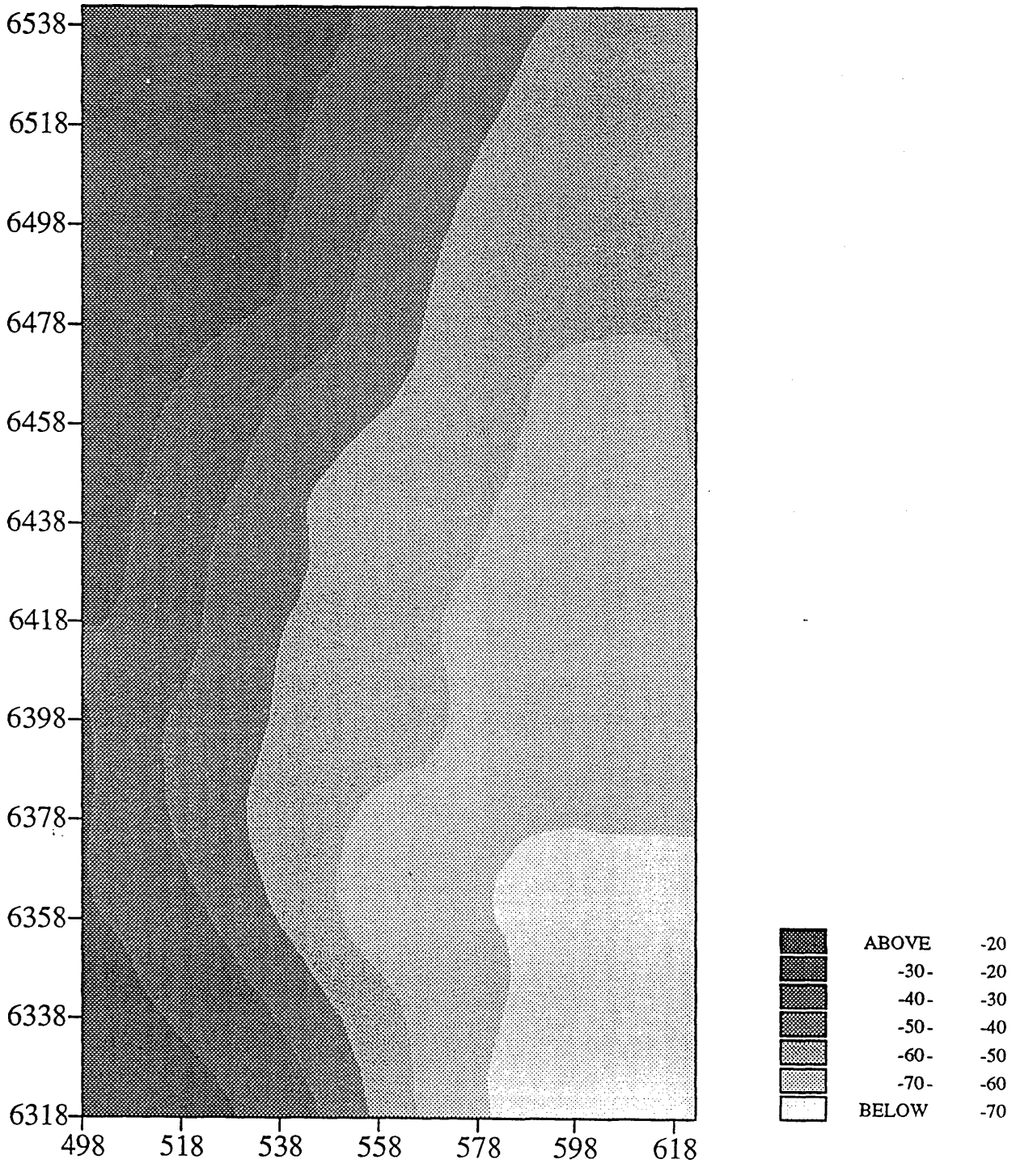


FIGURE 3.12 Calculated gravitational effect of the post-Palaeocene layer (units in mGals).

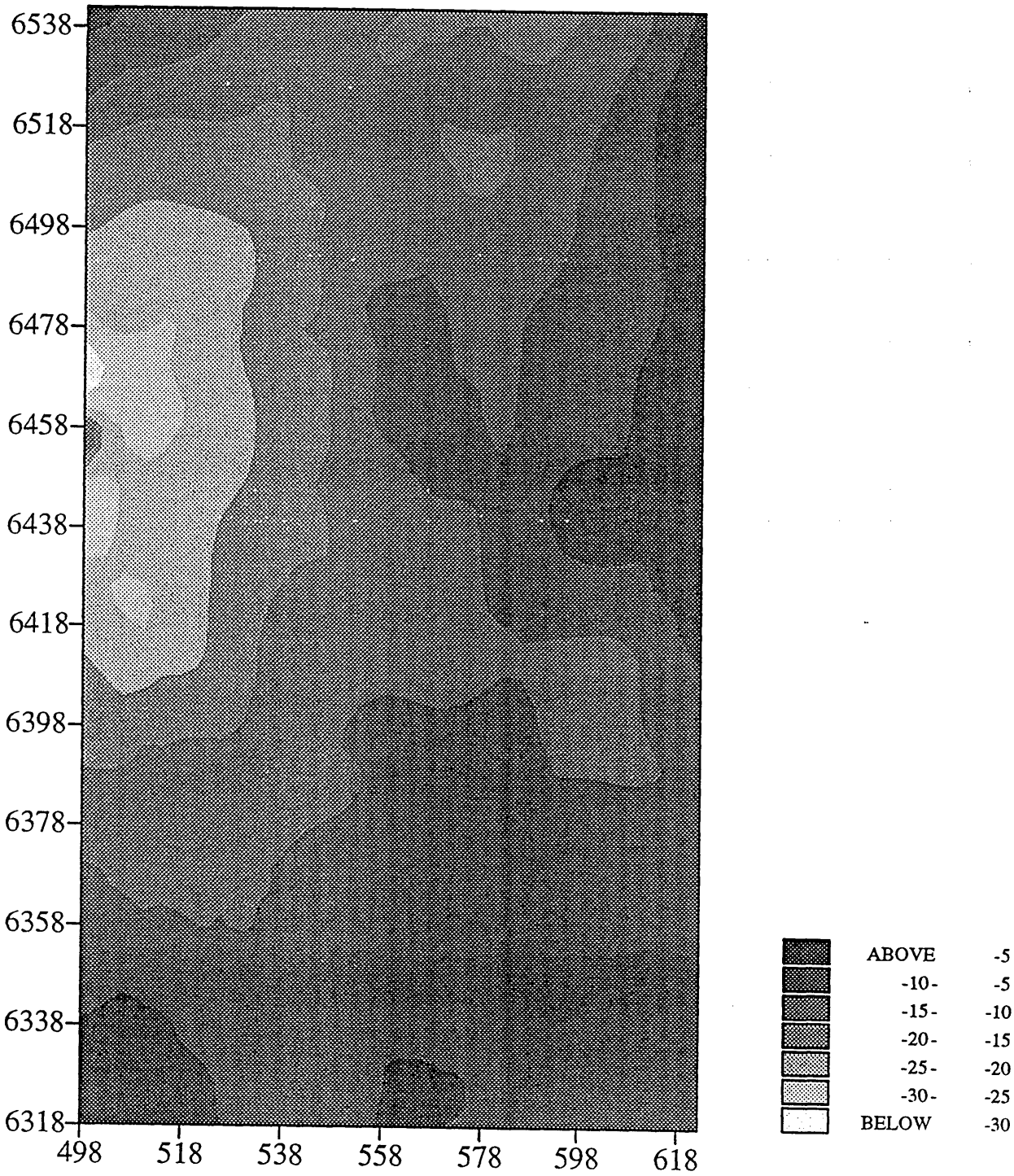


FIGURE 3.13 Calculated gravitational effect of the Palaeocene layer (units in mGals).

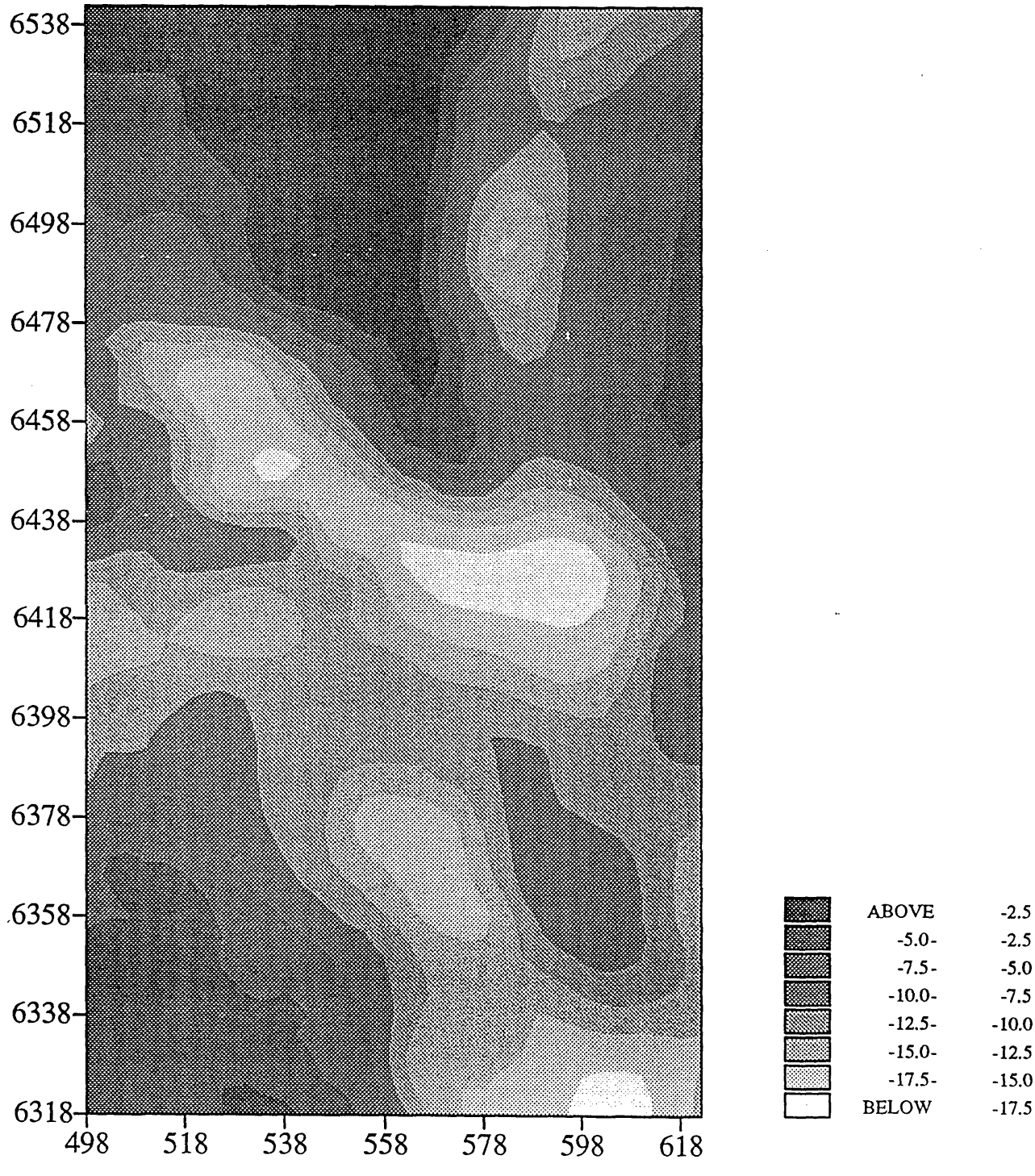


FIGURE 3.14 Calculated gravitational effect of the Cretaceous layer (units in mGals).

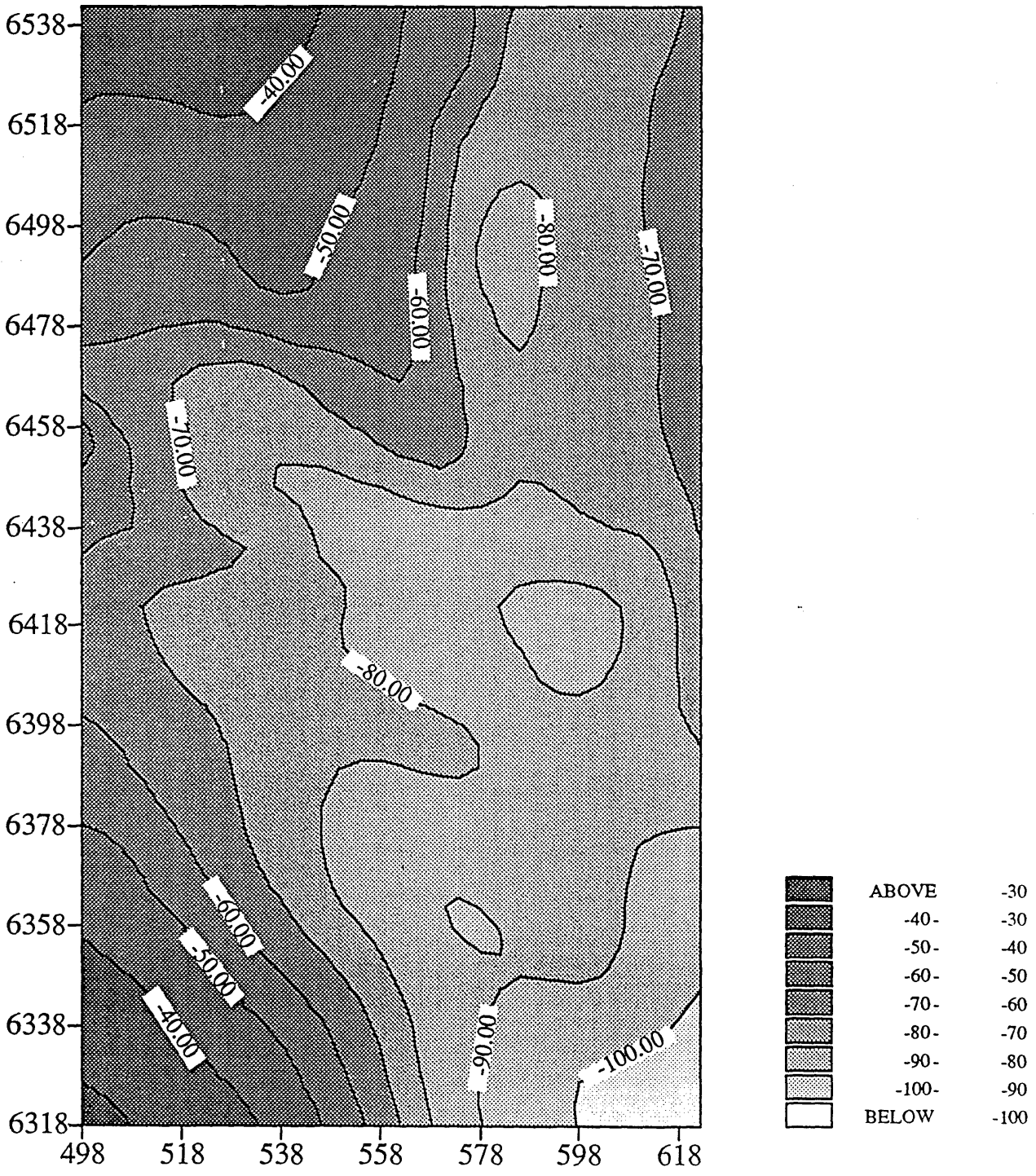


FIGURE 3.15 Total gravitational effect of the near-surface layers (units in mGals).

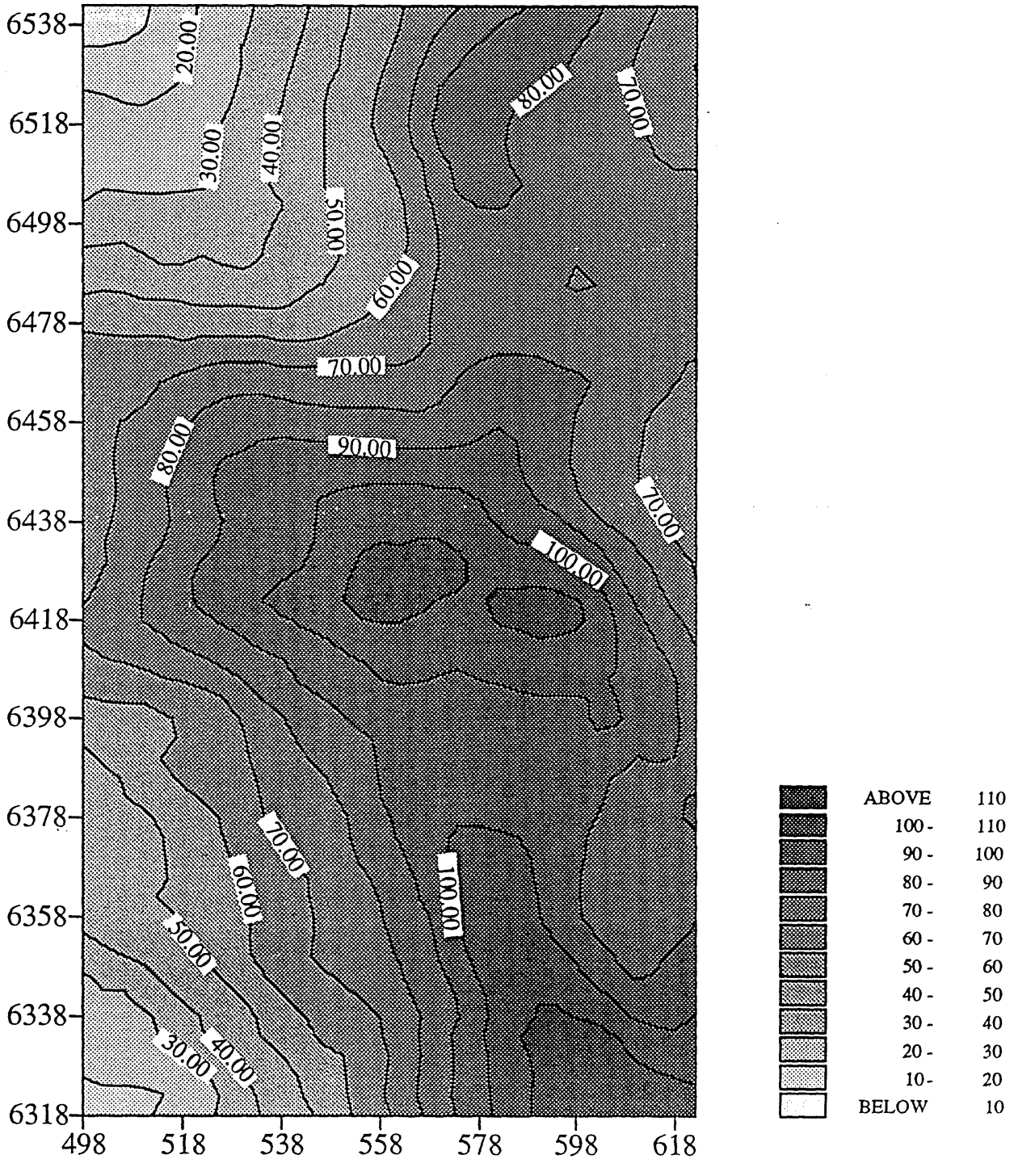


FIGURE 3.16 Residual gravity (in mGals), ie. the difference between the Bouguer anomaly and total gravitational effect of the near-surface layers.

and figure 3.18 shows the residual field when this is subtracted from the original Bouguer anomaly data. This residual field is approximately the same shape as in the previous case although the maximum values in the centre and south-east of the study area are somewhat smaller.

The large, positive anomalies in both residual fields tend to occur over the deepest parts of the basin, where the constant densities derived from well data used for each layer are most likely to be in error. Over the shallow parts where the residual fields are smooth and low in amplitude such densities are more likely to be correct. Figure 3.19 represents the difference between the residual field calculated using constant densities and the residual field calculated using variable densities with depth. At points where both residual fields reach a maximum the difference between the two is approximately 15 mGal. In the smooth low amplitude areas the difference is roughly -10 mGal.

The Base-Cretaceous is generally less than 3 km deep over the study area, therefore it is likely that the estimates of density made by Donato and Tulley (1981) will be more accurate than those derived using the compaction curves. It was therefore decided to continue the rest of this study using the field generated by the constant density method. Estimates of errors in the chosen densities are discussed in 3.5.4.

3.4.2 Analysis of the Residual Field

The wavelength of a gravity anomaly associated with a point source increases as the depth to that source increases (Spector and Grant, 1970 and Telford et al, 1976). High frequency variations in the field are therefore associated with relatively shallow density contrasts. The purpose of this research is to model large-scale variations in a deep structural feature. Low-pass filtering provides a means of removing the unnecessary high-frequency component of the residual gravity data which would be associated with near-surface sources.

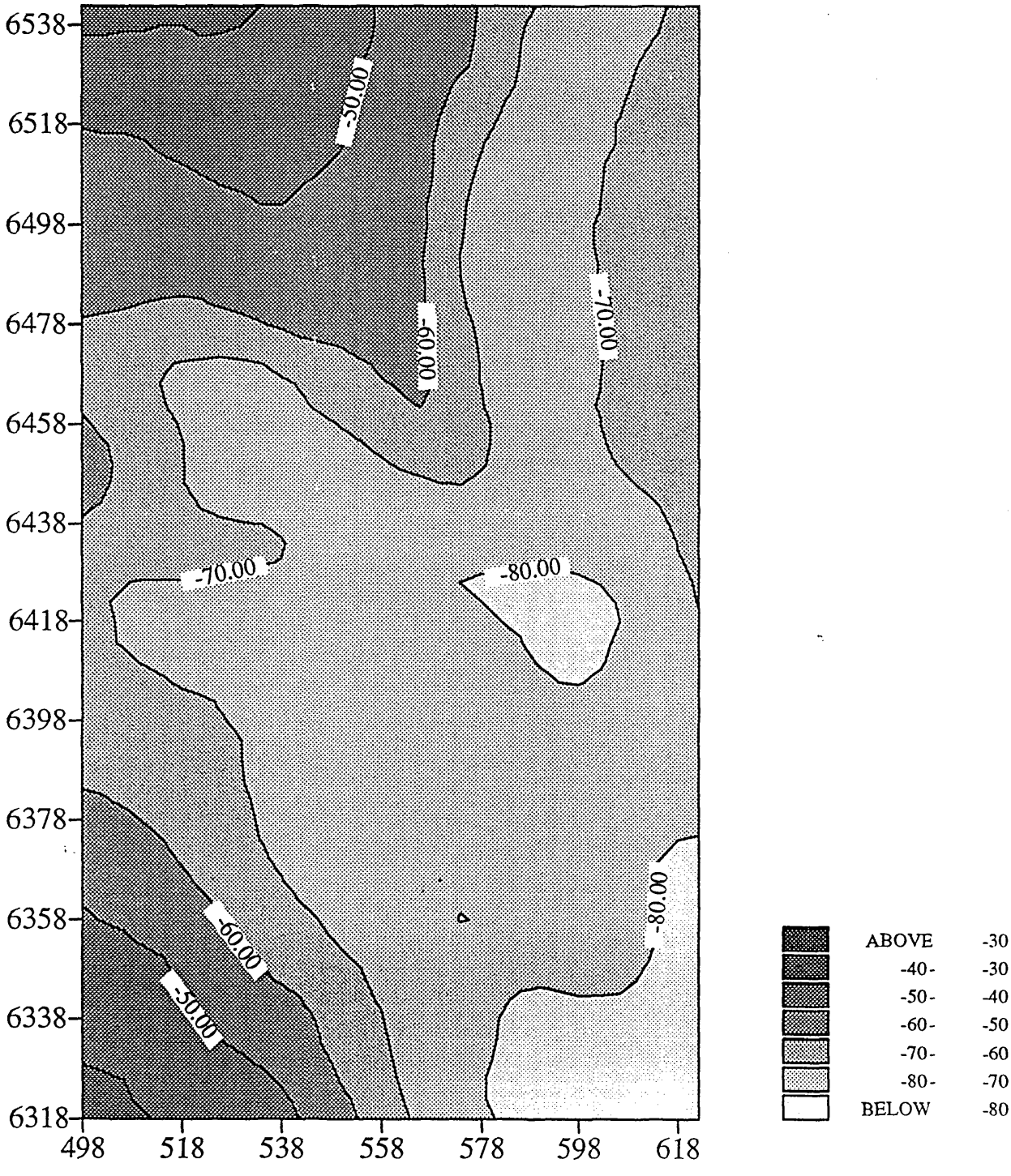


FIGURE 3.17 Total gravitational effect of the near-surface layers (units in mGals). Density contrasts have been calculated using compaction curves.

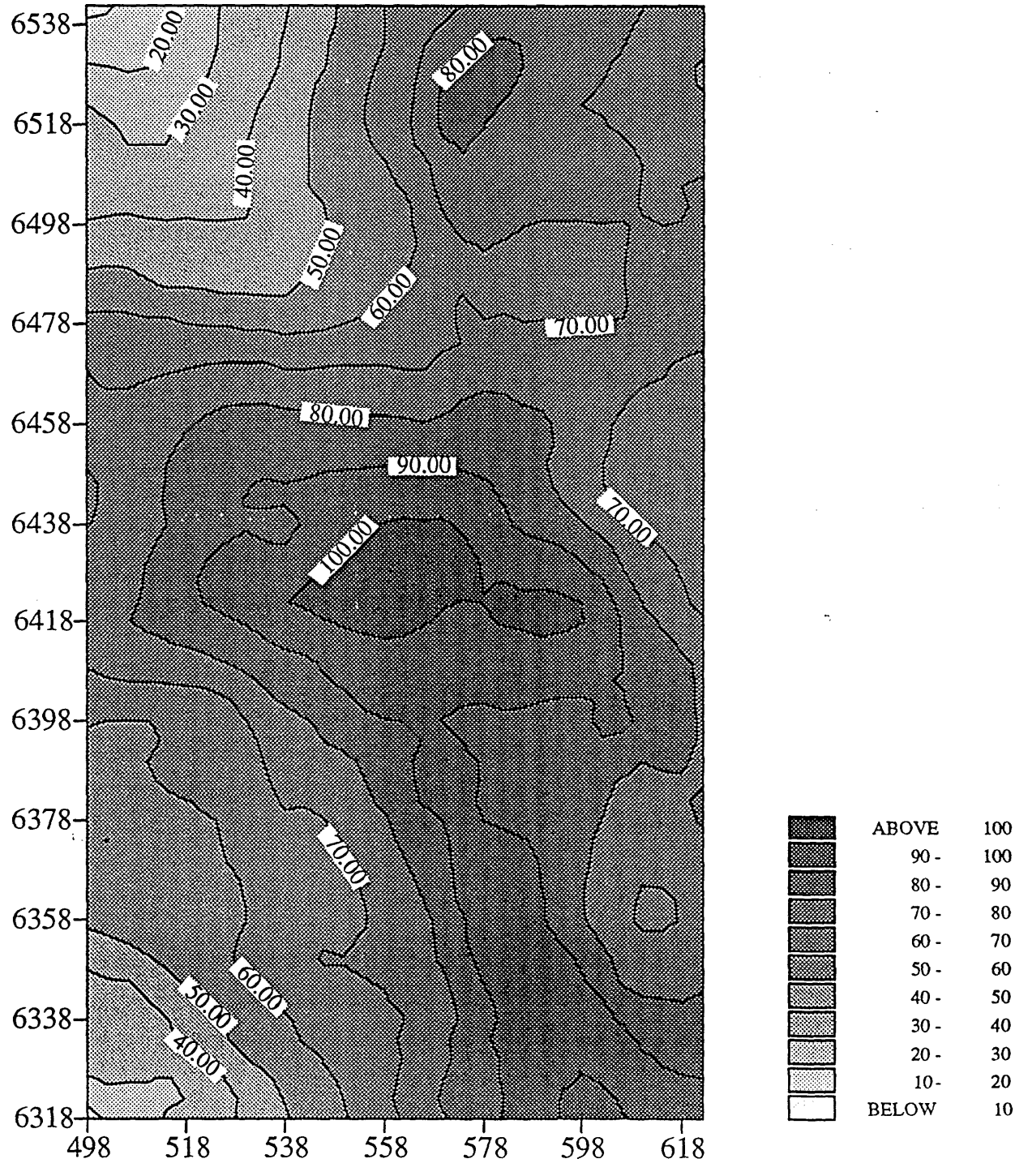


FIGURE 3.18 Residual gravity (in mGals). Density contrasts for the near-surface layers have been calculated using compaction curves.

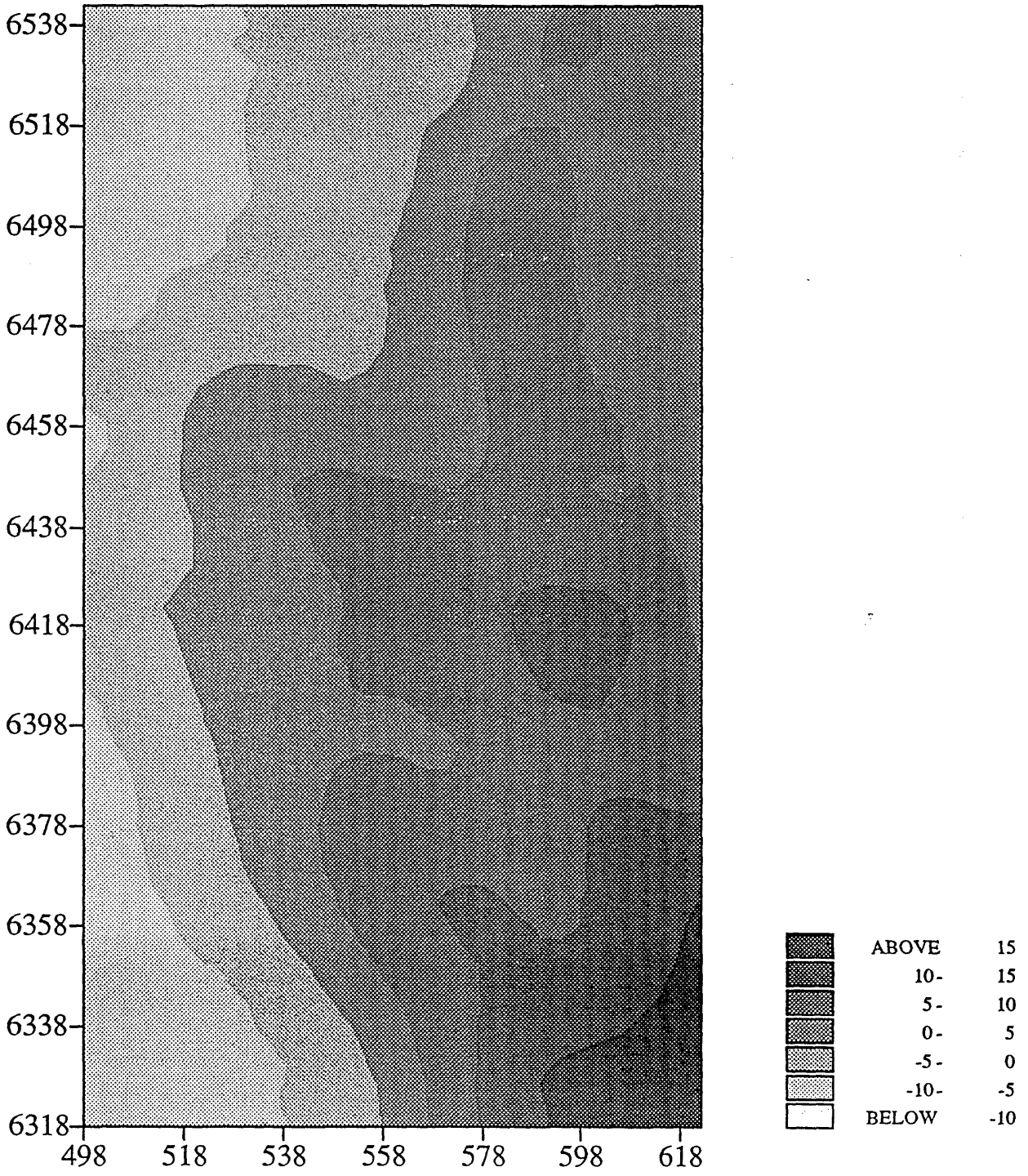


FIGURE 3.19 The difference (in mGals) between residual gravity where density contrasts are estimated from well data and residual gravity where density contrasts are calculated using compaction curves.

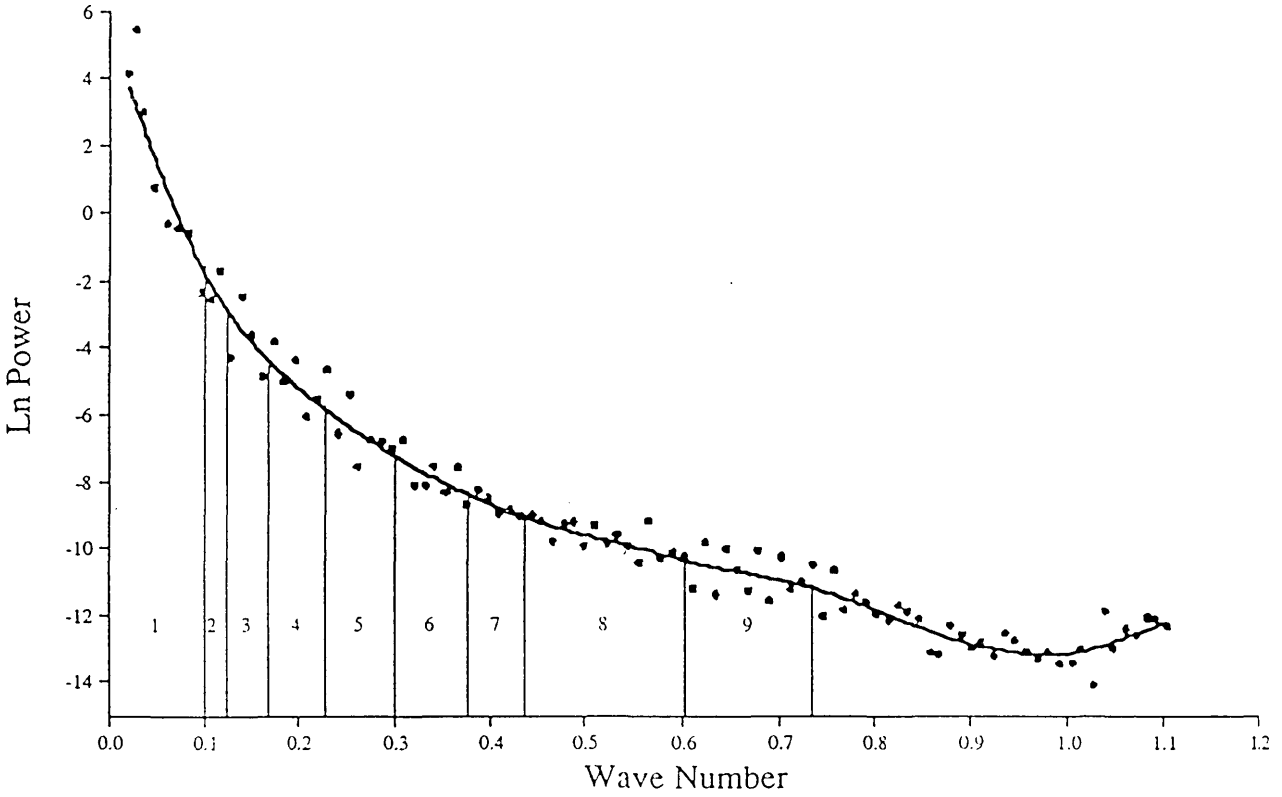
3.4.2.1 Spectral Analysis

Great care has to taken when designing the low-pass filter. If the cut-off frequency chosen is too low then useful data could be lost; too high and the output data will have an unnecessarily large high frequency component. As outlined in 3.4.3 the latter case causes an adverse effect on the final model resulting in a geologically unrealistic solution and severly degrading the quality of fit between the 'observed' and calculated fields for the model.

The azimuthally-averaged power spectrum of a potential field data set provides a basis for a method of designing wave number filters to separate anomalies due different groups of sources (Spector and Grant 1970). This technique was applied to the residual gravity data set.

The power spectrum derived from a three dimensional data set such as a grid of gravity data also has a three dimensional form. However, using a computer routine adapted from one kindly supplied by Dr. R. Hipkin (Edinburgh University) the azimuthal average of the three dimensional spectrum is taken to produce a simplified two dimensional output as shown in figure 3.20.

The natural logarithm of the power spectrum can be divided into several straight-line segments. The gradient of each segment is related to the depth of sources producing gravity anomalies which are within the range of spatial frequencies defined by that segment.



Segment	Wave No. Range	Av Depth(km)	Max.Wavelength (km)
1	0.000-0.100	32.0	62.8
2	0.001-0.124	27.7	50.6
3	0.124-0.168	18.3	37.5
4	0.168-0.228	11.6	27.5
5	0.228-0.300	10.2	20.8
6	0.300-0.377	7.2	16.7
7	0.377-0.436	6.0	14.4
8	0.436-0.603	3.9	10.5
9	0.603-0.734	3.1	8.6

FIGURE 3.20 Power spectrum calculated for residual gravity data. The table shows the average depth to source ensembles causing anomalies whose frequencies are defined by the wavenumbers bounding each straight-line section of the power spectrum (after Spector and Grant, 1970).

Average depth estimates for source ensembles are calculated using the relationship:

$$z = 0.5 \frac{\partial p}{\partial k}$$

Where:

z = Average depth to the source ensemble (in km)

p = Natural logarithm of the power

k = wavenumber = 2 pi/wavelength in km

The cut-off of spatial frequency (wave number) for filtering operations is marked by the wavenumber at the end of each segment.

It is immediately apparent from the power spectrum that most of the energy in the residual field is due to deep sources. This is perhaps not surprising since the field due to near-surface layers down to the Base-Cretaceous should have already been removed (3.4.1). Preliminary test models calculated using unfiltered residual data show that the Moho rarely rises to depths of much less than 12 km and the deepest sediments do not occur at depths of greater than 10 km. Using this as a guide a low-pass filter in the wave number domain was designed. The filter shape is a rectangular box-car modified by a cosine taper. The start and end of the taper is defined by cut-off wavelengths of 37.5 and 27.5 km. This effectively cuts off all data whose average depth to source is less than approximately 11 km (see table below figure 3.20).

3.4.2.2 Filtered Data

Low-pass filtering was carried out on the residual gravity data set using the program supplied by Dr. R. Hipkin (Grant Institute, Edinburgh). The result is shown in figure 3.21. A comparison of this with the unfiltered field (fig 3.16)

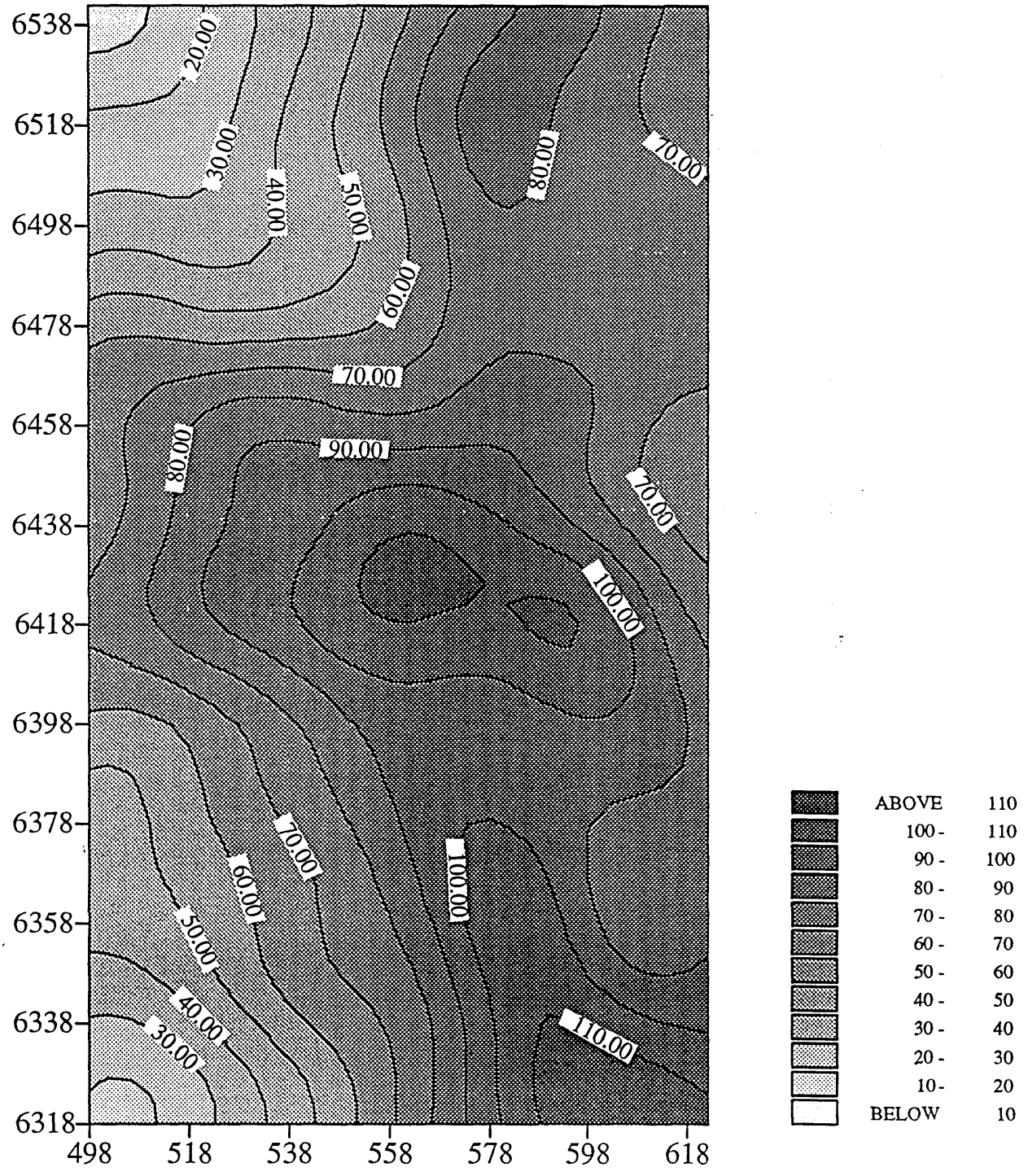


FIGURE 3.21 Residual gravity after low-pass filtering. The filter is a rectangular box-car modified by a cosine taper. The start and end of the taper are defined by wavelengths of 34.5 and 25 km. This should eliminate most of the field caused by sources shallower than approximately 11 km.

shows that they both have the same general shape and magnitude but, as expected, the filtered data is considerably smoother.

3.4.3 Automatic Iterative Forward Modelling.

Once the effects of all relatively shallow sources have been removed, modelling the 'Moho topography' can go ahead. The three dimensional modelling routine 'IT3DGRAV' was adapted from one kindly supplied and originally developed by Dr. M. Lee (BGS, Keyworth). It runs on a VAX Station 3100 and uses the following iterative technique.

A body of anomalously high density (a density contrast of 0.5 g cm^{-3} across the Moho is used) is defined by vertical prisms of square cross-section, one centred on each of the grid points in the filtered residual gravity data. The top of this body is a variable surface which is automatically adjusted by the program. The gravity anomaly of the entire model is calculated for each grid point by summing the gravitational effect of each prism. The thickness of each prism is then adjusted by the following formula:

$$T_n = T_{n-1} * \frac{(g_0 - g_c)}{2\Pi G \Delta \rho}$$

Where:

T_n = Thickness after n iterations

T_{n-1} = Thickness after n-1 iterations

g_0 = 'observed' residual gravity

g_c = calculated gravity

G = gravitational constant

$\Delta\rho$ = density contrast at the Moho

The gravity effect of the new model is then calculated and the calculation procedure continues for a preset number of iterations.

The routine is allowed to alter the data freely in this way but constrained so that the solution after each successive iteration lies between two depth limits. The minimum depth limit was defined as being 12 km. Such a value was chosen because the filtering technique (3.4.2) should have removed anomalies caused by sources at depths shallower than this. The maximum depth limit should correspond approximately with the thickness of unstretched crust, i.e. where the Moho is not anomalously shallow. Evidence from a deep seismic refraction line across the Witch Ground Graben (Christie and Sclater 1980) shows this depth to be approximately 35 km under the East Shetland Platform. Other authors such as Barton and Wood (1984) claim this depth to be approximately 31 km. In this experiment a maximum depth limit of 35 km was chosen although the results show (3.5) that the modelled Moho topography never quite reaches this depth. The ambiguous nature of potential field modelling means that there are an infinite number of possible solutions to the problem. The assumption of a maximum depth therefore, provides an important constraint on the model. If the assumption is not made, the solution will have a large associated absolute error in the Moho depth. Such an error could not be quantified with any degree of accuracy.

After the routine has completed its preset number of iterations the end result is a simple grid of data points representing one possible solution for depths to the Moho. A second grid is also produced representing the difference in mGals between the observed residual gravity and the calculated gravity for the final model.

3.5 RESULTS

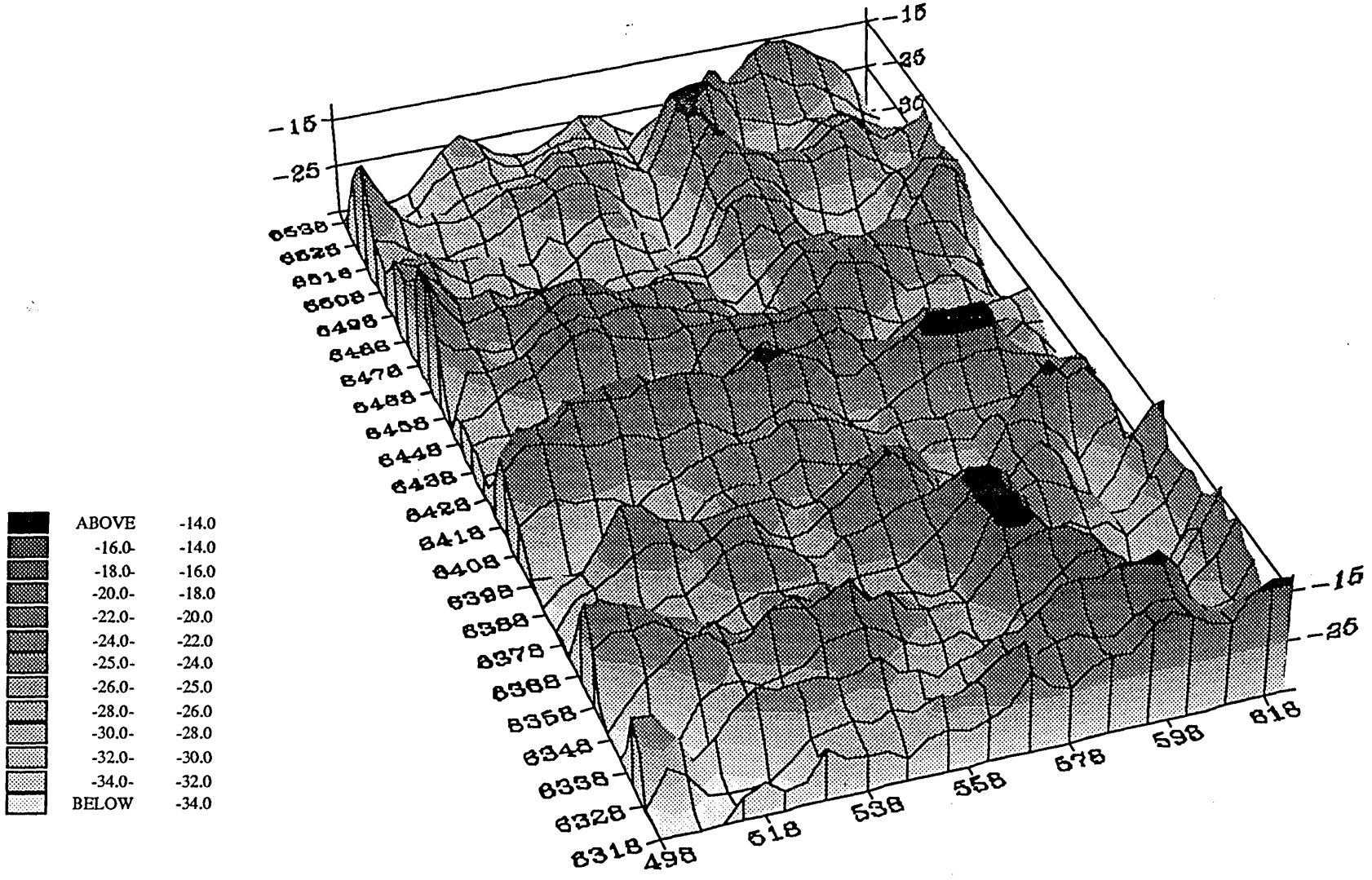
3.5.1 Results Obtained Using Unfiltered Residual Gravity

Figure 3.22 is an isometric projection of the solution obtained using unfiltered residual gravity after 50 iterations. The same solution is also shown as a grey-scale contour map in figure 3.23.

The high frequency nature of the unfiltered data is transmitted to the solution producing what appears to be a geologically unrealistic result. However, if the small wavelength features are ignored, a general shape for the Moho topography can still be picked out. This shape is much easier to see when the filtered residual gravity data is used (see 3.5.1.2 and 3.5.1.3). Depths to the Moho vary from slightly greater than 34 km to less than 12 km. The shallowest points occur in the centre of the area, in the Central Graben and South Viking Graben and over the East Forties Basin. The modelling routine has a limiting depth of 12 km thus Figure 3.22 shows the solution being 'planed-off' at this depth over the East Forties Basin and Central Graben.

Figure 3.24 shows the difference between the unfiltered residual gravity and that calculated for this solution. Again the high frequency nature of the result makes it difficult to decipher but errors range between roughly +/− 7 mGal. The largest errors tending to concentrate on areas where the Moho is relatively deep.

FIGURE 3.22 Isometric projection of the solution obtained after 50 iterations using unfiltered residual gravity. The surface represents depths to the Moho (in kilometres) for the study area.


ABOVE -14.0
-16.0- -14.0
-18.0- -16.0
-20.0- -18.0
-22.0- -20.0
-24.0- -22.0
-25.0- -24.0
-26.0- -25.0
-28.0- -26.0
-30.0- -28.0
-32.0- -30.0
-34.0- -32.0
BELOW -34.0
-15
-25
-15
-25
-30
6538
6528
6518
6508
6498
6488
6478
6468
6458
6448
6438
6428
6418
6408
6398
6388
6378
6368
6358
6348
6338
6328
6318
498
518
538
558
578
598
618
-15
-25

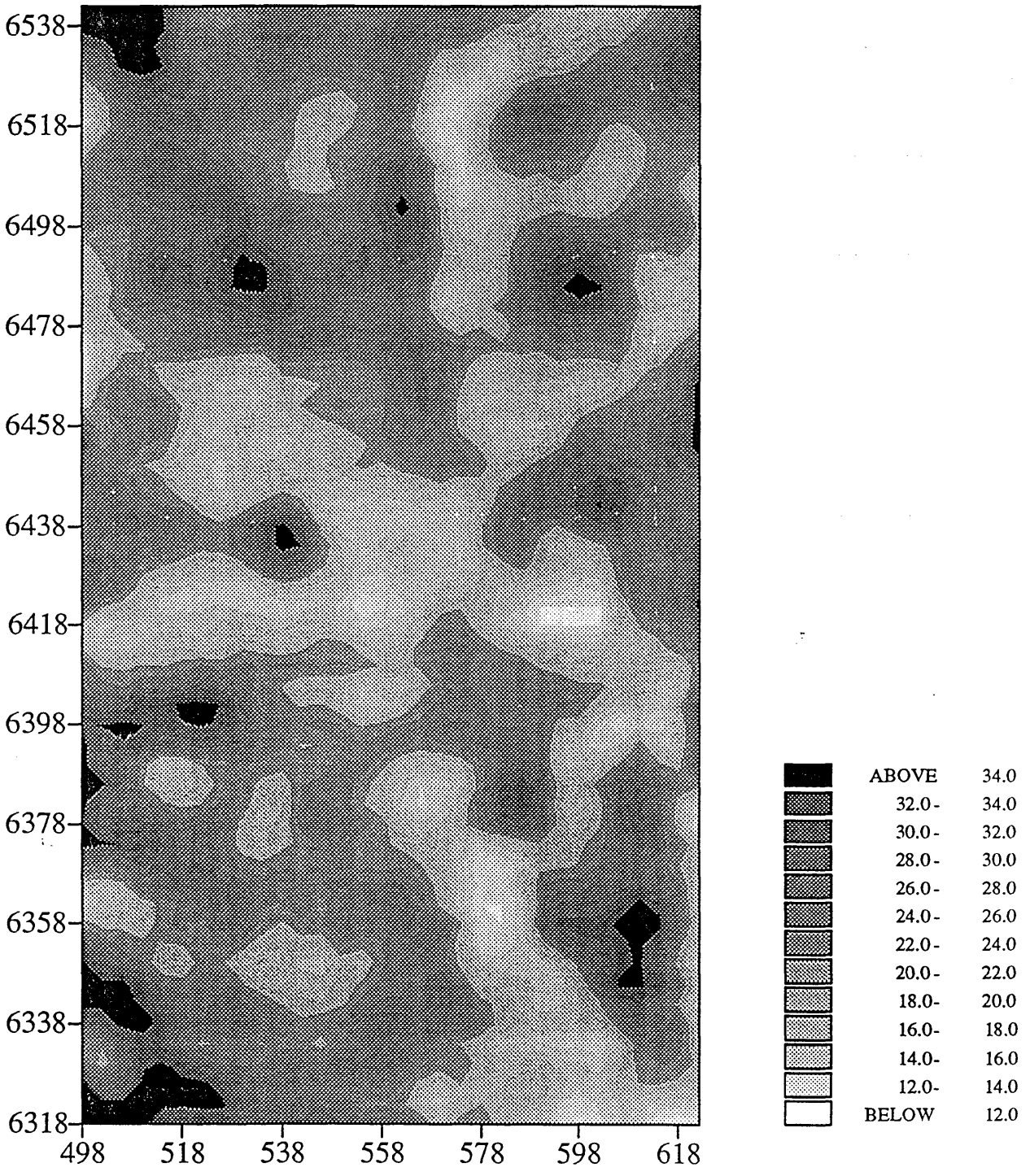


FIGURE 3.23 Grey-scale contour map of the solution obtained after 50 iterations using unfiltered residual gravity. Depths are in units of kilometres.

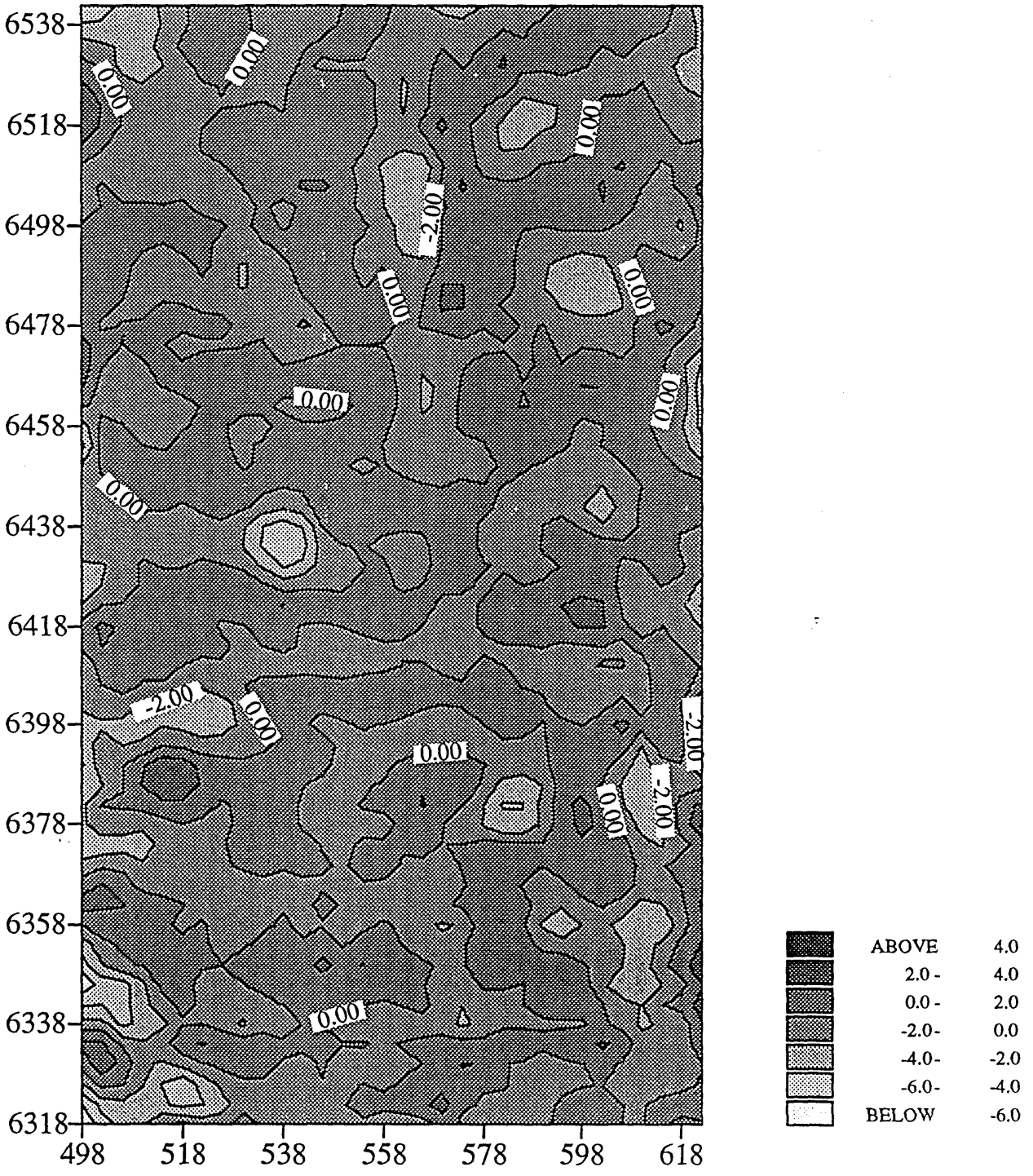


FIGURE 3.24 Grey-scale contour map representing 'goodness of fit' (i.e. the difference between the residual gravity and that calculated for this solution) for the solution obtained after 50 iterations using unfiltered residual gravity. Contours are in units of 2 mGal.

3.5.2 Results Obtained Using Filtered Residual Gravity After 50 iterations

Figure 3.25 is an isometric projection of this solution, the same result is also shown as a grey-scale contour plot in figure 3.26.

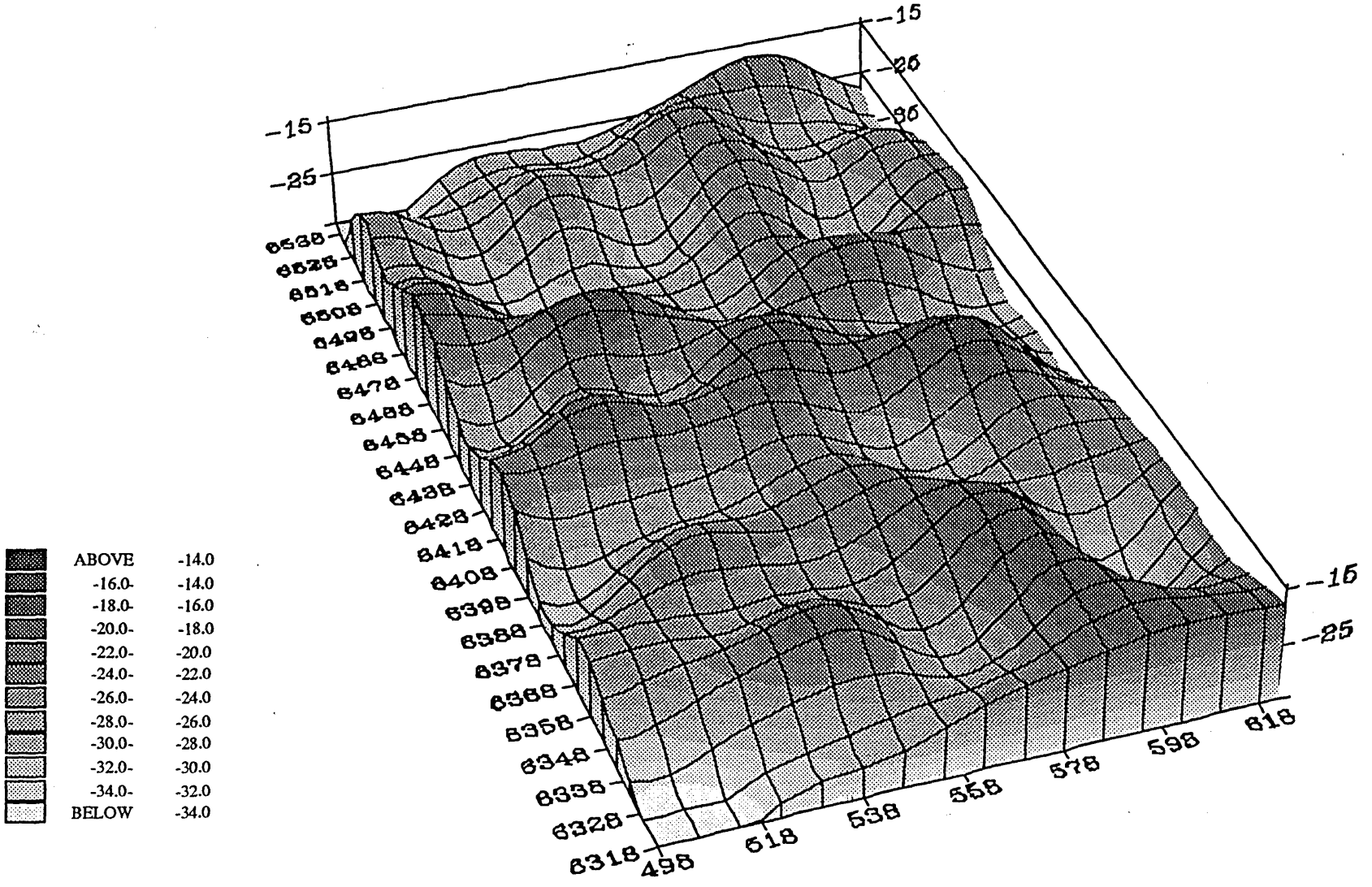
The general shape of the Moho topography in this solution follows the gross geological structure of the area. Three zones of anomalously shallow Moho can be identified: one trending NNW-SSE in the south-east of the study area, another trending WNW-ESE across the centre of the area and a third trending approximately N-S in the north. Depths to the Moho vary between approximately 34 km and approximately 15 km.

In the north of the study area the Moho topography forms a ridge-like structure trending N-S along the line of the South Viking Graben. The shallowest point on this ridge (approximately 18 km) occurs on the western side of the graben with a secondary 'high' at the extreme southern end. Off-axis to the west of the Viking Graben in the area of the East Shetland Platform the Moho is relatively deep (maximum depth of 34 km) and the general structure is smooth. The western boundary fault of the Viking Graben is also marked by a steep gradient in the Moho topography.

The centre of the study area is dominated by a broad WNW-ESE trending ridge in the Moho topography. Four centres of anomalously shallow Moho can be identified: one at the very centre of the study area where the Moho reaches depths of approximately 17.5 km, one at the centre of each of the Witch Ground and Buchan Grabens and a fourth centred on the East Forties Basin in the east. In the last case the Moho is as shallow as 15.0 km. The two shallow zones centred in the Buchan and Witch Ground Grabens are separated by a synformal feature where the Moho is comparatively deep.

In the south the dominant feature is a NNW-SSE trending ridge parallel to and centred on the Central Graben. In the centre of this ridge the Moho is very

FIGURE 3.25 Isometric projection of the solution obtained after 50 iterations using filtered residual gravity. The surface represents depths to the Moho (in kilometres) for the study area.


ABOVE -14.0
-16.0- -14.0
-18.0- -16.0
-20.0- -18.0
-22.0- -20.0
-24.0- -22.0
-26.0- -24.0
-28.0- -26.0
-30.0- -28.0
-32.0- -30.0
-34.0- -32.0
BELOW -34.0
-15
-25
-15
-25
6538
6528
6518
6508
6498
6488
6478
6468
6458
6448
6438
6428
6418
6408
6398
6388
6378
6368
6358
6348
6338
6328
6318
498
518
538
558
578
598
618

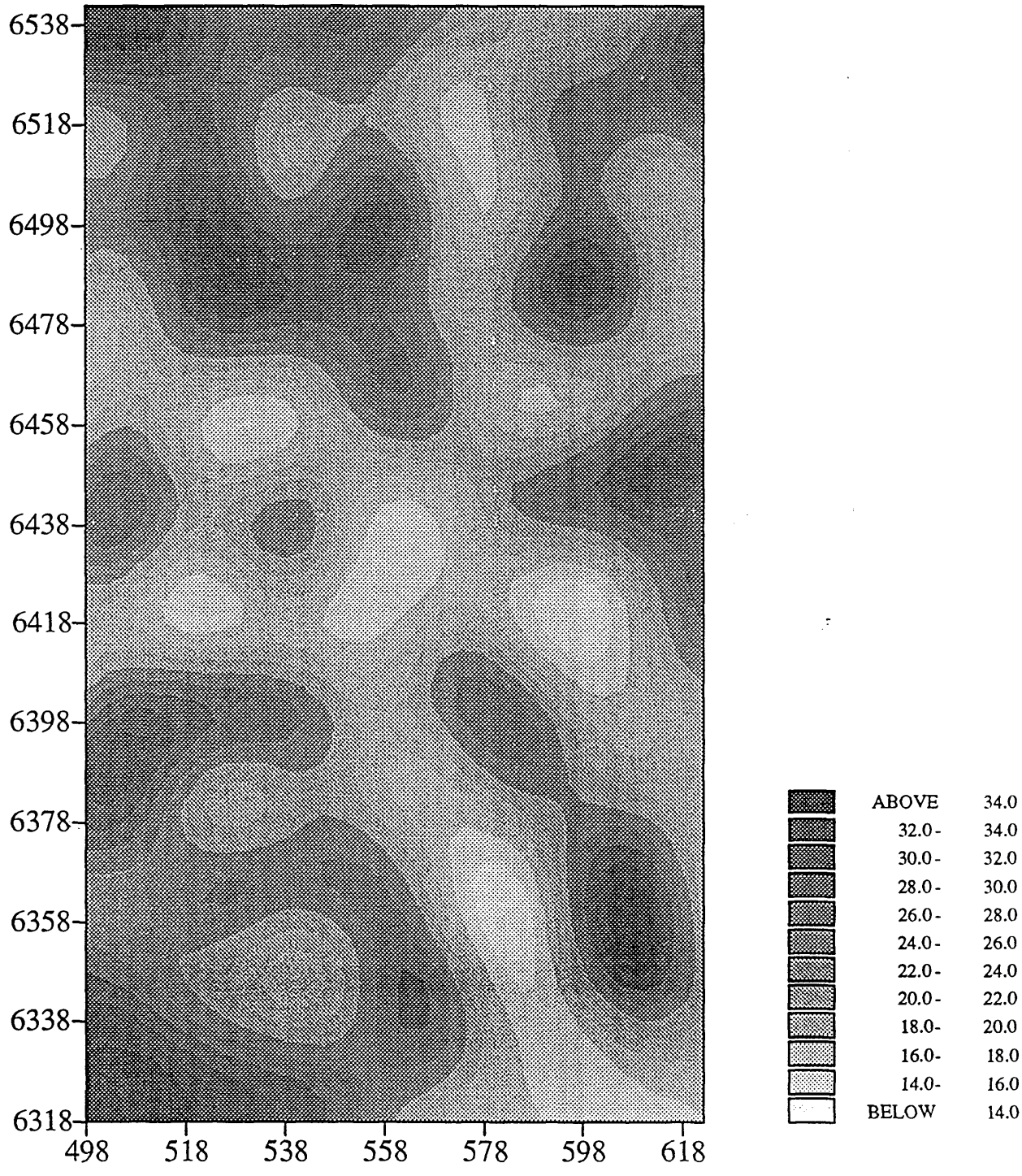


FIGURE 3.26 Grey-scale contour map of the solution obtained after 50 iterations using filtered residual gravity. Depths are in units of kilometres.

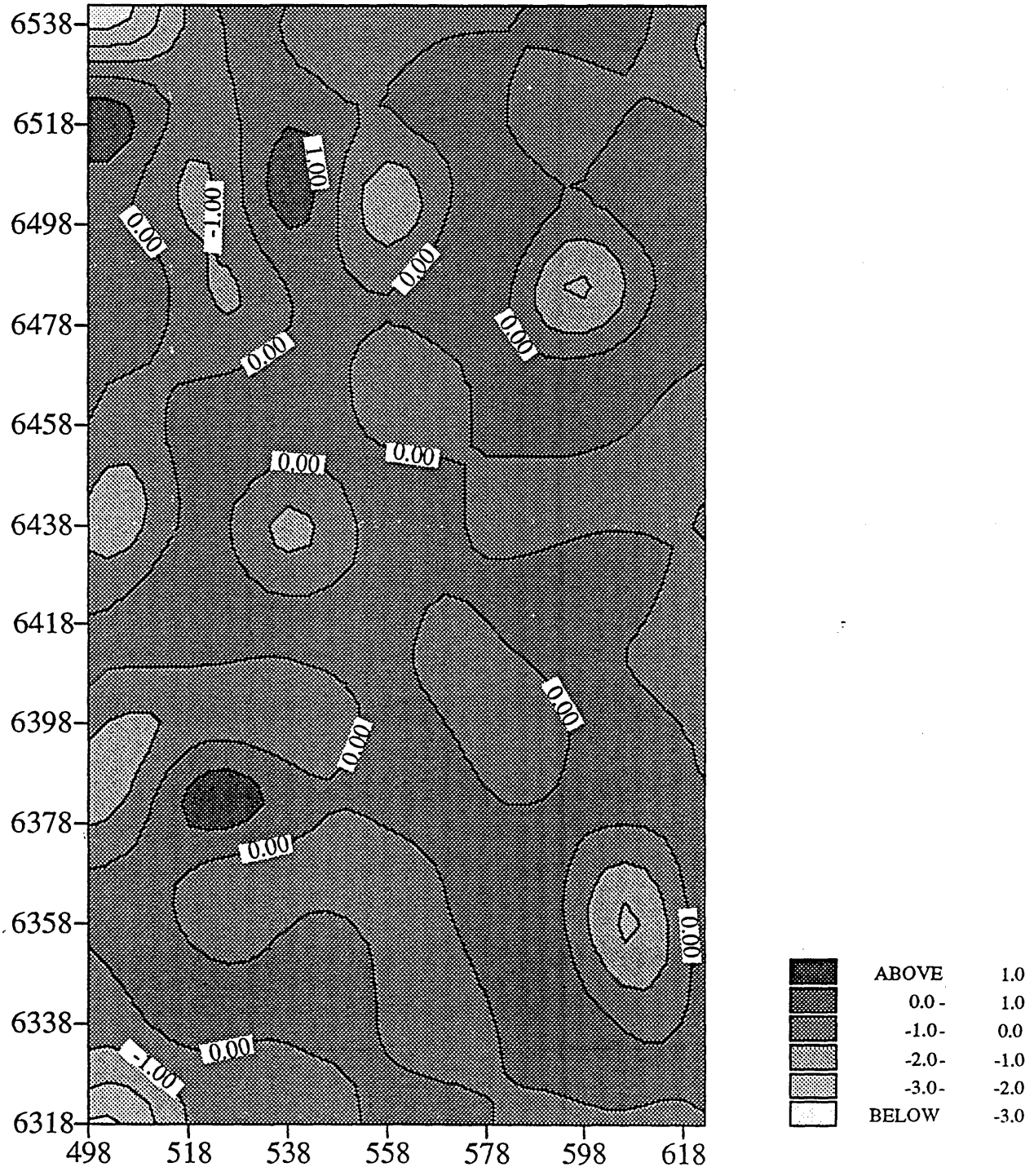


FIGURE 3.27 Grey-scale contour map representing 'goodness of fit' (ie. the difference between the residual gravity and that calculated for this solution) for the solution obtained after 50 iterations using filtered residual gravity. Contours are in units of 1 mGal.

shallow at approximately 15.5 to 16 km. Very steep gradients in the Moho topography separate this structure from two areas where the Moho is comparatively deep. To the east (and still within the Central Graben area) a valley in the Moho topography trends sub-parallel to the ridge. Here the Moho reaches depths of approximately 32 km. Off-axis to the west the general structure is smoother with the Moho increasing in depth up to 34 km in the extreme south-west of the study area. An isolated 'high' occurs just to the west of the Central Graben's western boundary fault where the Moho is at depths of roughly 20 km.

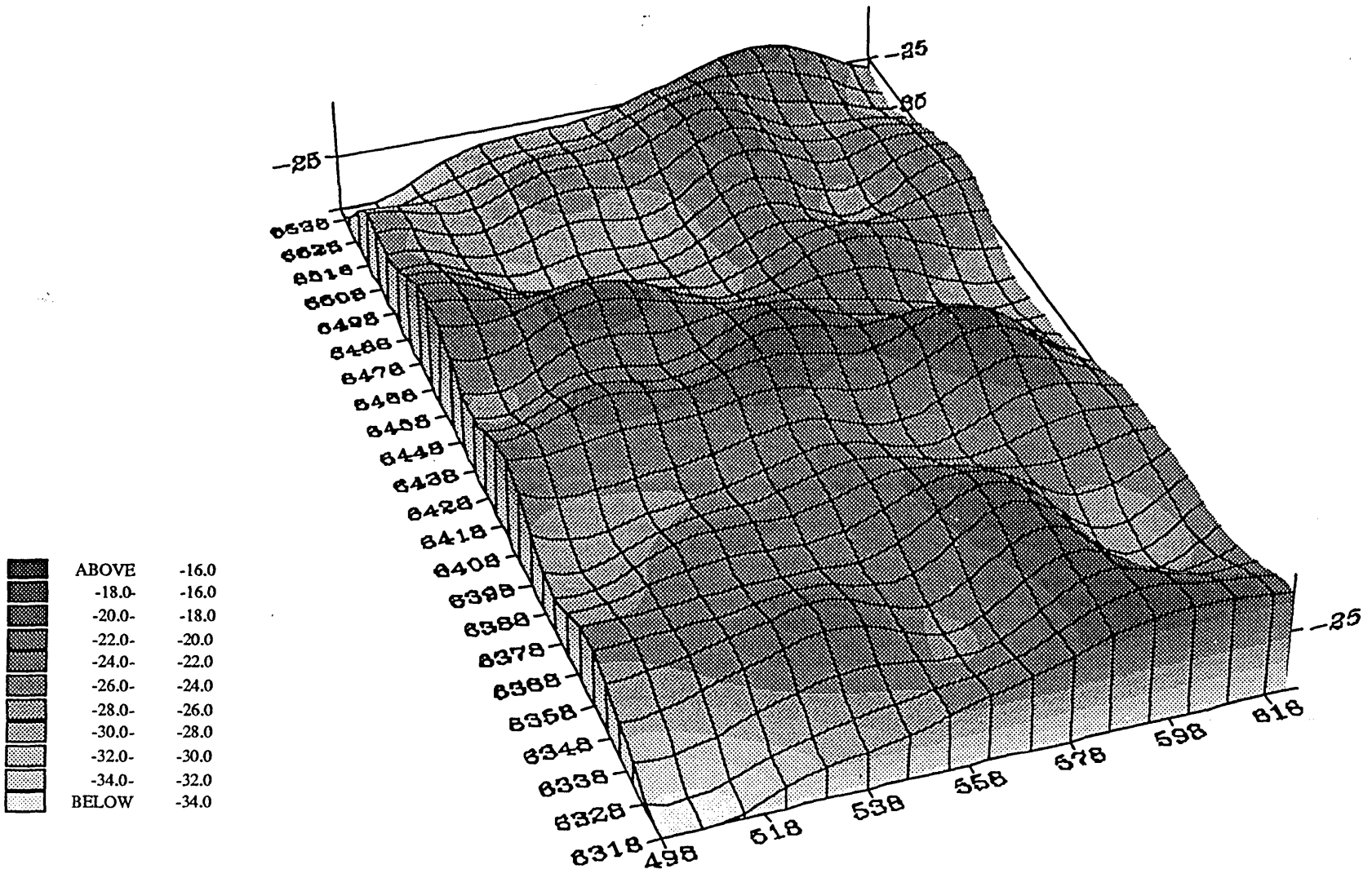
Figure 3.27 is a contour map showing the difference in mGals between the filtered residual gravity (figure 3.21) and the calculated anomaly that would be caused by the upper-mantle body modelled here. The fit is very good and varies between −3.5 and 1.5 mGal. In fact over most of the area the fit is within +/− 1.0 mGal. Deviations from this only occur locally and then generally in places where the Moho is at its deepest.

3.5.3 Results Obtained Using Filtered Residual Gravity After 20 iterations

No significant improvement in the fit of the model occurred beyond 50 iterations. However, it was noticed that with each successive iteration the model became less smooth, the steep gradients in the topography between features such as the ridge and valley in the south-east of the study area becoming more and more prominent. Using 20 iterations rather than 50 an alternative smoother model can be obtained where the 'goodness of fit' is not significantly reduced.

Figures 3.28 and 3.29 are respectively, the isometric plot and grey-scale contour plot for this solution. The general shape is the same as that obtained using 50 iterations although the structure is somewhat smoother. The Moho is at its shallowest in the East Forties Basin where it reaches depths of roughly 16 km slightly deeper than the solution obtained using 50 iterations.

FIGURE 3.28 Isometric projection of the solution obtained after 20 iterations using filtered residual gravity. The surface represents depths to the Moho (in kilometres) for the study area.


ABOVE -16.0
-18.0- -16.0
-20.0- -18.0
-22.0- -20.0
-24.0- -22.0
-26.0- -24.0
-28.0- -26.0
-30.0- -28.0
-32.0- -30.0
-34.0- -32.0
BELOW -34.0
-25
-25
-25
6538
6528
6518
6508
6498
6488
6478
6468
6458
6448
6438
6428
6418
6408
6398
6388
6378
6368
6358
6348
6338
6328
6318
498
518
538
558
578
598
618

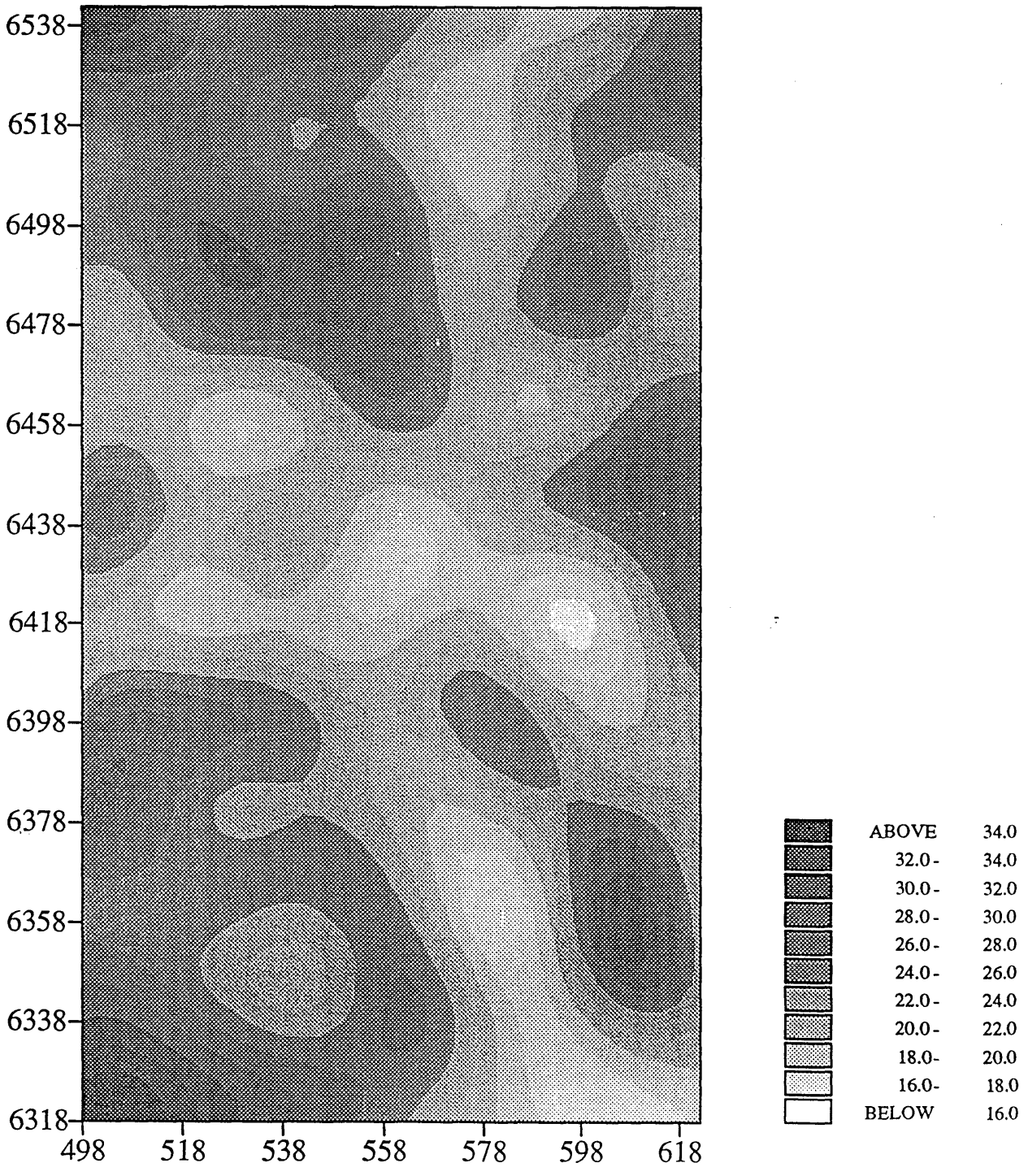


FIGURE 3.29 Grey-scale contour map of the solution obtained after 20 iterations using filtered residual gravity. Depths are in units of kilometres.

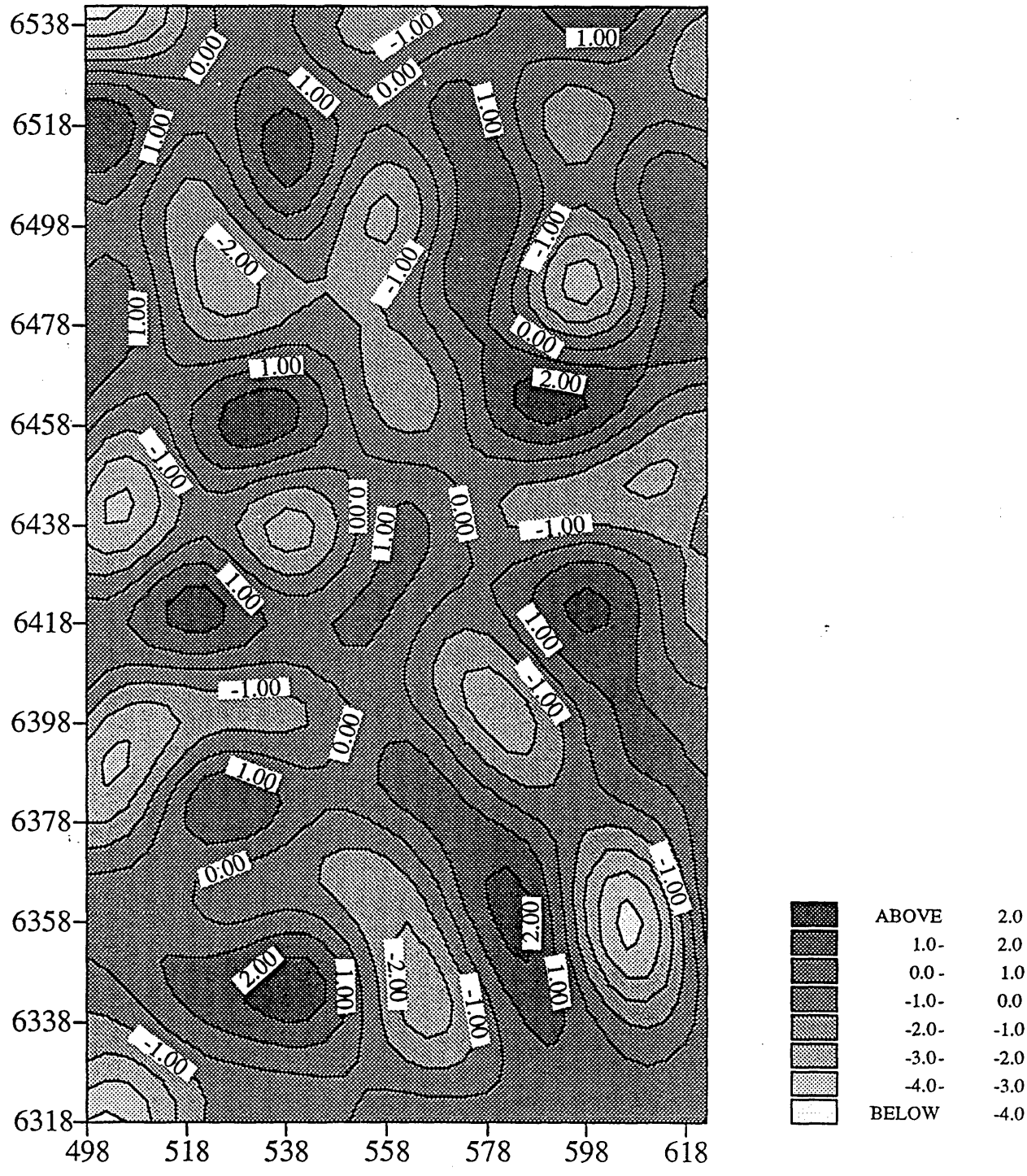


FIGURE 3.30 Grey-scale contour map representing 'goodness of fit' (i.e. the difference between the residual gravity and that calculated for this solution) for the solution obtained after 20 iterations using filtered residual gravity. Contours are in units of 1 mGal.

Figure 3.30 shows the 'goodness of fit' for this solution. The errors are slightly larger than those obtained for the 50 iteration solution but generally they lie between +/− 2 mGal. Again the largest errors (approximately −4 mGal) tend to be associated with areas where the Moho is deepest and those areas of steep gradient.

The geological implications of these models will be discussed in detail in chapter 6 which deals with the extensional history of the North Sea.

3.5.4 QUANTIFICATION OF ERRORS

The complex nature of the modelling procedure means that errors can be introduced at several stages. If the assumption of a maximum depth limit is made and the associated absolute error in the Moho depth is ignored then five principal sources can be defined:

1) The original Bouguer Anomaly Data
2) The accuracy of the seismic structure maps produced by Day et al (1981)
3) The transfer of these maps to digital format
4) The choice of density contrasts
5) The iterative 3D modelling routine.

3.5.4.1 Accuracy of the Original Survey

As mentioned in 3.2.1 the accuracy of marine gravity surveys is considerably less than the 0.1 mGal accuracy expected for a land-based survey. In this case Tulley and Donato (1985) report an internal accuracy for the survey of 1 mGal.

3.5.4.2 Accuracy of the Seismic Structure Maps

Day et al (1981) do not report on the accuracy of their maps other than to point out that the depth estimates will decrease in accuracy for the deeper horizons. The reflectors arising at the chosen horizons such as the Top-Palaeocene and Base-Cretaceous have very distinctive characters. Errors due to the picking of these horizons during seismic interpretation will therefore be minimal. The chief inaccuracy will arise during the conversion from time to depth. This is done using a time/depth curve derived from averaged well data for each area. Where well information is sparse (i.e. at large depths) this curve will be least accurate. However, for horizons younger than the Base Cretaceous it is unlikely that any error will be larger than approximately 0.25 km. It is also important to note that the deeper layers have smaller associated density contrasts and are generally less thick. Thus the error is largest where the contribution to gravity is relatively small.

3.5.4.3 Accuracy of the Gridding Process

The digital maps representing depths to each of the near-surface layers compare favourably with the original seismic structure maps. The chief errors arise will arise where the sedimentary sequences are complicated by faults. In these areas the gridding procedure will tend to smooth over the fault, spreading its effect over the space of one grid interval. However, in the study area only the Cretaceous layer is substantially affected by faulting, and this contributes a relatively small amount to the overall gravitational effect.

Overall, the maximum error for the depth to the Base Cretaceous is unlikely to be in error by more than +/− 0.5 km. If the near-surface layers are approximated to a horizontal slab with an average density contrast of -0.55 g cm^{-3} then a change in thickness of 0.5 km is equivalent to a change in gravitational attraction of 11.5 mGal.

3.5.4.4 Accuracy of Density Estimates.

Each model is derived by considering 6 separate layers each having a characteristic density. Errors in the estimates of density contrast will therefore, play an important part in determining the final solution.

The water layer contributes such a small amount to the total gravity effect (fig. 3.11) that any error in the density (which is unlikely) will have a negligible affect on the end result. As mentioned in 3.4.1.2 density estimates for the other three near-surface layers were made using well log information from the study area. It was also pointed out that due to the affects of compaction these estimates will be least accurate in places where the sequence is deepest.

Telford et al (1976) report that wet sandstone has an average density of 2.0 g cm^{-3} with a possible range of 1.7 to 2.3 g cm^{-3}. However, where the density of the sedimentary sequence has actually been measured directly and in several places then the error will be considerably less than +/− 0.3 g cm^{-3}. Holliger and Klemperer (1989) in a similar gravity modelling study in the North Sea estimate that the average uncertainty in all density contrasts is +/− 0.05 g cm^{-3}.

Using the approximation of the near-surface layers to a horizontal slab of variable thickness then the following estimations of accuracy can be made. For a total thickness of 1 km an error in the density contrast of 0.05 g cm^{-3} is equivalent to approximately 2.1 mGal for a thickness of 3 km the error is equivalent to 6.3 mGal and for 5 km the error is equivalent to 10.5 mGal.

At the Moho the density contrast chosen is 0.5 g cm^{-3}. Unlike the near-surface layers this contrast cannot be directly measured and has to be determined by other means such as correlating seismic velocity with density (Barton and Wood 1984 and Barton 1986). The error in this contrast may be larger than that associated with the sedimentary sequences. The effect of varying this contrast by +/− 0.1 g cm^{-3} is shown in 3.5.4.6.

3.4.4.5 Errors Due to the Three Dimensional Modelling.

As seen earlier in this section the quality of fit is very good for most of the models considered here. Errors are rarely in excess of +/− 4 mGal with any significant errors occurring on a relatively small scale and limited to specific locations. These being mainly in the area where the Moho is relatively deep and also in areas associated with steep gradients in the Moho topography.

3.5.4.6 Overall Estimation of Errors

The following estimations have been made:

Error due to survey inaccuracies = 1 mGal.
Errors due to inaccuracies in depth estimates = 11.5 mGal.
Max. error due to inaccurate density contrasts = 10.5 mGal
Errors due to quality of fit during modelling = 4 mGal.
Total = 27 mGal.

If the upper-mantle body is approximated to a horizontal slab then for a density contrast of 0.5 g cm^{-3} an error of 27 mGal is equivalent to a change in thickness of 1.3 km. For a density contrast of 0.6 g cm^{-3} the error is 1.1 km and for a density contrast of 0.4 g cm^{-3} (in line with the 0.39 g cm^{-3} predicted by Woolard (1966)) the error is 1.6 km.

3.6 SUMMARY

The most important conclusions of the present chapter are summarised as follows:

1) The most notable feature of the Bouguer anomaly map for the study area is

the low amplitude (between −28 and +35 mGal.) of the field. The thick sediments associated with the area would produce large negative anomalies, it follows that there must be a compensating mass at depth.

2) There is a change in the field from dominantly NE-SW (typically Caledonian) trends in the south west to NNW-SSE trending features in the east.

3) The total gravitational effect of sedimentary sequences down to the Base Cretaceous can be calculated in three dimensions. The greatest contribution to the resultant field comes from the thick low density sediments of the Tertiary although the general shape of the field is largely controlled by the effect of the Cretaceous layer.

4) A residual field has been calculated which is interpreted as being due to variations in the depth to the Moho. The general shape of this field follows the major structural elements of the study area. The field varies between 6 and 119 mGal. the largest values being associated with the Central Graben and the East Forties Basin.

5) Low pass filtering in the wavenumber domain was used to remove anomalies from the residual field which could have been caused by sources shallower than approximately 11 km.

6) The filtered residual field was modelled in three dimensions using an iterative forward modelling technique. The best solutions show an Upper Mantle body varying in depth to its upper surface from approximately 34 km to 16 km. Areas where the Moho is relatively shallow tend to be governed by the major structural elements in the study area. The shallowest points are found in the East Forties Basin and the Central Graben.

7) Sources of error in the modelling procedure can be identified and the errors themselves can be estimated using the formula for a horizontal slab. The total

error for modelled depths to the Moho is not in excess of +/− 1.6 km.

CHAPTER 4

ANALYSIS OF AEROMAGNETIC DATA

4.1 INTRODUCTION

In the previous chapter a detailed study was made of the Bouguer anomaly data. As a complement to this an interpretation was also made of all the available aeromagnetic data for the study area. This chapter outlines that interpretation.

The magnetic method is based on interpreting variations in the magnetic field generated by susceptibility contrasts and/or changes in remanent magnetisation within the Earth's crust. Both of these rock properties can only exist at temperatures cooler than the Curie point, which varies according to mineralogy. Almost all the magnetic properties of rocks are due to concentrations of the accessory mineral magnetite (Paterson and Reeves, 1985) which has a Curie point of 575°C. (Telford et al, 1976). Carstens and Finstad, 1981 report that the geothermal gradient for the northern North Sea varies between 25°C km^{-1} and 40°C km^{-1}, the larger gradients tending to occur toward the centre of the Viking Graben. If an average geothermal gradient of 32.5°C km^{-1} is assumed for the Central North Sea then the Curie point will occur at depths of approximately 18 km. Thus in the North Sea aeromagnetic interpretation is restricted to analyses of structures within the upper half of the crust.

The primary objectives of regional aeromagnetic surveys can be summarised as follows:

1) Delineating areas where there are thick accumulations of volcanic rock.

2) Identification and delineation of large intrusive bodies.

3) Recognition and interpretation of magnetic lineations, often associated with zones of faulting, shearing and fracturing.

4) Delineating the structure of the magnetic basement underlying sedimentary basins.

Other uses such as the direct detection of magnetic iron are not of use to this study.

Section 4.2 of this chapter summarises the details and acquisition parameters of the surveys used in this study. The subsequent processing to grid format is also outlined.

A detailed qualitative interpretation of the aeromagnetic data is presented in section 4.3. This section also includes several digitally enhanced images to aid interpretation. Two of the areas where the magnetic field is particularly intense (the Piper-Forties Volcanic Province and the East Forties Basin) are discussed in detail in section 4.4. Each area is dealt with separately. The anomalies in these areas are analysed and modelled using a combination of 2.5D forward and inverse modelling. The models obtained are later used in conjunction with the Bouguer gravity to modify the Moho topography models obtained in the previous chapter. This process is discussed in detail in chapter 5.

The chapter ends with a brief summary of the most important conclusions obtained during the interpretation.

4.2 AEROMAGNETIC DATA

4.2.1 Survey Details

The magnetic data set is made up of data from three separate surveys which have been digitised from maps and then amalgamated into a single digital grid.

South of latitude 58N. the data set has been digitised from British Geological Survey published aeromagnetic anomaly maps (Forties sheet 57N - 00 and Peterhead sheet 57N - 02W, 1:250 000 series). These maps have had the International Geomagnetic Reference Field subtracted from them and are presented at 5 nT contour intervals. The survey itself was flown in 1963 by Aeroservices Corporation. The flight elevation was 305 m. and flight-line spacing was 3 km. east-west with north-south tie lines at 40 km. spacing.

North of latitude 58 N. the data comes from two surveys performed by Huntings. Again maps were digitised along flight lines so that the digital product could be used as input to a gridding algorithm.

4.2.2 Processing

Digital data was processed into grid format using the minimum curvature technique outlined in 3.2.1. the resulting grid is in the same UTM projection as the Bouguer anomaly data and covers the same area. Like the Bouguer anomaly grid it consists of 113 by 121 points with a cell spacing of 2 km.

Levelling problems between the three surveys were largely solved using the program 'GRDLVL' (courtesy of Cowan Geodata Ltd.). However, the join between survey grids is still not perfect, thus there are spurious east-west and north-south orientated line effects in these regions (approximately north-south along the 1° longitude line down to 58°N. and also east-west along 58°N.).

In some areas (particularly in the north-east and along the edges of the grid) a lack of data in the original surveys means that these areas have been masked using dummy values in the grid.

4.3 REGIONAL INTERPRETATION OF AEROMAGNETIC DATA

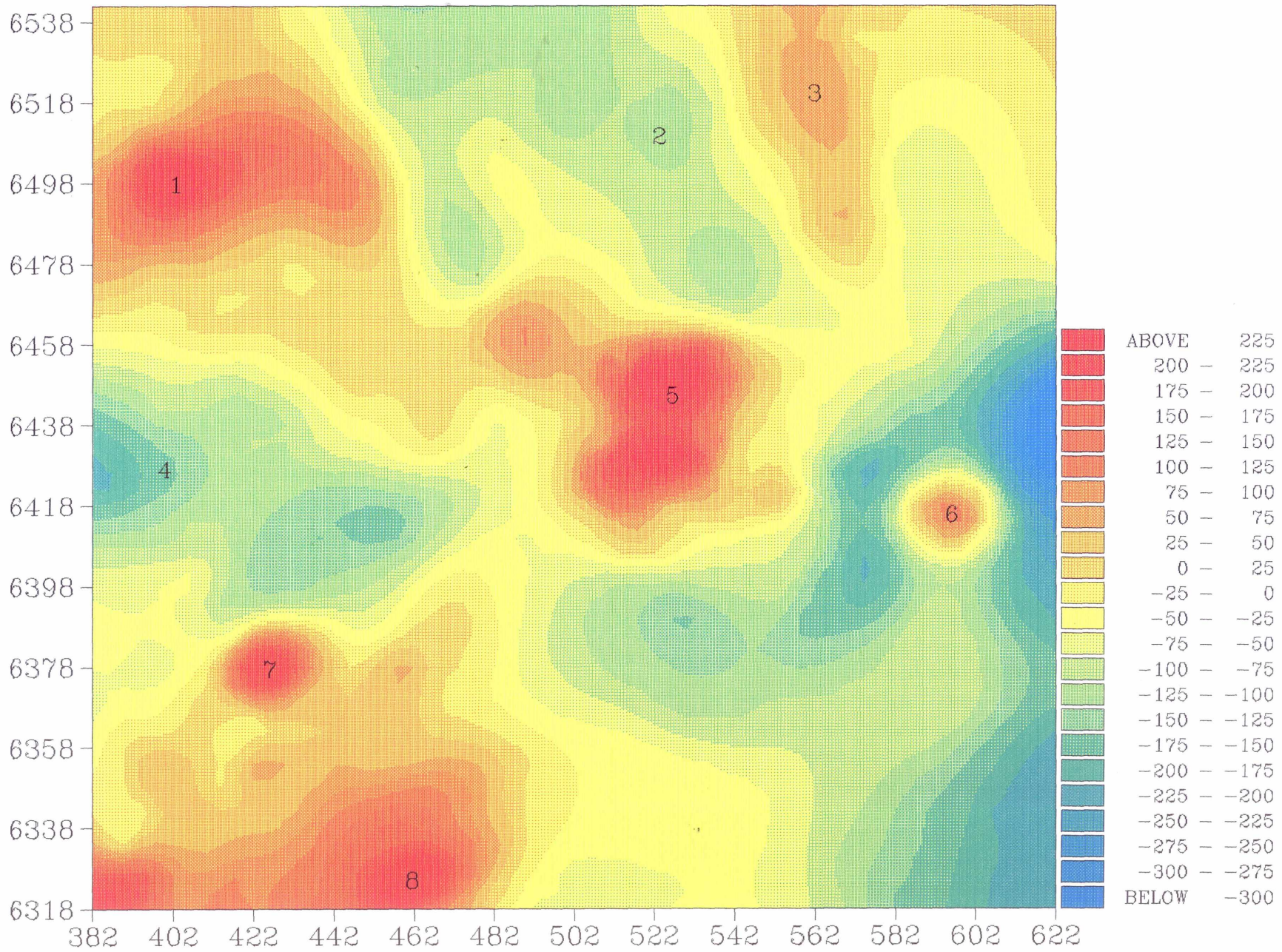
Several methods of interpretation are outlined in this section. A quantitative analysis of the aeromagnetic map is followed by a discussion of the features revealed using first horizontal and second vertical derivatives as well as shaded relief images. Digital filtering in the wavenumber domain is discussed and several results of high and low-pass filtering using different parameters are presented. Structural overlay 1 can be used in conjunction with all the images presented in this section. The principal results of the interpretation are shown on magnetic interpretation overlay 1.

The inclination of the magnetising vector can appreciably influence the size and shape of magnetic anomalies. This can be corrected by recalculating the field as it would have been observed if the causative body had been placed at the north pole. This process is known as reduction to pole and can lead to errors if any remanent magnetisation is present. Andreasen and Zietz (1969) show that at high inclinations this effect is relatively small. Since the inclination of the field in the study area is 71 degrees and no information is available regarding remanence it was decided that the data would not benefit greatly from polar reduction.

4.3.1 Qualitative Interpretation of the Aeromagnetic Map.

Figure 4.1 shows the gridded aeromagnetic data for the study area. It is presented in a rectangular UTM projection (central meridian at 0 degrees longitude). The axes coordinates are in units of kilometres and the data is presented at **25** nT contours (1 nanoTesla = 1 Gamma).

FIGURE 4.1 Total field aeromagnetic data from the Central North Sea. Contour interval is 25 nT. In some places (such as the extreme NE) interpolation has taken place to cover areas where there is no real data.


6538
6518
6498
6478
6458
6438
6418
6398
6378
6358
6338
6318
382
402
422
442
462
482
502
522
542
562
582
602
622
1
2
3
4
5
6
7
8
ABOVE 225
200 – 225
175 – 200
150 – 175
125 – 150
100 – 125
75 – 100
50 – 75
25 – 50
0 – 25
-25 – 0
-50 – -25
-75 – -50
-100 – -75
-125 – -100
-150 – -125
-175 – -150
-200 – -175
-225 – -200
-250 – -225
-275 – -250
-300 – -275
BELOW -300

The interpretation is made with reference to the interpretation of the Bouguer anomaly map for the same area (3.3). Wherever possible the two data sets are compared and contrasted. For ease of reference the study area has been divided into three zones: northern, central and southern (see structural overlay 1) and the principal anomalies have been numbered. The boundaries of these zones are not related to any geological boundaries however, they are the same as those used in the interpretation of the Bouguer anomaly data.

The author is not aware of any published regional interpretations of the whole of this data set. However, this interpretation is made with some reference to a non-exclusive interpretation of the data south of 58°N made by ARK GEOPHYSICS LTD in 1986. For the purpose of this research the conclusions made during the interpretation have been derived directly from the gridded data set shown in figure 4.1. Results obtained by ARK GEOPHYSICS which have not been derived in this research (due to software limitations, for instance) are given full credit.

4.3.1.1 Northern Zone

A large east-west trending magnetic high (feature 1) is the dominant feature in the western part of this zone. The anomaly reaches a maximum of 300 nT and is centred just to the south of the Wick fault which separates the Caithness Ridge to the north from the Outer Moray Firth Basin to the south. The Bouguer anomaly map (figure 3.1) also shows an elongate east-west trending positive anomaly in this area.

The magnetic anomaly is terminated to the east by a relatively strong magnetic gradient marking the south-western flank of the Dutch Bank Basin (Piper Embayment). The basin itself is marked by a broad SE - NW trending magnetic low (feature 2) reaching a magnetic minimum of approximately −130 nT in the north. The smooth nature of the field in this area suggests a deeply buried

basement. A large negative Bouguer anomaly is also present in this area.

The Fladen Ground Spur is marked by a magnetic high of less than 100 nT (feature 3) trending almost N - S. The anomaly is very well matched to the general shape of the spur and so is probably caused by the raised basement in this area. There is a positive Bouguer anomaly associated with this feature although it is centred approximately 10 km to the east of the magnetic high. This has been interpreted (see figure 3.1 and Donato and Tulley, 1981) as the southern edge of a basement ridge on the western flank of the Viking Graben.

4.3.1.2 Central Zone

The west of this zone is marked by a large, approximately, E - W trending magnetic low (feature 4) associated with the thick sediments of the Outer Moray Firth Basin. In places the anomaly reaches lows of over −200nT. South and south-east of this feature the magnetic field is characterised by NE - SW trending lineaments probably caused by faults in the Caledonian basement (4.2.1.3). The sudden change in the field from smooth and negative to complex and largely positive strongly suggests that this basinal area is fault bounded to the south. Since it is cut by Caledonian features it seems more likely that this area represents an region where the basement surface is relatively deep rather than an area of basement with an un-characteristically low susceptibility contrast. A large negative Bouguer anomaly is also associated with this area.

Although its shape is clearly defined in the gravity data, the Halibut Horst does not have a strong magnetic signature. A very low amplitude (less than 50 nT) magnetic ridge does follow the same trend as the Halibut Horst and the Halibut Platform to the North. An isolated magnetic high (approximately 100 nT) occurs on the eastern edge of the horst which may be associated with the Piper-Forties Volcanic Province to the east. This whole area is unfortunately disrupted by a N - S lineament which is purely an artifact of the gridding process and marks the join

between two surveys.

The Central zone is dominated by a broad magnetic high (feature 5) over the Witch Ground and Buchan Grabens. This consists of two magnetic maxima, one in the north of almost 300 nT and a slightly smaller one to the south in the Buchan Graben of approximately 250 nT. Unfortunately the anomaly is disrupted by a large E - W gridding artefact marking the boundary between the Aeroservice survey to the south from the Huntings surveys to the north. These large anomalies are in fact the magnetic signature of the Piper-Forties Jurassic Volcanic Province (Howitt et al,1975 and Woodhall and Knox, 1979). The alkali basalts associated with this region are discussed in more detail in 2.4). Detailed 2.5D modelling of this feature is discussed in 4.4.1. This feature is also associated with a broad high in the Bouguer anomaly data. Any Caledonian features in the basement tend to be obscured by the anomaly due to the basalts however some detail can be made out using shaded relief images (see 4.3.3).

The eastern flank of the Piper-Forties anomaly is marked by a steep gradient in the magnetic field running into a narrow N - S trending trough which reaches a low of approximately −210 nT. Another steep gradient separates this low from a very distinctive circular high of over 200 nT in the East Forties Basin (feature 6). The simple shape and size of this isolated anomaly suggests that it may be caused by a deep-seated intrusion. Detailed 2.5D modelling of this anomaly is discussed in 4.4.3. The East Forties Basin also has an associated positive Bouguer anomaly.

4.3.1.3 Southern Zone

As in the Bouguer anomaly data the western section of the southern zone is characterised by a complex field. In aeromagnetic data this is generally indicative of a relatively near-surface basement. The field is dominated by NE - SW trending lineaments, undoubtedly caused by Caledonian structural features within the

basement.

The Grampian arch is clearly outlined in the magnetic data as a relatively low amplitude (generally less than 50 nT) elongate 'ridge-like' anomaly trending NE - SW into the Buchan Graben. South-east of this the eastward extension of the Highland Boundary Fault is picked out by a series of small isolated magnetic highs with the characteristic Caledonian trend.

North-west of this, a second slightly weaker Caledonian lineament ends in a large positive magnetic anomaly of over 300 nT (feature 7). Its shape and isolation suggests that it may be caused by an intrusive body within the basement, although it may also be due to an unusually shallow area of basement. This is discussed in more detail in 4.3.5.

North of this anomaly a weak NNE - SSW trending lineament cuts into the broad magnetic trough discussed in 4.2.1.2. This weak lineament seems to terminate against the NE - SW trending Banff Fault.

South-east of the Highland Boundary Fault the field is less complex but still consists of at least three fairly strong Caledonian lineaments. The feature gradually increases in strength to the south and reaches a maximum of almost 300 nT (feature 8). The general shape of this anomaly suggests that there are more than one causative body. The structure of this area is revealed more clearly when the second vertical derivative map is analysed (4.3.4).

A secondary set of weaker NW - SE trending lineaments can be identified together with the Caledonian features in this region. ARK GEOPHYSICS have interpreted these lineations as being due to either compositional changes within the basement or the traces of ancient basement confined faults. Although this may be the case it does appear that these structures seem to cut across the Caledonian bodies suggesting that they are younger features. They also have a typically

Cimmerian trend. Johnson and Dingwall (1981) show similar Cimmerian faults (derived from seismic data) immediately east of this area on the north-western edge of the Forth Approaches. However, no such faults are recorded in the seismic structure maps of Day et al (1981) for this south-western zone of the study area.

There is a distinctive change in the character of the field toward the centre and east of this southern zone. The field changes from a complex of largely NE - SW lineaments in the west to much smoother E - W trending low amplitude features. The broad low amplitude troughs and ridge in the field are probably due to suseptability changes within the basement. ARK GEOPHYSICS have interpreted the E - W trending ridge as being caused by a deep-seated broad body at depths of between 6 and 11 km. This is discussed further in 4.3.5. The change in the character of the field from west to east suggests that there may be an important structural discontinuity within the Caledonian basement, the basement to the east being consistently deeper than that to the west. This feature trends NNW - SSE and is therefore exactly parallel to the Central Graben, which is the dominant structural feature 100 km to the east. Many of the Caledonian faults and bodies in the west would be cut off at this discontinuity. This phenomenon is more clearly seen in the shaded relief and second vertical derivative images (4.3.3 and 4.3.4).

In the east the Central Graben and Forties-Montrose Ridge do not have a strong magnetic signature. Rather the field seems to cross them almost at right-angles. The smoothness of the field in this area is indicative of a deeply buried basement; within the graben it is known that sediment thicknesses exceed 6 km (Ziegler 1982 and Day et al 1981). A broad, low amplitude magnetic 'high' (approximately −50 nT) changes from an E - W trend to a N - S trending feature in the centre of the graben. This terminates at the large anomaly (feature 6) in the East Forties Basin.

4.3.2 First Horizontal Derivative

The first horizontal derivative of the magnetic data was calculated in the same way as was done for the Bouguer anomaly data (3.3.2.1). As with the gravity data the first horizontal derivative is a very useful interpretive tool used to accentuate structural trends and lineations.

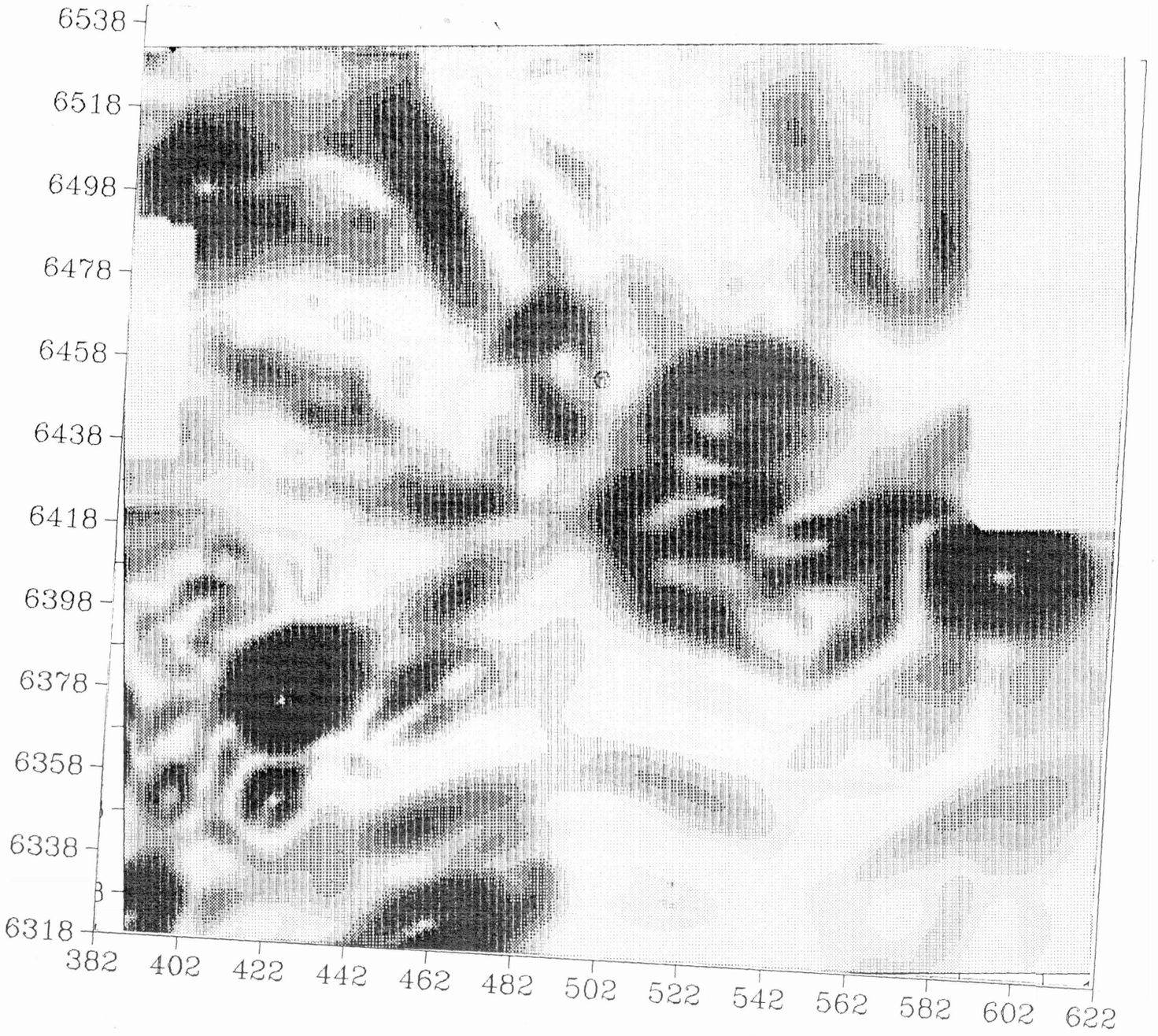
Figure 4.2 shows the first horizontal derivative for this data. the darker areas indicate steeper gradients within the field. Again structural overlay 1 can be used in conjunction with this image.

4.3.2.1 Northern Zone

The northern zone is dominated by the steep gradients associated with the Caithness Ridge anomaly in the extreme west. The Wick Fault is not easily recognised as a magnetic lineament in this image however, a strong lineation is seen just to the south of it. The Caithness Ridge and Wick Fault appear to be cut off to the east by a steep lineation trending NNW - SSE. This seems to continue southward cutting across the eastern boundary of the Halibut Horst. Two other weaker lineations on the same trend are seen cutting into the Piper Embayment and continuing southward into the With Ground Graben. If these are structural features than they may be related to the large discontinuity in the Caledonian basement in the south of the study area (4.2.1.3). The western-most (and strongest) of these lineations can almost be continued in a SSE. direction to join up with this basement feature.

To the east the western edge of the Fladen Ground Spur is clearly delineated as is the large N - S trending western boundary fault of the Viking Graben.

FIGURE 4.2 First horizontal derivative of the total magnetic field. Darker areas correspond to areas of increased local gradient in the field and tend to pick out steep geological contacts.


6538
6518
6498
6478
6458
6438
6418
6398
6378
6358
6338
6318
382
402
422
442
462
482
502
522
542
562
582
602
622

4.3.2.2 Central Zone

The most striking features of this zone are the lineations associated with the Piper-Forties Volcanic Province in the Witch Ground and Buchan Grabens. Several NE - SW trending features can be seen in the area as well as a more minor set of NW - SE Cimmerian lineaments. The Glen Horst is clearly picked out however, the centre of the area is degraded by the presence of an E - W trending gridding artefact.

West of the volcanic province the dominant trend is NW - SE. The western boundary fault of the Halibut Horst is clearly picked out. The trend is typical of Cimmerian structures. The NNW - SSE trending lineation on the SE side of the Halibut Horst which seems to be a continuation of a very strong lineation to the north (4.2.2.1) may in fact be due to a collection of smaller Cimmerian structures. The Banff Fault appears as a relatively weak lineation, however the presence of the large E - W trending gridding artefact makes this whole area difficult to interpret.

East of the volcanics the magnetic effect of any linear basement features is obscured by the steep gradients associated with the East Forties anomaly.

4.3.2.3 Southern Zone

As outlined in 4.2.1.3 the western section of this zone is characterised by a complex arrangement of NE - SW and NW - SE trending lineations. This is emphasised in the first horizontal derivative image.

In the north-west section of this area two elongate Caledonian lineaments are clearly visible together with two weaker lineations with the same trend in the north-western corner of the zone and just south of the Banff Fault. The secondary set of weaker lineations perpendicular to the Caledonian trend are also well

delineated in this area especially immediately north-west of the large anomaly in the Peterhead Ridge.

The eastern extension of the Highland Boundary Fault is not particularly easy to recognise on this image although there does seem to be evidence of it continuing further toward the NE cutting into the Grampian Arch. This structure is easier to delineate on the shaded relief images (4.3.3).

South-east of the Highland Boundary Fault at least three strong and one weaker Caledonian lineations are seen to be cut off to the east by the NNW - SSE trending basement discontinuity discussed in 4.2.1.3. In the extreme south the very dark and blurred nature of the image makes it difficult to interpret the exact nature of Caledonian faults present. ARK GEOPHYSICS have interpreted this region SE of the Highland Boundary Fault as consisting mainly of two large elongate relatively deep bodies bound on both sides by faults. These are probably the cause of the four lineations seen in this area on the first horizontal derivative. The second vertical derivative image (4.3.4) seems to confirm this interpretation.

In the centre of the southern zone there are only two features worthy of special note namely, a weak ESE - WNW trending lineation just west of the West Forties Basin and an even weaker isolated lineament of the same trend to the south. The northern-most of these may represent the edge of a deep basement feature or susceptibility contrast. It seems to be cut off in the east by the western boundary fault of the Central Graben which is also shown as a very weak WNW - SSE lineation.

Within the Central Graben the lineations cut across the main structural trend almost at 90 degrees. Two weak lineaments can be identified. The first (to the north) seems to be an extension of the ESE - WNW structure west of the West Forties Basin, albeit slightly offset to the north. This lineation changes from a NE - SW trend to almost N - S as it reaches the East Forties Basin. The southern most of these lineations trends NE - SW and cuts right across the Central Graben.

4.3.3 Shaded Relief Images

Figures 4.3 to 4.6 are shaded relief images of the first horizontal derivative field. Details of shaded relief production are given in 3.3.2.2. In the previous chapter shaded relief images of the Bouguer gravity field were presented. In this section shaded relief images of the first horizontal derivative field are discussed. The first horizontal field is commonly used to identify structural trends and fault lineations. Shaded relief images enhance these trends giving a more detailed view of the basement structure in the study area. It is important to note however, that these images cannot be used for direct mapping purposes since the technique displaces the highs and lows toward the illumination direction (figure 3.3).

Figure 4.3 is a shaded relief image of the first horizontal derivative field. The field has been 'illuminated' at an incident angle of 45 degrees from the north-west. A scaling factor of 10 has been applied to the initial data. Illumination from the north-west enhances all features which trend NE - SW The northern half of the study area is relatively free of Caledonian trending features. There are however, a weak set of such lineations north of the Halibut Horst on the Halibut Platform. Johnson and Dingwall (1981) show such a set of small Caledonian faults in this area. South-east of this within the area of the Piper-Forties Volcanic Province at least four Caledonian lineations can be seen although these features are somewhat degraded by the E - W trending gridding artefact which runs through this area.

In the South-west at least four Caledonian faults are delineated by weak lineations north-west of the large anomaly in the Peterhead Ridge. The northern-most of these seems to correlate with the Banff Fault. A strong lineation is seen

trending NE of the large positive anomaly into the Buchan Graben. This probably correlates with the fault complex associated with the Grampian Arch. South of this, two strong Caledonian lineaments can be seen terminating against the NNW - SSE trending basement discontinuity discussed in 4.3.1.3. the southern-most of these two lineaments seems to correlate with the eastern extension of the

Highland Boundary Fault. South of the Highland Boundary Fault a further set of six relatively strong Caledonian structures can be identified. The southern-most four of these terminate sharply against the NNE - SSW basement discontinuity. In the Central Graben area four relatively weak Caledonian lineations can be recognised.

Figure 4.4 is a shaded relief image of the first horizontal derivative field, this time illuminated from the south-east. at an incident angle of 45 degrees. Again Caledonian trends are emphasised in this image. It is not a significant improvement on the image illuminated from the north-west. however, the structures within the Piper-Forties Volcanic Province are perhaps a little easier to define in in this image.

Figure 4.5 is a shaded relief image of the same field illuminated at 45 degrees from the north-east. This illumination direction accentuates NW - SE trending structures. In the north the three NNW - SSE lineations in the Piper Embayment and Halibut Platform are clearly picked out as are the large Cimmerian faults in the west Halibut Platform and South Halibut Horst. A minor set of three Cimmerian faults seems to be situated on the south boundary of the Halibut Horst emphasising the complex nature of this feature. The Piper-Forties Volcanic Province is bound to the south-west by a strong NNW - SSE which changes direction (to the south) to a more NW - SE orientation. A second (and perhaps a third) NW - SE lineament can be identified further east. These are more clearly expressed in figure 4.6 where the illumination direction is from the south-west. They are probably caused by Cimmerian faulting cross-cutting the older Caledonian features within the basement.

FIGURE 4.3 Shaded relief image of the first horizontal derivative field. The field is 'illuminated' at an incident angle of 45 degrees form the north-west.

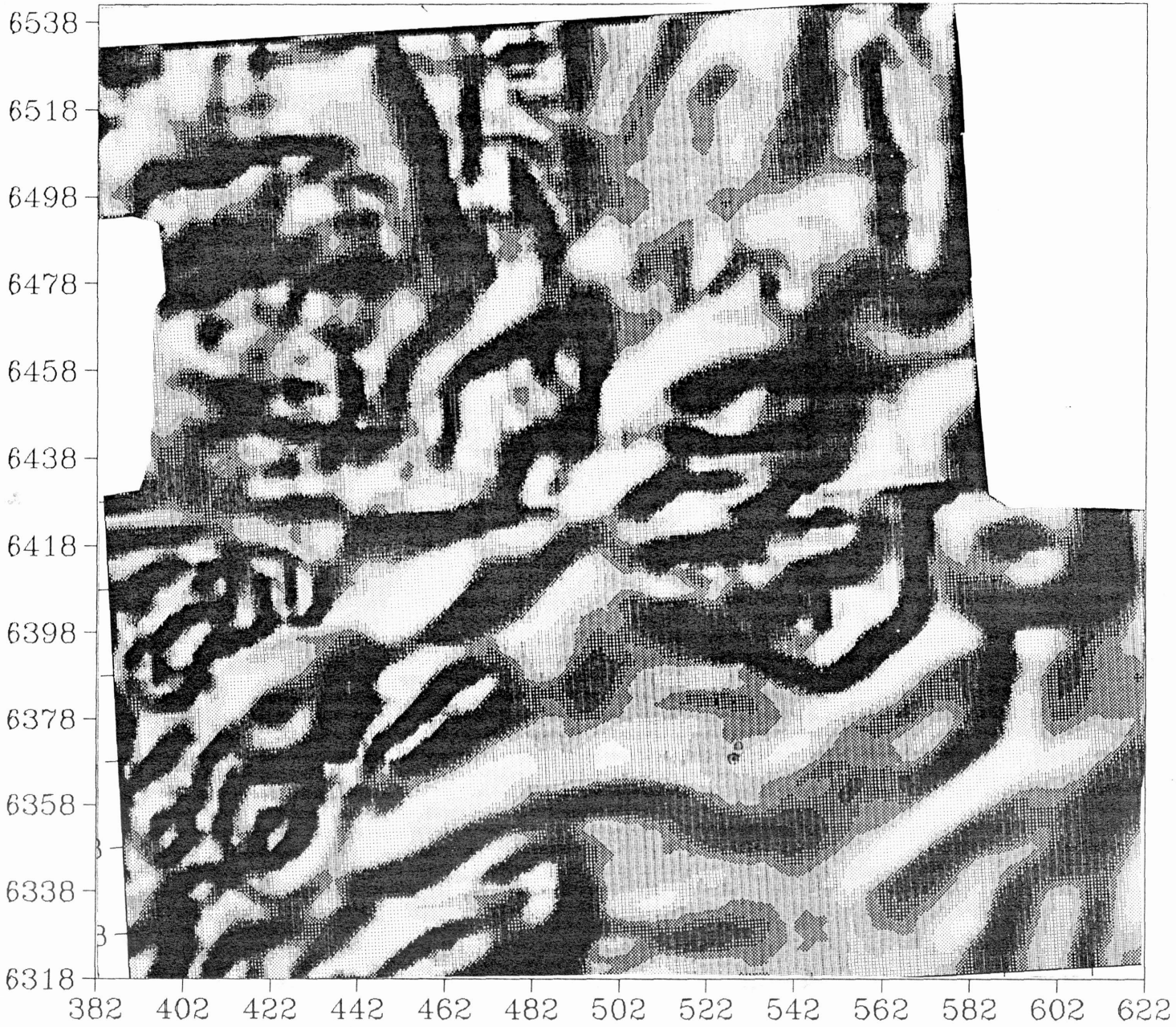

6538
6518
6498
6478
6458
6438
6418
6398
6378
6358
6338
6318
382
402
422
442
462
482
502
522
542
562
582
602
622

FIGURE 4.4 Shaded relief image of the first horizontal derivative field. The field is 'illuminated' at an incident angle of 45 degrees form the south-east.


6538
6518
6498
6478
6458
6438
6418
6398
6378
6358
6338
6318
382
402
422
442
462
482
502
522
542
562
582
602
622

FIGURE 4.5 Shaded relief image of the first horizontal derivative field. The field is 'illuminated' at an incident angle of 45 degrees form the north-east.

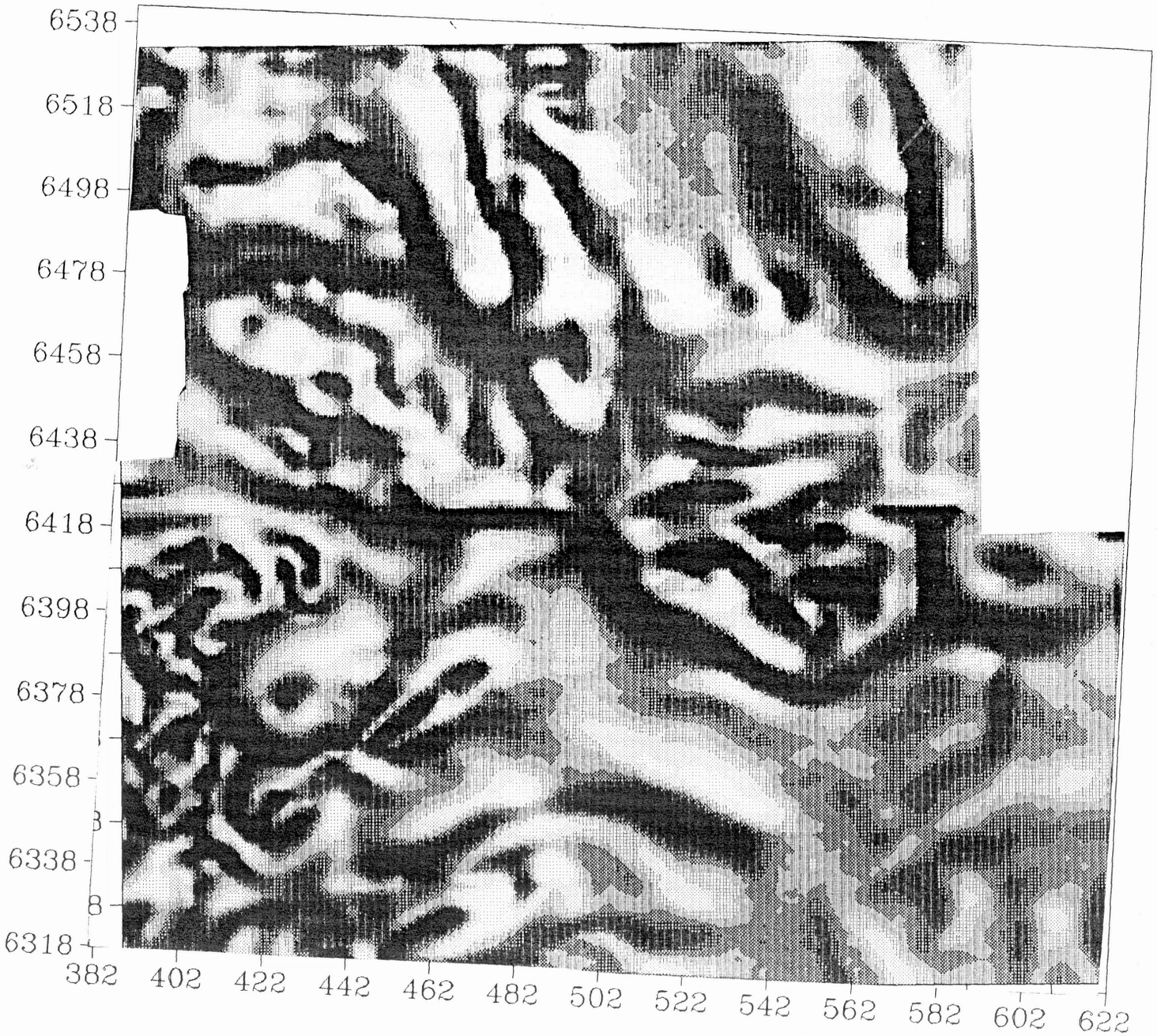

6538
6518
6498
6478
6458
6438
6418
6398
6378
6358
6338
6318
382
402
422
442
462
482
502
522
542
562
582
602
622

FIGURE 4.6 Shaded relief image of the first horizontal derivative field. The field is 'illuminated' at an incident angle of 45 degrees form the south-west.


6538
6518
6498
6478
6458
6438
6418
6398
6378
6358
6338
6318
382
402
422
442
462
482
502
522
542
562
582
602
622

In the south-west the secondary set of NW - SE weak lineaments cutting the Caledonian features is easy to pick out. Several such structures can be seen immediately south of the Banff Fault and at least two such features seem to cut across the trend of the Highland Boundary Fault extension.

The large NNW - SSE trending basement discontinuity discussed in 4.3.1.3 is present as a very weak lineation as is the western boundary fault of the Central Graben further to the east.

4.3.4 Second Vertical Derivative Image.

The analysis of second vertical derivative anomalies of potential field data is a commonly used method of emphasising shallow structures and discontinuities often relating to faulting (eg. Hildenbrand and Kucks, 1985 and Behrendt and Grim, 1985).

Laplace's equation for potential fields states:

$$\frac{\partial^2 f}{\partial x^2} + \frac{\partial^2 f}{\partial y^2} + \frac{\partial^2 f}{\partial z^2} = 0$$

Thus the second vertical derivative of the field is given by:

$$\frac{\partial^2 f}{\partial z^2} = -[\frac{\partial^2 f}{\partial x^2} + \frac{\partial^2 f}{\partial y^2}]$$

i.e. the second vertical derivative is the negative sum of the curvature of the field in the x and y directions (Berhendt and Grim, 1985)

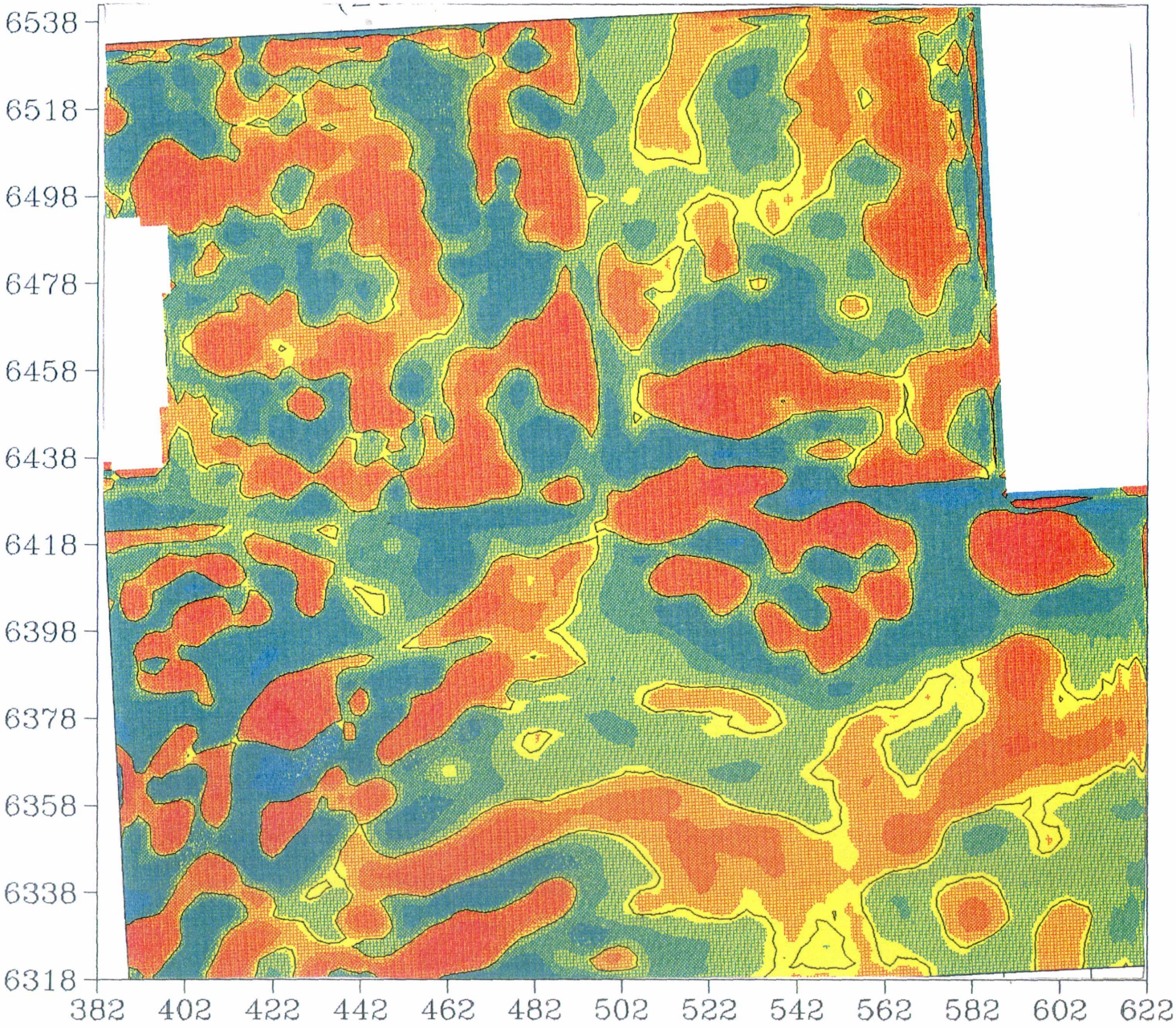
In this research it is calculated using a wavenumber-domain filtering technique available on the 'GEOSOFT' PC-based potential field analysis software package. The linear transform operator is derived in Gunn (1975).

The operator is basically a high-pass filter therefore shallow features are emphasised at the expense of deeper ones. Apart from accentuating discontinuities, second vertical derivative maps are a particularly useful interpretive tool as the zero contour represents the point of inflexion of the anomaly. Vacquier et al (1981) show that this approximates to the edges of the causative body. Contours immediately above and below the zero contour can be used to give an estimate of the reliability of this approximation. Where there are few contours then any bodies outlined using the zero contour will be less accurate than where there are steep gradients in the second vertical derivative field about the zero level.

Figure 4.7 shows the second vertical derivative field for the study area, the zero contour is marked. Unfortunately since high-frequency components are accentuated the image is a little noisy. This could be cured by applying a low-pass filter but, the problem is not so great that the image cannot be interpreted.

In the north, there are few significant bodies defined by the zero contour. This is probably due to the deep basement in these areas. A notable exception occurs at the Caithness Ridge and further south in the region of the Halibut Horst. The central region of the study area is dominated by the E - W trending gridding artefact making interpretation impossible. In the area of the Piper-Forties Volcanic Province several 'bodies' can be identified which at first may appear to relate to zones of anomalously thick basalt sequences, however detailed modelling (4.4) later proved this assumption to be false for the south-east of this area. The large body (interpreted as a large mafic intrusion) which is responsible for the East Forties Basin anomaly is clearly outlined by the zero contour.

FIGURE 4.7 Second vertical derivative of the total magnetic field. Tightly grouped contours around the zero contour (marked) tend to outline the edges of causative bodies.


6538
6518
6498
6478
6458
6438
6418
6398
6378
6358
6338
6318
382
402
422
442
462
482
502
522
542
562
582
602
622

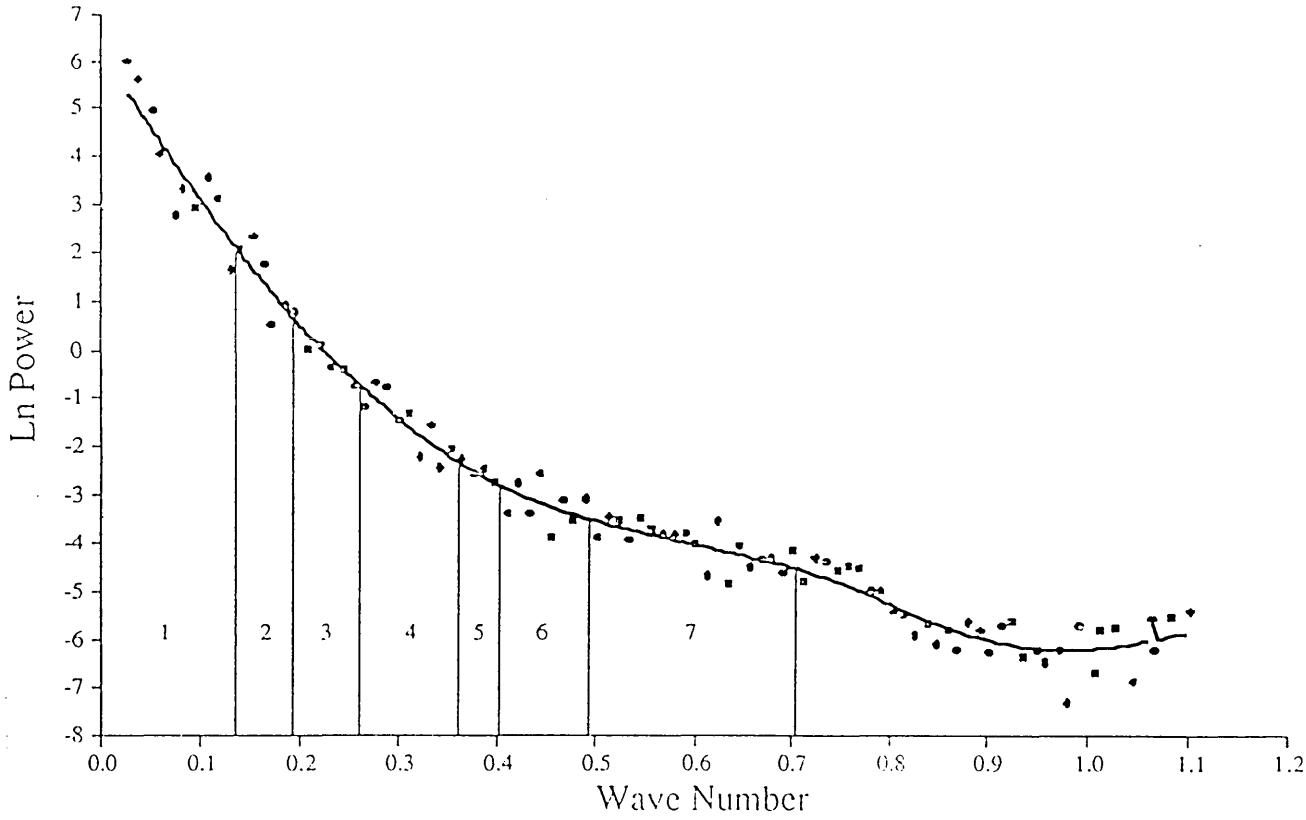
The most significant results are seen in the south-west of the study area. Several small bodies are outlined by the zero contour and the steep gradients in the field around it. Most of these have typically Caledonian trends. Apart from the large positive anomaly on the Peterhead Ridge, here interpreted as an intrusive body (see 4.3.5), they probably represent areas of raised basement bound by faults. In the south, two clongate bodies are clearly outlined by the zero contour. The zero contour exactly matches the relatively poorly defined lineations seen on the first horizontal derivative map. Both bodies are probably fault bound areas of raised basement. West of these features the zero contour appears to outline a broad E - W to ENE - WNW trending body. The contours around the zero-level are widely spaced suggesting that this is an unreliable interpretation. However, it is possible that this feature may be caused by a deep seated body which would not be accentuated by taking the second vertical derivative.

The west boundary fault of the Central Graben is picked out by a weak NNW - SSE lineation in the zero contour. In the Central Graben itself, south of the East Forties Basin anomaly there is some evidence to suggest the presence of a narrow N - S trending body. The northern edge of this body by a relatively steep gradient around the zero contour.

4.3.5 Depth Estimates from Spectral Analysis

As outlined in 3.4.2.1 any potential field data set contains a range of frequencies which relate to different source ensembles (Spector and Grant 1970). Using the same routine used on the gravity data (3.4.2.1) the azimuthally averaged power spectrum for the aeromagnetic data was obtained and analysed. The result is shown in figure 4.8.

The power spectrum can be divided into seven straight-line segments. The gradient of each line is equal to twice the average depth to the source ensembles



Segment	Wave No. Range	Av Depth(km)	Max.Wavelength (km)
1	0.000-0.137	14.64	45.86
2	0.137-0.194	12.23	32.39
3	0.194-0.260	10.16	24.17
4	0.260-0.360	7.31	17.45
5	0.360-0.403	5.23	15.59
6	0.403-0.491	3.47	12.78
7	0.491-0.703	2.06	8.94

FIGURE 4.8 Power Spectrum of the aeromagnetic data. Explanation in text.

causing anomalies with frequencies defined by the end-points of each segment. The power spectrum shows these average depths and the wavelengths associated with them. Much of the energy is associated with large wavelengths indicating the large depth to magnetic basement over much of the study area.

By designing successive high-pass filters at increasingly small cut-off wavelengths then analysing the results at each stage it should be possible to make rough depth estimates for various points in the study area.

Figure 4.9 shows the field after high-pass filtering where the filter has a cut-off wavelength of 17.45 km. Figure 4.8 shows that this should eliminate all sources whose depths are greater than approximately 7 km i.e. the only anomalies to appear on figure 4.9 will have sources shallower than 7 km. Much of the plot consists of random noise (between +/− 10 nT in figure 4.9) but some anomalies can still be made out. These are mainly found in the Piper-Forties Volcanic Province or in the south-west of the study area however, anomalies are also seen in the extreme north-west in the Caithness Ridge area. In the East Forties Basin the large anomaly is totally absent indicating a minimum depth of more than 7 km.

Figure 4.10 shows the field after high-pass filtering where the filter has a cut-off wavelength of 15.59 km. In this case only those anomalies caused by bodies shallower than approximately 5 km should be present. The Caithness ridge anomaly has disappeared indicating a minimum depth to its source of between 5 and 7 km. In the Piper-Forties Volcanic Province only those anomalies in the centre of this area remain although some of these may be due to the gridding artefact degrading data in this region. In the south-west much of the useful signal has been removed especially in the south indicating that the elongate bodies interpreted here occur at depths between 5 and 7 km. Some signal is still present on the southern-most of these indicating that it may be slightly shallower than the more northerly of the two.

FIGURE 4.9 Magnetic field after high-pass filtering. The cut off wavelength is 17.45 km. Sources deeper than 7 km should be eliminated, explanation in text.

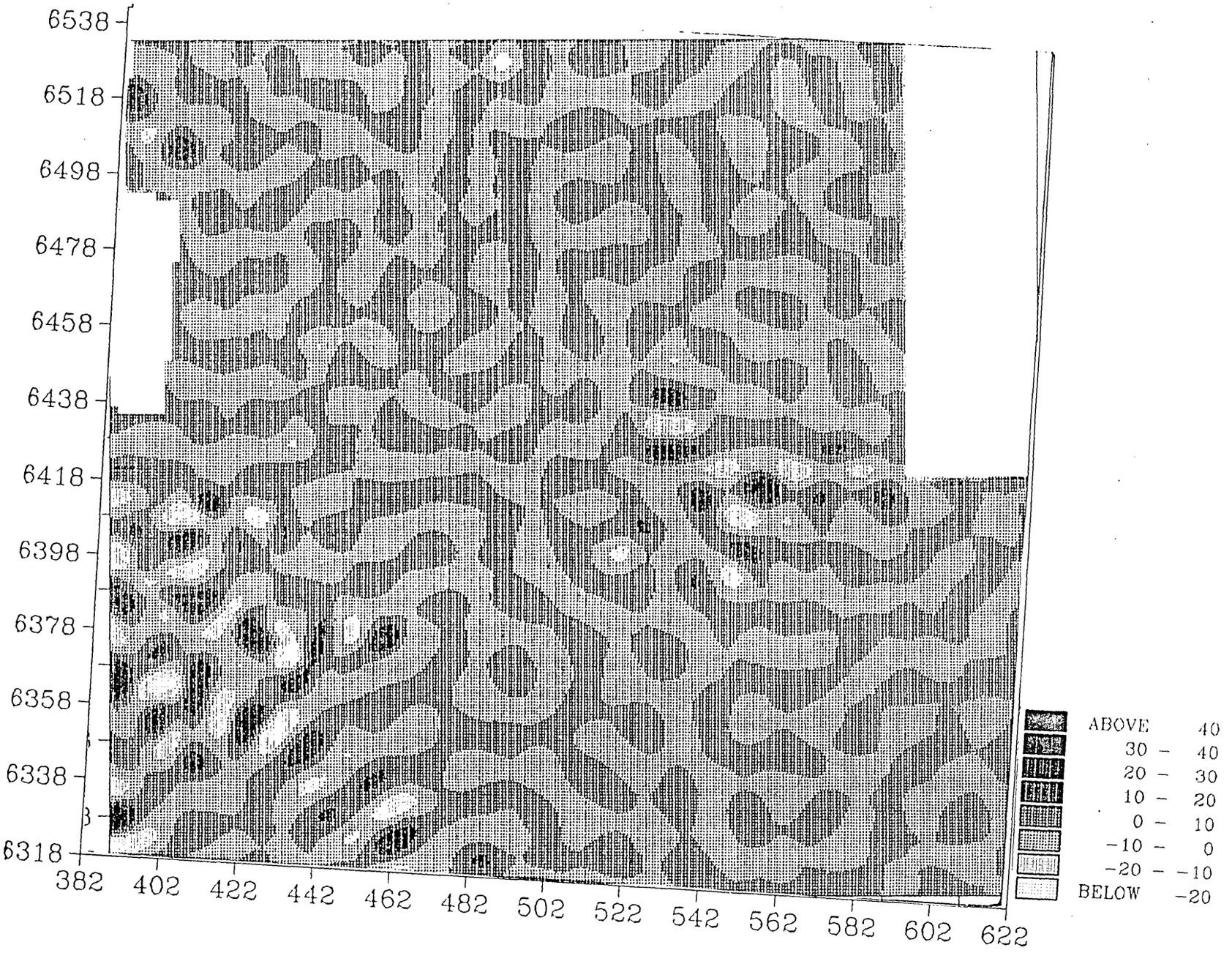

6538
6518
6498
6478
6458
6438
6418
6398
6378
6358
6338
6318
382
402
422
442
462
482
502
522
542
562
582
602
622
ABOVE 40
30 – 40
20 – 30
10 – 20
0 – 10
−10 – 0
−20 – −10
BELOW −20

FIGURE 4.10 Magnetic field after high-pass filtering. The cut off wavelength is 15.59 km. Sources deeper than 5 km should be eliminated, explanation in text.

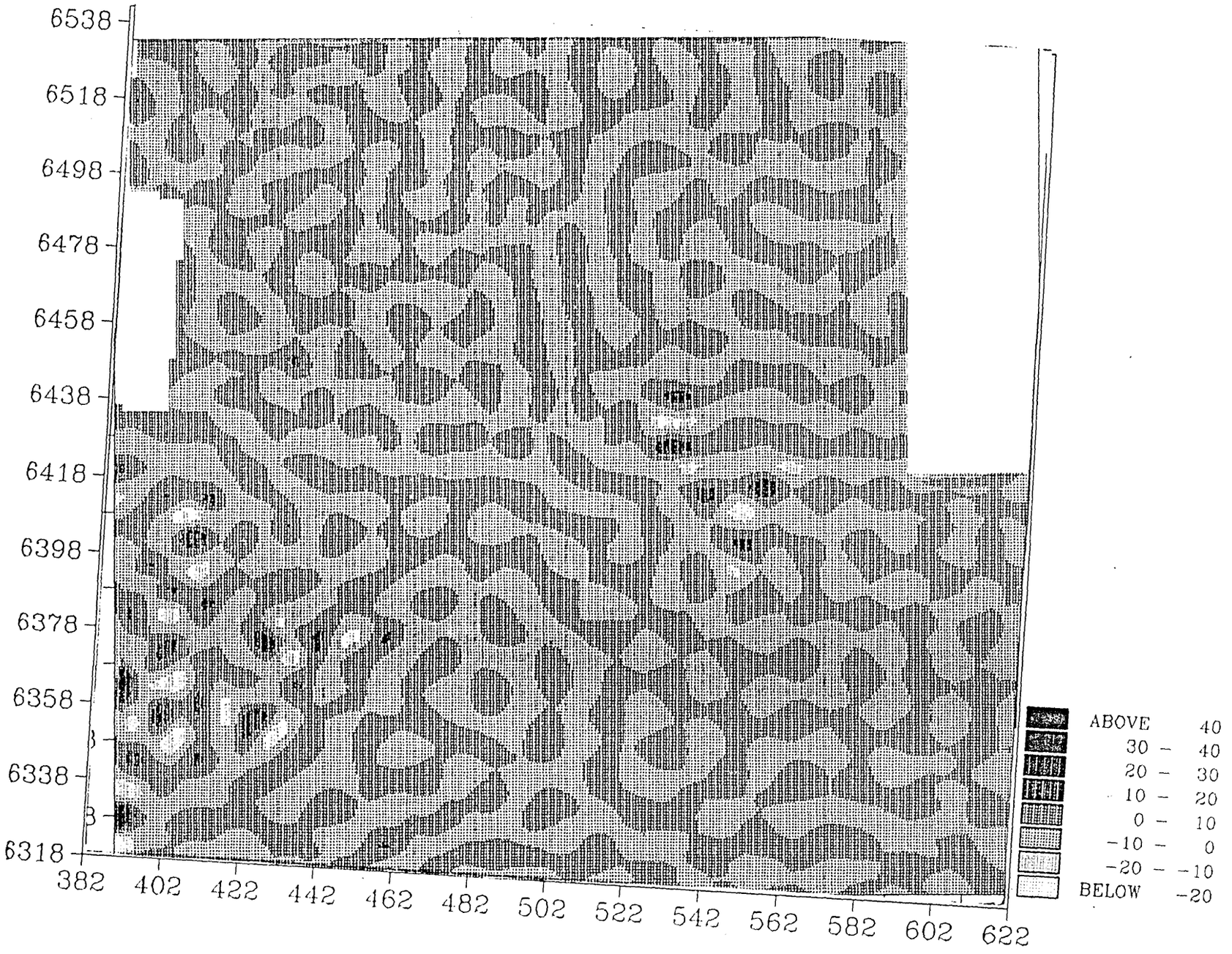

6538
6518
6498
6478
6458
6438
6418
6398
6378
6358
6338
6318
382
402
422
442
462
482
502
522
542
562
582
602
622
ABOVE 40
30 - 40
20 - 30
10 - 20
0 - 10
-10 - 0
-20 - -10
BELOW -20

Figure 4.11 shows the field after high-pass filtering at a cut-off wavelength of 12.78 km. In this case only those anomalies caused by sources shallower than approximately 3.5 km. The only signal present is in the south-west indicating the shallow basement in this area. The large anomaly seen in the unfiltered data has virtually disappeared suggesting that its source is likely to be an intrusive body rather than an area of anomalously shallow basement. If the latter were true then its associated high amplitude anomaly would suggest that the basement was shallower here than anywhere else in the near vicinity. This is clearly not the case.

Figure 4.12 shows what might be described as the 'regional component' of the magnetic field, although there is perhaps too great a high-frequency component for this to be strictly true. It is obtained by filtering the data with a low-pass filter at a cut-off wavelength of 24.17 km. Sources producing these anomalies should be greater than approximately 10 km. In certain areas (eg. the south-west) these represent very deep intra-basement magnetic contrasts. An interesting point to note is the diffuse low-amplitude WNW - ESE trending anomaly just north of the Forth Approaches. This may indicate a very deep seated basement structure probably at depths of around 8 to 9 km.

This method is very crude and depth estimates are likely to have large errors associated with them (maybe as large as +/− 1.5 to 2 km). For instance it is reasonably well known that the basalts of the Piper-Forties Volcanic Province occur at depths of approximately 3.5 to 4 km (4.4.1) yet figure 4.10, showing anomalies supposedly caused by bodies shallower than 5 km shows very little signal associated with the volcanic province. The technique is better used to distinguish between areas of relatively shallow or deep basement.

FIGURE 4.11 Magnetic field after high-pass filtering. The cut off wavelength is 12.78 km. Sources deeper than 3.5 km should be eliminated, explanation in text.

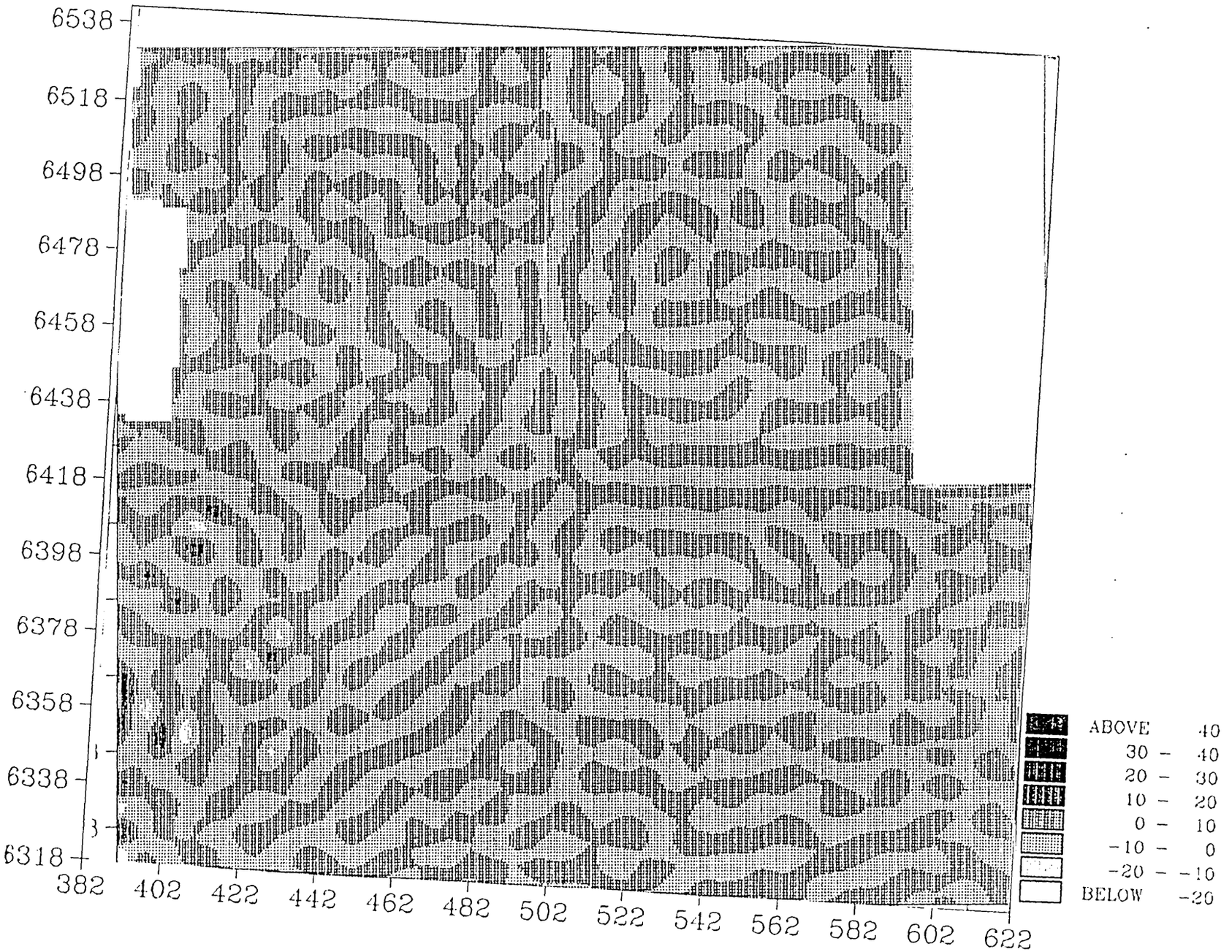
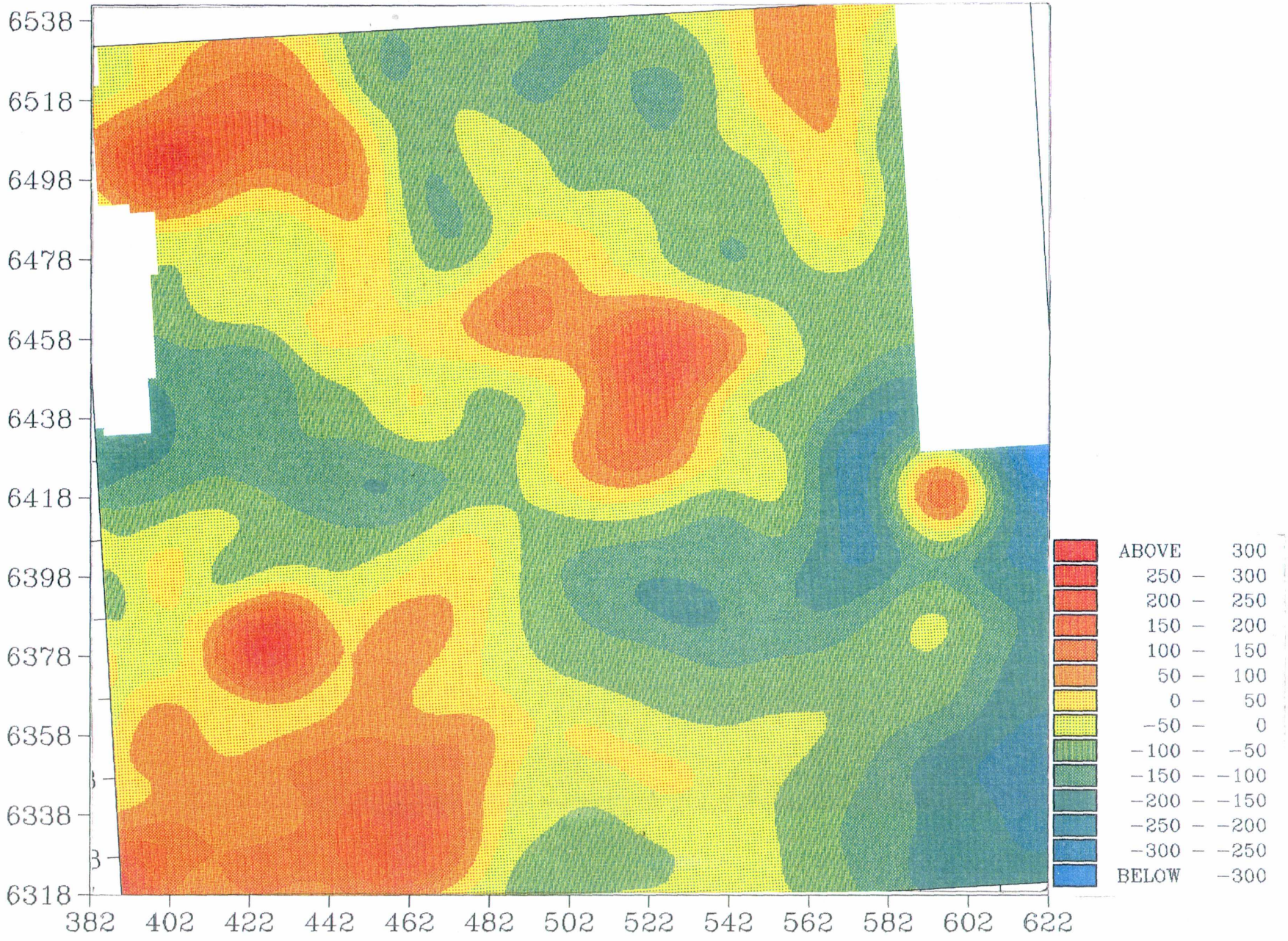

6538
6518
6498
6478
6458
6438
6418
6398
6378
6358
6338
6318
382
402
422
442
462
482
502
522
542
562
582
602
622
ABOVE 40
30 - 40
20 - 30
10 - 20
0 - 10
-10 - 0
-20 - -10
BELOW -20

FIGURE 4.12 Magnetic field after low-pass filtering. The cut off wavelength is 24.17 km. Sources shallower than 10 km should be eliminated, explanation in text.


6538
6518
6498
6478
6458
6438
6418
6398
6378
6358
6338
6318
382
402
422
442
462
482
502
522
542
562
582
602
622
ABOVE 300
250 – 300
200 – 250
150 – 200
100 – 150
50 – 100
0 – 50
−50 – 0
−100 – −50
−150 – −100
−200 – −150
−250 – −200
−300 – −250
BELOW −300

4.4 QUANTITATIVE MODELLING

In order to improve the Moho topography models obtained from the gravity data (3.5) it was decided to calculate the gravitational effect of both the body causing the East Forties Basin anomaly and the basalts of the Piper-Forties Volcanic Province. More details of this process are given in chapter 5. The shape of the East Forties Basin intrusion and the distribution of the basalts in the Piper-Forties Volcanic Province can be determined by modelling the aeromagnetic data. This section outlines the modelling process and the results obtained.

4.4.1 Modelling the Piper-Forties Volcanic Province

From the second vertical derivative map (figure 4.7) 10 separate centres believed to represent areas of anomalously thick basalts can be identified. These are shown in magnetic interpretation overlay 2. The largest centres appear on the northern side of the province. It seems likely that these may represent the location of magma vents. For modelling purposes 5 S - N trending profiles running across the province were extracted from the gridded data. There locations were designed to pass through the centres of all of the 'bodies' defined on the second vertical derivative map. An E - W trending gridding artefact runs through the centre of the province. Nothing can be done to correct for this so the models shown here must inevitably be in error, especially in the central area of the province. Since the artefact causes a slight magnetic low the models are likely to show too little basalt rather than too much.

The modelling routine 'SAKI' (Semi-Automatic 'K'- parameter Inversion) works in two and a half dimensions and allows a combination of both inversion and forward modelling. It runs on a standard IBM PC and was adapted by Duncan Cowan (Cowan Geodata Ltd.) from algorithms originally developed by the Canadian Geological Survey.

There is no published literature giving depths to the surface of the basalt sequences. Latin (pers. comm.) has studied many commercial wells in this area and reports that in most cases the top surface of the basalt is usually just below the Base-Cretaceous. In the absence of any other data all the models shown here have the top surface of the basalt at the same level as the Base-Cretaceous. During the modelling process this remains a fixed surface allowing the lower surface of the basalts to be varied in depth.

The five profiles and the models obtained are shown in figures 4.13 to 4.17. For each model a susceptibility contrast of 0.00226 e.m.u. was used to represent the basalt. Since no information was available, no account of remanent magnetisation was made during the modelling process.

The basalt layer is seen to thicken toward the centre of the province. Profiles 2 and 3 show areas in the centre where thicknesses are in excess of 8 km. In order to get a clearer picture of the distribution of the basalt the lower surfaces of each model were digitised and made into a digital grid using the minimum curvature method outlined in 3.2.2. By subtracting the depths to the upper surface of the basalts (here taken as the Base-Cretaceous) from the depths to the lower surface a thickness (isopach) grid for the Piper-Forties Volcanic Province was obtained. This is shown in figure 4.18. The solution shows broad regional thickness variations but there is a definite thickening toward two centres in the Witch Ground Graben. These two centres appear to be so localised that they probably represent vent sites. The difference of thickness of basalt in the Witch Ground Graben and Buchan Graben suggests that there may be a large degree of ponding against the Cimmerian fault which separates the two grabens. Using magnetic overlay 2 on this image reveals that many of the 'bodies' (particularly those in the south-east) previously defined on the second vertical derivative map (4.3.4 and figure 4.7) are not at all connected with the volcanic province.

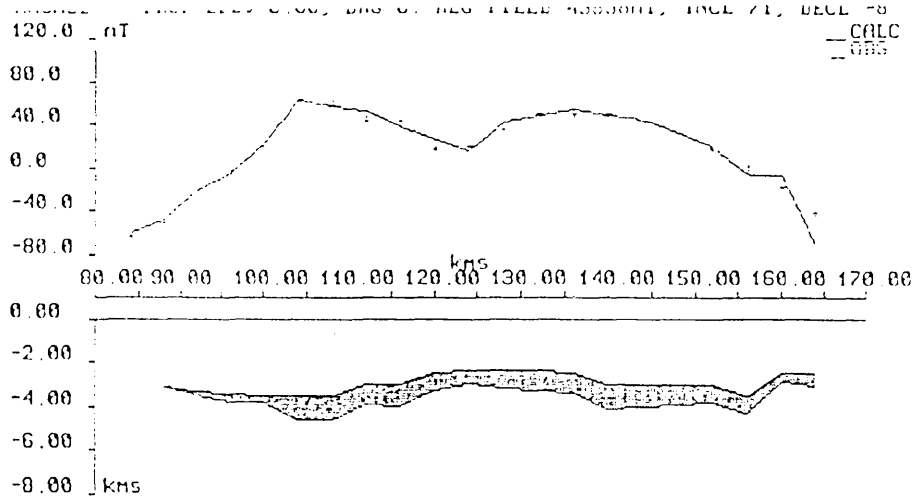


FIGURE 4.13 Profile 1: 2.5D Model of the Piper-Forties Volcanic Province. See Magnetic Interpretation Overlay 2. Susceptibility contrast = 0.00226 e.m.u.

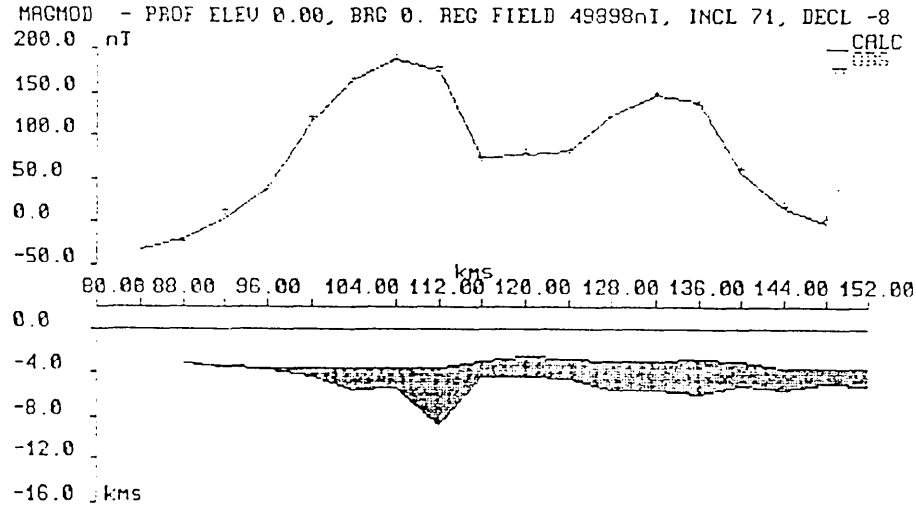


FIGURE 4.14 Profile 2: 2.5D Model of the Piper-Forties Volcanic Province. See Magnetic Interpretation Overlay 2. Susceptibility contrast = 0.00226 e.m.u.

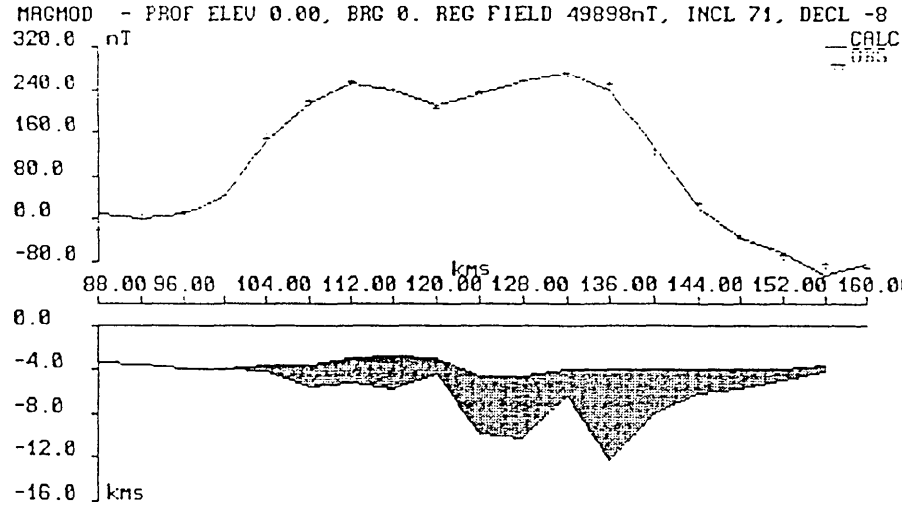


FIGURE 4.15 Profile 3: 2.5D Model of the Piper-Forties Volcanic Province. See Magnetic Interpretation Overlay 2. Susceptibility contrast = 0.00226 e.m.u.

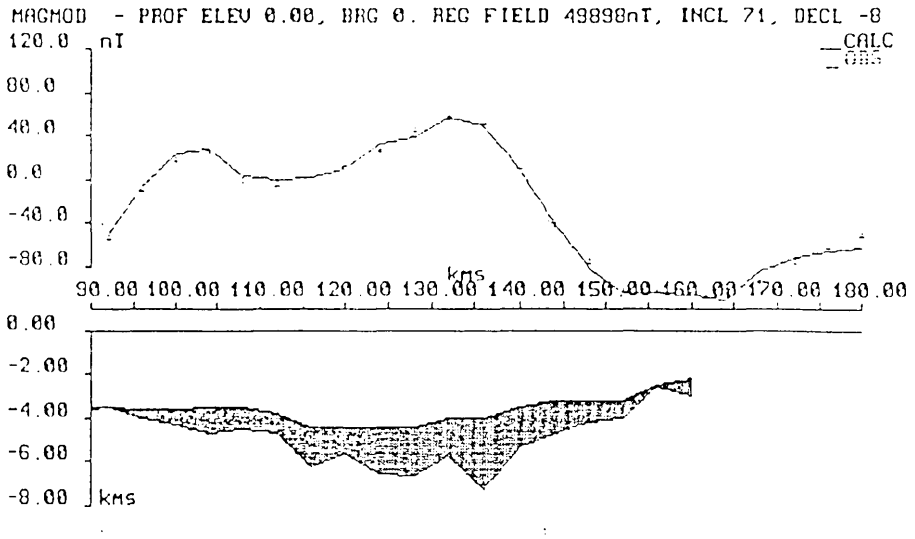


FIGURE 4.16 Profile 4: 2.5D Model of the Piper-Forties Volcanic Province. See Magnetic Interpretation Overlay 2. Susceptibility contrast = 0.00226 e.m.u.

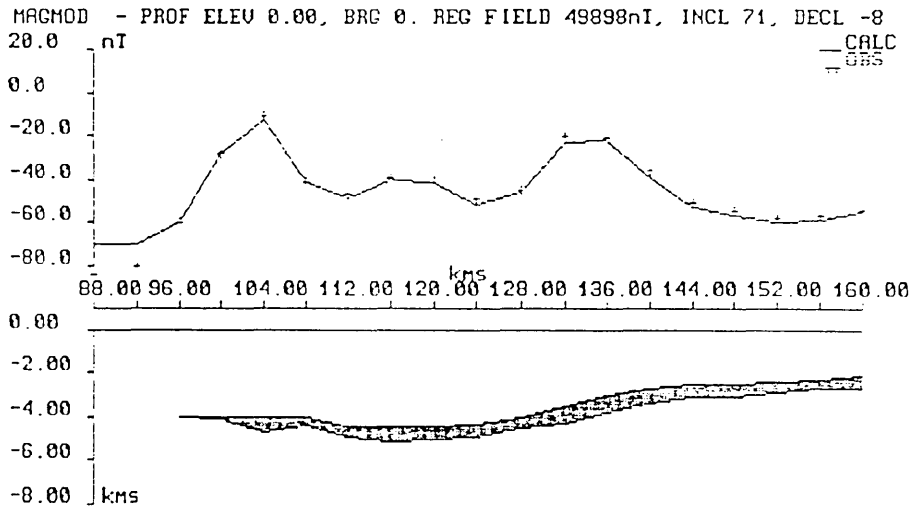
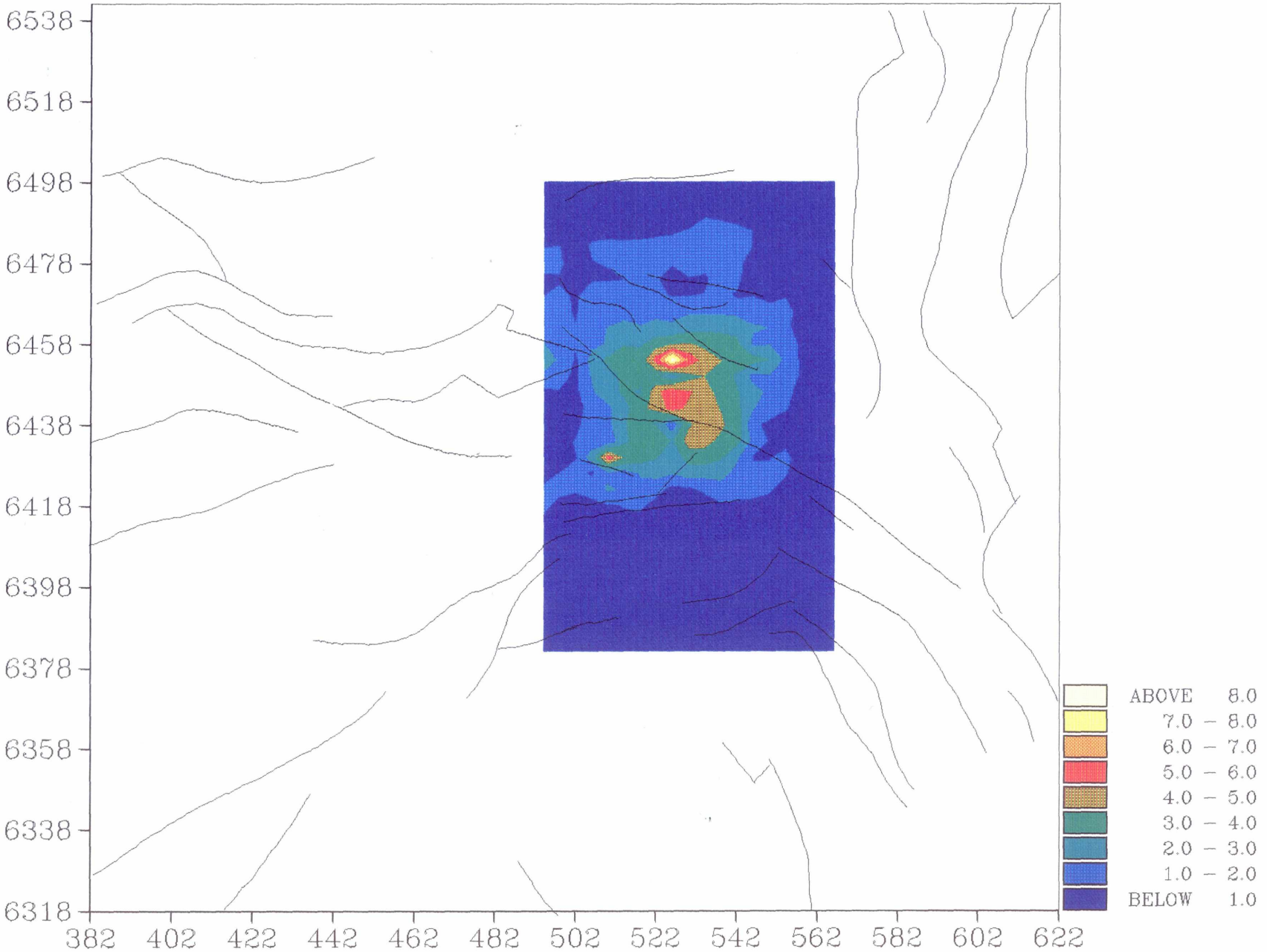


FIGURE 4.17 Profile 5: 2.5D Model of the Piper-Forties Volcanic Province. See Magnetic Interpretation Overlay 2. Susceptibility contrast = 0.00226 e.m.u.

FIGURE 4.18 Isopach of the Piper-Forties basalts derived from 2.5D modelling of the magnetic field. Thicknesses are in kilometres.


6538
6518
6498
6478
6458
6438
6418
6398
6378
6358
6338
6318
382
402
422
442
462
482
502
522
542
562
582
602
622
ABOVE 8.0
7.0 - 8.0
6.0 - 7.0
5.0 - 6.0
4.0 - 5.0
3.0 - 4.0
2.0 - 3.0
1.0 - 2.0
BELOW 1.0

4.4.2 Comparison with Previous Work

To the author's knowledge only two other detailed interpretations of the magnetic data in this area exist. The first (Howitt et al, 1975) only deals with the area south of 58° N. They calculate a maximum general thickness of 1000 m. with three possible vent sites identified by anomalously thick sequences of up to 1500 m. The models derived in this research show thicknesses of 3-4 km. in this area. A second previous interpretation is presented in Woodhall and Knox (1979). This is based on a marine magnetic data set rather than the aeromagnetics used here. Unlike Howitt et al (1975) their data covers the whole of the Piper-Forties Volcanic Province area. Their isopach for the basalts is shown in figure 4.19. This is derived by a combination of magnetic modelling and well data. Their model indicates thickness of more than 3 km. in the north Buchan Graben area (similar results are shown in figure 4.18) and the possibility of even thicker sequences in the Witch Ground Graben. These results are more akin to the results obtained in this research however, they do not recognise any large thickening of the basalt sequence just north of 58° N. They point out that an appreciable proportion of inter-bedded sediments between the basalt sequences would serve to increase the calculated volume of the volcanics. Unfortunately they do not state the susceptibility contrast used in their modelling other than stating it was that "of basalt". If they used a higher value than the 0.00226 e.m.u. used in this research then their models would tend to show a thinner basalt layer.

4.4.3 Modelling the East Forties Basin Anomaly

The isolated nature of this anomaly and its near-symmetry makes its interpretation relatively easy. Rough depth estimates from spectral analysis show that the source is very deep (greater than 7 km). Its shape suggests that the source is an intrusive body. Howitt et al (1975) have interpreted it's minimum depth to be 8 km. It has never been sampled by drilling, so its age is unknown.

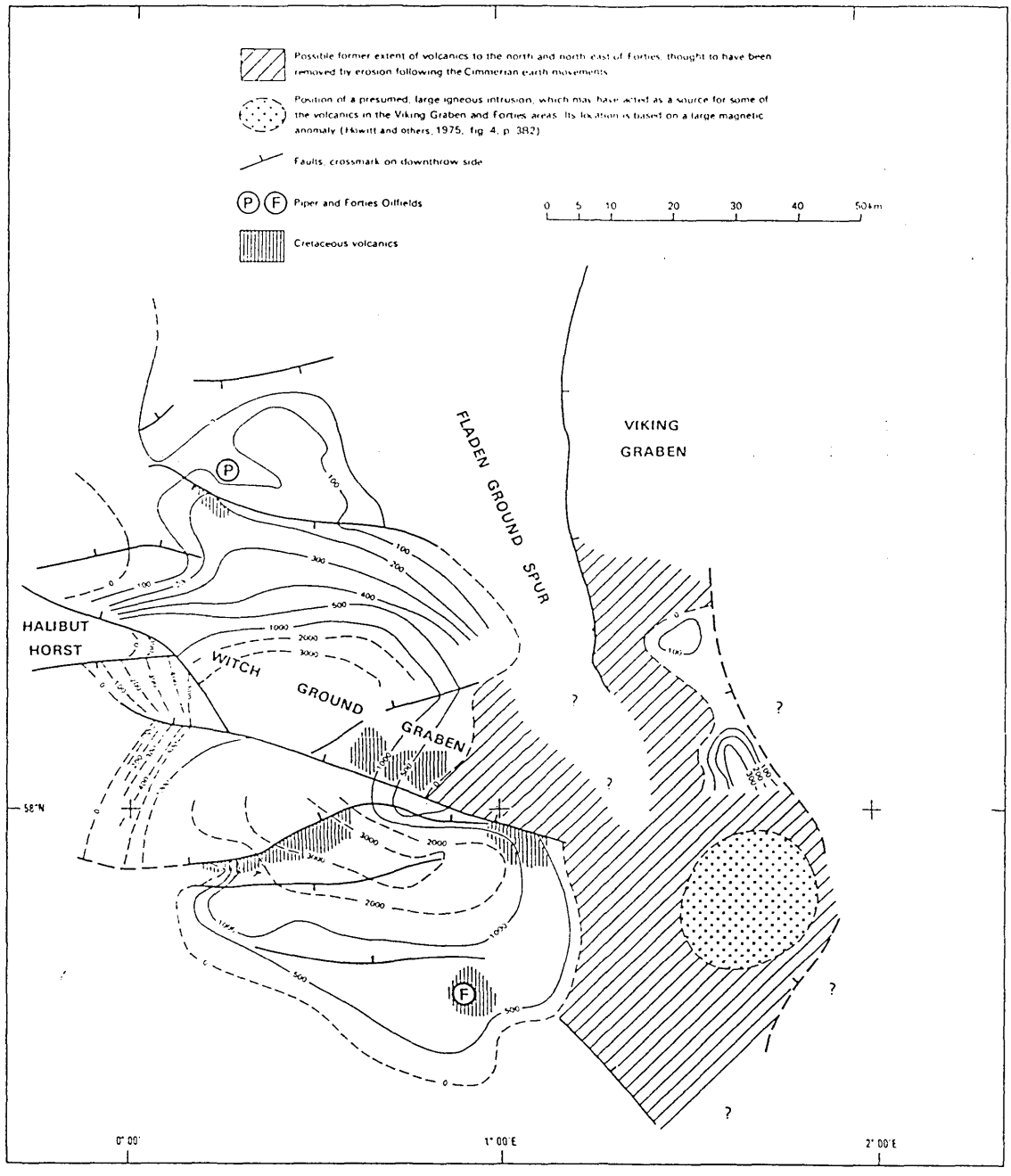


FIGURE 4.19 "The distribution of Mesozoic volcanics in the Eastern Moray Firth Basin", after Woodhall and Knox (1979). Thickness isopachs (in metres) for the Jurassic basalts are shown.

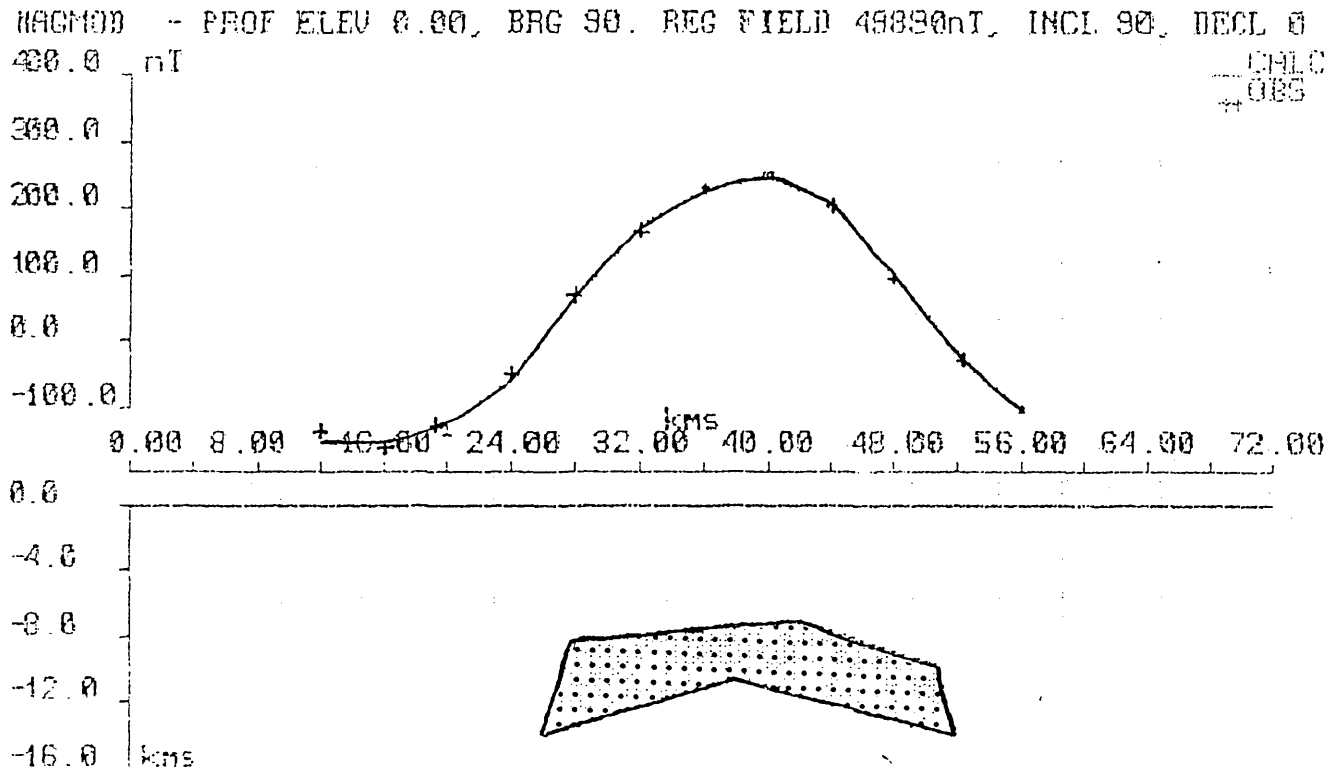


FIGURE 4.20 2.5D model of the East Forties Basin intrusion. See Magnetic Interpretation Overlay 2. Susceptibility contrast = 0.00787 e.m.u.

Woodhall and Knox (1979) suggest that it may have acted as a source for some of the volcanics seen in the South Viking Graben and Forties area (figure 4.19).

A single E - W profile was extracted from the magnetic data across the East Forties basin and modelled using the same 2.5D routine mentioned in 4.4.1. One solution is shown in figure 4.20.

4.5 SUMMARY

The most important conclusions of the present chapter are summarised as follows:

1) A compilation of all available aeromagnetic data for the study area can be used to map out the principal magnetic structures in the upper 18 km. of the crust.

2) The west (and particularly the south-west) of the study area is characterised by a complex collection of strong NE - SW trending lineations. These are interpreted as being caused by Caledonian faults and bodies in a relatively shallow basement.

3) A secondary weaker set of NW - SE trending lineations is present together with the Caledonian features in the south-west. Although their trend is characteristic of Cimmerian features they do not correlate with any known faults previously defined on seismic surveys.

4) The elongate Caledonian bodies are 'cut off' to the east by a poorly defined NNW - SSE trending lineation parallel to the Central Graben. The basement to the east of this line is at least 6 km deeper than that to the west of it. It may therefore represent a major discontinuity in the Caledonian basement.

5) The NNW - SSE structural trend is not at all represented in the magnetic field.

6) The Piper-Forties Volcanic province is very well defined by a large positive anomaly in the centre of the study area.

7) Many structures, particularly in the north such as the Caithness Ridge and Fladen Ground Spur have both distinctive magnetic and Bouguer anomalies associated with them.

8) There are at least three fairly strong Cimmerian trending (NW - SE) lineations in the Piper Embayment (Dutch Bank Basin).

9) Shaded relief images of the first horizontal derivative field proved to be very useful interpretation tools especially in delineating the weaker lineaments in the complex south-western part of the study area.

10) Spectral analysis can be used to provide rough depth estimates of the magnetic basement.

11) The basalts of the Piper-Forties Volcanic Field can be modelled along several profiles. The solutions show broad regional thickness variations of up to 8 km and a ponding of basalt in the Witch Ground Graben against the major fault separating it from the Buchan Graben. A possible vent site can be identified in the Witch Ground Graben.

12) The source of a large anomaly in the East Forties Basin is interpreted as a very large intrusive body occurring at depths in excess of 7 km. It may be possible that this could have served as a source for the nearby volcanics in the Forties and South Viking Graben Areas.

CHAPTER 5

COMBINING MAGNETIC AND GRAVITY MODELLING

5.1 INTRODUCTION

In chapter 3 models for the depth to the Moho were produced by modelling the residual gravity field after the effect of near-surface layers had been stripped off. Several solutions were obtained, the best of which is shown in figures 3.28 and 3.29. It was noted that in several places the Moho appears to be more shallow than might be expected. This is the case in the areas of the East Forties Basin, the Forties-Montrose Ridge and the Witch Ground and Buchan Grabens. If the models are indeed incorrect and the Moho in these areas is deeper than the best solution suggests, it follows that the amplitude of the residual gravity field has been over-estimated (i.e. it is too positive in the above areas). The residual field is the filtered result of subtracting the calculated gravitational effect of the near-surface layers from the Bouguer anomaly for the study area. There are two principal causes which would result in this residual field being too positive:

1) The negative gravitational effect of the near-surface layers has been over-estimated.

2) A positive gravitational effect (other than that caused by the Upper Mantle) has not been recognised and taken into account.

Since the effect of sediments occurring below the Base-Cretaceous has not been calculated it is unlikely that the total effect of the near-surface layers has been over-estimated. The very localised nature of the anomalously shallow Moho (especially in the East-Forties Basin) also tends not to support the first conclusion. The second conclusion therefore, seems to be the more likely of the two.

A positive gravity anomaly could only be the result of rocks with a larger density than the 2.75 g cm^{-3} used to represent crystalline basement. Such high densities are generally limited to mafic igneous and metamorphic rheologies. It follows that such rocks are also likely to have a characteristic magnetic signature. In the previous chapter a detailed interpretation of the magnetic data for the study area was presented. In this chapter the results of this interpretation are combined with gravity modelling in order to improve the models presented at the end of chapter 3.

In section 5.2 the magnetic field is re-analysed and compared directly to the model for the Moho shown in figures 3.29 and 3.30. Areas where the crust is anomalously thin which also have an associated distinctive magnetic anomaly are identified. The next section outlines the calculation of a pseudo-gravitational anomaly made directly from the magnetic data. This technique is commonly used to identify magnetic bodies which may also have a strong gravitational signature.

In section 4.4 the results of magnetic modelling in the Piper-Forties Volcanic Province and the East Forties Basin were presented. Section 5.4 of this chapter shows how these models are used to calculate gravity anomalies, whilst section 5.5 shows the final results of 3D modelling after these effects have been removed from the residual field. This section is followed by an attempt to quantify the additional errors introduced during the revised modelling process.The chapter ends with a brief summary of the most important conclusions made in this chapter.

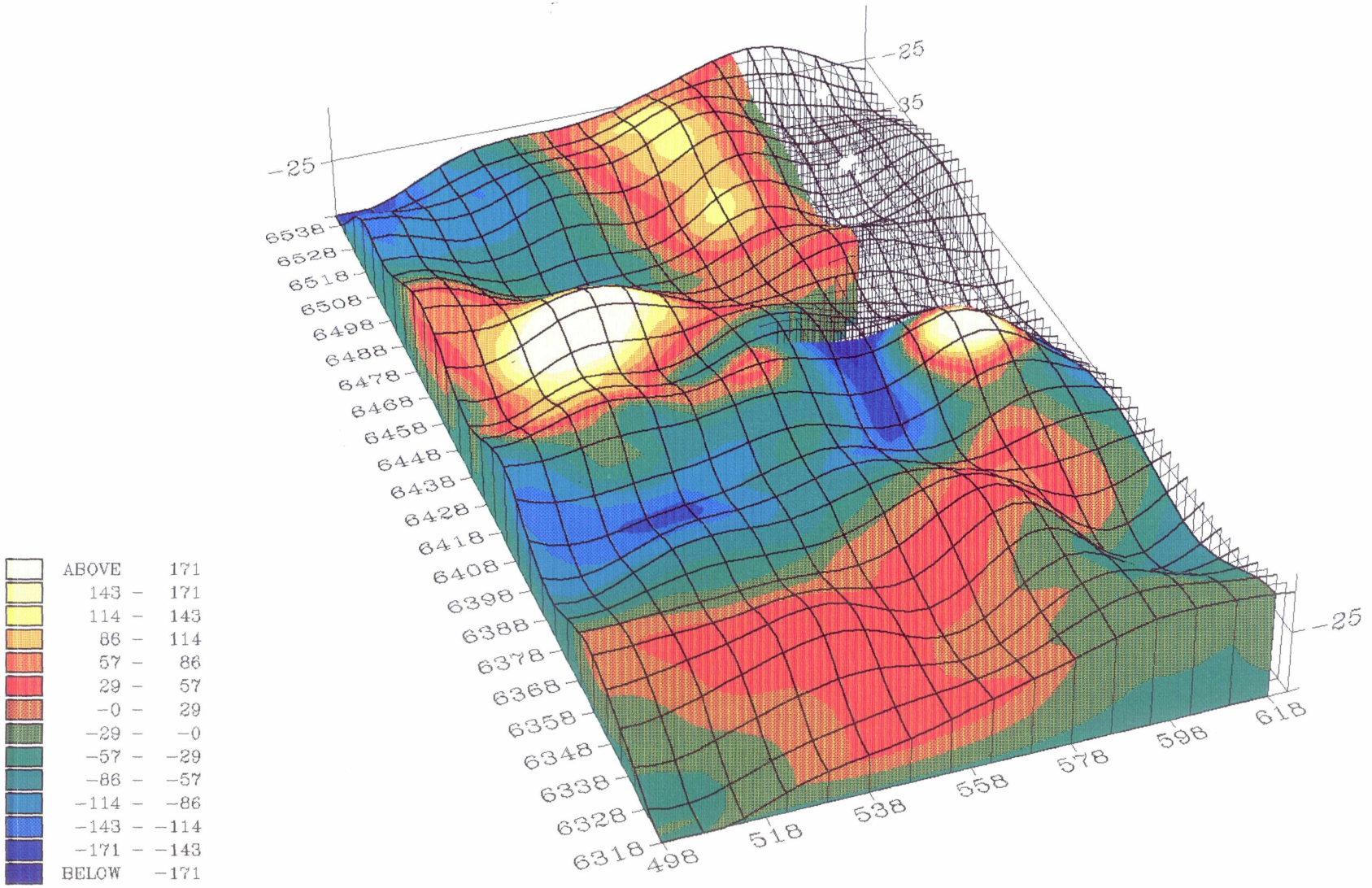
5.2 THE RELATIONSHIP BETWEEN THE MODELLED MOHO AND THE MAGNETIC FIELD

Figure 5.1 is a four-dimensional image showing the relationship of the magnetic field with the Moho topography derived from gravity modelling (see figures 3.28 and 3.29). The vertical axis of the plot represents the Moho whilst the overlying contour plot is the magnetic field for the study area.

In the west the large magnetic anomaly caused by the basalts of the Piper-Forties Volcanic Province coincides with the area of anomalously thinned crust in the Witch Ground Graben and to a lesser extent with that in the Buchan Graben. The basalts in this area have been dated as Callovian (approx 160 Ma) in age (Richie et al, 1988) and only sequences down to the Base-Cretaceous have been accounted for in the gravity modelling. If they have a significantly large and positive gravitational effect, then not including them in the modelling process may have resulted in large errors in the solution. This may explain why the crust appears to be anomalously thin in this area.

The only other coincidence of anomalously thin crust with high amplitude features in the magnetic field occurs in the East Forties Basin. The source of this magnetic anomaly was modelled as being a large mafic intrusion with a minimum depth of approximately 7 km (see 4.4.3). As with the Piper-Forties basalts the gravitational effect of this body was not accounted for in the gravity modelling process. The relatively isolated nature of the region of thinned crust in this area (figure 3.28) strongly suggests that it may be a modelling error caused by ignoring the effect of this intrusive body.

FIGURE 5.1 'Four-dimensional' image showing the relationship between the magnetic field and the modelled Moho topography. The magnetic field is represented by contours (interval = 30 nT) and the surface represents the depth to the Moho (see figures 3.28 and 3.29).


ABOVE 171
143 - 171
114 - 143
86 - 114
57 - 86
29 - 57
-0 - 29
-29 - -0
-57 - -29
-86 - -57
-114 - -86
-143 - -114
-171 - -143
BELOW -171
-25
35
-25
6538
6528
6518
6508
6498
6488
6478
6468
6458
6448
6438
6428
6418
6408
6398
6388
6378
6368
6358
6348
6338
6328
6318
498
518
538
558
578
598
618
-25

5.3 CALCULATING THE PSEUDO-GRAVITATIONAL FIELD

The magnetic and gravitational fields associated with any given source are implicitly related to each other by Poisson's Relation which states:

$$V = \frac{J}{G\Delta\rho} \frac{\delta U}{\delta i}$$

Where: V = magnetic potential
U = gravitational potential
$\Delta\rho$ = density contrast
J = magnetisation intensity
i = direction of magnetisation
G = Universal Gravitational Constant

Thus it is possible to transform measured magnetic field values to what might have been the gravity anomaly if a density contrast exists. The resulting values make up what is known as a 'Pseudogravity' field. The prefix 'Pseudo' is used as the source of the magnetic anomaly need not actually have an associated gravity anomaly.

In the previous section two areas of interest were identified from the magnetic data. The causative bodies of these two anomalies have been modelled as either sequences of basalts or gabbroic intrusions. Such lithologies generally have characteristically high densities (Telford et al, 1976) and will therefore almost certainly have associated gravity anomalies. Thus the pseudogravity field calculated from the magnetic data in these areas should (in shape at least) be similar to the actual gravitational field associated with these bodies.

Baranov (1957) describes the spatial convolutions required to produce a pseudogravity field from magnetic data. The whole procedure can be carried out by deconvolution in the wavenumber domain by applying the transfer function W_{PG}

to the Fourier transform of the magnetic field where:

$$W_{PG} = \frac{G}{4T_0} \frac{\Delta\rho}{\Delta k} \frac{e^{\Delta hr}}{r} \bullet W_{MP}$$

and W_{MP} is the transfer function for calculating magnetic pole reduction given by:

$$W_{MP} = (\sin I_E + i\cos I_E \bullet \sin(D_E + \theta))^{-2}$$

Where:

I_E and D_E are respectively the inclination and declination of the Earth's magnetic field.

G = Universal Gravity Constant

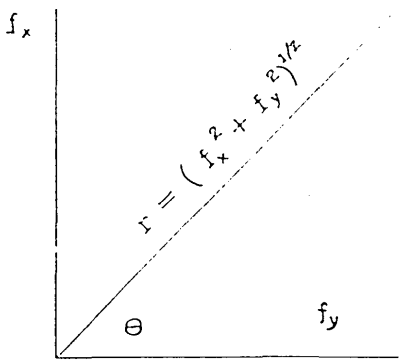
T_o = Geomagnetic field intensity

Δk = Average susceptibility contrast

$\Delta\rho$ = Average density contrast

Δh = Mean separation between aeromagnetic survey altitude and gravity survey elevation.

r and θ are defined by:



where f_x and f_y are wavenumbers in the x and y directions.

After reducing to pole, the magnetic data was filtered in the wavenumber domain using the transfer function W_{PG} as defined above. The result is shown in figure 5.2. Note, all data east of the Fladen Ground Spur down to the northern

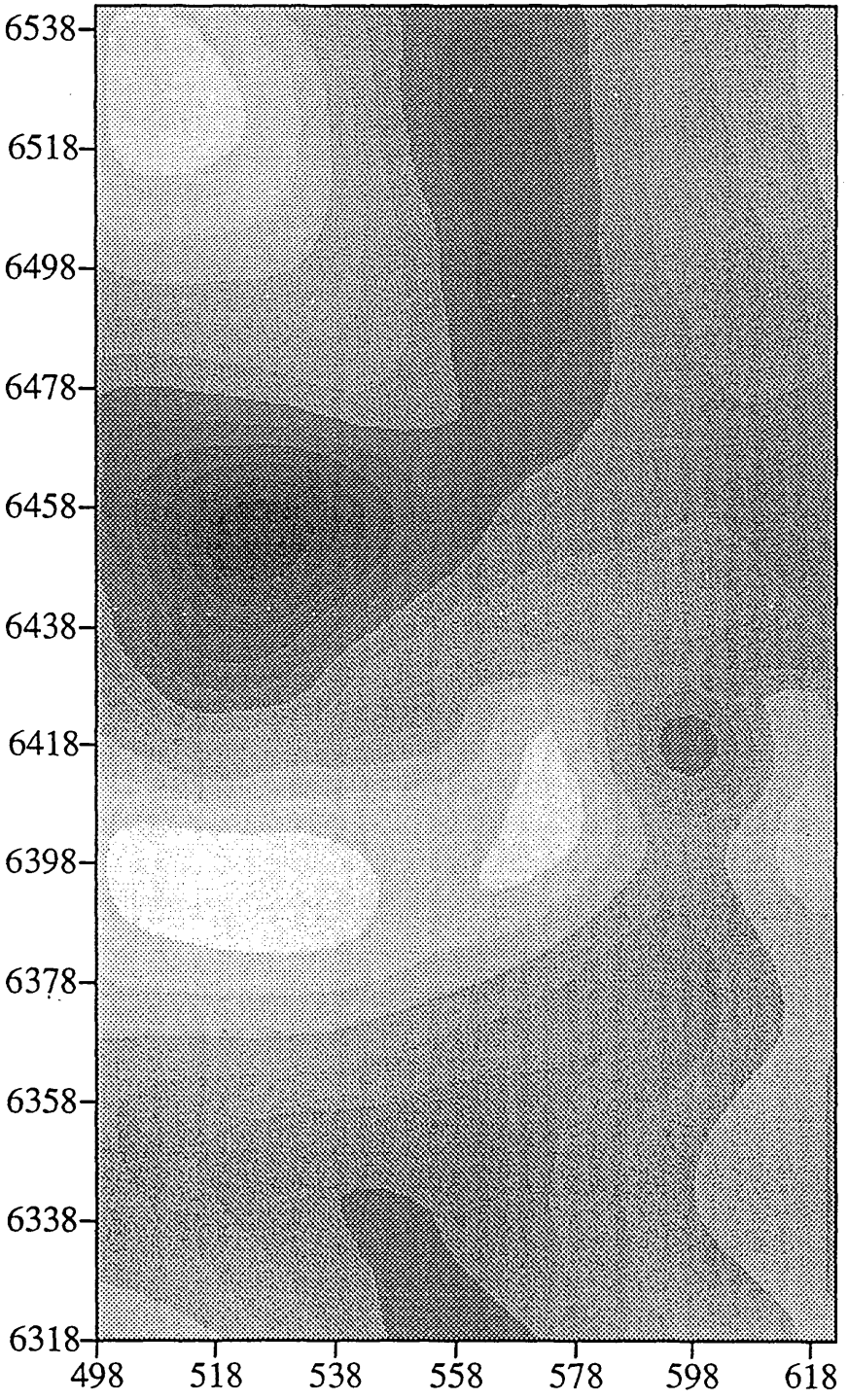


FIGURE 5.2 Unscaled pseudogravity calculated for the study area. The north-eastern area of the plot is interpolated since there are no aeromagnetic data for this area.

side of the East Forties Basin is unreliable. This area of the grid is normally masked by dummy values. To make the pseudogravity calculation possible these dummy values were replaced with values of 0 nT. The average density and susceptibility contrasts together with the Geomagnetic Field Intensity and the Gravity Constant are all constant values and have been taken out of the calculation for the pseudogravity field. The values shown in figure 5.2 could, in theory, be multiplied by the coefficient defined by these constants to yield a quantified estimation of the gravity field. However the uncertainties involved with the density and susceptibility contrasts are so great that such a quantification is pointless. This is especially true when, as in this study, no information regarding remanent magnetisation is known. The average effective susceptibility contrast is partially dependent on the direction of remanent magnetisation. Thus, it could be reduced to an effective zero value which would make the scaling coefficient infinitely large.

The pseudogravity field can therefore, only be used in a qualitative manner to outline the shape of the gravity field associated with the magnetic bodies. If however, a constant density and susceptibility contrast for the whole study area can be assumed then it is possible to scale the pseudogravity field to any given value. Figure 5.3 shows the result of scaling to a maximum value of 30 mGal. As expected the Piper-Forties Volcanic Province has a large pseudogravitational signature. The East Forties Basin intrusion also has a significant signature albeit relatively small when compared with that of the Piper-Forties basalts. It should be noted however, that this technique relies entirely on the assumption of a constant susceptibility and density contrast for the whole of the study area and this is not likely to be the case.

5.4 CALCULATING THE GRAVITY FIELD FROM MAGNETIC MODELS

In section 4.4 of chapter 4 the large magnetic anomalies associated with the Piper-Forties Volcanic Province and the East Forties Basin were modelled in 2.5

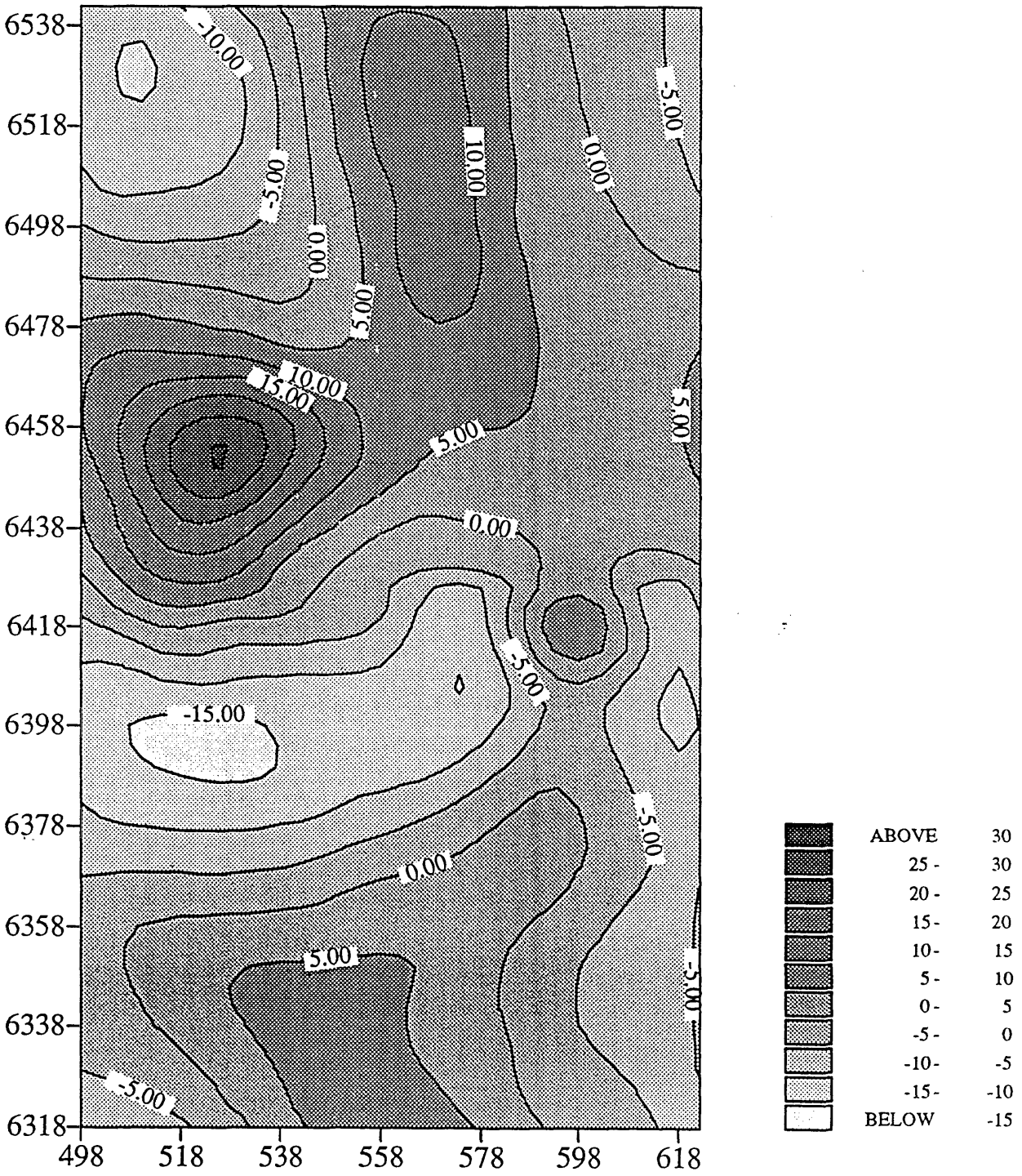


FIGURE 5.3 Pseudogravity scaled to a maximum value of 30 mGal. The north-eastern area of the plot is interpolated since there are no aeromagnetic data for this area.

dimensions. It is possible to calculate the gravitational effect associated with these areas using these magnetic models and estimations of the density contrasts associated with the causative bodies.

Digital grids of both the top and bottom surfaces of the bodies defined by magnetic modelling were produced using the minimum curvature method outlined in 3.2.2. Taking each area separately the Plouff three-dimensional gravity modelling program (see 3.4.1.3) was used to calculate the gravitational effect of each body.

Telford et al (1976), state that the average density of basalt is approximately 3.0 g cm^{-3}. This is equivalent to a density contrast of 0.25 g cm^{-3} with respect to the 2.75 g cm^{-3} taken as the density of crystalline basement. The calculated gravity anomaly for the Piper-Forties Volcanic Province using this density contrast is shown in figure 5.4. Values reach a maximum of approximately 31 mGal in the centre of the field where the basalt is modelled as being thickest (up to 8 km in the interpreted vent site).

Calculating the gravitational effect of the East Forties Basin intrusion is more problematical than the calculation made for the Piper-Forties Basalts. Firstly, the intrusive body has never been directly sampled. It's lithology can therefore only be estimated. Its proximity to the Piper-Forties basalts suggests that it is not unreasonable to assume a similar source for both magmatic areas. The intrusive equivalent of basalt is gabbro. The susceptibility contrast of 0.00727 e.m.u. used in the magnetic modelling is slightly on the high side for gabbro (Telford et al, 1976 quote a range of between 0.00008 and 0.0072 e.m.u with an average of 0.006 e.m.u.), although not enormously so. The second problem is that while the upper surface of the body is relatively simple to define using magnetic modelling, the lower surface is far more difficult. Since the calculation of the gravitational effect of the body is dependent on its volume, the ambiguity associated with the depth of its lower surface becomes a significant source of error.

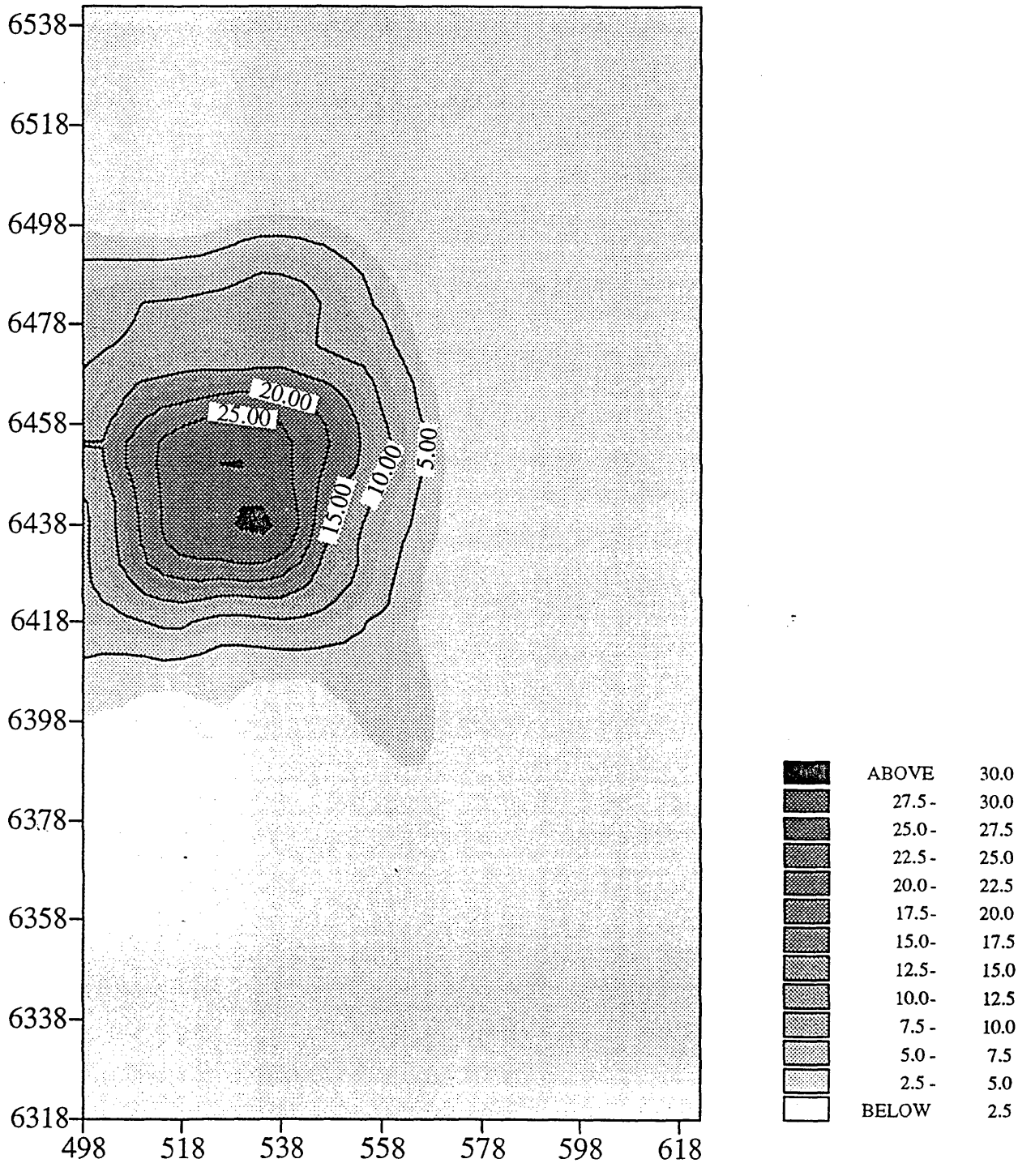


FIGURE 5.4 Estimated gravitational effect of the Piper-Forties basalts. Units are mGals.

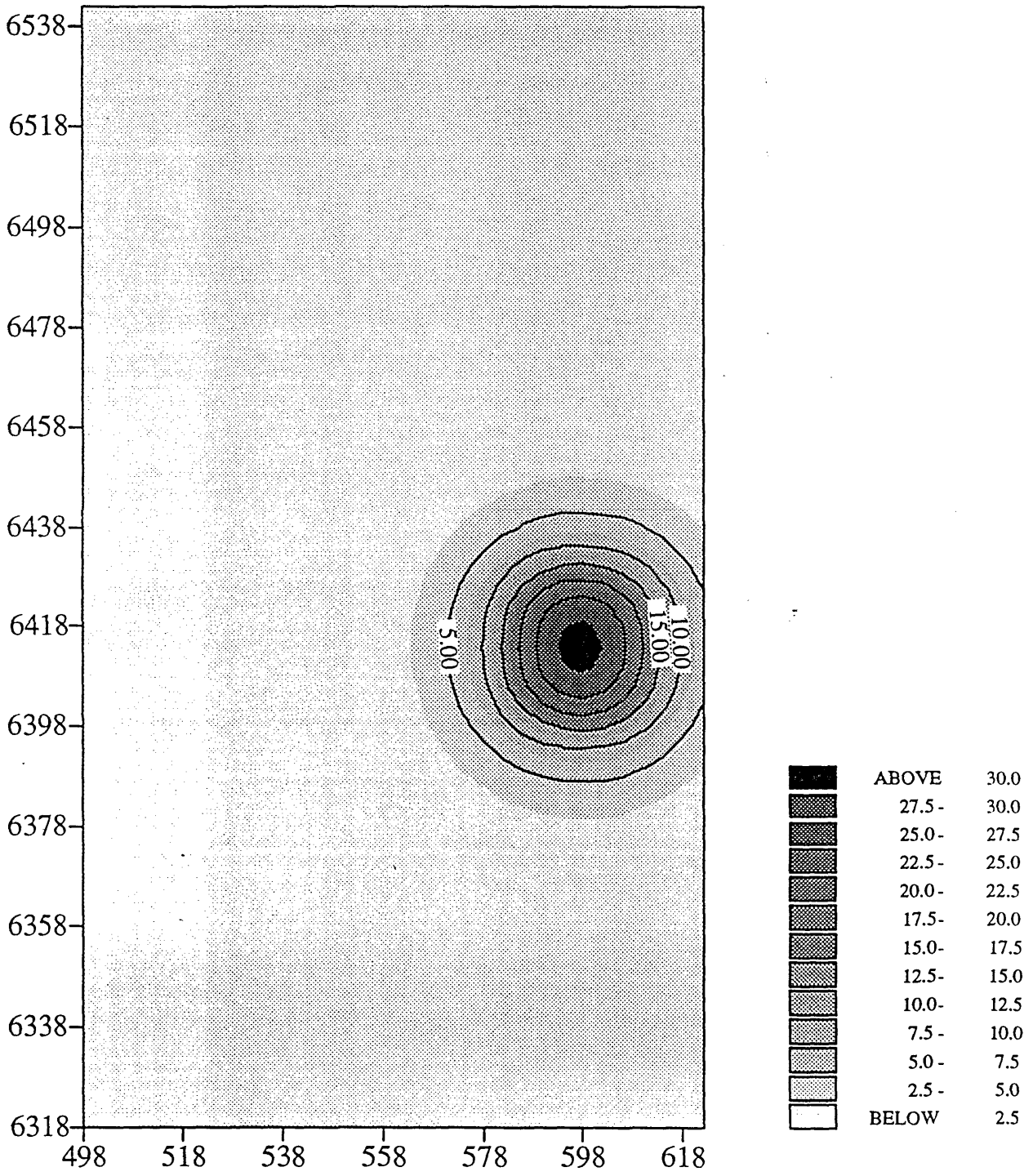


FIGURE 5.5 Estimated gravitational effect of the East Forties Basin intrusion. Units are mGals.

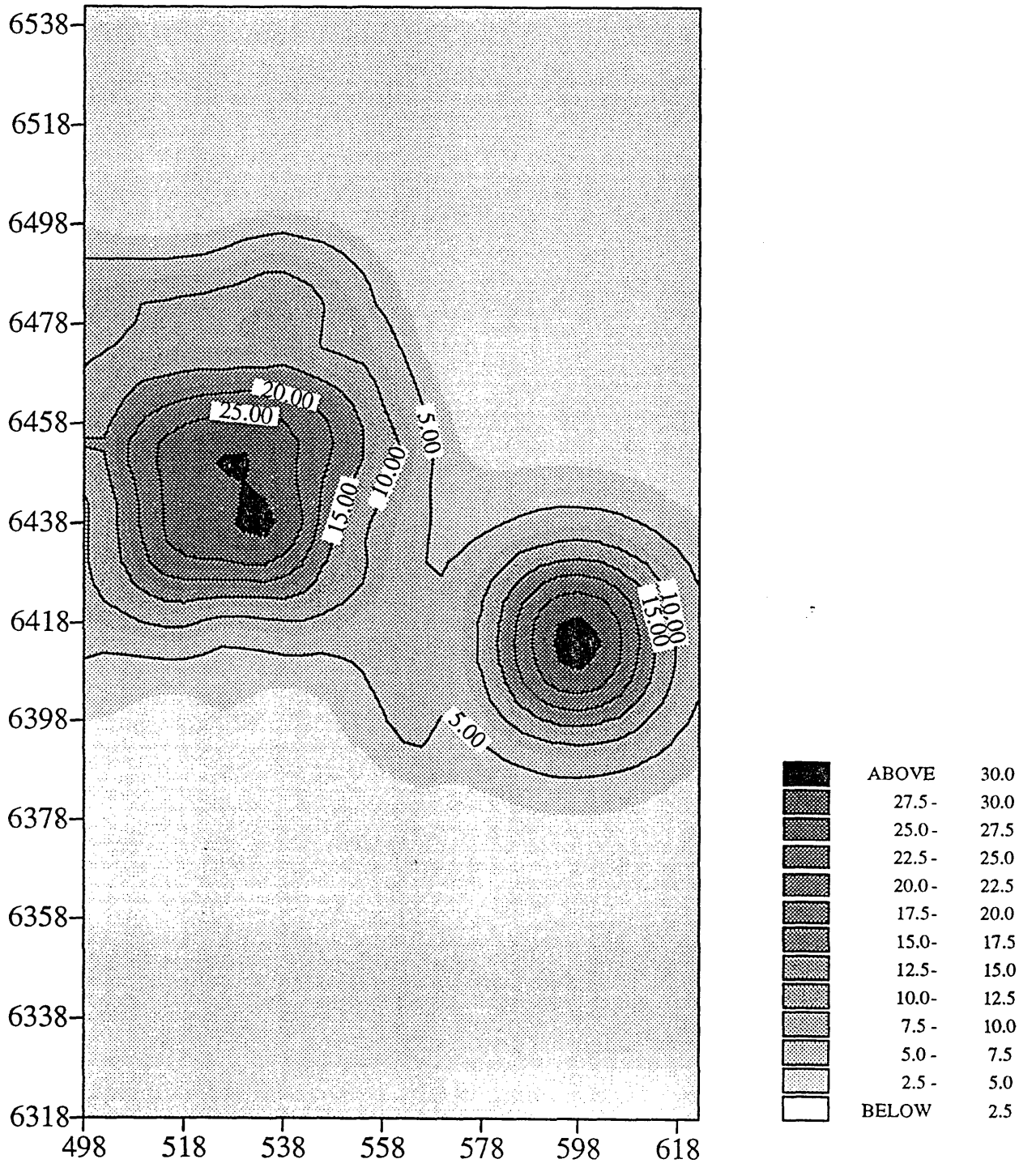


FIGURE 5.6 Total estimated gravitational effect of igneous bodies in the study area. Units are mGals.

Telford et al (1976) quote an average density of 3.03 g cm^{-3} for gabbro giving a density contrast of 0.28 g cm^{-3} with respect to the 2.75 g cm^{-3} taken as the density of crystalline basement. Figure 5.5 shows the calculated gravity anomaly for the body using this density contrast and the model shown in figure 4.20. As in the case of the Piper-Forties basalts the anomaly reaches a maximum of approximately 31 mGal although the effect is concentrated on a smaller area reflecting the smaller spacial extent of the East Forties Basin body.

Figure 5.6 shows the total effect of both the Piper-Forties basalts and the East Forties Basin intrusion. Figure 5.7 shows the result of subtracting this field from the un-filtered residual field calculated in 3.4.1. (figure 3.16). A comparison of this revised field with that shown in figure 3.16 shows that the isolated high associated with the East Forties Basin has been removed. In the west the broad E - W trending high associated with the Witch Ground and Buchan Grabens has also been reduced in size especially in the north of this area.

Before this new residual field can be used as an input to the 3D iterative forward modelling routine it needs to be smoothed using the low-pass filtering technique outlined in 3.4.2.1. The azimuthally averaged power spectrum of the new field is shown in figure 5.8. The useful part of the spectrum is divided into 9 straight-line segments each of which corresponds to a particular depth of source ensembles (See 3.4.2.1 and Spector and Grant, 1970). With reference to this spectrum the data was filtered using a low-pass rectangular box-car filter modified by a cosine taper defined by cut-off wavelengths of 34.5 km and 24.5 km. The filtered result is shown in figure 5.9. Values range between approximately 8 and 118 mGal the largest values occurring in the extreme south-east over the Central Graben and in the centre of the triple-junction area.

The filtered field was then used as an input to the 3D automatic iterative forward modelling routine outlined in 3.4.3. The next section shows the results obtained during the modelling process.

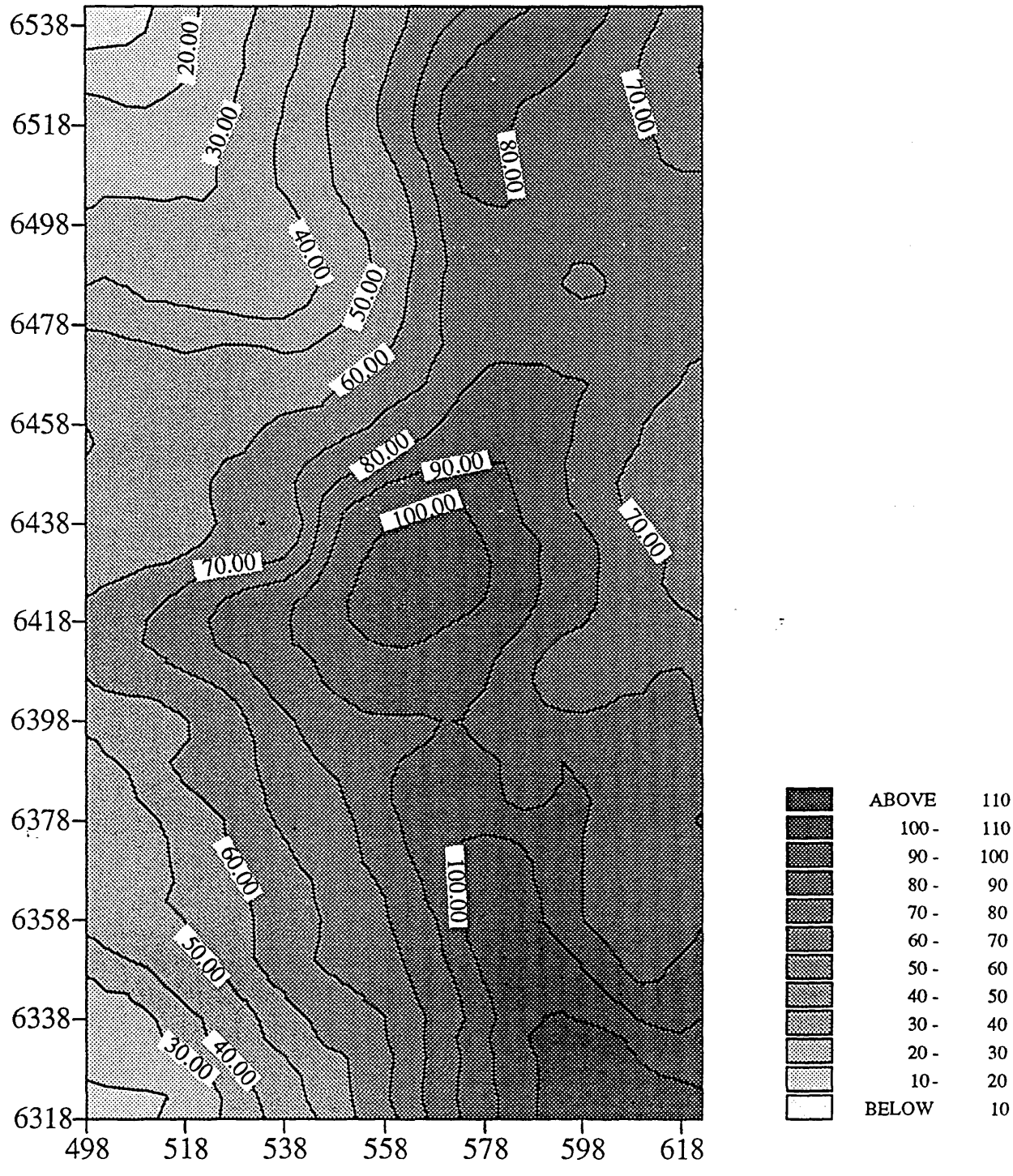
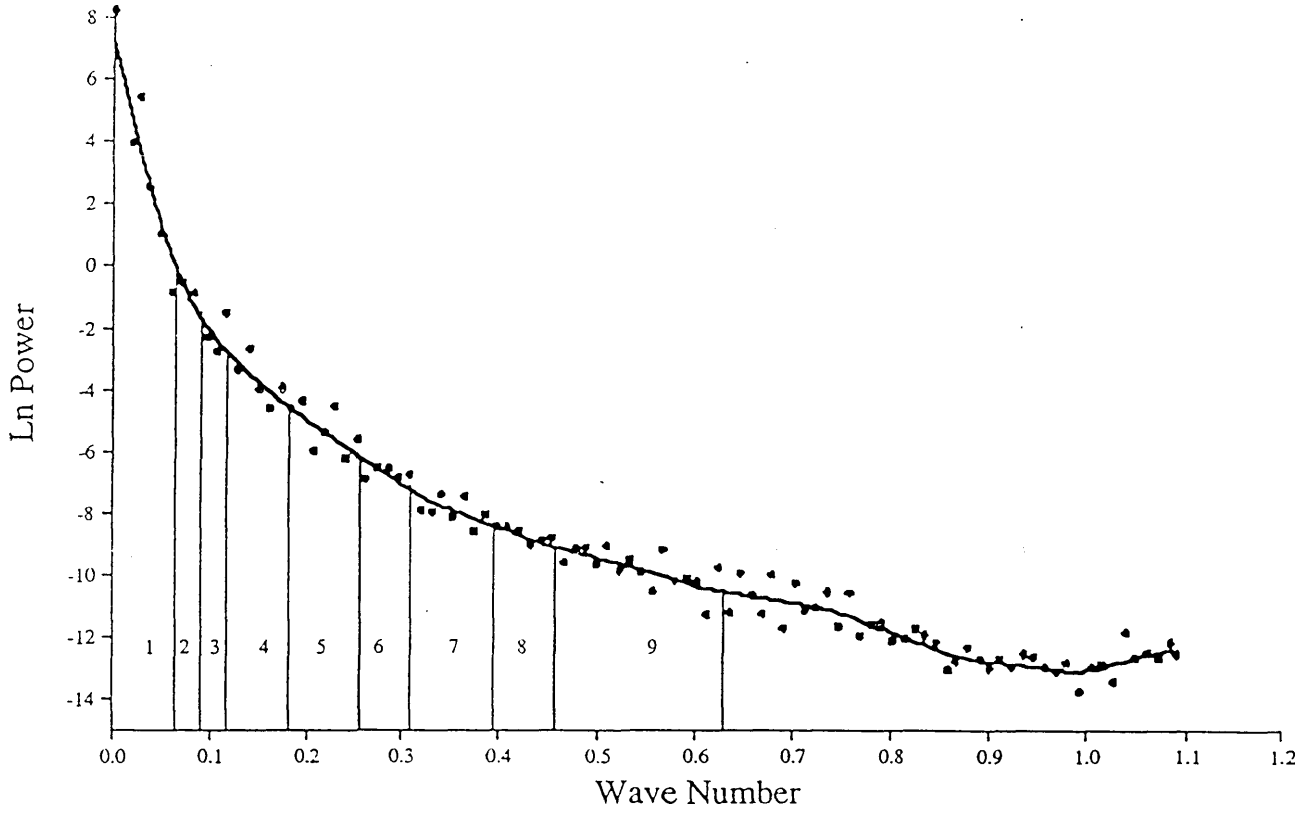


FIGURE 5.7 Result of subtracting the total estimated gravitational effect of igneous bodies from the unfiltered residual gravity field (see figure 3.16).



Segment	Wave No. Range	Av Depth(km)	Max.Wavelength (km)
1	0.000-0.064	58.3	98.2
2	0.064-0.090	32.1	69.8
3	0.090-0.117	23.1	53.7
4	0.117-0.182	14.1	34.5
5	0.182-0.257	11.3	24.5
6	0.257-0.310	8.7	20.3
7	0.310-0.395	7.2	15.9
8	0.395-0.458	5.2	13.7
9	0.458-0.629	4.0	10.0

FIGURE 5.8 Power Spectrum of the modified residual gravity field (explanation in text).

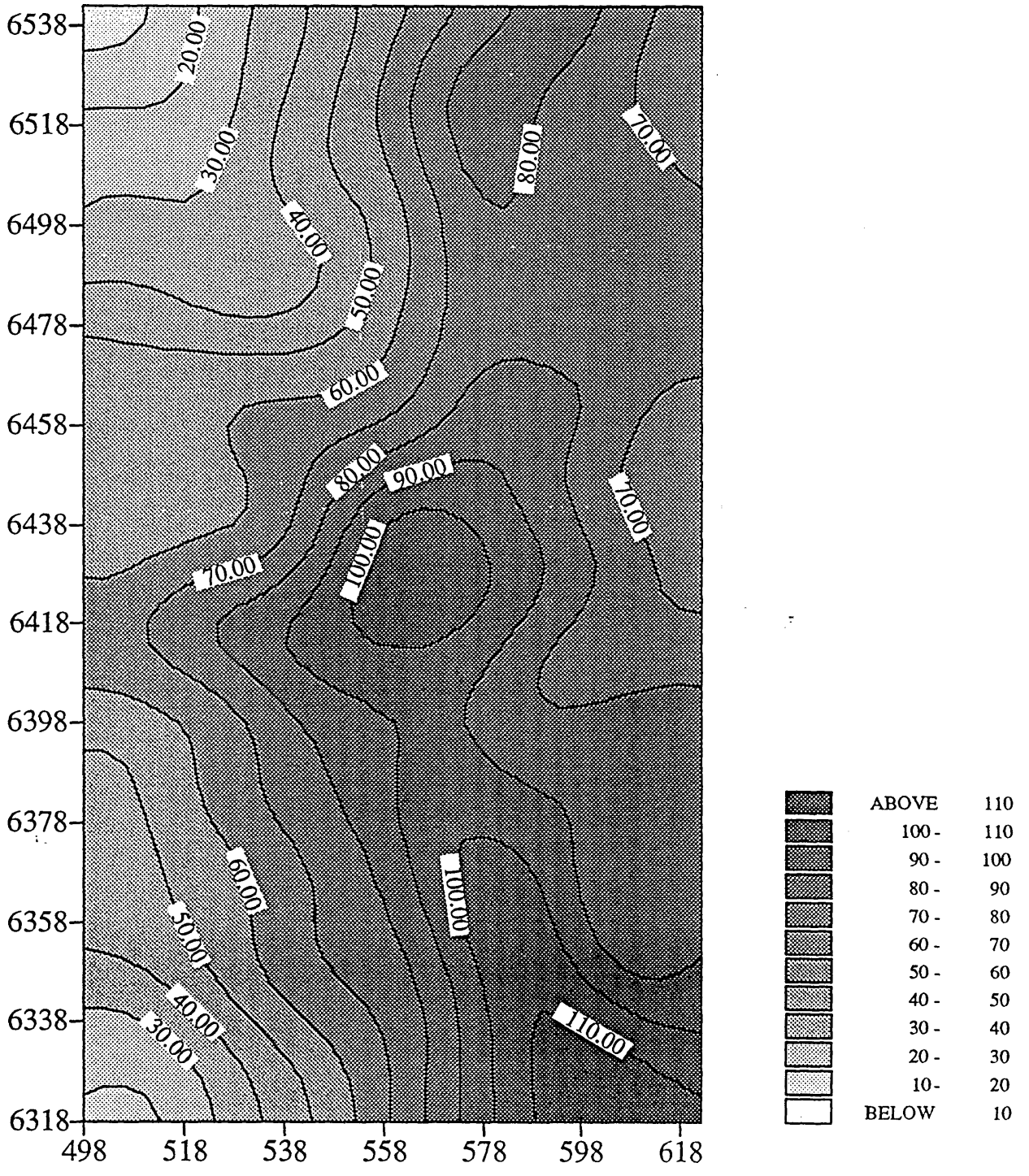


FIGURE 5.9 Modified residual gravity field after low-pass filtering. Units are mGals.

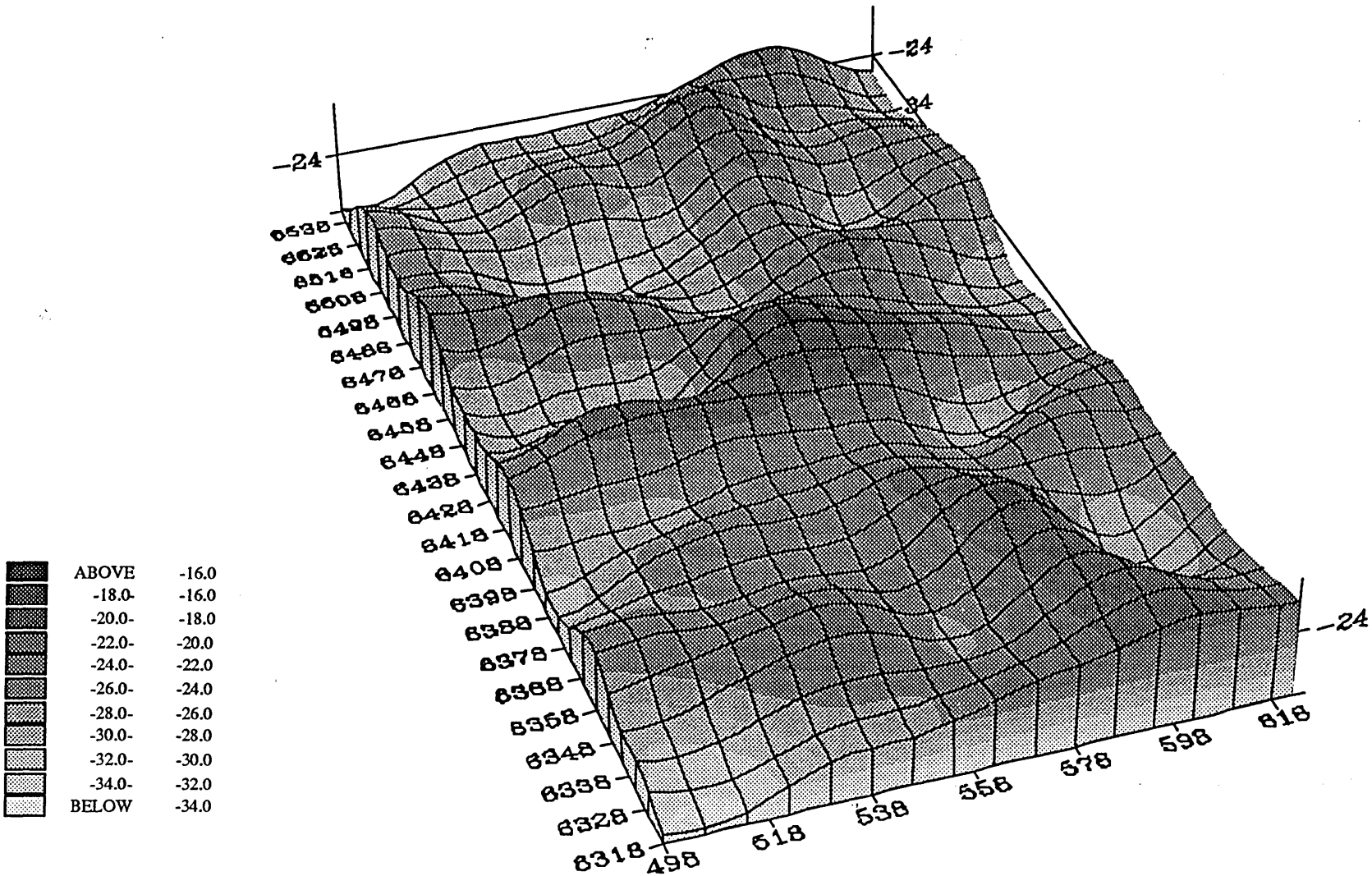
5.5 RESULTS OF 3D MODELLING

Figure 5.10 is an isometric plot of the solution obtained after 20 iterations using the filtered version of the revised residual field and a density contrast of 0.5 g cm^{-3} for the Upper-mantle body. Figure 5.11 is the same solution shown as a grey-scale contour map. The goodness-of-fit for this solution is shown in figure 5.12.

The Moho is at its shallowest over the Central Graben and in the centre of the 'triple-junction' area where it occurs at depths of approximately 16 km. Unlike the model shown in figures 3.28 and 3.29 there is no isolated 'high' in the Moho topography in the East Forties Basin area. Removing the effect of the intrusive body has therefore been very effective in reducing the Moho topography in this region. A similar effect is seen in the Witch Ground Graben area. The model shown in figures 3.28 and 3.29 shows the Moho topography to be approximately equal below the Witch Ground and Buchan Grabens. Removing the gravitational effect of the Piper-Forties basalts results in a deepening of the Moho below the Witch Ground Graben.

Figure 5.13 shows the difference (in kilometres) between the depth to the Moho calculated in chapter 3 (figures 3.28 and 3.29) and the depth to the Moho calculated using the revised residual gravity field (figures 5.10 and 5.11). The negative areas on this plot represent regions where the earlier model has a shallower Moho than the final model. In the East Forties Basin the later model has the Moho more than 10 km deeper than the earlier model. In the Witch Ground Graben area the effect is more diffuse although the final model is still deeper by some 8 km at the centre.

FIGURE 5.10 Isometric projection of the solution obtained after 20 iterations using filtered modified residual gravity. The surface represents depths to the Moho (in kilometres) for the study area.


ABOVE -16.0
-18.0- -16.0
-20.0- -18.0
-22.0- -20.0
-24.0- -22.0
-26.0- -24.0
-28.0- -26.0
-30.0- -28.0
-32.0- -30.0
-34.0- -32.0
BELOW -34.0
-24
-24
-24
6538
6528
6518
6508
6498
6488
6478
6468
6458
6448
6438
6428
6418
6408
6398
6388
6378
6368
6358
6348
6338
6328
6318
498
518
538
558
578
598
618

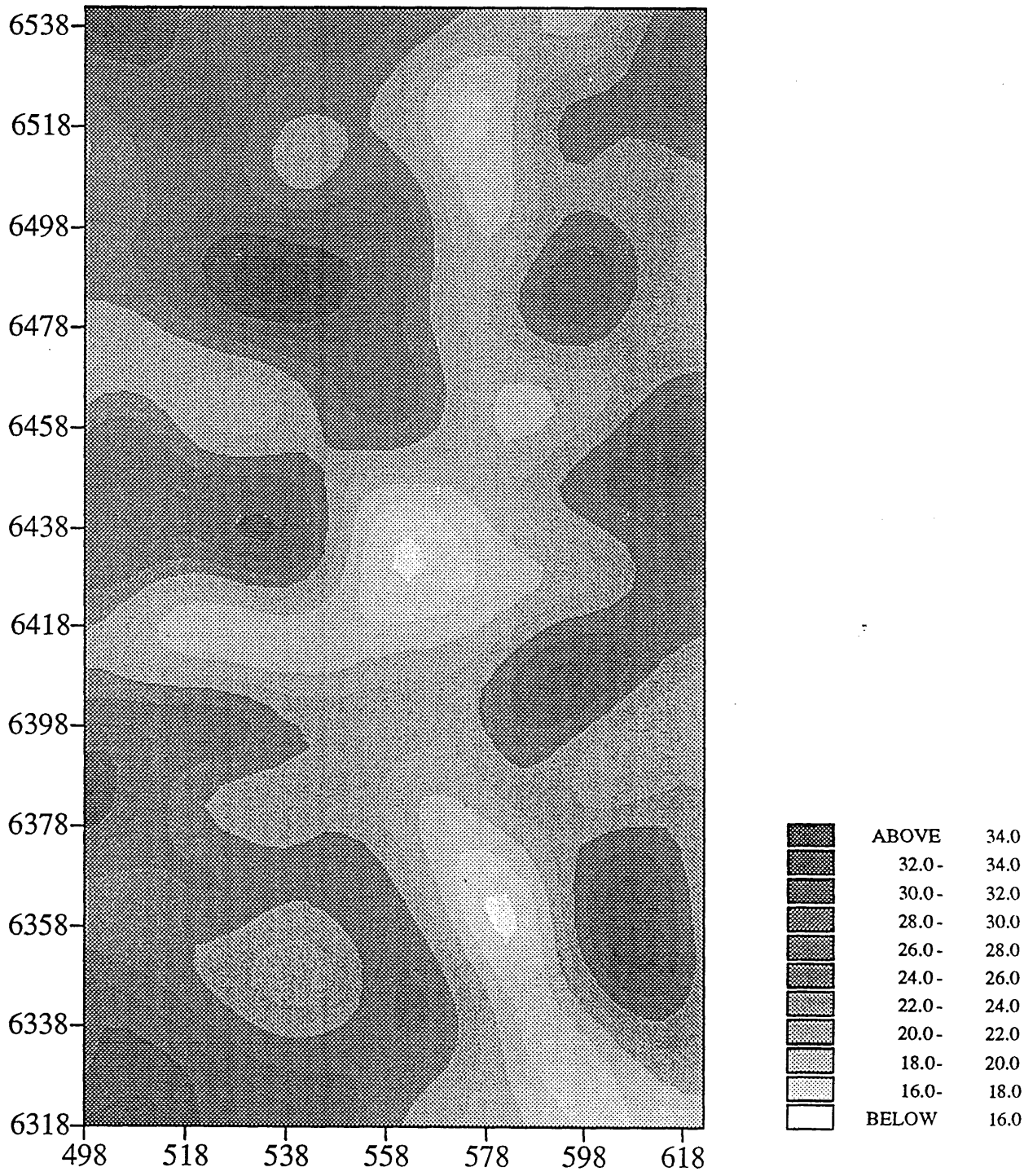


FIGURE 5.11 Grey-scale contour map of the solution obtained after 20 iterations using filtered modified residual gravity. Depths are in units of kilometres.

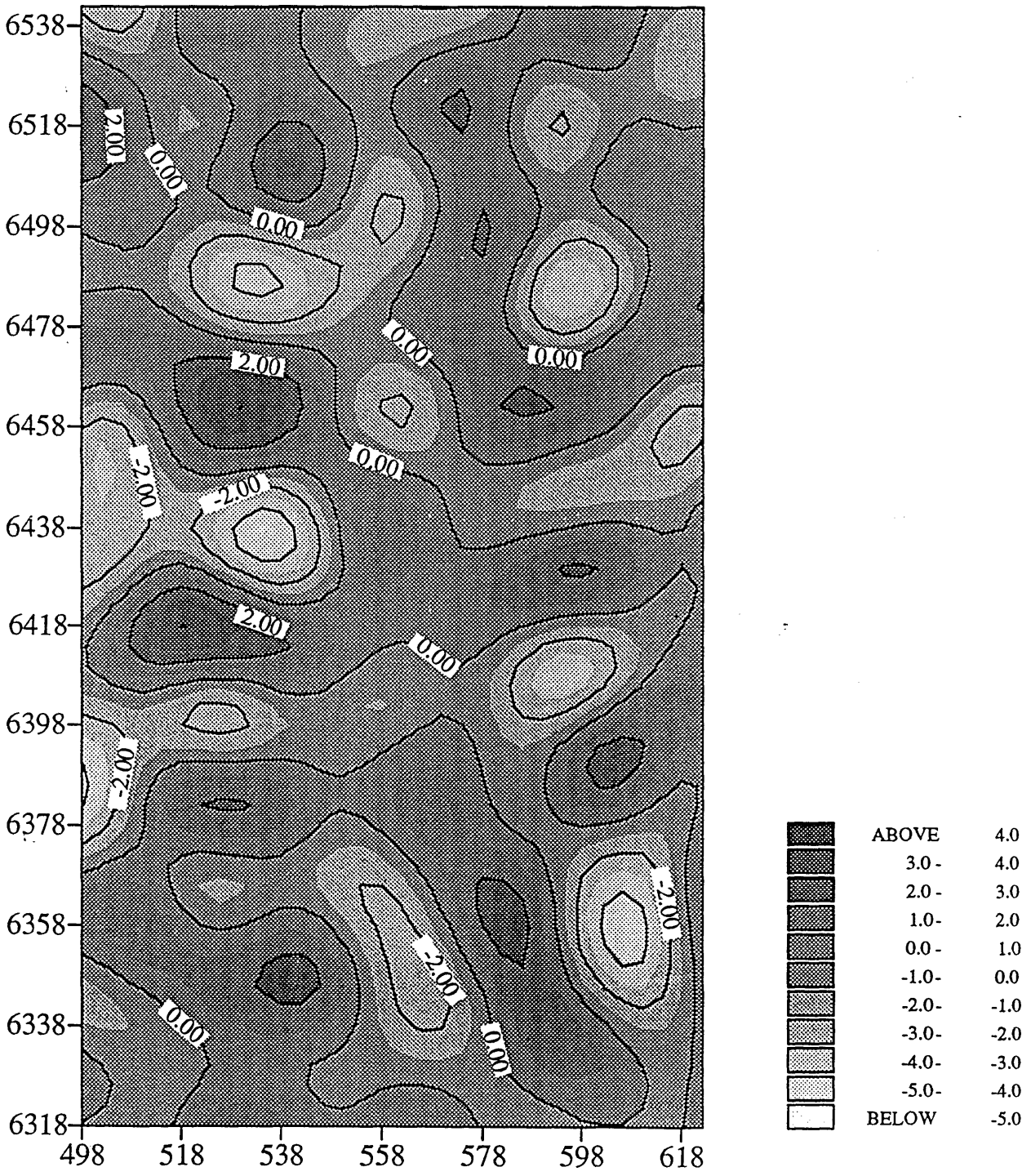


FIGURE 5.12 Grey-scale contour map representing 'goodness of fit' (i.e. the difference between the residual gravity and that calculated for this solution) for the solution obtained after 20 iterations using filtered residual gravity. Contours are in units of 1 mGal.

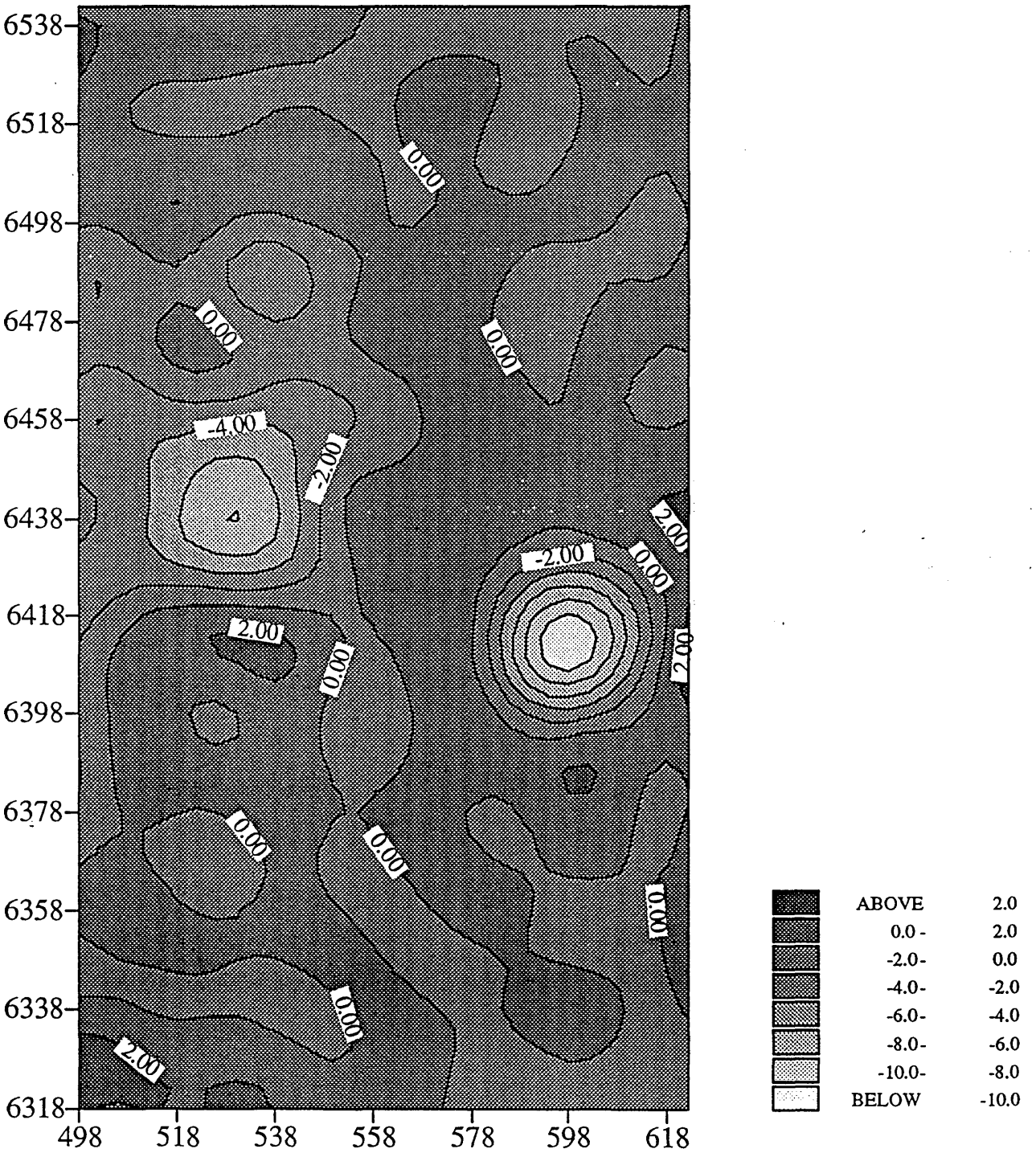


FIGURE 5.13 The difference (in kilometres) between the depth to the Moho calculated in Chapter 3 (figures 3.28 and 3.29) and the depth to the Moho calculated using the modified residual field which has accounted for the effect of igneous bodies in the area.

5.6 ESTIMATION OF ERRORS

The final model is a definite improvement on any of the earlier attempts at modelling the Moho. Errors over most of the study area will be the same as those quantified in 3.5.4 i.e. approximately +/− 1.5 km. However, an extra level of uncertainty has been introduced in the areas which have been modelled using the magnetic data. The ambiguities inherent in the magnetic modelling process and the subsequent calculation of the gravitational effect of the East Forties Basin intrusion and the Piper-Forties basalts were outlined in section 5.4 of this chapter. Quantification of these additional errors is very difficult. In section 3.5.4 of chapter 3 the total average error for the earlier models was calculated by quantifying the error at each stage of the modelling process in terms of miligals. These were summed and the total effect in terms of depth was calculated using the formula for a simple slab with an average density contrast of 0.5 g cm^{-3}. For an error of say 30 mGal the depth equivalent would be approximately 1.43 km. However, in this section a difference of approximately 31 mGal in the residual gravity over the East Forties Basin resulted in a difference in depth to the Moho of some 10 km. A similar difference but spread over a larger area for the Piper-Forties basalts, resulted in a smaller and much more diffuse effect in terms of depth. It seems that when the gravity error is concentrated over a very restricted area the resulting depth error cannot be estimated using a simple slab formula.

It is likely that the error in the calculated gravitational effect for the East Forties Basin intrusion is as much as 50 percent. Thus there is an additional uncertainty of approximately 5 km in the modelled Moho depth in this area. Magnetic models for the Piper-Forties basalts were better constrained than in the East Forties Basin. The error for the calculated gravitational effect of the basalts is estimated at 25 percent. This would cause an additional error of approximately 2 km in the modelled depths for this area.

An interesting point to note is that the location of magmatism may be governed (at least partially) by the location of areas where the crust is particularly

thin (see 6.5). If this is the case then it is likely that beneath centres of magmatism such as the East Forties Basin and the Piper-Forties Volcanic Province the crust may indeed be anomalously thin. Thus the model shown in figures 5.10 and 5.11 where the anomalously shallow Moho has been deepened, may represent one extreme of the possible solutions. A more realistic answer may lie somewhere between this model and those presented in chapter 3.

5.7 SUMMARY

The most important procedures and conclusions outlined in the present chapter are summarised as follows.

1) Using the model for depth to the Moho obtained at the end of chapter 3 it was noted that there were areas where the Moho appears to be anomalously shallow. A possible cause was identified as being the presence of large high-density bodies not accounted for in the gravity modelling.

2) Two areas where the Moho was modelled as being unusually shallow also have large associated magnetic anomalies. These were the East Forties Basin and the Piper-Forties Volcanic Province.

3) An attempt to quantify the gravitational effect of the bodies causing these large magnetic anomalies, by calculating the pseudogravity field for the study area proved unsuccessful. This was due to the uncertainties involved in making estimations of average density and susceptibility contrast for the whole area.

4) The total gravitational effect of the East Forties Basin intrusion and the Piper-Forties basalts was estimated using the magnetic models calculated for these areas in chapter 4. A revised residual gravity field was calculated using these estimations and a new model for the depth to the Moho was calculated.

5) The new model shows a maximum deepening of the Moho of some 10 km in the East Forties basin area and a more diffuse and widespread deepening of approximately 8 km in the Piper-Forties region.

6) The revised modelling process may introduce an additional error of up to 5 km in the depth to the Moho in the East Forties Basin area and up to 2 km in the Piper-Forties area. These errors are largely due to the high degree of ambiguity inherent in the magnetic modelling process. Particularly in determining depths to the lower surface of the intrusive body.

7) If the amount of crustal thinning affects the location of magmatism then a particularly thinned crust might be expected in areas such as the Piper-Forties Volcanic Province and the East Forties Basin. The new model may therefore represent an extreme in possible solutions. If this was the case a more realistic answer would lie somewhere between this and those presented in chapter 3.

CHAPTER 6

EXTENSION IN THE NORTH SEA BASIN

6.1 INTRODUCTION

The primary purpose of this research was to quantify crustal thinning in the Central North Sea using potential field modelling. The previous three chapters gave details of the modelling process and presented models for the depth to the Moho for the Central North Sea. In this chapter these models are used to estimate extension factors (Beta factors) for every point in the study area. The extension factor is defined as being the ratio of the thickness of unstretched crust (here taken to be 32 km) to the thickness of the basement at a point were the crust has been stretched.

In section 6.2 the basic mechanisms by which the lithosphere can be extended are outlined. These can be broadly divided into two groups; coaxial or pure shear models and non-coaxial or simple shear models. The next section (6.3) is a review of the major pieces of research which have attempted to quantify extension in the North Sea basin. There are three principal methods of measuring extension: by palinspatic reconstruction of major faults, by measuring crustal thinning and by analysing basement subsidence. The review is divided into three main sub-sections each dealing with one of these techniques. In the case of subsidence analysis particular reference is made to the work of Latin (1990).

Section 6.3 outlines the technique used to convert the models of Moho topography derived in chapters 3 and 5 into crustal extension factors for the study area. The results are presented and an attempt is made to quantify the errors involved in the technique. The extension factors obtained are compared and contrasted with those estimated by previous workers.

As well as analysing subsidence data in the Central North Sea, Latin (1990) did extensive work in relating the magmatism seen in certain parts of the North Sea (eg. the Piper Forties Volcanic Province) with his estimates of extension. Section 6.5 summarises some of the key points of his research in this field. Using the technique of McKenzie and Bickle (1988) the volume and composition of melt generated during extension can be related to extension factors. In this section the predictions made by the McKenzie and Bickle technique are compared with the extension factors estimated for areas associated with magmatism (eg. the Piper-Forties Volcanic Province) and the models of magmatic bodies made in chapter 4. The final section (6.6) is a summary of the main conclusions and observations made in this chapter.

6.2 MODELS FOR LITHOSPHERIC EXTENSION

6.2.1 Introduction

In this section the principal models of lithospheric extension which have been presented by various workers over the last 15 years are outlined and summarised. The models can be divided into two distinct groups, those based on coaxial or pure shear mechanisms (6.2.2) or those based on non-coaxial or simple shear mechanisms (6.2.3). The application of these models specifically to the North Sea basin is dealt with in section 6.3.

6.2.2 Extension by Pure Shear

6.2.2.1 Uniform Stretching Models

This simple model was first proposed by McKenzie (1978) to explain the crustal rifting and thermal subsidence evident in many continental basins such as the North Sea and Pannonian basins (Boccaletti et al, 1976). The model is

illustrated in figure 6.1.

The thermally equilibrated continental lihosphere is instantaneously and uniformly extended by a stretching factor Beta. In the relatively brittle upper crust the extension is accommodated by large scale faulting, whereas in the ductile lower crust and mantle extension takes place via penetrative flow. Isostatic compensation causes upwelling of hot asthenopshere resulting in a steeper geotherm. McKenzie (1978) shows that the sign of the initial subsidence (negative subsidence is equivalent to uplift) is dependent on the initial thickness of the continental crust but is actually independent of the stretching factor. He demonstrates that for an initial lithospheric thickness of approximately 125 km. the initial subsidence will be positive provided the initial crustal thickness is greater than approximately 18 km. Thus areas of relatively thick crust will subside but other regions where the crust is relatively thin may be elevated during extension.

After the stretching event the hot material of the upwelled asthenosphere cools exponentially by vertical conduction of heat. As an isostatic response to this cooling a slow thermal subsidence takes place. McKenzie (1978) demonstrates that assuming there is no sediment loading the variation of total basement subsidence and heat flux with time are functions of the stretching factor and the equilibrium geotherm.

McKenzies's model assumes that stretching occurred instantaneously and that the resulting thermal anomaly is produced entirely by vertical advection. Jarvis and McKenzie (1980) adapted this model to account for rifting over a finite duration. They point out that when stretching occurs over a period greater than the thermal time constant for conduction (approx. $60/\beta$ My.) some heat will diffuse away before the extensional event is completed. Since the resulting thermal anomaly will be smaller than that predicted for instantaneous stretching, the subsequent thermal subsidence will also be reduced.

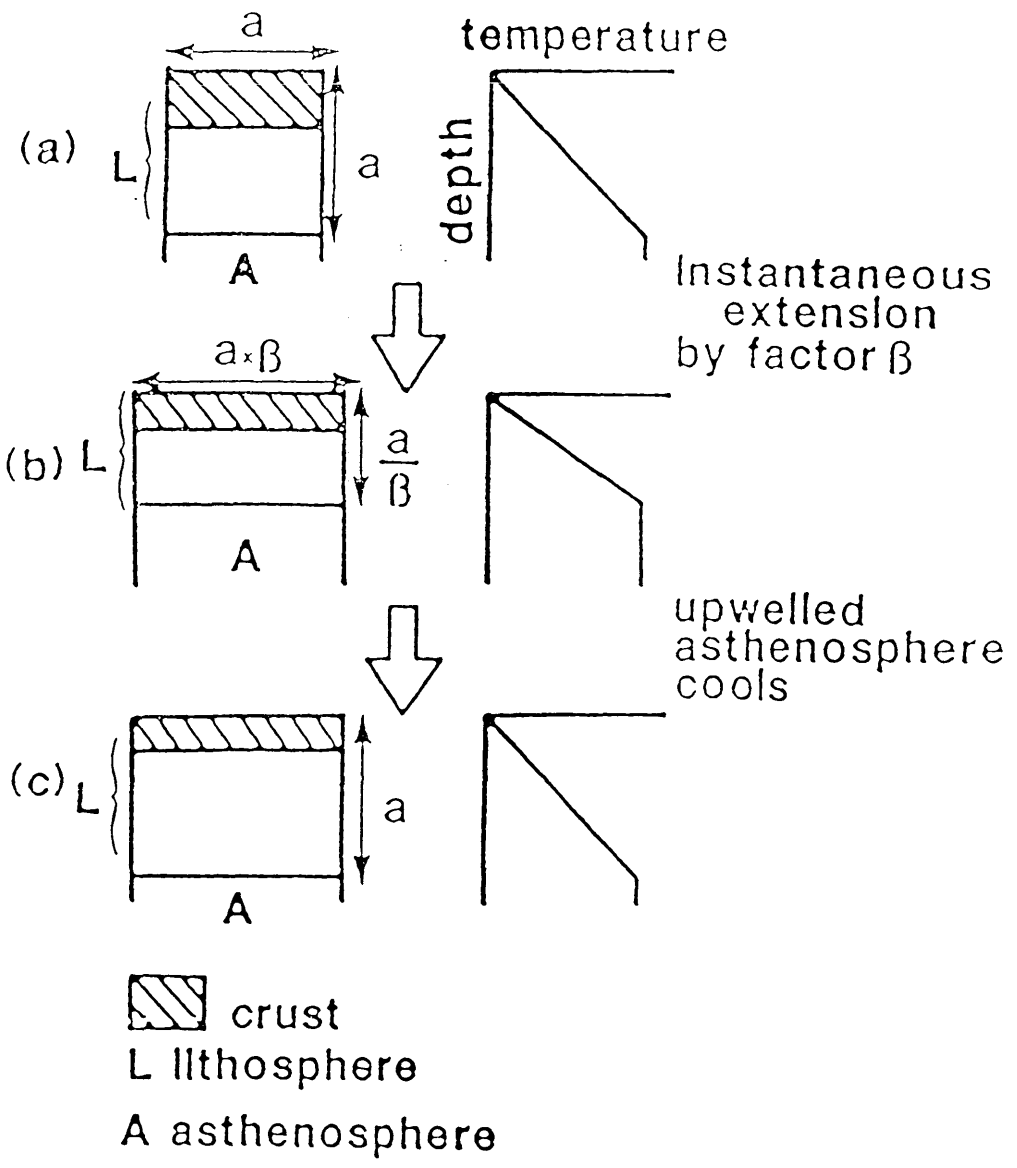


FIGURE 6.1 The uniform stretching model for the development of extensional basins (McKenzie, 1978). (a) Column of thermally equilibrated lihosphere.. (b) Instantaneous stretching. Note perturbation of the temperature gradient. (c) Perturbed temperature gradient gradually returns to the steady state position. After White (1988).

6.2.2.2 Non-Uniform Depth Dependent Stretching.

The simple uniform stretching model of McKenzie (1978), has been successfully applied to several basins and continental shelf areas (eg. Sclater and Christie (1980), Wood and Barton (1983), Royden and Keen (1980)). Many authors (eg. Royden and Keen (1980)) however, noted that in many areas the amount of crustal extension and the initial subsidence are less than that predicted by McKenzie's model and the amount of thermal subsidence is greater than that predicted by measuring crustal extension. To explain this phenomenon Royden and Keen (1980) and Sclater et al (1980) proposed a two layer model in which the ductile lower crust and sub-crustal lithosphere were thinned more than the upper crust during the extensional event. Thus more heat is introduced during extension and the amount of post-rift thermal subsidence is increased.

Hellinger and Sclater (1983) point out that this model allows crustal thinning to be significantly less than sub-crustal thinning at places within the region of extension. At such places "the initial subsidence will be drastically reduced compared to that which would be observed if the sub-crustal thinning were the same". If mass and volume are conserved during the extension process then the amount of crustal thinning and mantle thinning should balance when summed over the entire region. Thus if there are areas where the amount of crustal thinning is much less than mantle thinning then there must also be areas where the converse is true. In such areas the initial subsidence will be comparatively large.

The non-uniform stretching models presented by workers such as Hellinger and Sclater (1983), Sclater et al (1980), Royden and Keen (1980), Rowley and Sahagian (1986) and White and Mckenzie (1988) all involve the use of coupled strain rates between the crust and mantle. In such models the relative values of crustal and mantle thinning cannot vary with time. Latin (1990) presents speculative models incorporating decoupled strain rates in which mantle thinning is much greater than crustal thinning at the start of rifting but by the end of the rifting event the amount of crustal thinning may exceed that of the mantle (see

later in this chapter).

The application of the above models to the North Sea Basin are discussed in greater detail in 6.3.

6.2.3 Extension by Simple Shear

In non-coaxial stretching (by simple shear) the zones of maximum crustal and sub-crustal thinning are displaced from one another and are not symmetric about the rift axis (Wernicke, 1985).

Wernicke's model of lithospheric simple shear (Wernicke, 1981 and 1985) is perhaps the most well known example of non-coaxial stretching. Although it was originally developed to explain various features of the Basin and Range Province it has since been widely applied to other sedimentary basins and passive margins. Applications of his model to the North Sea (Beach, 1986, Beach et al, 1987, Gibbs 1987, 1990) are discussed in detail in 6.3.3.

In Wernicke's model a very low angle (less than 30°) normal fault or 'detachment' penetrates the entire lithosphere dividing it into two distinct 'plates' (figure 6.2). Extension is largely accommodated by slip along this shear zone.

Wernicke (1985) divides his model into five distinct zones (figure 6.2). The first of these (zone A on figure 6.2) is characterised by unstrained lithosphere within the 'lower' of the two plates. In this region no extension is observed in either the crust or the mantle. However, Wernicke (1985) points out that this zone may undergo a slight amount of uplift due to either an isostatic 'edge-effect' (Hellinger and Sclater, 1983) or lateral conduction of heat from the rift zone. The next zone (zone B on figure 6.2) is characterised by a region where the upper crust is extended by faulting whereas the mantle remains unstretched.

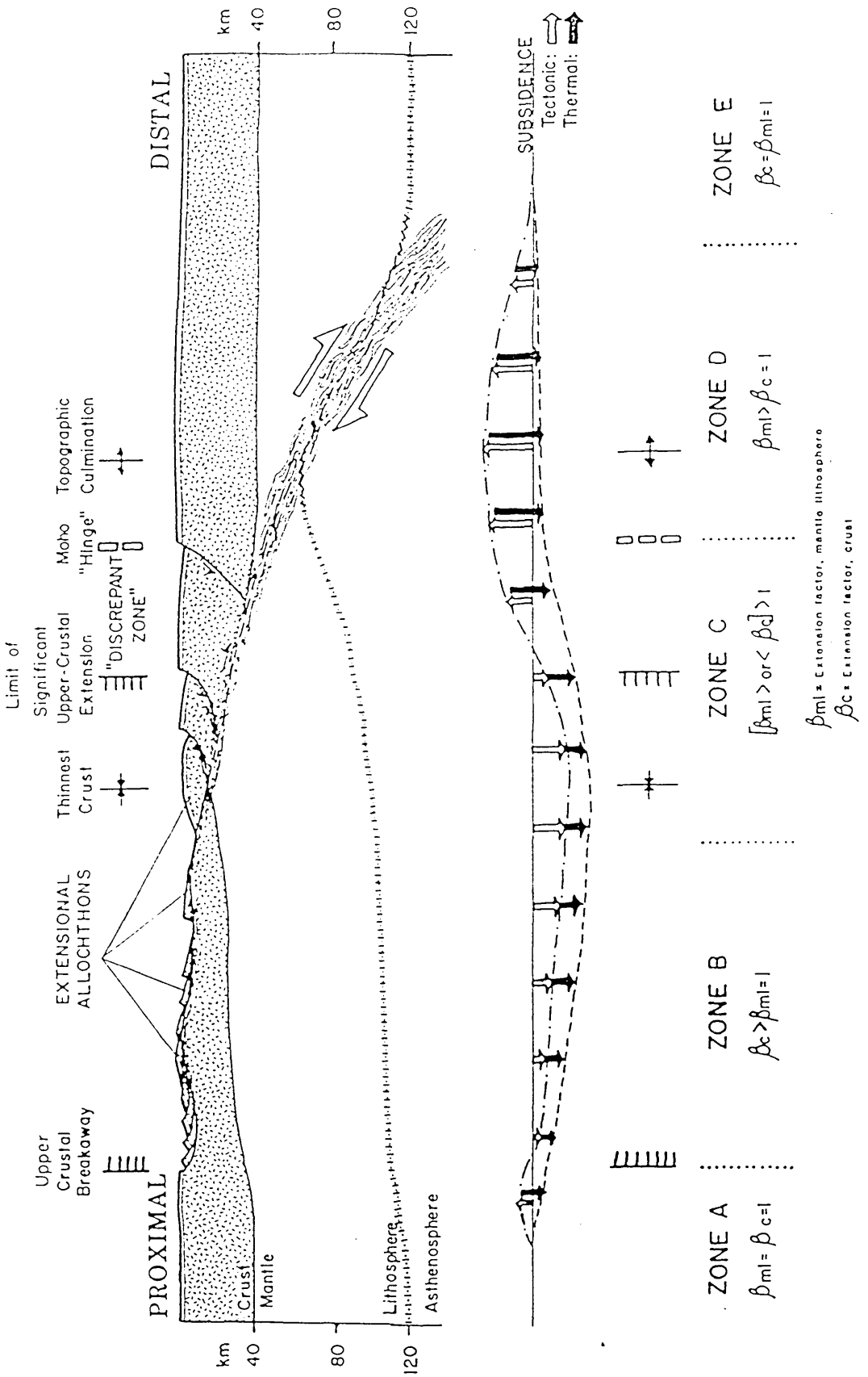


FIGURE 6.2 Hypothetical normal simple shear of the entire lithosphere. See text for explanation. After Wernicke (1985).

Within zone C both the mantle and crust are extended. The point of maximum thinning usually occurs in this zone but Wernicke (1985) points out that it is also geometrically possible for it to lie within zone B. The distal boundary of this zone is defined by the point where the crust is no longer attenuated and all extension takes place within the mantle, a situation which characterises the lithosphere within zone D. Since this zone contains the point of maximum lithospheric thinning it will also be characterised by pronounced uplift which should result in broad topographic doming during the extension. The most distal zone (zone E on figure 6.2) like zone A consists of unstrained lithosphere however, its proximity to the point of maximum lithospheric attenuation may result in it being uplifted either due to an isostatic edge-effect or lateral heat conduction from zone D.

As with the pure shear stretching models discussed in 6.2.2 the extension begins with a rifting stage in which the crust is thinned and subsidence is fault controlled (the 'initial subsidence' of McKenzie (1978)). As the upwelled asthenosphere cools and the base of the lithosphere gradually returns to its original position the whole basin undergoes slow thermal subsidence.

Latin (1990) points out that numerical models of the thermal response of the lithosphere to simple shear (Voorhoeve and Houseman, 1988, Buck et al, 1988, White, 1988, 1989, Latin and White, 1990, Latin et al, 1990) have provided quantitative predictions (for a given amount of horizontal extension) of the distribution and extent of asthenospheric upwelling and the distribution and thickness of the fault controlled and thermal subsidence through time.

An example of one of these models is shown in figure 6.3 (from White, 1988). The lithosphere is divided into seven distinct sections (similar to the 5 zones of Wernicke, 1985). If local Airy isostasy is assumed each vertical column within the seven sections can be treated independently in the calculations. For a given amount of horizontal extension the amount of crustal thinning and mantle thinning can be calculated. The isostatic and thermal response to stretching in

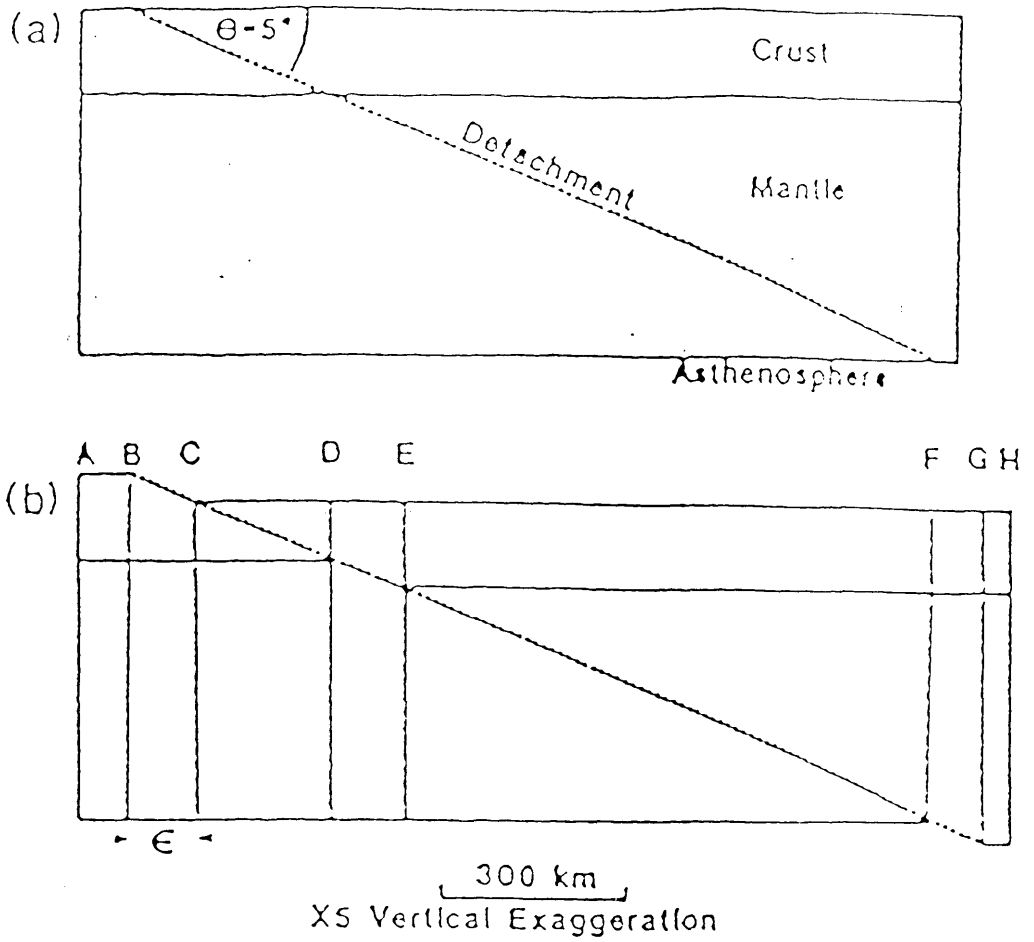


FIGURE 6.3 (a) Cross-section of lithosphere with incipient planar detachment fault. (b) Same section after extension by simple shear before isostatic compensation. After White (1988).

each column are calculated using equations similar to those of McKenzie (1978). The results of this modelling show three important differences between the effects of extension by pure shear and simple shear (Latin 1990):

1) In pure shear models sediment sequences are symmetrically distributed about the rift whereas in simple shear models the sequences pinch out toward the detachment giving rise to a marked asymmetry of sedimentary infill within the basin.

2) In pure shear models the thickness of the sediments associated with the thermal subsidence is greater than the thickness of those associated with initial subsidence. The converse is true in simple shear models where syn-rift sediments should be approximately three times more abundant than the sediments associated with thermal subsidence.

3) Unlike pure shear models, in simple shear extension maximum thinning of the mantle occurs away from the rift axis. This means that any melt generated during extension should also be located in off-axis regions (Latin and White, 1990).

6.3 EXTENSION IN THE NORTH SEA BASIN: A SUMMARY OF PREVIOUS WORK

6.3.1 Introduction

Theories regarding the extensional history of the North Sea Basin have been very well documented over the past 10 - 15 years. This section is by no means a complete review, rather it concentrates on those studies which have attempted to quantify values of crustal attenuation and extension. These values are compared and contrasted with similar estimates made by potential field modelling in this study in section 6.4.

The following summary is divided into three sub-sections each of which deals with extension estimates made by a particular method, namely: the measurement of extension on faults, measurements of crustal thinning and subsidence analysis.

6.3.2 Measuring Extension on Faults

This was one of the first methods of estimating extension in rifted regions. Ziegler (1983) presented palinspatic reconstructions of faults on profiles across the North Sea Basin which produced a total 'heave' of 25 km. across his profile. This is approximately equivalent to a crustal extension factor of 1.2. Similar results were obtained by Sclater and Shorey (1989) and Ziegler and Van Hoorn (1990).

Estimates of stretching using palinspatic methods are invariably smaller than those obtained from other methods such as crustal thinning or subsidence analysis. The method is prone to very large errors. It assumes that all the important faults in the basin together with their associated stratigraphic displacements can be identified and measured accurately. Another approach which applies simple trigonometry to the geometries of fault blocks, approximating them to rigid rotating 'dominoes' has been shown by White (1988, 1990) to produce minimum estimates of extension since the dip of the faults and the amount of rotation needs to be known very accurately before estimates of extension can be made, even assuming the simplest possible model.

6.3.3 Measuring Crustal Thinning

Determining levels of crustal thinning is a very commonly used method of estimating extension in the North Sea basin. The method involves comparing measurements of crustal thicknesses within the rifted area with those made in areas unaffected by the rifting process, in order to estimate the amount of thinning in the rift. This provides a time-integrated estimate of the crustal

stretching factor which is given by the ratio of unstretched crustal thickness outside the rift to the stretched thickness under the rifted area. The method relies on an assumption of crustal conservation within the rifted area, thus no account is taken of any material added to the crustal section due to magmatic underplating.

There are three principal methods of measuring crustal thicknesses: interpretation of seismic refraction lines, identification of the Moho on deep seismic reflection profiles and, as in this study, determining the depth to the Moho by modelling the regional gravity field.

The first estimates of crustal thinning in the North Sea were made by Solli (1976). This was based on a seismic refraction line running orthogonal to the Viking Graben at approximately 60° N. At its most thinned point Solli interpreted the crustal thickness to be 14 km. The crust at either end of the line was measured to be approximately 35 km. thick giving a maximum time-integrated stretching factor of approximately 2.5 for this region.

Christie and Sclater (1980) published their estimates of crustal thinning based on studying a seismic refraction line across the Witch Ground and Buchan Grabens (figures 6.4 and 6.5). They assumed that stretching had stopped by the base of the Upper-Cretaceous and that crustal material had been conserved. In the most stretched part the depth from the Base Upper-Cretaceous to the refraction Moho was found to be approximately 20 km. This gives a time-integrated stretching factor of 1.6 provided the unstretched crust had a thickness of 32 km. (as seen below the East Shetland Platform). If an unstretched thickness of 35 km. is used (as seen beneath the Shetland Islands) the crustal stretching factor is increased to 1.7 - 1.8. Sclater and Christie (1980) performed a subsidence analysis from several wells in this area, their results are discussed in 6.3.4.

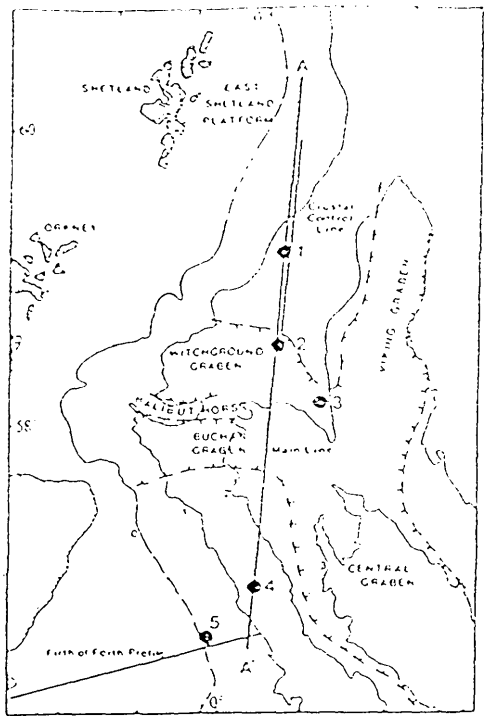


FIGURE 6.4 The Seismic refraction lines of Christie and Sclater (1980) across the Witch Ground and Buchan Grabens. Numbers refer to those on the section shown in figure 6.5. After Christie and Sclater (1980).

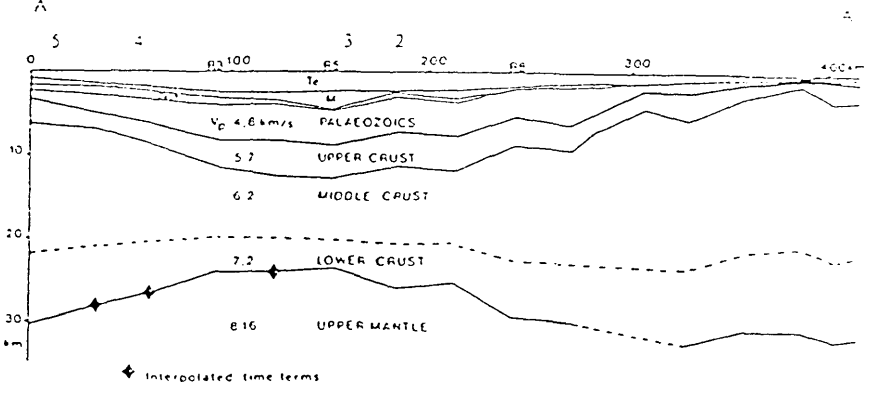


FIGURE 6.5 Velocity and depth section obtained from the refraction line shown in figure 6.4. After Christie and Sclater (1980).

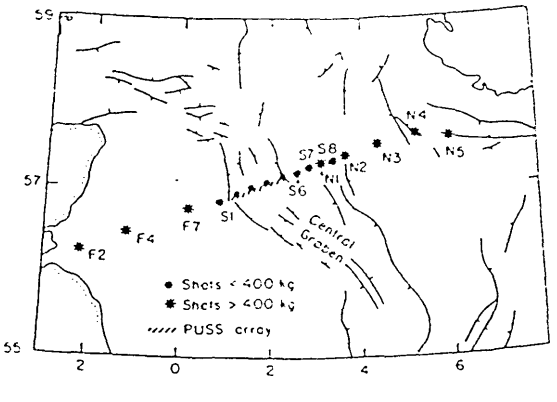


FIGURE 6.6 Map of the refraction experiment of Barton and Wood (1984). The study area used in this research is outlined. Modified from Barton and Wood (1984).

Barton and Wood (1984) also used a seismic refraction line to measure crustal thicknesses. This line runs approximately orthogonal to the northern part of the Central Graben (figure 6.6). Their results show a maximum thinning of approximately 2.46 in the rift axis. They also performed a subsidence study from wells around the refraction line and found a considerable discrepancy between their estimates of crustal extension using this method and those obtained from the seismic experiment. The results of their subsidence study are discussed in more detail in 6.3.4.

A number of studies have been made in which crustal thinning has been measured using gravity modelling. Donato and Tulley (1981), make use of very widely spaced 2D profiles across the UK sector of the North Sea in order to determine crustal thinning over the whole of the basin. Their method involved modelling the depth of the Moho along 9 widely spaced profiles between 53° and 62° N. From these models they re-calculate a regional anomaly which would have been caused by the implied Moho topography of the 2D profiles. This is then re-modelled in 3D to produce a 'Moho map' for the whole region. Their results, which are somewhat difficult to interpret, show time-integrated Beta factors of upto 1.9 in the centre of the basin at approximately 56.5° N. and something like 1.8 in the centre of the Viking Graben. These results are very approximate and are made from the map shown in figure 6.7. In this case the crustal thickness is taken as the distance between Moho and Base-Tertiary and an un-stretched crustal thickness of 32 km. The methodology behind this modelling must be prone to very large errors chiefly due to the large amount of interpolation which is necessary to link up the 2D profiles. The Moho map shown in figure 6.7 is also the product of two modelling stages (one in 2D and one in 3D) which will also introduce large errors into the result. Apart from this, no account is taken of variations in the gravity field east of the Median line and yet the final model covers the whole of the basin.

Hospers et al (1985) used a similar method to that of Donato and Tulley (1981) to analyse gravity data from the UK. and Norwegian sectors of the North

Sea between 56° and 62° N. Unfortunately they did not produce a map of implied Moho topography however, one of their profiles running across the Viking Graben at 50°50' N. shows an apparent crustal thinning of approximately 1.8 where the thickness of the crust is taken as the base Jurassic and the unstretched thickness is taken as 30 km. Again this is a gross approximation.

Zervos (1986 and 1987) made use of 2D and 3D modelling of the filtered regional Bouguer anomaly field to determine crustal thicknesses in the northern North Sea. His model shows a maximum crustal stretching factor of approximately 2.5 located at roughly 2° E., 60° N. This was calculated using a Moho depth of approximately 21 km. and a basin fill of approximately 8 km. and an original crustal thickness of 32 km.

In a study over a similar area Fichler and Hospers (1990) make use of 2D and 3D gravity modelling together with interpretations of the deep seismic reflection profiles of the BIRPS NSDP 84 data set. In this case their calculated crustal extension factors reach a maximum of greater than 3.5 at approximately 60°40' N. and 2°30' E. (figure 6.8). The unstretched crustal thickness is taken to be 31 km. and the base of the sediments is at least as deep as the base Triassic but may also include some Permian and Devonian sediments in places.

In a similar study to that of Fichler and Hospers (1990), Holliger and Klemperer (1989) have modelled the gravity data along the deep seismic reflection profiles NSDP85 1-4 which were previously interpreted by Klemperer (1988) (figure 6.9). Figure 6.10 shows Klemperer's (1988) interpretation of crustal thicknesses taken from the reflection lines across the Viking Graben. He suggests a total crustal thinning factor of at least 2.0. The gravity models of Holliger and Klemperer (1989) generally show good agreement with the seismic interpretations of Klemperer (1988). However, in the deeper parts of the Viking Graben the Moho derived using reflection data is approximately 5 km. deeper than that derived using gravity. To explain this discrepancy they mention the possibility of magmatic intraplating or underplating occurring where the crust

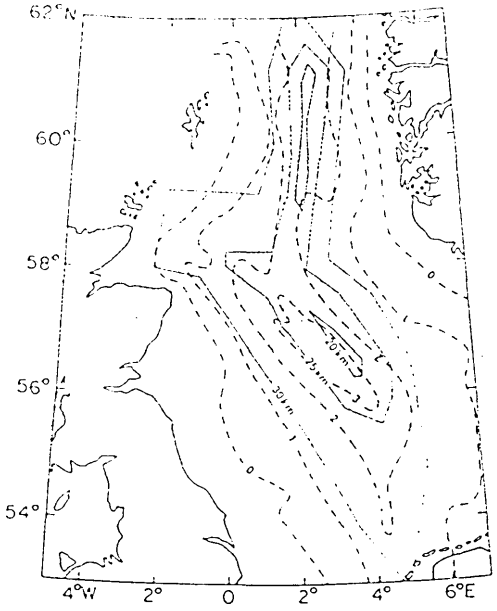


FIGURE 6.7 Base Tertiary contours (km) and three-dimensional model showing implied crustal structure beneath the Viking and Central Grabens. From Donato and Tulley (1981).

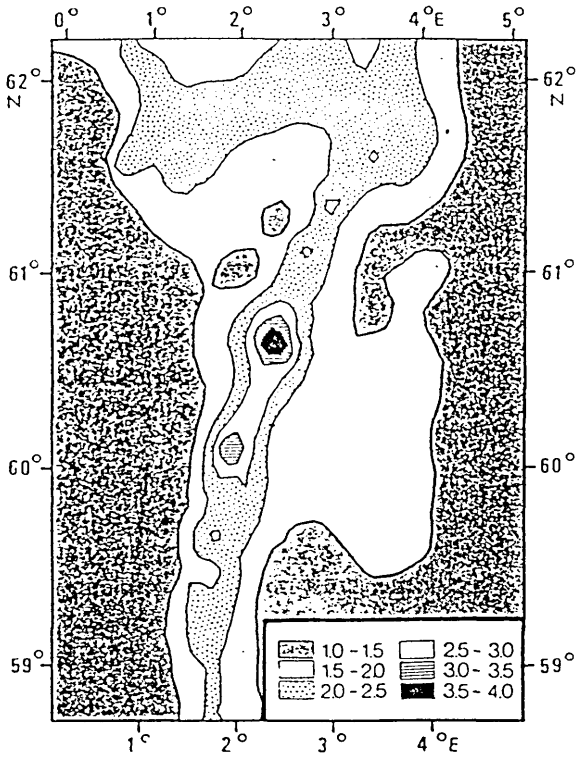


FIGURE 6.8 Map of crustal stretching factors for the Northern North Sea, estimated from measuring crustal thinning using 2D and 3D gravity modelling and interpretations of deep seismic reflection profiles. From Fichler and Hospers (1990).

is most attenuated. In the latter case the base of a layered upper-most mantle would appear as the reflection Moho. Provided the underplated material was nearly of mantle density this would appear below the large density contrast which marks the gravity Moho. The maximum time-integrated crustal extension factor derived by Holliger and Klemperer (1989) is given as approximately 3.2 with an uncertainty of +/− 0.5.

Holliger and Klemperer (1990) studied a series of deep seismic reflection lines and produced regional-scale gravity models along them. In this case the seismic lines included the BIRPS NSDP85 lines across the Central North Sea together with the SALT 1 and SALT 2 refraction lines across the Central Graben and the SNST83-7 line across the southern North Sea. They derive a maximum extension factor of 1.3 in the southern North Sea and 2.0 in the Central North Sea. Again they quote errors of between 0.5 and −0.3 for a typical extension factor of 2.0. As with the study of the northern North Sea (Holliger and Klemperer, 1989) the gravity Moho and the reflection Moho are in good agreement.

All of the workers mentioned so far explain their estimates of crustal attenuation in terms of coaxial lithospheric extension. Diametrically opposed to these ideas Beach (1986), Gibbs (1987) and Beach et al (1987) have proposed a non-coaxial Wernicke-type origin for the Viking Graben. They argue that unmigrated deep seismic reflection data from the Viking Graben area can be interpreted to show strong evidence of low-angle detachments penetrating the mantle. This evidence is based on the presence of some strong shallow angle reflectors seen penetrating the mantle and also zones of laterally differing reflectivity (figures 6.11 and 6.12). Beach et al (1987) attribute the Triassic to early Jurassic extensional development of the Viking Graben to a Wernicke-type model with a gently eastward dipping detachment shear zone passing eastward through the crust and ramping down beneath the Moho. Early Mesozoic basin development thus occurred in the hanging wall above the shear zone in a similar way to that proposed by Wernicke (1981, 1985) for the development of the Basin and Range Province.

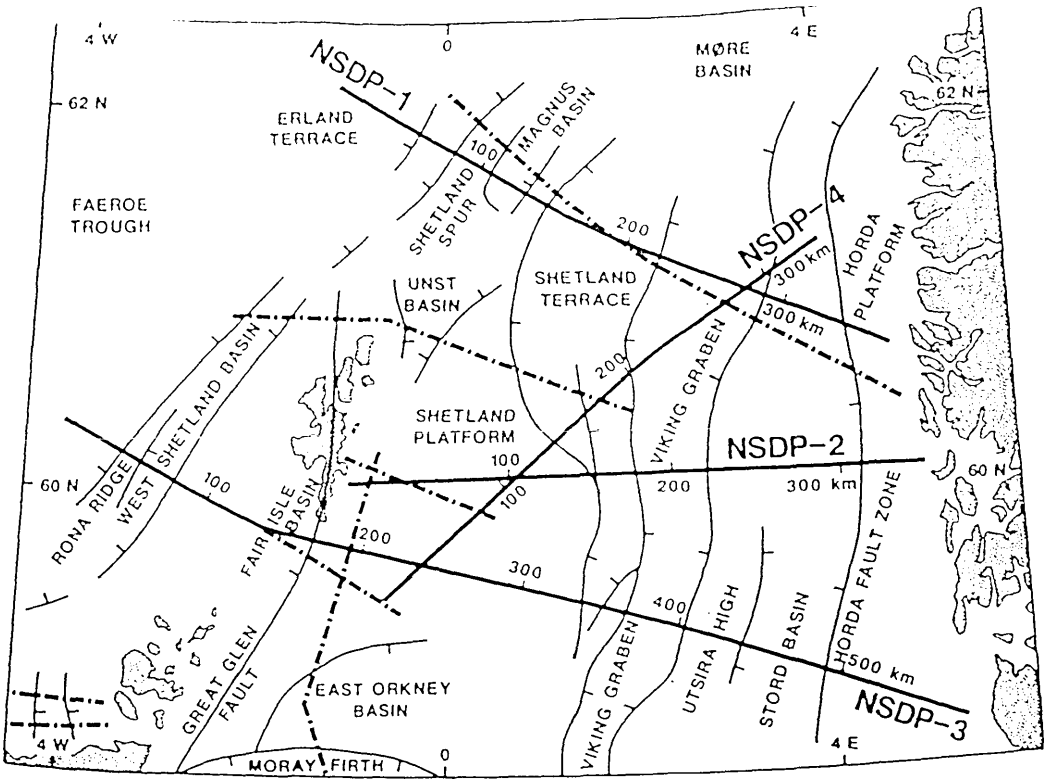


FIGURE 6.9 Map of the northern North Sea showing the locations of the NSDP-84 deep seismic reflection profiles (solid lines). Previous surveys are shown as dotted lines. After Klemperer (1988).

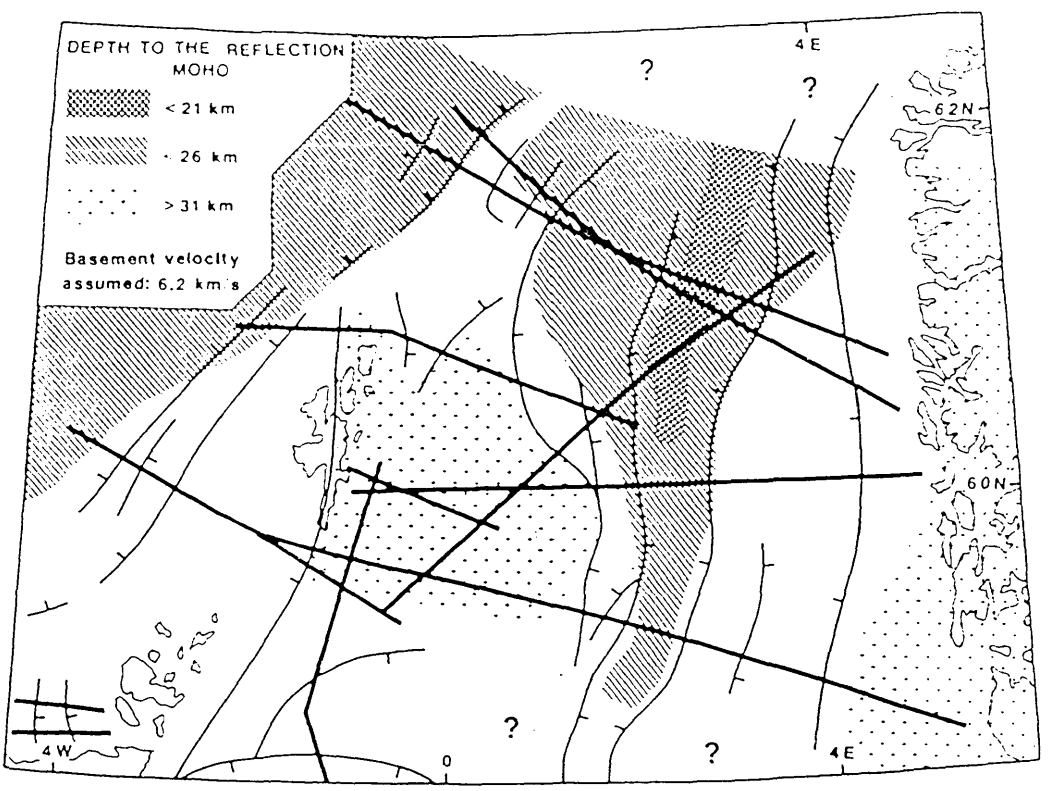


FIGURE 6.10 Contoured map of the depth to the reflection Moho in the northern North Sea. Interpreted from seismic reflection data. After Klemperer (1988).

Maximum syn-rift subsidence occurred above the zone of maximum crustal thinning, thus creating the Viking Graben. Thinning of the mantle caused uplift during the extension period of the region east and south-east of the Viking Graben, Horda Platform hinge line. Thermal subsidence was superimposed on the tectonic subsidence of the Viking Graben as the upwelled mantle lithosphere cooled. In the late-Jurassic to early-Cretaceous Beach et al (1987) propose a change in the mechanism of movement from one affecting the whole of the crust to a more discrete strike-slip movement occurring on the primary shear zones that cut through the crust and offset the Moho. They propose a dominoe structure being imparted to the crust by these fault zones. Crustal extension in the late-Jurassic occurs by dip-slip movements on this fault set and the rotation of major crustal blocks bounded by these faults.

From their interpretation of the seismic data Beach et al (1987) propose a thinning of the crust to a minimum of 14 km. beneath the rift, equivalent to a time-integrated crustal extension factor of 2.3 in the centre of the Viking Graben.

Klemperer (1988) has argued that the seismic data, when depth-migrated, are quite consistent with a coaxial stretching model since the crust appears to be thinned symmetrically and because both syn-rift and post-rift sediments are superimposed directly on top of thinned crust. White (1988) however, has shown that through numerical modelling of the simple-shear model it is in fact possible to produce both crustal thinning that is symmetric about the basin and having the locus of initial and thermal subsidence sediments coinciding spatially within the rift. Arguments against the simple shear model on the basis of melt generated during lithospheric extension are presented in 6.4

There are two principal problems associated with estimating crustal extension factors from measurements of crustal thinning. The first of these has already been mentioned. This is that the values obtained are always time-integrated i.e. different phases of extension cannot be recognised, delineated and quantified. The other problem is that errors made in the initial estimate of crustal thinning

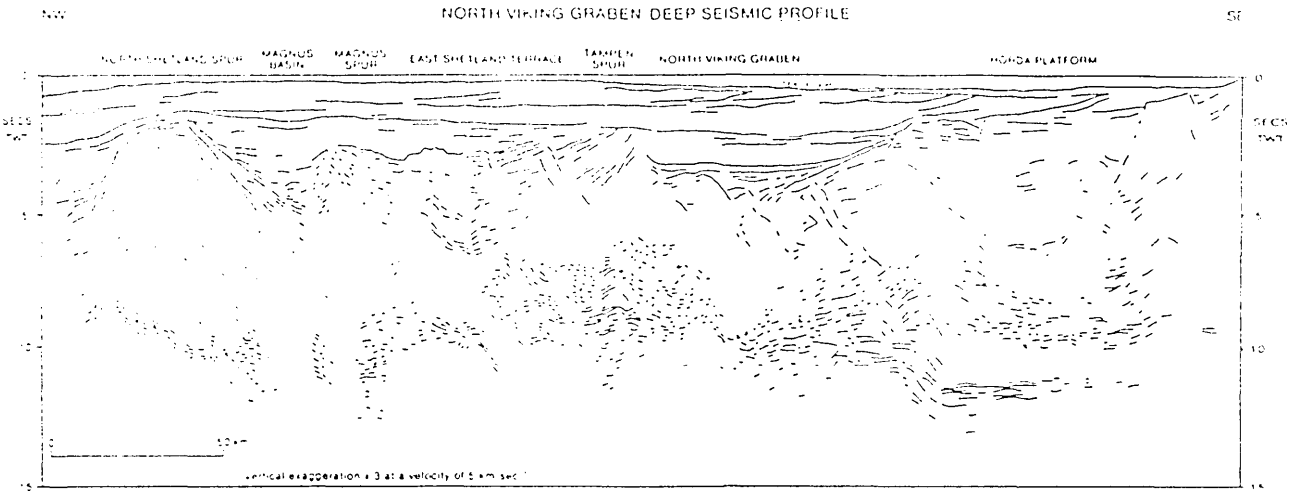


FIGURE 6.11 Line drawing of principal reflectors on a deep seismic reflection profile across the Viking Graben. After Beach et al (1987).

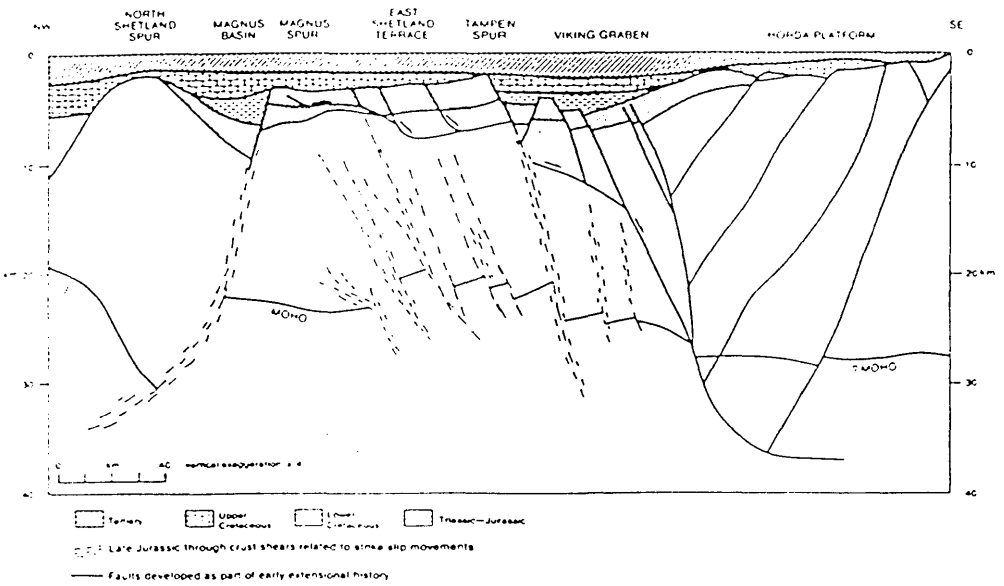


FIGURE 6.12 Simple geological model for the profile shown in figure 6.11. After Beach et al (1987).

are compounded when the conversion to a stretching factor is made. That is, the larger the amount of thinning, the larger is the error in the Beta factor. For example, Holliger and Klemperer (1989) quote an accuracy of +/− 2km. for their estimates of the depth to the gravity Moho. For an initial crustal thickness of 32 km the following estimates of Beta can be made:

Crustal thickness = 16 km +/− 2 km Beta factor = 2.0 with error bars at 1.78 and 2.29.
Crustal thickness = 12 km +/− 2 km Beta factor = 2.67 with error bars at 2.29 and 3.20
Crustal thickness = 10 km +/− 2 km Beta factor = 3.2 with error bars at 2.67 and 4.0.

6.3.4 Subsidence Analysis

Subsidence analysis is a commonly used method to estimate the amount of extension in an extensional sedimentary basin. It has an advantage over other methods such as measuring crustal thinning in that in areas which have undergone a number of discrete rifting episodes the amount of extension during each rifting event can be evaluated.

In principal the method is simple; using either seismic or well data the basin stratigraphy is decompacted and is used to progressively unload the crystalline basement. This allows curves to be generated which show the water-loaded basement subsidence of the basin as a function of time. These curves can then be compared with theoretical curves generated for different amounts of stretching and for various stretching models (e.g. uniform or heterogeneous stretching). In order to fully appreciate the relevance and accuracy of extension factor estimates made using subsidence analysis, it is important to understand how these estimates are obtained. The method is described below but for more detail refer to Steckler and Watts (1978) and Sclater and Christie (1980).

6.3.4.1 Modelling Subsidence

Estimating extension factors from subsidence analysis involves seven principal stages, each is described below.

1) A large number of wells are selected from the area of interest. Ideally the wells need to be evenly distributed over the area since the extension factors calculated from any one well can only be truly applied to that location and the amount of extension may vary from area to area. Latin (1990) points out that it is also important that the wells penetrate the basin as deeply as possible and that each well samples at least the complete post-rift sequence. It is also desirable that they are not located on the tips of fault blocks since it is likely that in these areas the syn-rift sequence will be incomplete due to uplift and subsequent erosion.

2) From each well the thickness and average sediment-type deposited over different stratigraphic intervals through time are noted. The sediments are divided into several layers each of which is assumed to be a homogeneous lithology (eg. Shale, Sandy-Shale, Sand or Chalk). Each layer is bound above and below by points of known stratigraphical age (derived from micropalaeontological studies). These stratigraphical ages are then converted into absolute ages using a time-scale such as that of Harland et al (1982). Since errors in stratigraphical ages are likely to be small (less than +/− 5 Ma, Latin (1990)) in comparison with the time intervals chosen to display the final subsidence curves it is usually assumed that they will not adversely affect the final shape of the curve.

3) As mentioned in 3.4.1 the density of sedimentary layer will increase with depth due to the effects of compaction and de-watering. It is necessary to correct for these effects in order to determine the subsidence history of a basin (figure 6.13). This process, known as decompaction, was outlined by Sclater and Christie (1980) who noted that the decay of porosity with depth of burial for lithologies such as: sand, shaley-sand, sand and chalk was exponential and could be approximated by the relationship:

$$\Phi_{(z)} = \Phi_0 e^{(-\frac{z}{\lambda})}$$

Where:

$\Phi_{(z)}$ = Porosity at depth z

Φ_0 = Initial porosity

z = depth of burial

λ = Characteristic decay length (lithologically dependant).

The effect of decompaction is to increase the depth to the basement. However, the method assumes that the sediments lie on a completely compacted basement which in the Central North Sea is taken as either the Top-Triassic (approx. 213 Ma) or the Top-Permian (approx. 250 Ma). It also assumes that each stratigraphic sequence is not over-pressured (i.e. when the pore fluids support some of the weight of the over-burden). These two assumptions tend to maximise the estimate of decompaction since: a) it is likely that the basement will not be fully compacted at the time of deposition of the earliest sediments and b) in over-pressured sections a layer at a given depth will appear thicker than it would at normal pore-fluid pressures.

4) After calculating the effect of decompaction the total load of the sedimentary pile can be calculated together with its effect on basement subsidence. This is actually done layer by layer in conjunction with the decompaction calculation in a process known as 'back-stripping'. As each layer is removed and the underlying sequences are decompacted the depth to the basement is recalculated (figure 6.13).

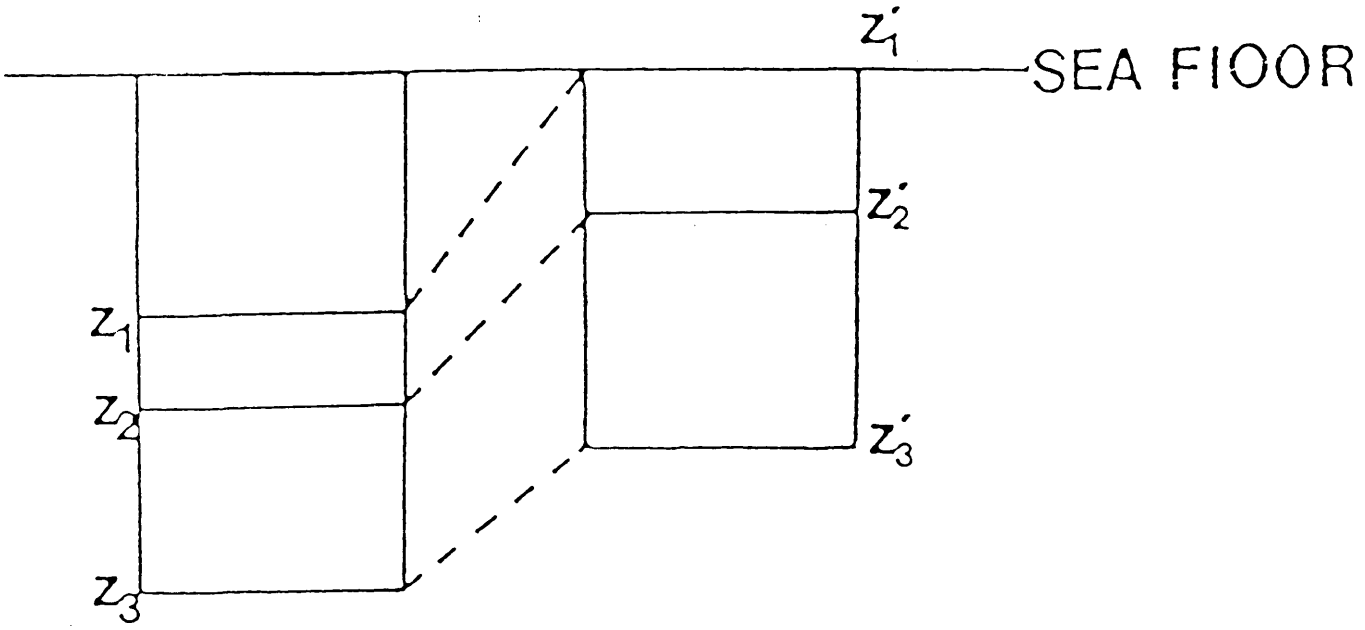


FIGURE 6.13 Decompaction of sediment layers (Z_2 and Z_3) as a layer of sediment (Z_1) is removed. After Sclater and Christie (1980).

Sclater and Christie (1980) shows that the density of the remaining column is given by:

$$P_s = \Sigma[\Phi_i \rho_w + (1 - \Phi_i)\rho_{sgi}]\frac{Z_{i'}}{S}$$

Where: Φ_i = Mean porosity of the i^{th} layer

P_{sgi} = Sediment grain density of the i^{th} layer

$Z_{i'}$ = Recomputed depth to the top of the i^{th} unit

S = Recomputed total sediment thickness

ρ_w = Density of water

The decompacted thickness of the sediment column (less any layers previously stripped off) can then be 'unloaded' and the space left filled by water. This leaves the water-loaded depth to the basement (D) which is given by:

$$D = S(\rho_m - \rho_s)/(\rho_m - \rho_w)$$

Where: S = Total Sediment Thickness

ρ_m = Average Mantle Density

ρ_w = Average Water Density

The degree to which the lithosphere responds to loads not only at one point but also to loads from a surrounding area is a function of the effective elastic thickness (T_e) of the lithospheric plate (Turcotte and Schubert, 1982). In the calculation above an assumption of total Airy isostasy has to be made in which the lithosphere is assumed to have zero lateral strength and responds only to the size of the load directly above the point of calculation. Barton and Wood (1984) show that the effective value of T_e for the North Sea was less than 5 km. for the whole of the post-rift phase. Thus many workers (eg. Barton and Wood, 1984, Latin, 1990) conclude that the assumption of Airy isostasy is valid. Isostasy in the North Sea is discussed in more detail in chapter 7.

5) The depth of water at the time of sediment deposition (palaeobathymetry) has an important effect on the calculation of subsidence. It is therefore necessary to correct for this effect at each stage in the back-stripping process. Estimates of palaeobathymetry are difficult to make and rely on the identification of either sedimentary facies indicators to make distinctions between different depositional environments or assemblages of fossils known to have lived at certain depth ranges. An indication of the errors introduced during this process is shown in figure 6.14 which is taken from Latin (1990).

6) Related to the correction for palaeobathymetry a further correction can be made to take into account global changes in sea-level. Estimates of such global sea-level changes are extremely difficult to quantify and separate from local tectonic events (Watts and Thorne, 1984). The overall uncertainty involved in making corrections due to global sea-level changes causes extreme irregularities to appear in otherwise smooth subsidence curves (Wood, 1982 and Latin, 1990). This correction is therefore, often ignored.

7) The Final stage of subsidence analysis is the interpretation of the water loaded basement subsidence curves produced for each well. Each curve consists of a series of error bars reflecting uncertainties in the palaeobathymetry correction (figure 6.14). Using the equations developed to describe finite extension (Jarvis and McKenzie, 1980) a series of theoretical subsidence curves for various extension factors can be generated. For uniform extension where the crust and mantle are stretched by equal amounts (6.2.2.1) the parameters needed to generate a series of such curves are, the starting age and duration of the extension event together with various physical properties of the lithosphere and Upper-Mantle such as: thickness, density, temperature etc. A set of such curves together with the parameters used to generate them are shown in figure 6.15.

Once the theoretical curves are generated an attempt is made to fit them to the observed subsidence curves for each well. The end result is an estimate of

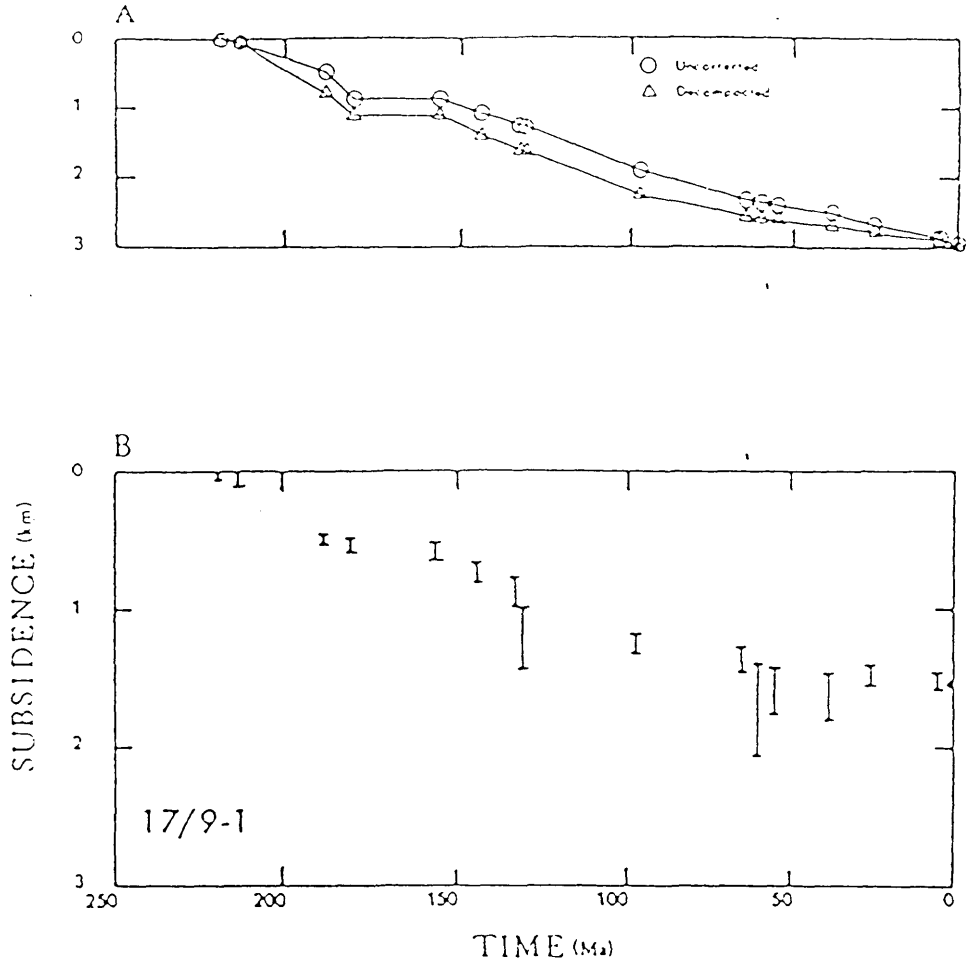
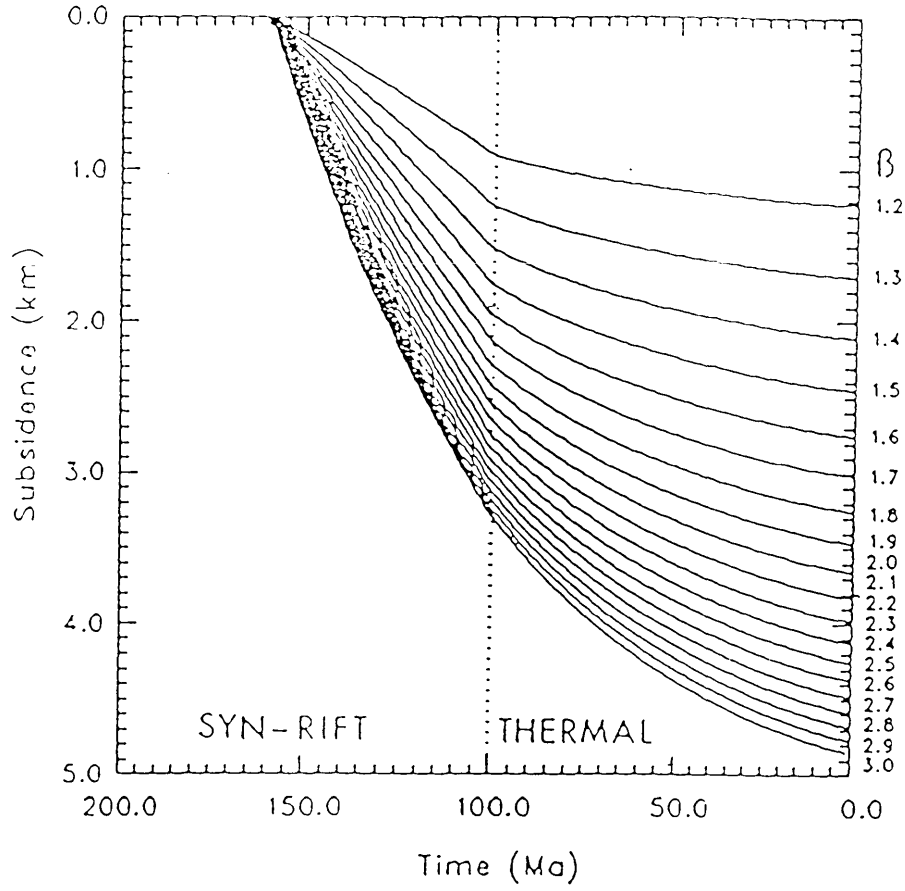


FIGURE 6.14 Subsidence curves from a well in the Egursund Basin. Upper diagram (A) shows uncorrected (circles) and decompacted (triangles) basement subsidence. Lower diagram (B) shows water-loaded basement subsidence (error bars); i.e. subsidence after the effects of sediment loading have been removed and a palaeowater depth correction has been applied. After Latin (1990).



: Model Parameters

a	lithospheric thickness	125 km
t_c	crustal thickness	30 km
ρ_w	sea water density	1.0 g cm^{-3}
ρ_s	sediment density	2.0 g cm^{-3}
ρ_c	crustal density (at 0°C)	2.8 g cm^{-3}
ρ_m	mantle density (at 0°C)	3.33 g cm^{-3}
ρ_a	asthenosphere density (at 1333°C)	3.2 g cm^{-3}
T_a	asthenosphere temperature (at 125 km)	1333°C
α	thermal expansion coefficient	3.28×10^{-5} $°C^{-1}$
κ	thermal diffusivity	$8 \times 10\text{-}7 m^2 s^{-1}$
τ	decay time	62.8 Ma

FIGURE 6.15 Theoretical subsidence curves for a range of Beta values. Homogeneous stretching is assumed to have started at 160 Ma and to have continued with a constant strain rate for 60 Ma. The table shows the model parameters used to generate these curves. After Latin (1990).

the stretching factor made from the best-fit theoretical curve. If the observed curve cannot be easily matched to a theoretical curve a new set can be generated using a different stretching model (eg. heterogeneous stretching).

6.3.4.2 Previous Work

In the previous section the basic theory behind subsidence analysis was outlined. This section summarises the research of various workers who have applied this method to the North Sea. Particular emphasis is placed on the work of Latin (1990) who has performed the most up-to-date analysis in the 'triple-junction' area of the North Sea.

The first study of basin subsidence in the North Sea was carried out by Sclater and Christie (1980). They examined a total of eight wells within the Central Graben and its flanks. By applying a simple instantaneous, uniform stretching model (McKenzie, 1978) to the area they estimated stretching factors of between 1.5 and 2 in the graben and less than 1.5 on the flanks. However, their approach to the subsidence analysis was, perhaps rather simplistic. They effectively ignored the effect of syn-rift subsidence since their analysis only included subsidence over the past 100 My and rifting probably started between 180 and 160 Ma (Ziegler, 1982). Latin (1990) however, points out that this approach is probably the best one to take in this area (see later in this section). Other errors may also have been introduced into their work since the only model they consider is the instantaneous, uniform stretching model (McKenzie, 1978) It is known that rifting was of finite duration (60 Ma according to Wood, 1982) also Latin (1990) and White and McKenzie (1988) point out that a model of heterogeneous stretching is more likely in the some parts of the rift (see later in this section).

In addition to their study of crustal thinning using a refraction line across the Witch Ground and Buchan Grabens, Christie and Sclater (1980) also analysed the

thermal subsidence of five wells along the profile using a similar method to Sclater and Christie (1980). They produced estimates of stretching factors which reached a maximum of approximately 2.0. These values compared very favourably with their estimates derived from their study of crustal thinning in which maximum stretching factor of approximately 1.8 was estimated at the thinnest point.

The next major study of subsidence in the Central North Sea was made by Wood (1982). She studied 19 wells in the Central Graben and Outer Moray Firth Basin. This work was an improvement over the work of Sclater and Christie (1980) since she assumed a model of uniform extension over a finite period. She assumed that the Jurassic rifting phase began at approximately 180 Ma in the Bajocian and continued for 60 Ma, finally ending in the early-Cretaceous (approx. 120 Ma). Her work also included an extensive study of micro-fauna in order to minimise errors due to inaccurate estimates of palaeobathymetry. In modelling subsidence she attempted to match theoretical curves to both the syn-rift and post-rift thermal stages of extension. Latin (1990) points out that she effectively ignored the fact that the syn-rift sequence is extremely sensitive to the location of the well. For instance if the well is located on the tip of a fault block a considerable amount of syn-rift sediment may have been uplifted and and lost due to subsequent erosion (Yielding, 1990).

The maximum estimation of extension factors from her study was for a well approximately in the centre of the basin where a value of approximately 1.55 was obtained.

Barton and Wood (1984) compared these results with measurements of crustal thinning made from a refraction profile across the Central Graben (6.3.3). and noted large discrepancies between the two estimates. They attributed this discrepancy to the effect of pre-Jurassic rifting on crustal thickness. The mismatch at each well was used to refine the estimate of initial crustal thickness down from 31.2 km. to whatever value eliminated this discrepancy.

Hellinger et al (1989) used the refraction data of Barton and Wood (1984) and recalculated extension factors at 25 km intervals along it. In their study they attempt to separate the subsidence data into that which would be caused by two major rifting events. The first event is actually considered to be the sum of two smaller events occurring in the Permian and the Triassic. The second event is that occurring in the Mid-Jurassic to Early-Cretaceous. By assuming that the first event lasted 95 My they approximated the extension due to this event (equation 5 of Hellinger et al 1989). The total extension is estimated is estimated using the same method as Barton and Wood (1984). Then, by assuming that the total extension factor is the product of the extension factors due to the first and second events they calculate the extension due to the late Mid-Jurassic to early Cretaceous event. Unlike every other workers in this field Hellinger et al (1989) estimate much more extension occurring in the pre-Jurassic events than in the later Jurassic - Cretaceous episode. Their maximum estimation of total extension is a Beta factor of 2.27 assuming an elastic plate thickness of 5 km. This is the product of an extension factor of 2.04 for the first event and 1.11 for the second. In contrast to this, Latin (1990) points out that in general subsidence data fits very well with a pre-mid Jurassic rifting event with extension factors not exceeding 1.2.

In the northern North Sea White (1988, 1990) compared extension estimates made in the Shetland Terrace region by considering both complex fault block rotations and subsidence analysis. He found that both methods produced similar results with a maximum mid-Jurassic to early-Cretaceous extension factor of between 1.5 and 2.2 . He also noted a considerable discrepancy between these results and those obtained from crustal thinning estimates made along the deep seismic reflection profile NSDP-84-1. This he found could be corrected by assuming a Triassic extension factor of between 1.05 and 1.2 depending on location.

The most recent analysis of subsidence data from the Central North Sea is that of Latin (1990). He analysed 19 wells from the Central North Sea area (figure 6.16) many of which (unlike the studies of Wood, 1982 and Barton and Wood,

1984) where from the deepest parts of the basin. Latin noticed that in many cases the subsidence profiles were characterised by a relatively condensed syn-rift sequence (mid-Jurassic to early-Cretaceous) in comparison to the large thicknesses of post-rift sediments associated with the thermal subsidence. This phenomenon has been attributed to the location of wells on basement highs and the tips of fault blocks where an incomplete syn-rift sequence might be expected. However, figure 6.16 shows that many of the wells in Latin's study came from deep parts of the basin where the syn-rift sequences should be complete. The relatively thin syn-rift sequences are actually a characteristic of the Central North Sea. Ziegler (1982) shows that in relation to the north Central Graben the Viking Graben contains much more significant thicknesses of mid-Jurassic to early Cretaceous sediments whilst the thickness of Tertiary sediments is similar in both regions suggesting that the two rifts may have different extensional histories.

Latin (1990) found that the subsidence curves derived from wells containing a relatively thin syn-rift sediment thickness could not readily be matched to theoretical curves generated using a uniform stretching model, suggesting that this is not the correct mechanism for this part of the basin. Without resorting to local tectonic effects the most obvious method of reducing the amount of syn-rift subsidence relative to post-rift subsidence is to invoke the heterogeneous stretching model of Hellinger and Sclater (1983) in which the crust is extended by a smaller amount than the mantle in the centre of the rift.

Latin considered two types of heterogeneous stretching models. In the first type he considered a coupled strain rate model in which the rates of strain in the crust and mantle may be different and variable but are coupled such that if, for instance, the strain rate increases in the crust at any point and at any time then it will also do so in the mantle by proportionally the same amount. This means

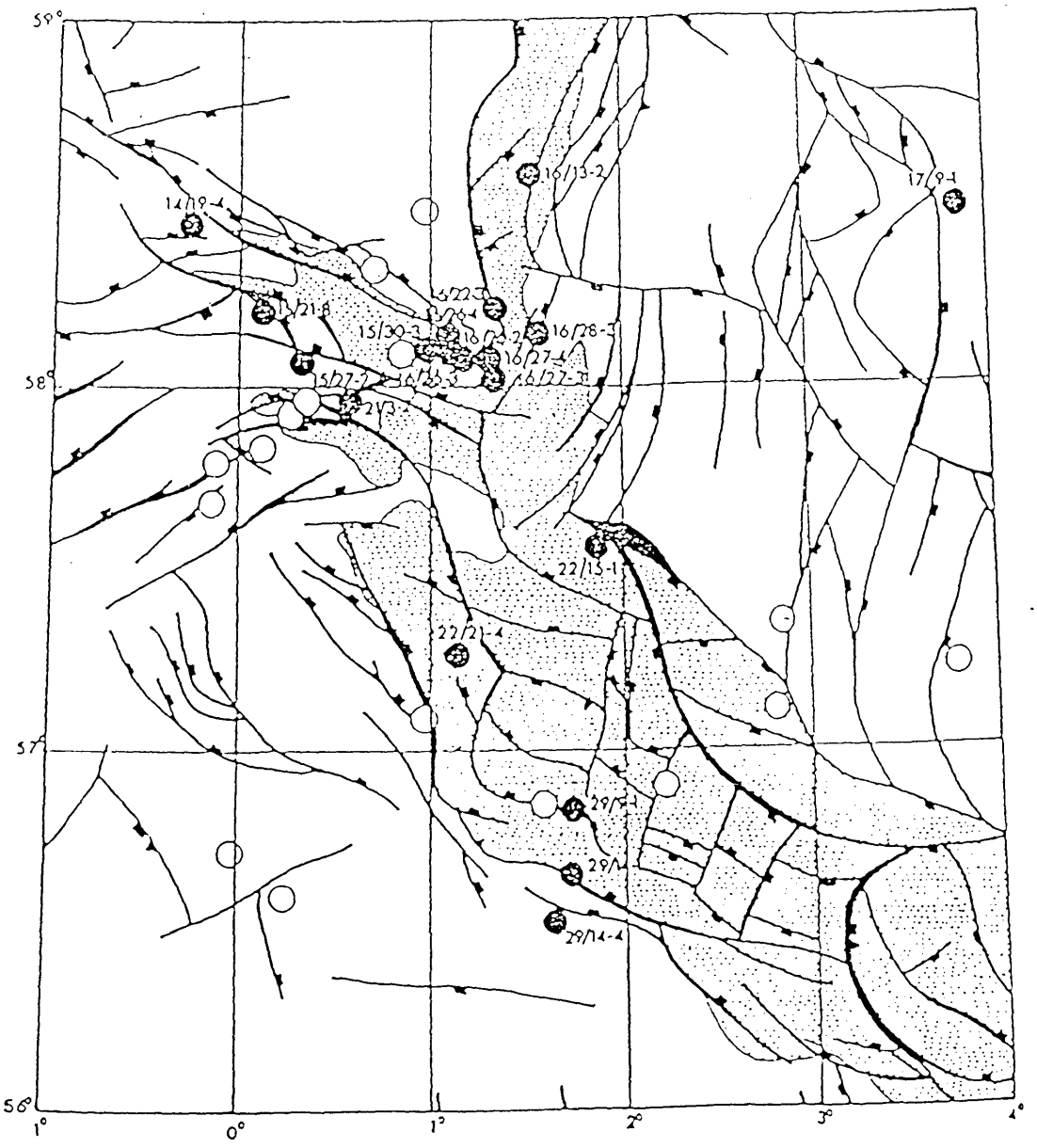


FIGURE 6.16 Map showing the locations of wells used in the subsidence analysis of Latin (1990) (filled circles) and that of Wood (1982) (open circles). After Latin (1990).

that if at the start of rifting, the crustal extension is less than the mantle extension in any vertical lithospheric column then it will remain less than the mantle extension throughout the rifting period (figure 6.17). In the second type of model he considered a de-coupled strain rate. In this case the strain rates within the crust and mantle may be different and may vary disproportionately during the rifting period. Thus, the relative values of crust and mantle extension may be varied within a single lithospheric column during rifting (see 6.5.4 and figure 6.30). Latin notes, "In this type of model while stretching at any stage during rifting may be heterogeneous the time-integrated total stretching need not be".

Using a program developed by Condon (1988) Latin produced theoretical curves for a coupled strain rate model and obtained good fits to subsidence curves from wells showing the characteristic relatively small syn-rift subsidence associated with the deep parts of the Central North Sea. In these models the crustal extension is always less than that of the mantle. Crustal and mantle strain rates were constant throughout the 60 My rifting event with the crustal strain rate being the smaller of the two.

$$\epsilon_c \propto \frac{\beta_c}{60} \qquad \epsilon_m \propto \frac{\beta_m}{60}$$

Where:
ϵ_c = crustal strain rate
ϵ_m = mantle strain rate
β_c = crustal extension factor
β_m = mantle extension factor

In one well from the 'triple-junction' area Latin estimated crustal extension factors of between 1.55 and 1.7 and mantle extension factors of between 2.8 and 3.2. The pressure drop due to thinning the mantle and crust by these amounts

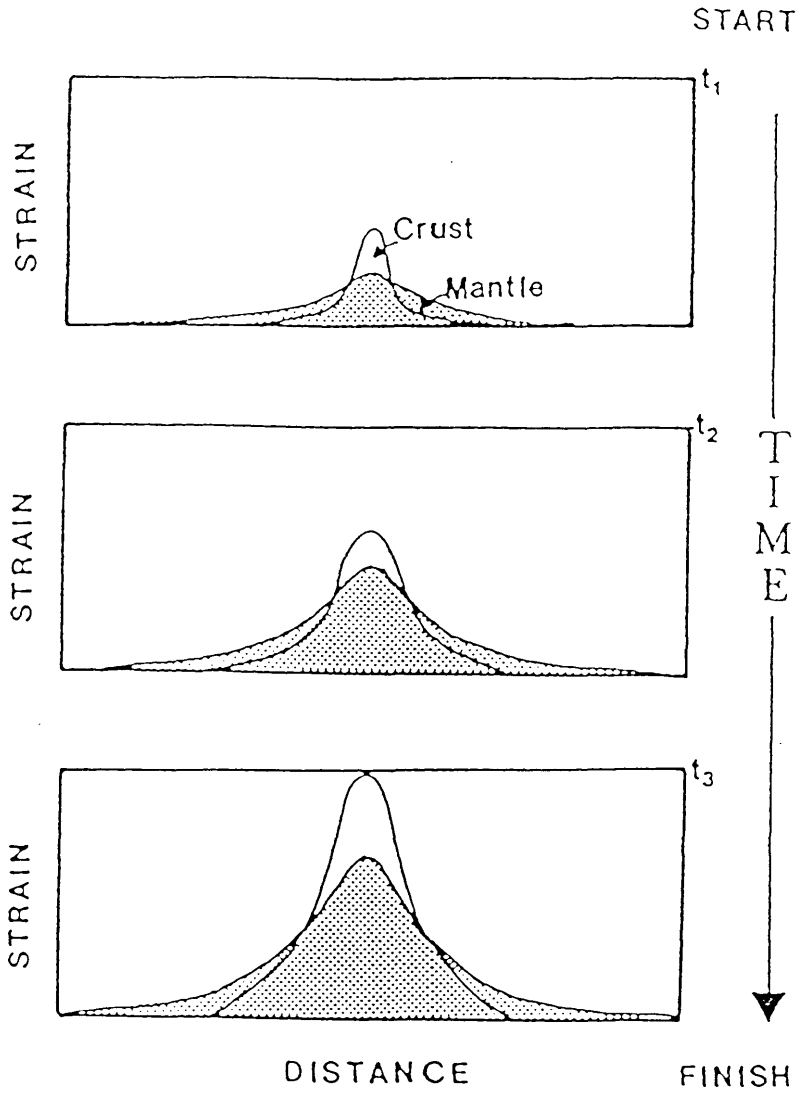


FIGURE 6.17 Coupled strain rate heterogeneous stretching. The diagram shows that crustal stretching and mantle stretching must balance at any time across the region. In this model the amount of crustal stretching is always greater than that of the mantle in the rift centre whilst the converse is true at the rift flanks. After Latin (1990).

can be calculated and the homogeneous stretching factor which results in approximately the same amount of decompression is then determined. An equivalent homogeneous stretching factor of 2.4 to 2.75 was calculated for this well. He notes that if homogeneous curves are fitted only to the thermal parts of the subsidence curves where there is a relatively thin syn-rift sequence, the results are very similar to those obtained for the equivalent homogeneous stretching factors calculated for the heterogenous stretching model (figure 6.18).

The main problem associated with coupled strain rate models is that if the crustal extension in the centre of the rift is always less than that of the mantle at the same point, there must exist off-axis areas where the converse is true. In these areas there will be a large amount of crustal thinning and a relatively small amount of thermal subsidence. Such areas are not observed in the North Sea. Studies of crustal thinning (including this study) invariably show that the crust is thinnest in rift areas whilst off-axis areas are relatively unaffected by the extension.

The de-coupled strain rate model is far more flexible and may be used to explain many of the features of the Central North Sea. Such features include the presence of relatively thin syn-rift sequences in the axis areas, low off-axis crustal thinning and the emplacement of igneous bodies (eg. the Piper-Forties Volcanic Province) very early in the rifting process. The model has never been quantified however, it is discussed in a qualitative manner in section 6.5.4 of this chapter.

Latin's results are shown in figure 6.19. These were obtained by fitting theoretical curves for a homogeneous stretching model to the thermal part of the observed subsidence curves. Figure 6.19 also shows his re-interpretation of the wells originally analysed by Wood (1982). Extension factors are as large as 2.5 in the centre of the triple junction area whilst off-axis values are often less than 1.2. These values are for the mid-Jurassic to early-Cretaceous only and will therefore be slightly less than the total extension for the basin which would include the effects of pre-Jurassic rifting. Latin (1990) points out, however, that

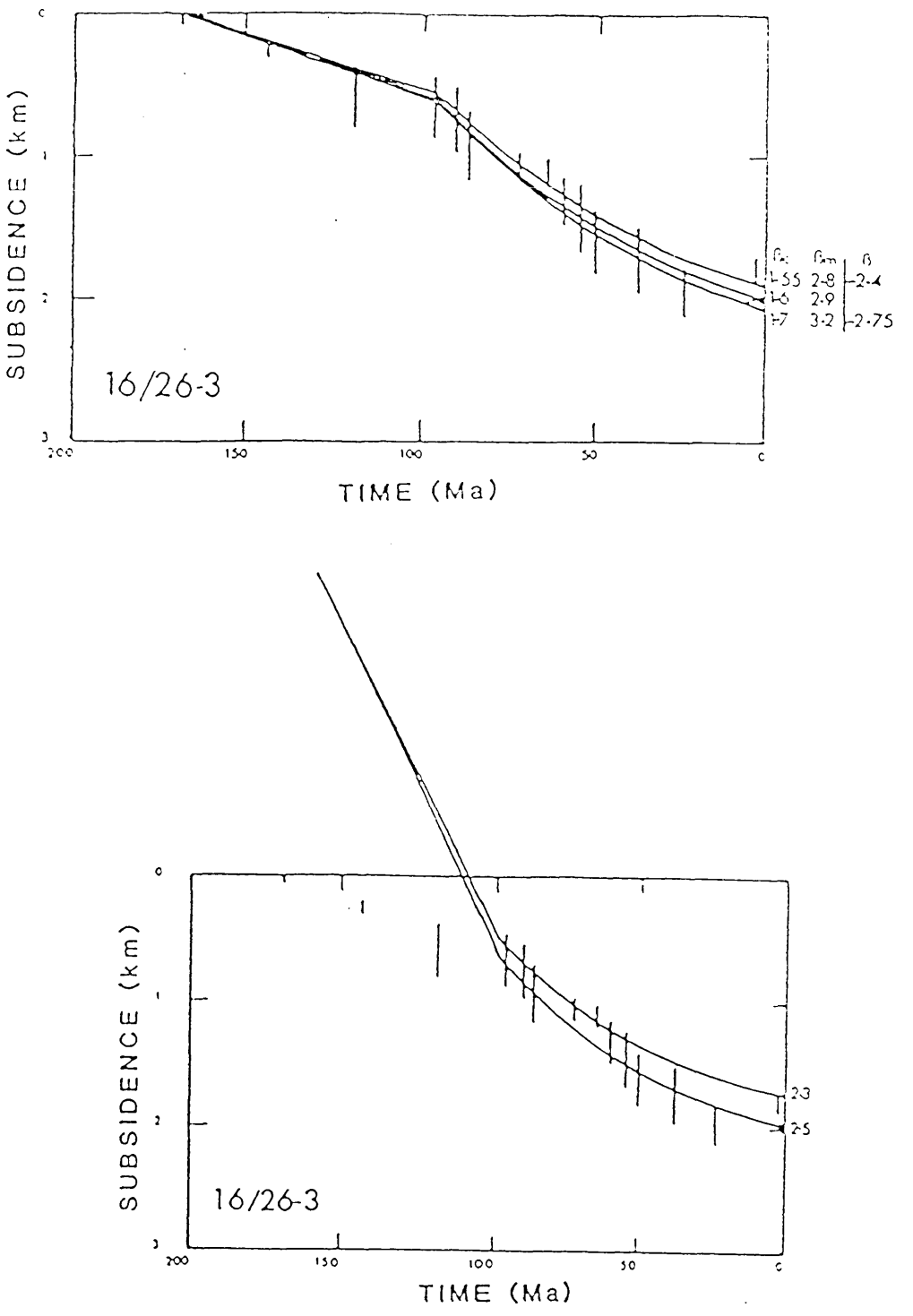


FIGURE 6.18 Upper diagram (a) Fitting curves for heterogeneous stretching to water-loaded subsidence data from a well in the Forties region. Rifting is assumed to start at 160 Ma and to finish at 100 Ma. Beta factors for crustal and mantle thinning are shown together with an effective equivalent homogeneous stretching factor which represents an equivalent amount of decompression. Lower diagram (b) shows the results of fitting homogeneous stretching curves to the thermal part of the subsidence curves only. Both diagrams from Latin (1990).

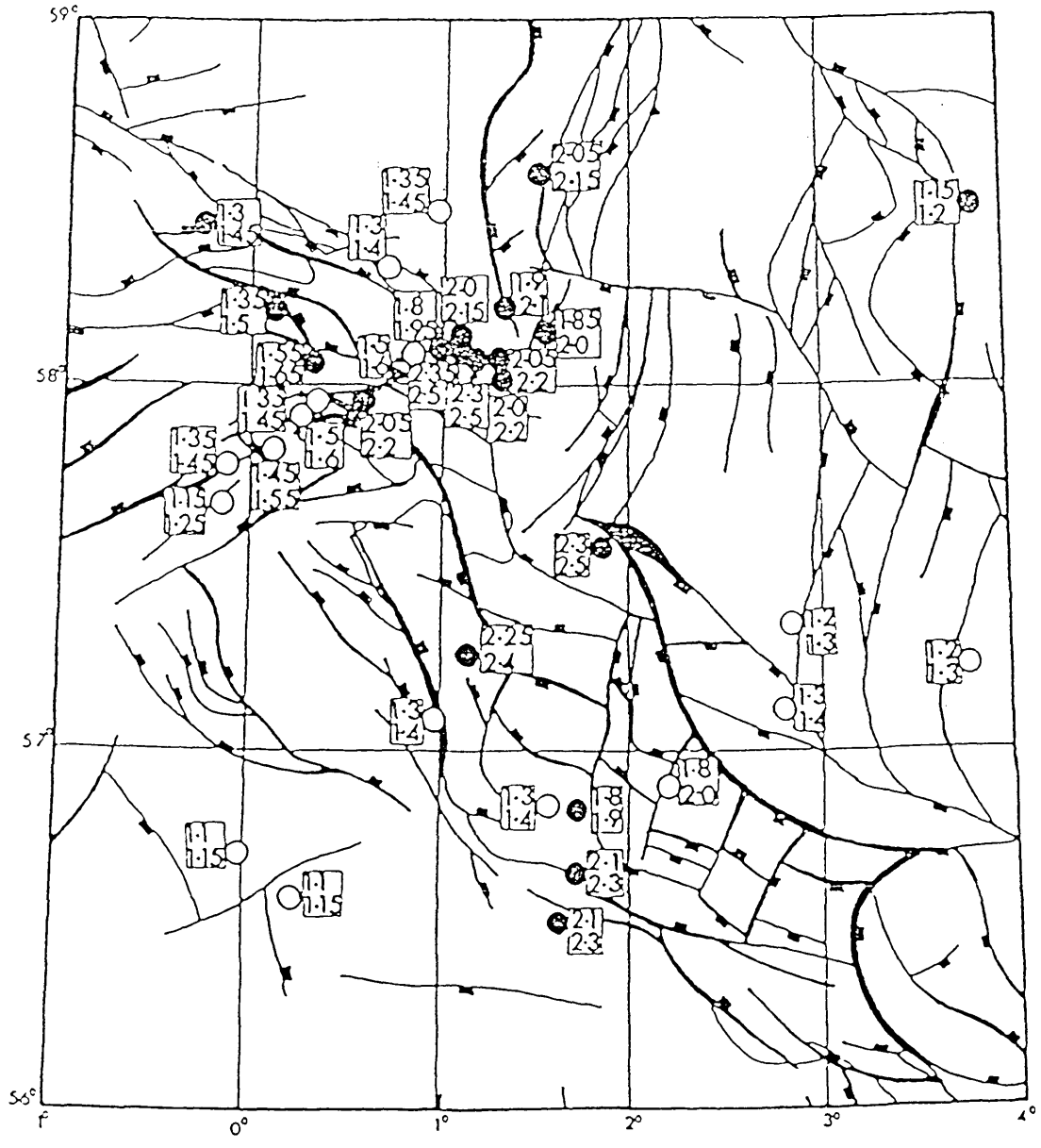


FIGURE 6.19 Map showing estimates of Beta factors for the mid-Jurassic as obtained by Latin (1990) by fitting homogeneous stretching curves to the thermal part of the water-loaded subsidence data. After Latin (1990).

this effect is likely to be very small (a maximum of 1.2). The total extension factor is the product of the factors from all rifting episodes.

6.4 ESTIMATING CRUSTAL EXTENSION FROM 3D GRAVITY MODELLING

6.4.1 Introduction

In this section the 3D models of the Moho topography derived in chapters 3 and 5 are used to estimate crustal thinning and crustal extension factors. The errors involved in these calculations are discussed in 6.4.3. These estimates are compared and contrasted with those obtained by other workers in 6.4.4.

6.4.2 Crustal Thinning and Extension

The calculation of crustal extension factors from the Moho models shown in chapters 3 and 5 is very simple. The first stage is to determine the thickness of the 'basement' at every point in the study area. In the gravity modelling the basement was taken as everything between the Base-Cretaceous and the Moho. Thus by subtracting the grid representing the depth to the Base-Cretaceous from that representing the depth to the Moho for any model it is possible to obtain a grid representing the thickness of the basement. Figure 6.20 shows the depth to the Base-Cretaceous for the study area whilst figure 6.21 is a grey-scale contour map showing the depth to the Moho for the final solution obtained by gravity and magnetic modelling (see chapter 5). The thickness of the basement associated with this model is shown in figure 6.22.

A grid of extension factors from the whole area is derived by dividing the basement thickness into the thickness of un-stretched crust. To facilitate direct comparisons between these estimations and those obtained by other workers

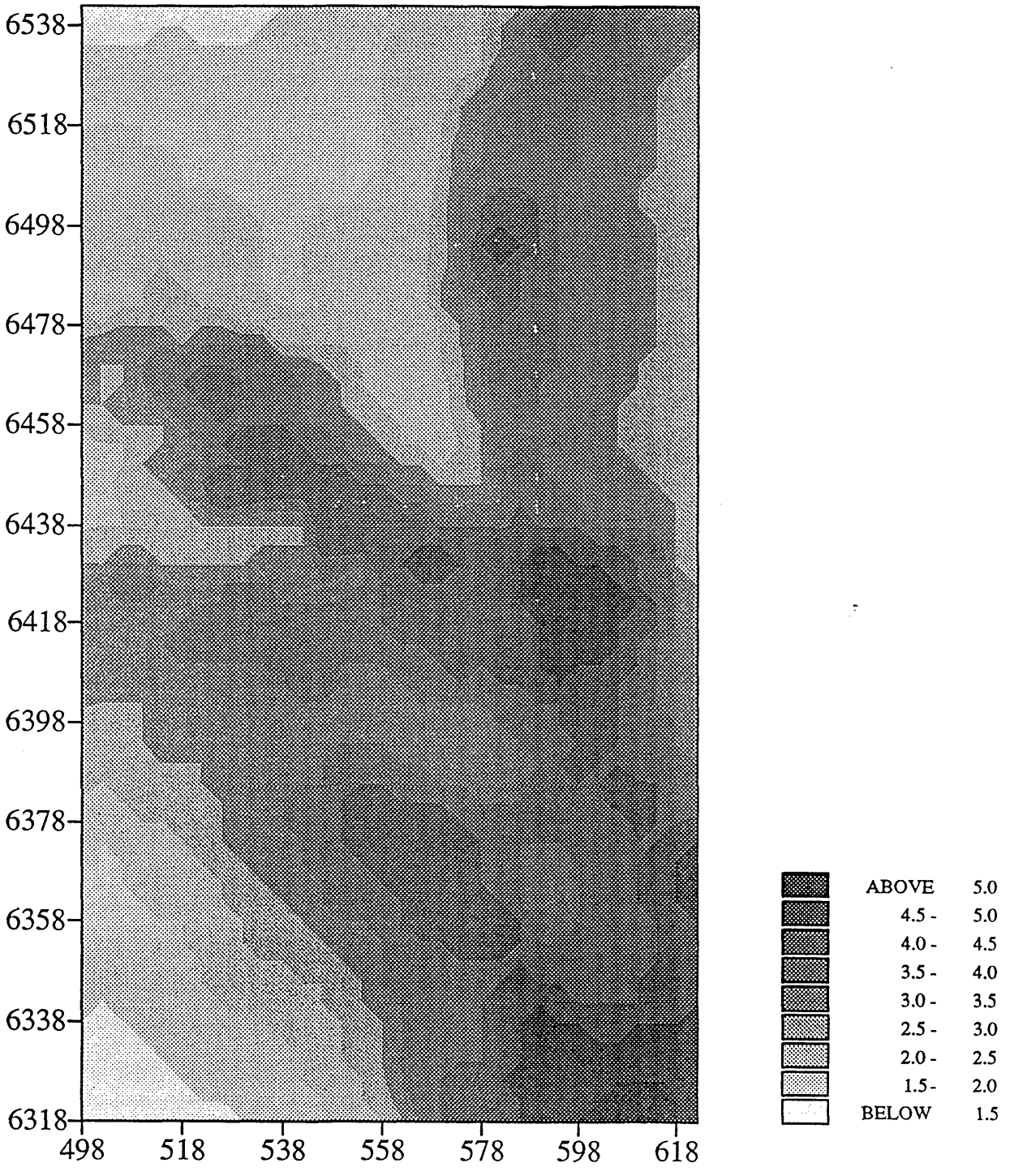


FIGURE 6.20 Depth to the Base Cretaceous. (From Day et al, 1981). Units are in kilometres.

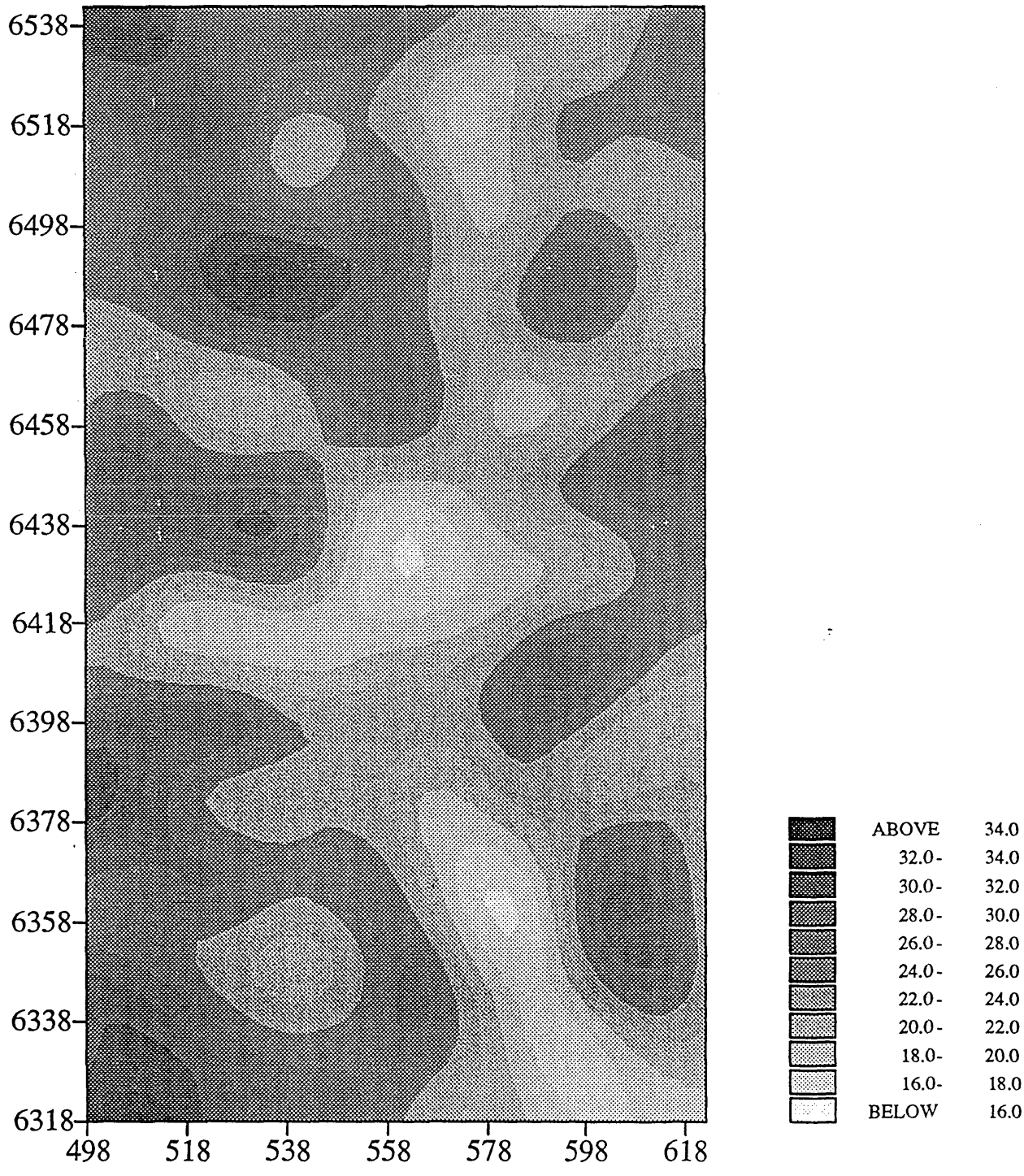


FIGURE 6.21 Depth to the Moho derived by gravity modelling (see chapter 5). Units are kilometres.

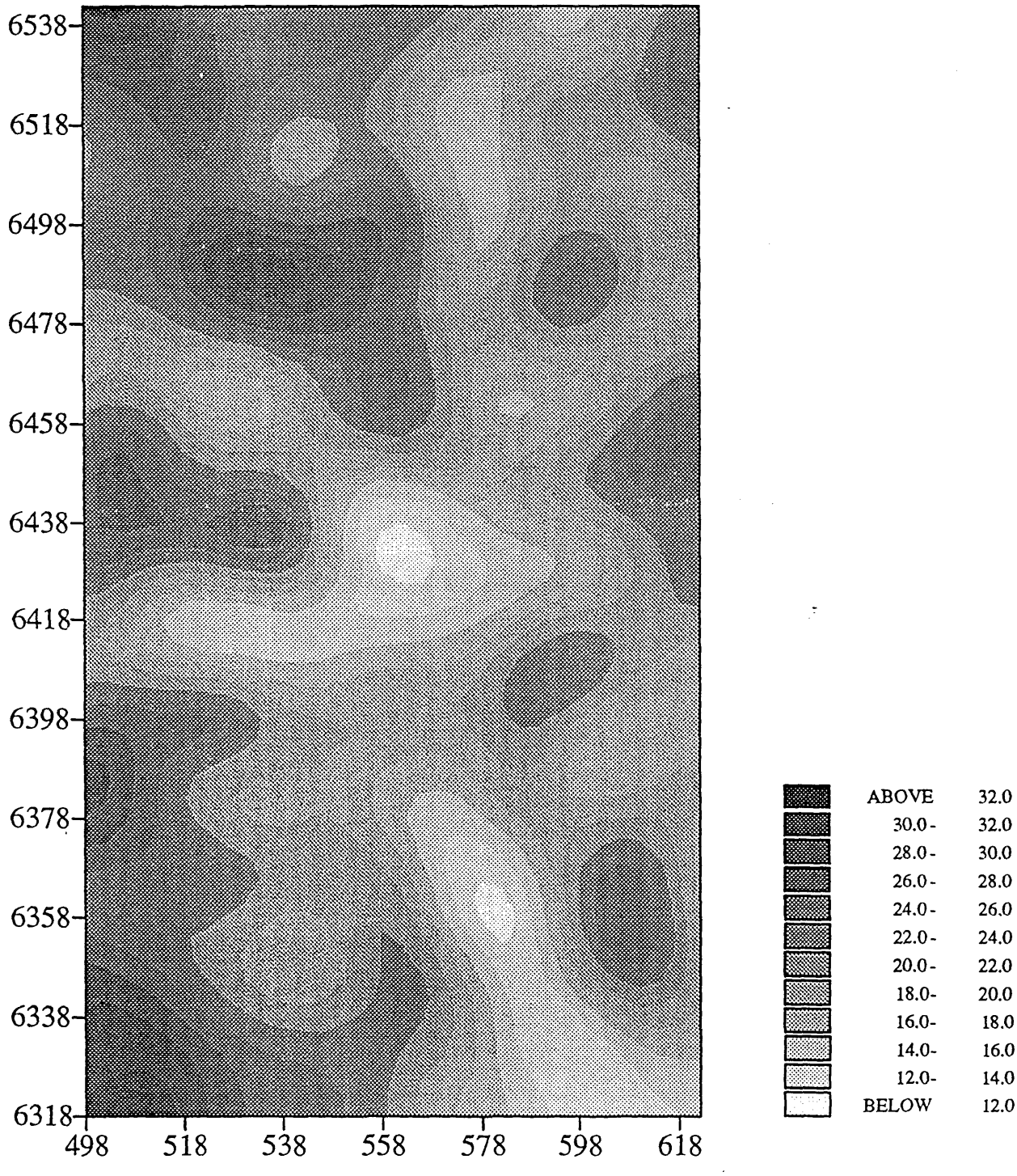


FIGURE 6.22 Thickness of the basement (in kilometres), derived by subtracting the depth to the Base-Cretaceous from the depth to the modelled Moho.

such as Latin (1990) an un-stretched crustal thickness of 32 km was chosen. As can be seen from figure 6.21 the Moho reaches depths of approximately 34 km in some very localised areas (e.g. the extreme south-western corner of the study area). Wherever this is the case such that the resulting calculated extension factor is less than unity then it has been rounded up to equal one. The results are shown in figure 6.23.

The maximum extension factor is approximately 2.8 and occurs in the centre of the 'triple-junction' area. A second centre of extension trends along the Central Graben where again, the maximum stretching factor is approximately 2.8. More minor centres of extension are found in the Witch Ground and Buchan Grabens and the South Viking Graben.

6.4.3 Possible Errors

The extension factors shown in figure 6.23 do not represent the true total extension. This is because the top of the basement has been taken as the Base-Cretaceous in the calculation outlined in 6.4.2. Therefore, no account is taken of the effect of pre-Cretaceous sediments. Latin (1990) reports that syn-rift sediments of the Jurassic-Cretaceous rifting event are relatively thin in the deeper parts of the basin however, little is known of Triassic and Permian sediment thicknesses. The seismic structure maps of Day et al (1981) show depths to the Base-Zechstein for part of the study area. Coverage is only complete in the south-east sector of the study area however, it shows the base Zechstein occurring at depths of greater than 7 km locally in the Central Graben area. It should also be noted that the original gravity modelling only involved low density near-surface layers younger than the Base-Cretaceous. Had more sediments been taken into account then the resulting residual gravity would have been larger and more positive. The final model of Moho topography obtained by modelling this residual gravity would therefore be more shallow in areas where pre-Cretaceous sediments are relatively thick. However, the relatively low density

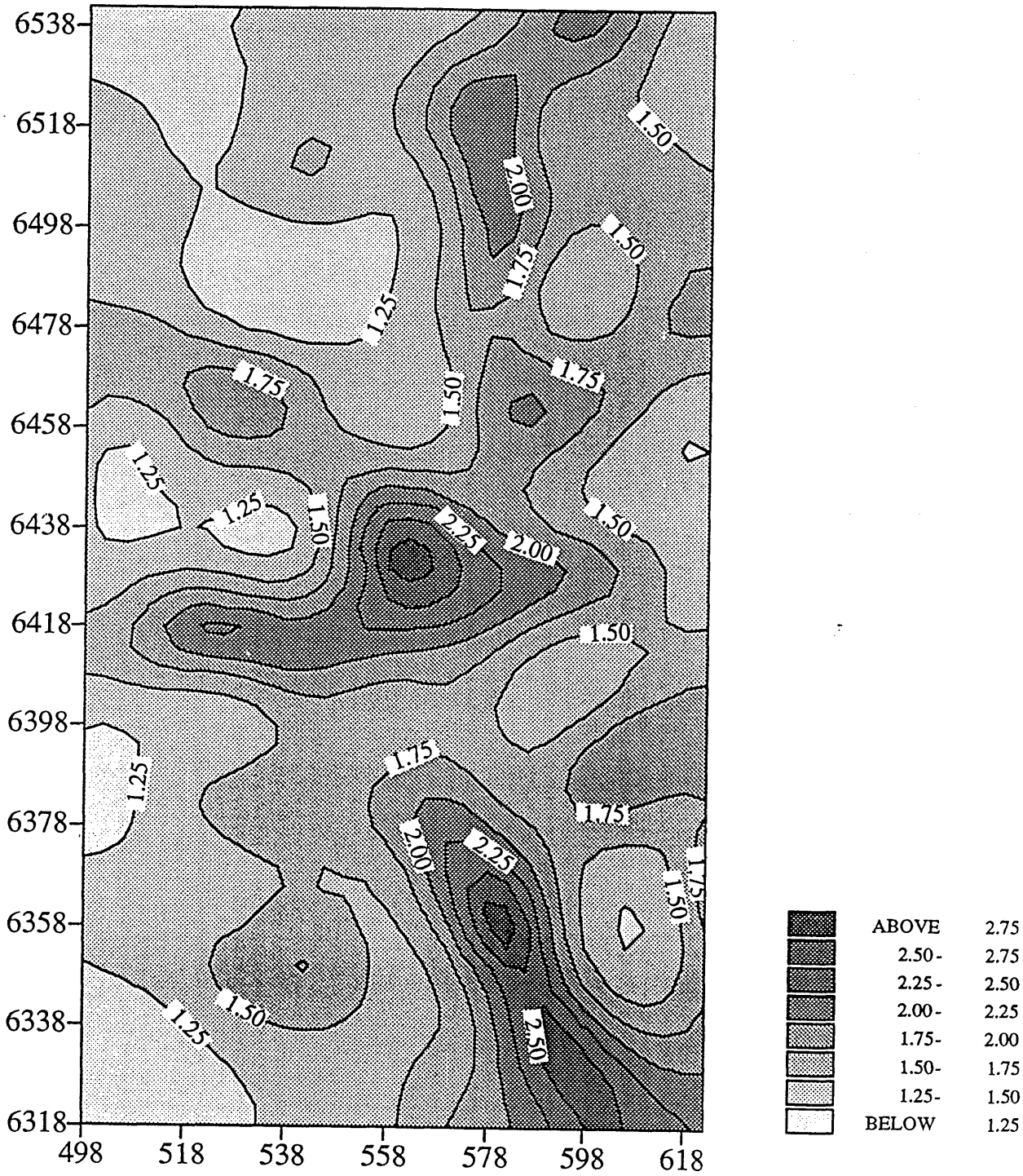


FIGURE 6.23 Estimated crustal stretching factors for the study area. The thickness of unstretched crust is taken to be 32 km.

contrasts associated with very deep sediments should result in this effect being rather small. The extension factors shown in figure 6.23 therefore represent minimum estimates of the true crustal extension.

As mentioned in 6.3.3 the errors involved in estimating crustal extension factors from measuring crustal thinning are always rather large and increase with increased values of Beta. In 3.5.4 the maximum estimation in the depth to the Moho was put at +/− 1.6 km. Table 6.1 below shows how this error affects the calculation of various extension factors using an un-stretched crustal thickness of 32 km.

Table 6.1 Errors in Estimated stretching Factors

Crustal Thickness (km.)	Min. Beta Factor	Av. Beta Factor	Max. Beta Factor
21.33 +/- 1.6	1.40	1.50	1.62
18.29 +/- 1.6	1.61	1.75	1.92
16.00 +/- 1.6	1.82	2.00	2.22
14.22 +/- 1.6	2.02	2.25	2.54
12.80 +/- 1.6	2.22	2.50	2.86
11.64 +/- 1.6	2.42	2.75	3.19
10.67 +/- 1.6	2.61	3.00	3.53

Thus the calculated extension factors can be in error by greater than 0.5 for the higher values.

In chapter 5 it was noted that due to the errors inherent in the magnetic modelling of the Piper-Forties Volcanic Province and the East Forties Basin intrusion the final model of the Moho as shown in figure 6.21 is likely to be in considerable error in these regions. It was shown that the model presented in figure 6.21 is likely to show too little crustal attenuation in the East Forties Basin and the Witch Ground Graben areas, since it seems likely that magmatism is more likely to occur in locations where the crust is highly attenuated. If this is

the case then the extension factors calculated in these areas will also be in error. Consider the East Forties Basin as an example. Figure 6.23 shows that a typical Beta factor for this area is 2.0 representing a crustal thickness of 16 km. If this was in error by say, 5 km and the crustal thickness was more like 11 km then the resulting Beta factor would be approximately 2.9.

Figure 6.24 shows the depth to the Moho for a model in which none of the magmatic bodies have been accounted for (see Chapter 3). The crustal thickness associated with this model are shown in figure 6.25. The crustal extension factors calculated for this model are shown in figure 6.26. The most likely model of crustal extension factors probably lies somewhere between the two end members shown in figures 6.23 and 6.26.

6.44 Comparison With Previous Work

Subsidence Overlay 1 shows the results of the subsidence analysis of Latin (1990). In the Central Graben area Latin's results agree very favourably with those obtained in this study. In most cases they are within the large error limits associated with the results obtained using crustal thinning. However it is apparent that the Beta factors calculated using crustal thinning are generally larger than those obtained via subsidence analysis. If the estimates of crustal extension made in this study are reasonably accurate (i.e. within the error limits outlined in 6.4.3) then this phenomenon could be explained if there was more pre-Jurassic extension than inferred from subsidence analysis. Latin's Beta factors refer only to the mid-Jurassic to early-Cretaceous event and therefore represent a minimum value for the total extension. However, as mentioned in 6.4.3 the crustal thinning models are also likely to be minimum estimates of extension as no account is taken of pre-Cretaceous sediments.

The large values of extension associated with crustal thinning models suggest that the relatively thin syn-rift sedimentary sequences found in the centre of the

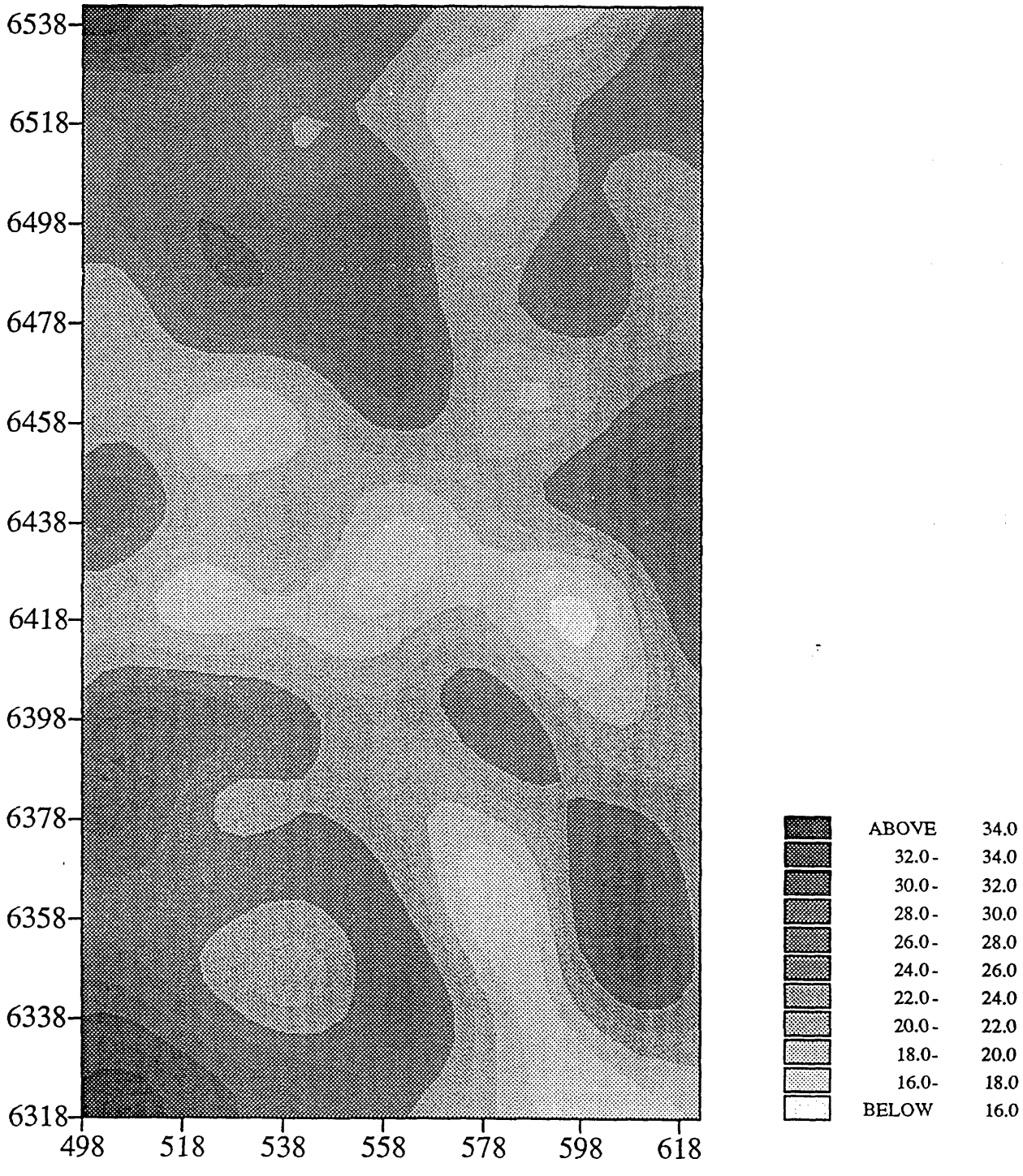


FIGURE 6.24 Depth to the Moho (km). The effects of igneous bodies in the study area are not taken into account during the modelling (same as figure 3.29).

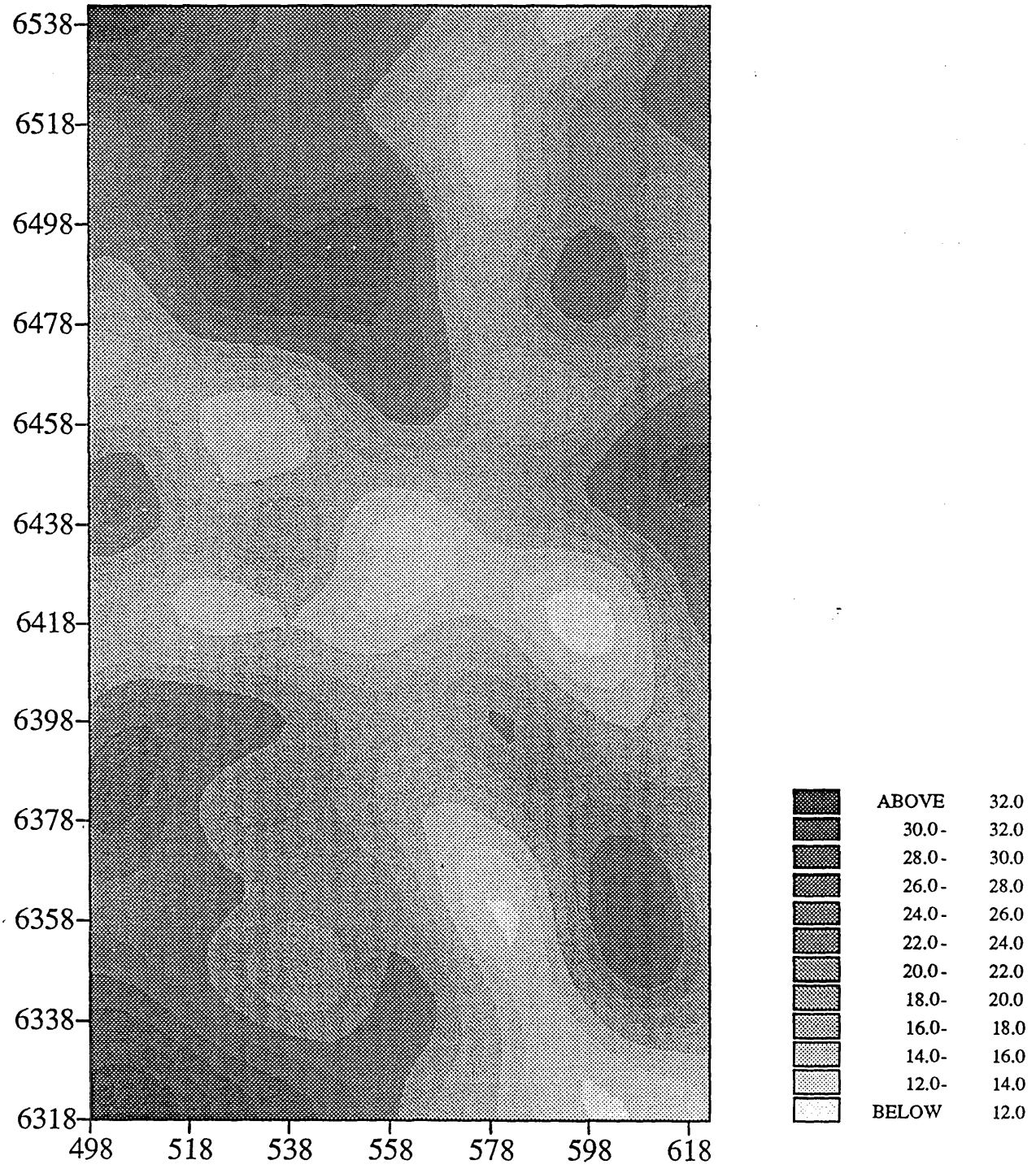


FIGURE 6.25 Thickness of the basement (km), derived by subtracting the depth to the Base-Cretaceous from the depth to the Moho (as shown in figure 6.24)

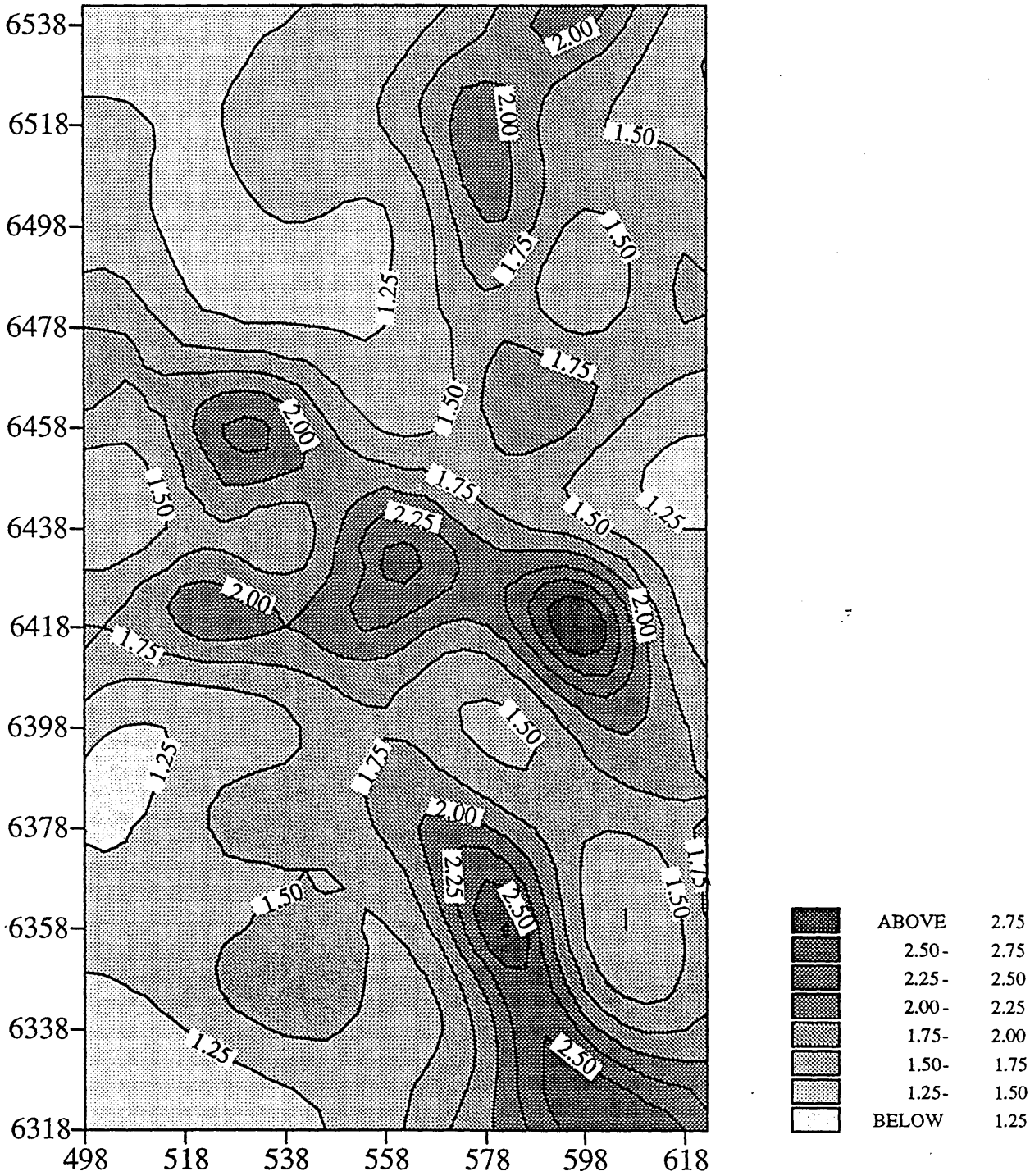


FIGURE 6.26 Estimated crustal stretching factors for the study area using the basement model shown in figure 6.25. The thickness of unstretched crust is taken to be 32 km.

basin (see 6.3.4.2 and Latin 1990) cannot be explained by invoking a coupled strain rate heterogeneous stretching model in which crustal thinning is always much lass than mantle thinning along the rift-axes. The coupled strain rate model also implies that in off-axis areas crustal extension will be much greater than mantle extension. The crustal thinning models show that this is evidently not the case since in off-axis areas the crustal Beta factors are generally close to unity. If a decoupled strain rate model is invoked the large values associated with crustal thinning are more readily explained (6.5.4).

As might be expected the crustal extension factors obtained in this study are always much greater than those obtained using Palinspatic reconstructions of major faults in the area. As outlined in 6.3.2 this method relies on every fault being recognised and the associated heaves being accurately measurable. Estimates of crustal extension made using this method are therefore always very conservative.

In the north of the study area the Beta factors calculated in this study match well with those obtained in a similar study for the northern North Sea made by Fichler and Hospers (1989) (6.2.3 and figure 6.8). They show a maximum crustal Beta factor of between 2 and 2.5 in the South Viking Graben at 59° N. For the same point in this study the crustal Beta factor is estimated at between 2 and 2.22.

As noted in chapter 1 there is very little deep seismic reflection data associated with it. This is due to the very thick sedimentary sequences in areas such as the East Forties Basin. The seismic reflection technique cannot easily penetrate these sequences making deep crustal interpretations impossible (pers. comm. M.R. Warner, Imperial College). The only seismic line(s) crossing the study area is the BIRPS NSDP-85-5 line which cuts across the Central Graben in the south-eastern corner of the study area. This line has been analysed and modelled using gravity data by Holliger and Klemperer (1990). Their results show less crustal thinning in the Central Graben area than obtained in this study and produce maximum crustal Beta factors of 2.0 centred on the rift axis. However, they have only

considered perfectly two-dimensional models. Relatively high-frequency lateral variations in the deep crustal structure of the basin may considerably affect the end result. This will be taken into account in the three-dimensional technique used in this study. Their profiles are also on a much larger regional scale. The NSDP-85-5 profile is greater than 550 km long whereas the study area in this study is only 124 km east-west. Their models are therefore not so detailed and the quality of fit is not so high.

The refraction line of Barton and Wood (1984) lies just to the south and east of the study area. Their maximum crustal Beta factor of 2.46 (6.3.3) is very similar to those obtained for the Central Graben in the south-east of the study area.

In the west the refraction line of Christie and Sclater (1980) which crosses the Witch Ground and Buchan Grabens produced maximum crustal Beta factors of 2.0. These are well in line with those estimates obtained in this study for the extreme west of the study area.

Table 6.2 below is a summary of the Beta factors obtained from various studies and from various regions in or near the study area.

Table 6.2 Summary of Extension Estimates from Various Sources

	C.Graben	Forties	S.Viking Graben	Outer Moray Firth
Gravity Beta	>2.5	>2.75	2.0	>2.0
Seismic Beta	>2.0	-	-	1.8
Max. Subs. Beta	2.1 - 2.3	2.5	-	2.0
Min. Subs. Beta	1.3 - 1.4	2.0	-	-

So far comparisons have only been made with estimates of crustal extension made by workers who favour coaxial stretching models. To the author's knowledge no estimates of extension have been made for the Central North sea by workers who favour the non-coaxial Wernicke-type models discussed in 6.2.3. The models

of Moho topography presented in chapters 3 and 5 show many regions where the large topographical gradient might suggest large-scale faults penetrating the mantle and off-setting the Moho. This is reminiscent of the models of the Viking Graben presented by Beach et al (1987) (6.3.3 and figure 6.12). However, as outlined in 6.2.3 simple shear models result in a marked asymmetry of sedimentary sequences about the rift, this is not the case in the Central North Sea. Simple shear models also result in thickened syn-rift sequences. Syn-rift sediments should be approximately three time thicker than those associated with the post-rift stage. As noted in 6.3.4.2 the converse is true in the Central North Sea. Latin and White (1990) have also presented convincing arguments against the simple shear model based on the location and volume of melt generated during rifting. Using the McKenzie and Bickle (1988) technique (outlined later in 6.5) which relates melt volumes and composition with Beta factors they show that it is necessary to invoke very large Beta factors (well in excess of 3.0) in order to generate any melting at all using a simple-shear model for the Central North Sea. Such very large Beta factors are not indicated even from crustal thinning measurements. Latin and White (1990) also show that the location of magmatism predicted using simple shear models is considerably offset from the rift axis. In the Central North Sea the principal magmatic bodies (ie. the Piper-Forties Volcanic Province and the East Forties Basin intrusion) are all located in axis areas.

6.5 THE RELATIONSHIP BETWEEN EXTENSION AND MAGMATISM IN THE NORTH SEA.

6.5.1 Introduction

It is beyond the scope of this research to present the complex relationship between magmatism and extension in any great detail. This has been dealt with in theoretical form by McKenzie and Bickle (1988) and has been applied specifically to the North Sea by Latin (1990), Latin et al (1990a) and Latin et al (1990b). It is useful however, to outline the method and application in order to

show how the melting observed in the Central North Sea relates to the crustal thinning measured in the previous chapters. For a more detailed study see Latin (1990). This section is made in reference to this work.

6.5.2 Summary of Method

McKenzie and Bickle (1988) explain how the volume and average composition of melt generated by adiabatic decompression of the asthenosphere may be predicted for a given amount of extension. Before any predictions can be made for any area the following parameters need to be quantified:

1) Potential Temperature of the Asthenosphere.
This is simply defined as the temperature the asthenosphere would have if it was allowed to rise adiabatically to the surface without melting.

2) Thickness of the Mechanical Boundary Layer.
This refers to the upper part of the lithospheric plate which is characterised by a more-or-less linear temperature gradient which is governed by conductive heat loss.

3) Lithospheric Stretching Factors and Strain Rate.

6.5.2.1 Potential Temperature

The potential temperature of the asthenosphere during rifting is an extremely important factor in governing the volume and composition of melt generated in the event (McKenzie and Bickle, 1988). The higher the potential temperature the larger is the volume of melt for any given amount of extension. Similarly, less extension is needed to induce melting if the potential temperature is relatively high.

The average asthenospheric potential temperature is given by McKenzie and Bickle (1988) as 1280 +/− 40° C Ziegler (1982) and Ziegler and Van Hoorn (1990) have put forward several arguments for the presence of a mantle plume in the Central North Sea during the Jurassic. Such a plume would result in an increased asthenospheric potential temperature of up to 1480° C. It is therefore important to decide whether or not a mantle plume was involved in the rifting process. Latin (1990) points out that there would be three predictable consequences of plume involvement.

1) Regional Doming. This would cause axi-symmetrical uplift of 1 - 2 km over a region of up to 2000 km in diameter.

2) Plume Trail. Migration of the European plate over a convective plume should lead to the temporal migration of the uplift and magmatism which would be associated with the plume.

3) Convective Thinning. A hot asthenospheric plume should cause a dramatically increased amount of mantle thinning with respect to crustal thinning.

Evidence in support of regional doming is mainly based on the fact that syn-rift sequences are so thin in the Central North Sea. However, it has been demonstrated that this phenomenon need not be solely due to uplift and erosion but could be explained by a heterogeneous stretching model.

A principal argument against the presence of a Jurassic plume is the paucity of any evidence of a plume trail. Figure 6.27 shows the path of the European plate across a stationary plume centred on the Forties region at 160 Ma. Using the palaeogeographic reconstructions of Ziegler and Van Hoorn (1990), Latin

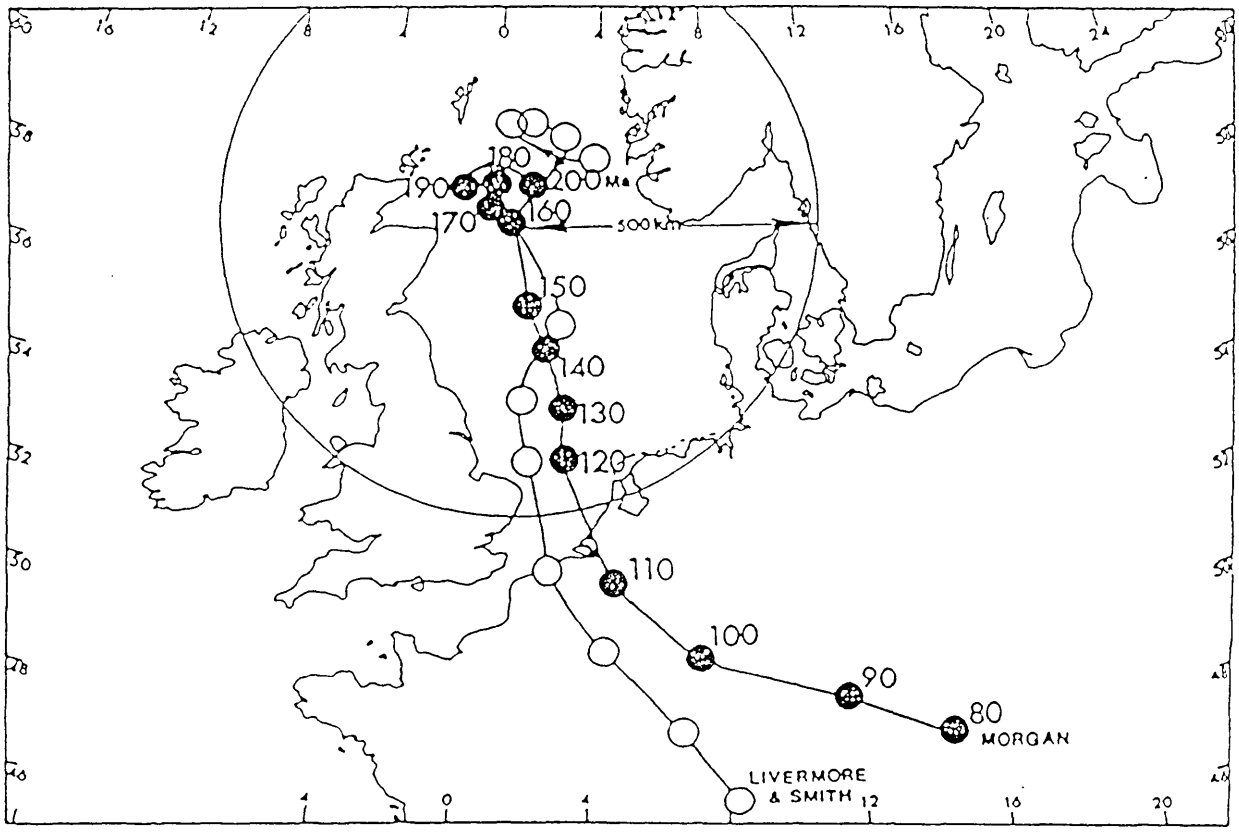


FIGURE 6.27 Motion of the European plate from 200 Ma to 80 Ma. Filled circles derived from Morgan (1981), open circles derived from Livermore and Smith (1985). Points mark the position of a stationary hot-spot, assumed to be centred on the Forties region at 160 Ma, at different times. The large circle (1000 km in diameter) represents the minimum region of plume-related uplift predicted by White and McKenzie (1988). After Latin (1990).

(1990) has shown that the plume was apparently absent immediately prior to the rifting event but may have been effective in causing uplift for a period of less than 30 My following the onset of rifting in the mid-Jurassic. After this period there is no evidence of a southward migration of plume-induced regional uplift or magmatism.

There is no direct evidence of convective thinning due to a plume which could be interpreted from either basement subsidence or studies of crustal thinning. Extension factors derived from subsidence analysis by fitting the thermal part of the subsidence curves refer to whole lithospheric thinning. There is no great mismatch between these values and those obtained from studies of crustal thinning. Assuming that there was only a relatively small amount of pre-Jurassic extension, this suggests that the mantle thinning is not hugely in excess of crustal thinning. The converse would be true had a plume been involved in the extension.

Using these arguments against the presence of a Mesozoic mantle plume Latin (1990) concluded that the most likely potential temperature for the asthenosphere is the 'normal' value of 1280 +/− 40° C.

6.5.2.2 Initial Mechanical Boundary Layer Thickness

There is no way of directly measuring the thickness of the mechanical boundary layer in the North Sea as it would have been immediately prior to the mid-Jurassic rifting event. It is important to quantify this thickness as it controls the minimum pressure obtained by upwelled asthenosphere after stretching. Generally speaking, a thinner mechanical boundary layer will result in a greater volume of melt for any given amount of lithospheric extension. Latin (1990) has estimated the thickness at between 90 and 100 km. This estimate is based on a detailed study of the thermal re-equilibration of the lithosphere following the Triassic extensional event.

6.5.2.3 Lithospheric Extension

Beta values for the lithosphere can either be taken from the values obtained from crustal thinning or subsidence analysis. As seen in the previous section (6.4) these values can be almost 3.0 in the Forties region. It was also mentioned that it is likely that these are minimum estimates.

Since it seems likely that a plume was not involved in the Jurassic rifting it is necessary to have very high strain rates early on in the rifting to explain the very early emplacement of the Piper-Forties basalts. The maximum decompression is assumed to take place in the first 10 - 20 My of rifting which, for the purposes of modelling means that extension can be approximated to an instantaneous rifting model.

6.5.3 Results

Figure 6.28 (after Latin, 1990) shows the relationship between Beta factor, potential temperature and mechanical boundary layer thickness using the McKenzie and Bickle (1988) method. Each diagonal line represents the values of Beta and potential temperature required to induce melting for a given mechanical boundary layer thickness. It appears that at the preferred potential temperature of 1280° C and a mechanical boundary layer thickness of between 90 and 100 km, melting will be induced at all points where extension is greater than 2.5. This is entirely compatible with the results obtained for crustal thinning in the Forties region. More difficult to explain is the fact that no melt is observed in the Central Graben area where Beta factors are also in excess of 2.5 in places.(see 7.22).

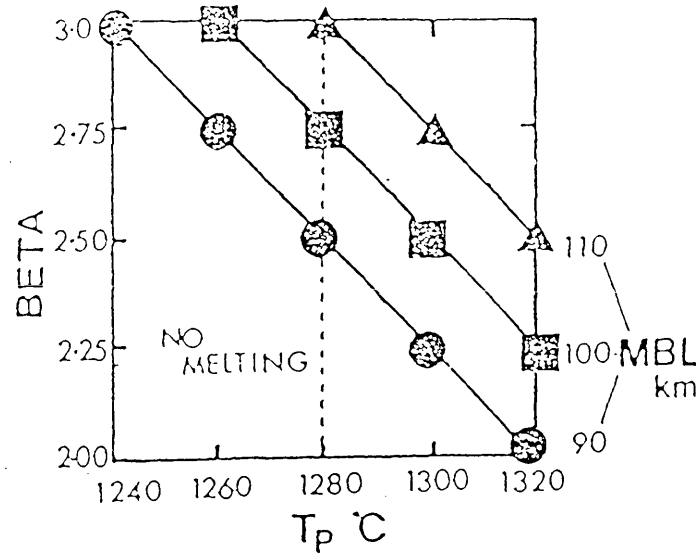


FIGURE 6.28 The relationship between Beta factor, Potential temperature and initial mechanical boundary layer thickness. The region of parameter space to the left of the dotted line and between the squares and the circles is considered to be the most likely in the Forties area of the North Sea. After Latin (1990).

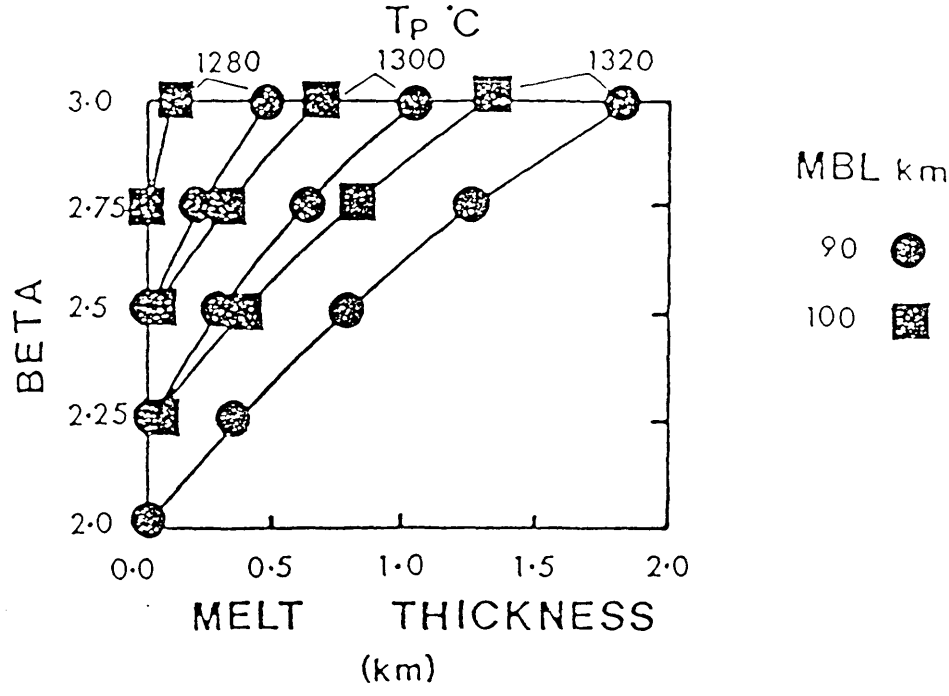


FIGURE 6.29 The predicted thickness of melt (km) in the Forties region as a function of Beta factor, potential temperature and initial thickness of the mechanical boundary layer. After Latin (1990).

Figure 6.29 shows the relationship between stretching factor, potential temperature and melt thickness for a given mechanical boundary layer thickness of 90 - 100 km. At potential temperature of approximately 1280° C the predicted melt thickness for stretching factors of over 2.75 (such as are seen in the Forties region) are anything between 0 and 0.7 km. The magnetic modelling of the Piper-Forties Volcanic Province (chapter 4) showed an average thickness of less than 1.2 km taken over the whole area. Given the ambiguities inherent in magnetic modelling and the errors involved with the McKenzie and Bickle method, the predicted thickness and the thickness obtained from modelling are in reasonably good agreement. If (as suggested in 6.4.3) the estimates of Beta are minimum values then the larger volumes of melt suggested by the magnetic modelling may be justified. It should be noted that the large igneous intrusion in the East Forties Basin has not been taken into account in the estimations of melt thickness. This is primarily because its age is unknown (it may be totally unconnected with the Jurassic rifting event). Its total volume is also extremely difficult to quantify with any degree of accuracy using the magnetic technique. For a detailed study of the melt composition predicted using the McKenzie and Bickle technique see Latin (1990).

6.5.4 Magmatism and Decoupled Strain Rate Extension

In section 6.3.4.2 it was mentioned that a decoupled strain rate heterogeneous stretching model might be used to explain a variety of features apparent from the subsidence data form the deeper parts of the study area. In this section the argument for a decoupled strain rate model is continued this time showing how the early emplacement of the Piper-Forties basalts might be explained.

The Forties region is characterised by four important observations which have yet to be explained:

1) There is evidence of uplift in the Central North Sea occurring at 180 - 160 Ma.

This is prior to the emplacement of the basalts in the Piper-Forties Volcanic Province (160 - 150 Ma) and the main phase of faulting (<150 Ma).

2) The basalts are emplaced prior to syn-rift sedimentation.

3) The syn-rift sediments are considerably thinner than the post-rift thermal sequence.

4) The post-rift thermal subsidence is very rapid.

The decoupled strain rate model proposed by Latin (1990) can be used to explain these observations. Figure 6.30 (after Latin 1990) shows a qualitative model of the variation of crustal and mantle extension with time for the 'triple-junction' area of the Central North Sea. The upper diagram shows the situation just after the onset of rifting. In the centre of the rift the mantle strain rate is much greater than that of the crust resulting in increased mantle extension over crustal extension. This would cause an early phase of uplift in axis areas. The mantle has thinned by its maximum amount (M) and the resulting adiabatic decompression will cause the asthenosphere and lower lithosphere to melt. Latin (1990) has interpreted this period as being equivalent to the Bathonian - Callovian of the Central North Sea. The centre diagram is characterised by a rapid increase in crustal strain rate such that the crustal extension exceeds that of the mantle in the rift centre causing subsidence in the rift axis. In off-axis areas the mantle thinning exceeds that of the crust causing uplift. This stage corresponds with the main phase of faulting in the Upper-Jurassic. The lower diagram shows the situation towards the end of the rifting event. In the rift centre crustal thinning has reached a maximum (C). Subsidence will continue in the rift axis both because crustal thinning exceeds that of mantle thinning and conductive cooling will be taking place. The flanks of the rift will continue to until the rifting is complete when the whole area will undergo thermal subsidence.

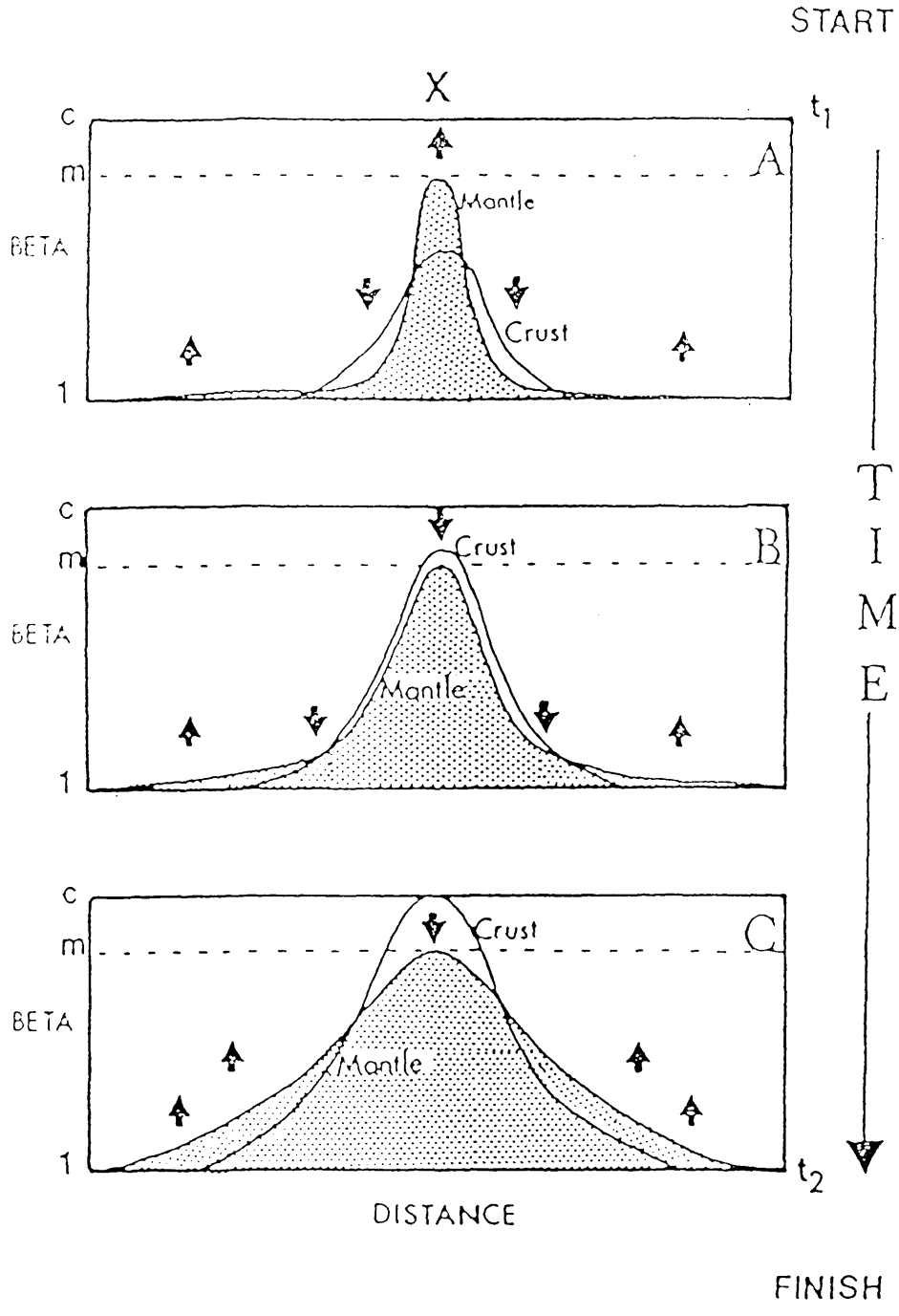


FIGURE 6.30 The decoupled strain-rate heterogeneous stretching model. Cartoons showing the possible variation of crustal and mantle strain (curves) with time and according to location during rifting across the 'triple-junction' area of the North Sea. See text for explanation. After Latin (1990).

6.6 SUMMARY

This section is a summary of the most important observations and conclusions made in this chapter.

1) Lithospheric extension models can be broadly divided into two types, coaxial or pure shear models and non-coaxial simple shear models.

2) Previous work on estimating extension in the North Sea Basin is based on either Palinspatic reconstruction of faults, measuring crustal thinning or subsidence analysis.

3) From the potential field modelling shown in chapter 3, 4 and 5 time-integrated estimates can be made of extension factors (Beta factors) in the study area. This is done by comparing the thickness of the basement in rifted areas with that of unstretched crust. These Beta factors (which are considered to be minimum estimates since no account is taken of pre-Cretaceous sediments) reach values of approximately 2.81 in the centre of the 'triple-junction' area.

4) Extension factors estimated by measuring crustal thinning are in good agreement with those estimated from subsidence analysis. However, they are persistently larger than estimates made from Palinspatic reconstructions of major faults.

5) In order to explain many features of the subsidence history of the Central North Sea, the best model appears to be one of coaxial, heterogeneous stretching involving decoupled strain rates between the crust and the mantle.

6) The McKenzie and Bickle (1988) modelling technique predicts that melting will occur in the Central North Sea provided the stretching factors are in excess of 2.5. This is consistent with the stretching factors observed in the region of the Piper-Forties Volcanic Province.

7) The volume of melt predicted by the McKenzie and Bickle technique is reasonably consistent with that indicated by magnetic modelling of the Piper-Forties Volcanic Province.

CHAPTER 7

CONCLUSIONS AND DISCUSSION.

7.1 CONCLUSIONS

The North Sea basin owes its complex geological history primarily to a series of extensional episodes the last phase of which occurred in the mid-Jurassic to early-Cretaceous. The main purpose of this research has been to estimate the amount of crustal extension which has occurred in the Central North Sea. This was achieved by measuring the amount of crustal thinning which has occurred in the rifted areas and comparing it with the thickness of the crust which has been unaffected by extension. Estimates of crustal thinning were made by modelling the regional gravity field. This section summarises the main conclusions and observations made during this research.

The Bouguer anomaly map for the Central North Sea shows a relatively smooth field of low amplitude (between −28 and 35 mGal). The thick sediments associated with the area should produce large negative gravity anomalies which are clearly not observed in the study area. It follows that there must be a compensating mass at depth. This mass was assumed to be high density mantle material. By determining the distribution of this mass it was possible to measure crustal thinning in the area. The total gravitational effect of sedimentary sequences down to the Base-Cretaceous was calculated in three dimensions and subtracted from the Bouguer anomaly data to obtain a residual gravity field. The basement (everything between the Base-Cretaceous and the Moho) was assumed to be homogeneous and the residual field was assumed to be caused by the high density compensating mass. After low-pass filtering the field was modelled in three dimensions to determine the depths to the gravity Moho in the study area. The best solutions show an upper-mantle body varying in depth to its upper surface

from approximately 34 km to approximately 16 km. Areas where the Moho is relatively shallow are governed by the major structural elements of the area, i.e. the Central Graben, the Buchan and Witch Ground Grabens, the South Viking Graben and the 'triple-junction' area. The shallowest parts were found in the East Forties Basin in the 'triple-junction' area and in the rift axis of the Central Graben. By quantifying the errors introduced at each stage in the modelling process, a total error was obtained for the depths to the Moho. This error was found not to be in excess of +/- 1.6 km.

It was noted that in some areas (e.g. the East Forties Basin) the modelled Moho appears to be particularly shallow. A possible cause was identified as being the presence of high density bodies not accounted for in the modelling process. It was also noted during a qualitative interpretation of the aeromagnetic data for the study area, that two of these areas of anomalously shallow Moho (the East Forties Basin and Piper-Forties Volcanic Province) are also associated with large magnetic anomalies. The causative bodies associated with these magnetic anomalies were identified as being a large, deep-seated igneous intrusion in the East Forties Basin and the Piper-Forties alkali basalts. Using a 2.5D combined forward and inverse magnetic modelling technique both of these magnetic bodies were modelled. In contrast with some earlier workers (e.g. Howitt et al, 1975) who have concluded that the Piper-Forties Volcanic Province consists of a maximum thickness of 1.5 km of basalt, these models show large thickness of basalt of between 6 and 8 km occurring in and around a possible vent site in the Witch Ground Graben. Over the whole area however, the average thickness is approximately 1.2 km.

Using these magnetic models the total gravitational effect of the East Forties Basin intrusion and the Piper-Forties basalts was estimated and was removed from the gravity field in the same way as the net effect of the near-surface layers. The new field was then re-filtered and re-modelled. The revised model shows a considerably deeper Moho in the Forties and Witch Ground Graben areas. However, the ambiguities inherent in the magnetic modelling process cause large

uncertainties in the final model of gravity Moho topography in the regions where it has been most altered. The errors cannot be accurately quantified but were estimated to be approximately 5 km in the East Forties Basin and perhaps 2 km in the Witch Ground Graben. Since it seems likely that magmatism will occur in areas where the crust is thinnest a more accurate solution will lie somewhere between the revised model and the original in which no account was made of the magmatic bodies.

Using the models of Moho topography crustal extension factors (Beta factors) were estimated for every point in the study area by finding the ratio of unstretched crustal thickness (here taken to be 32 km) to the thickness of the basement. The basement is defined as being everything between the Base-Cretaceous and the Moho. The values obtained reach a maximum of approximately 2.81 in the Forties and Central Graben areas. Errors associated with these estimates increase with an increased size of the Beta factor. For Beta factors of around 2.75 the uncertainty is −0.33 or +0.44 for an error of +/− 1.6 km in the depth to the gravity Moho. Errors will be larger in the East Forties Basin and Witch Ground Graben areas due to the additional uncertainties involved in calculating the gravitational effect of the igneous bodies in these areas.

Measuring crustal thinning provides only time-integrated estimates of extension, i.e. the effects of individual rift phases cannot be separated. In this research the Beta factors obtained are likely to be minimum estimates of the total extension since no account is taken of any pre-Cretaceous sediments. The results obtained are in good agreement with those estimated by Latin (1990) using subsidence analysis. Latin reports that the subsidence data for the Central North Sea is often characterised by a relatively thin syn-rift sedimentary sequence when compared with the thermal post-rift sediments. The large amount of crustal thinning evident from the gravity modelling suggest that this phenomenon cannot be explained by a model of heterogeneous stretching by pure shear in which the crustal stretching is always less than that of the mantle. Such a mantle would also require more crustal thinning in the off-axis areas than in the rift centres, this is not observed

in the gravity models. A better model would be one involving heterogeneous coaxial stretching in which the strain rates in the mantle and crust are not coupled. This would allow mantle stretching to exceed crustal thinning in the early stages of extension and the converse to be true as the rifting event continues. This would explain both the early emplacement of the Piper-Forties basalts and the relatively thin syn-rift sequences.

The steep gradients observed in the model of gravity Moho topography might suggest a Wernicke-type simple shear mode of extension in which large faults penetrate the lithosphere and offset the Moho. However, other observation in the Central North Sea suggest that this is not the case. These include: the axi-symmetrical distribution of sediments, the relatively compressed syn-rift sequences and the presence of magmatism in axis areas.

The McKenzie and Bickle (1988) modelling technique predicts that melting will occur in the Central North Sea provided the Beta factors are in excess of 2.5. This is entirely consistent with the stretching factors estimated from crustal thinning in the Piper-Forties Volcanic Province region. Magnetic modelling of these basalts revealed an estimated average thickness of approximately 1.2 km. The Mckenzie and Bickle technique predicts a somewhat smaller thickness of approximately 0.7 km. for Beta factors of roughly 2.8. However, when the large uncertainties involved in both modelling techniques are considered the two estimates are in reasonably good agreement.

7.2 DISCUSSION

7.2.1 Isostatic Equilibrium.

The assumption of Airy isostasy is critical to the calculations involved in the back-stripping process of subsidence analysis. Perfect Airy isostasy requires that the elastic thickness (T_e) (Turcotte and Schubert, 1982) of the lithosphere is zero. As outlined in 6.3.4.1 Wood (1982) and Barton and Wood (1984) have shown that on a regional scale in the North Sea the value of T_e was less than 5 km. The assumption of Airy isostasy is therefore usually considered to be valid.

The gravity models of Moho topography derived in chapter 3 and 5 are not in perfect local isostatic equilibrium. In many areas (principally the rift-axis areas) the modelled Moho appears to be too shallow. It was found that in regions such as the Forties area the gravity Moho needs to be up to approximately 9 km deeper than the model suggests in order to achieve Airy-type isostatic equilibrium with compensation at the Moho. Such a change in the model would result in an unacceptably poor quality of fit between the 'observed' gravity used in the 3D modelling procedure and the calculated gravity for the modified model.

It was decided to solve this dilemma by testing the assumption of local Airy isostasy on the relatively small scale of the study area. The theory behind the test is simple. Given that the thickness and density contrasts of all sedimentary sequences are known, it is possible to determine the shape of the compensating mass which would give rise to perfect isostatic equilibrium provided the density of that mass is known. The gravitational effect of this mass can then be calculated in three dimensions. If the study area is in perfect Airy-type isostatic equilibrium then the sum of this calculated gravity and the known gravitational effect of the near-surface layers should be closely matched to the observed Bouguer gravity for the area.

Using a depth of compensation of 32 km for the compensating upper-mantle

body and a density contrast of 0.5 g cm^{-3}, the depth to the Moho which would give rise to perfect isostatic equilibrium is given by:

$$D = 32 + (\Sigma \Delta\rho_i t_i / 0.5)$$

Where:

D = Depth to the Moho

$\Delta\rho_i$ = Density contrast of the i^{th} near-surface layer (w.r.t. 2.75 g cm^{-3})

t_i = Thickness of the i^{th} layer.

As in the gravity modelling four near-surface layers are considered: Water, Tertiary, Palaeocene and Cretaceous. No account is taken of any pre-Cretaceous sediments or the igneous rocks in the Forties area.

Figure 7.1 shows the depth to the Moho using the above calculation. As might be expected the general shape is a almost a mirror image of the depth to the Base-Cretaceous (figure 3.9) and it is considerably deeper than the Moho models shown in figures 3.25, 3.28 and 5.10.

Using the Plouff 3D modelling routine outlined in 3.4.1.3 the gravitational effect of this body was calculated. The result is shown in figure 7.2. This was then added to the total gravitational effect of the near-surface layers, the result is shown in figure 7.3. Figure 7.4 shows the observed Bouguer anomaly data for the study area. It is clearly seen that the calculated field and the observed field are very different, strongly suggesting that the area is not, in fact, in perfect local isostatic equilibrium. The estimated value of up to 5 km for T_e (Barton and wood ,1984) would tend to support this theory.

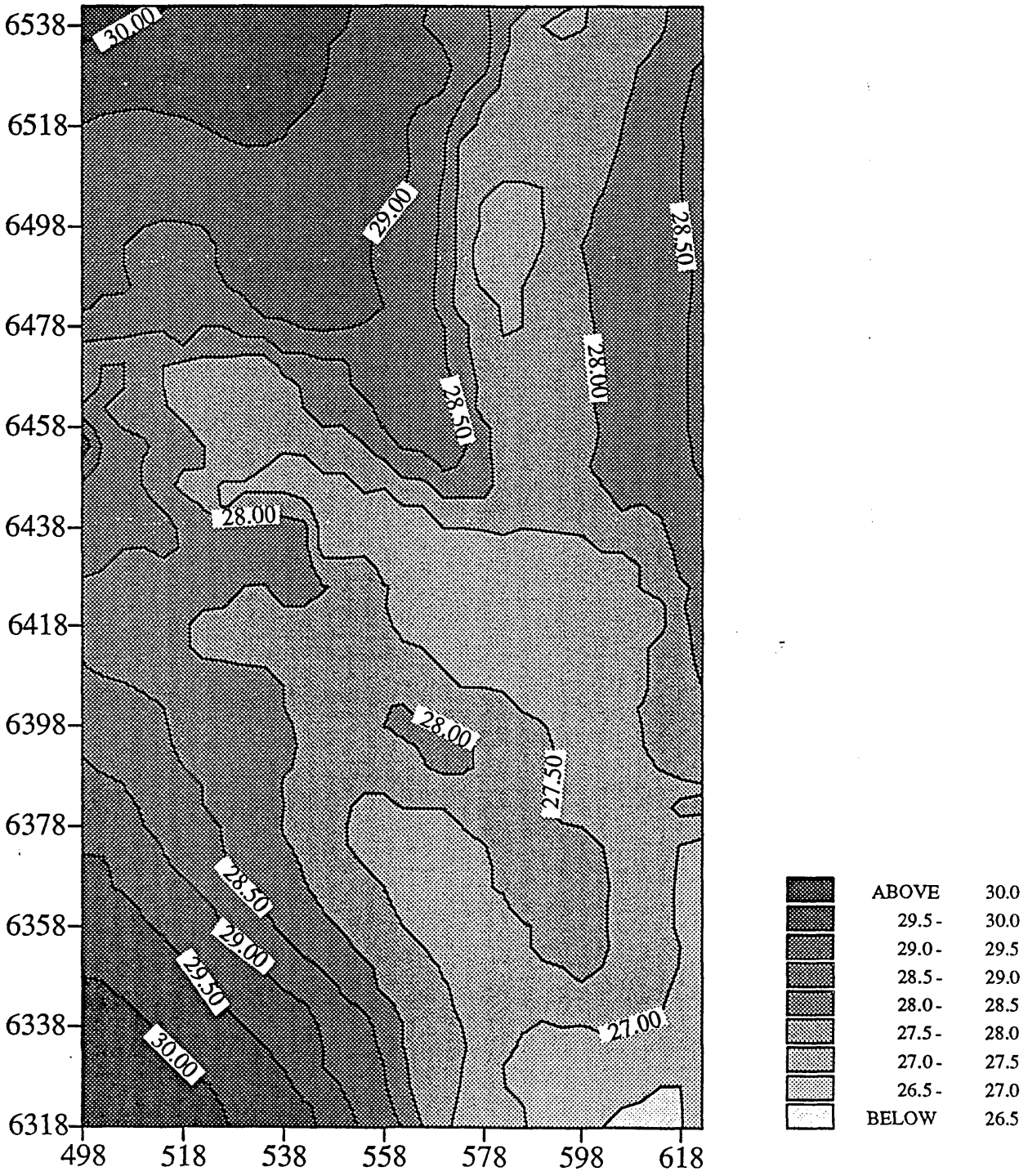


FIGURE 7.1 The calculated depth to the Moho (km) which would give rise to perfect isostatic equilibrium in the study area.

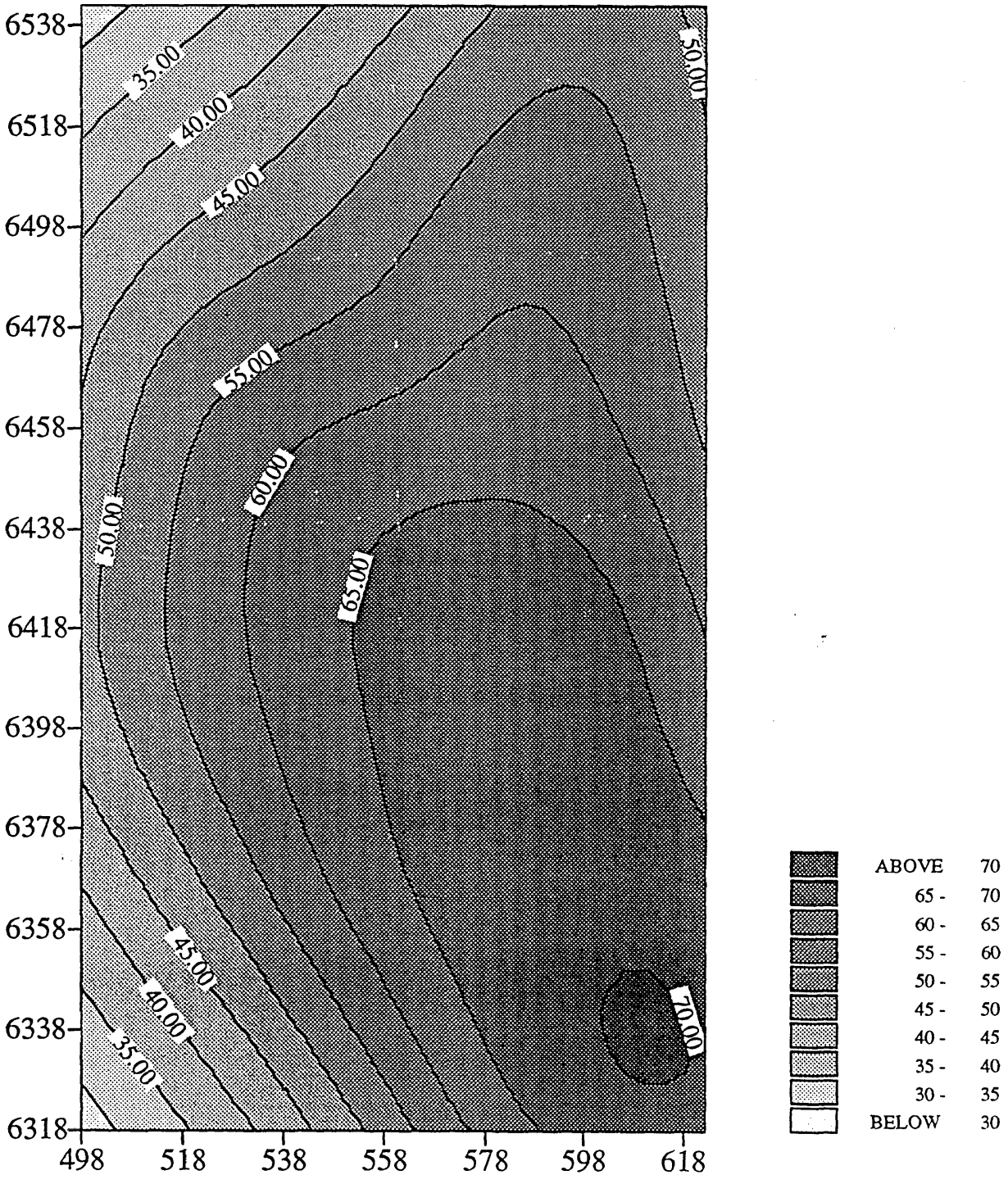


FIGURE 7.2 Calculated gravitational effect (mGals) of the upper-mantle body which would give rise to perfect isostatic equilibrium.

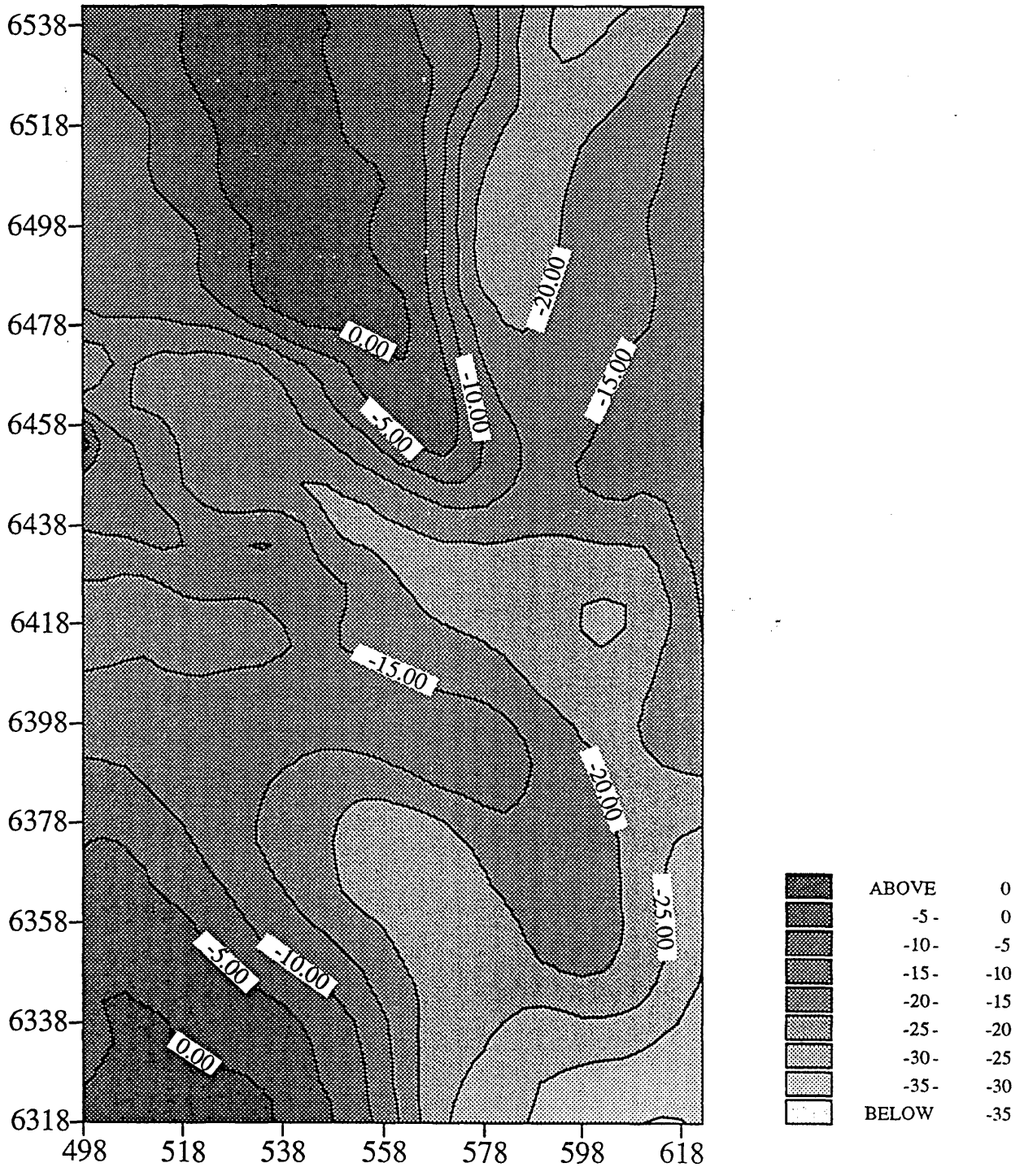


FIGURE 7.3 The sum of the total gravitational effect of the near-surface layers and the calculated effect of the upper-mantle body which would give rise to perfect isostatic equilibrium.

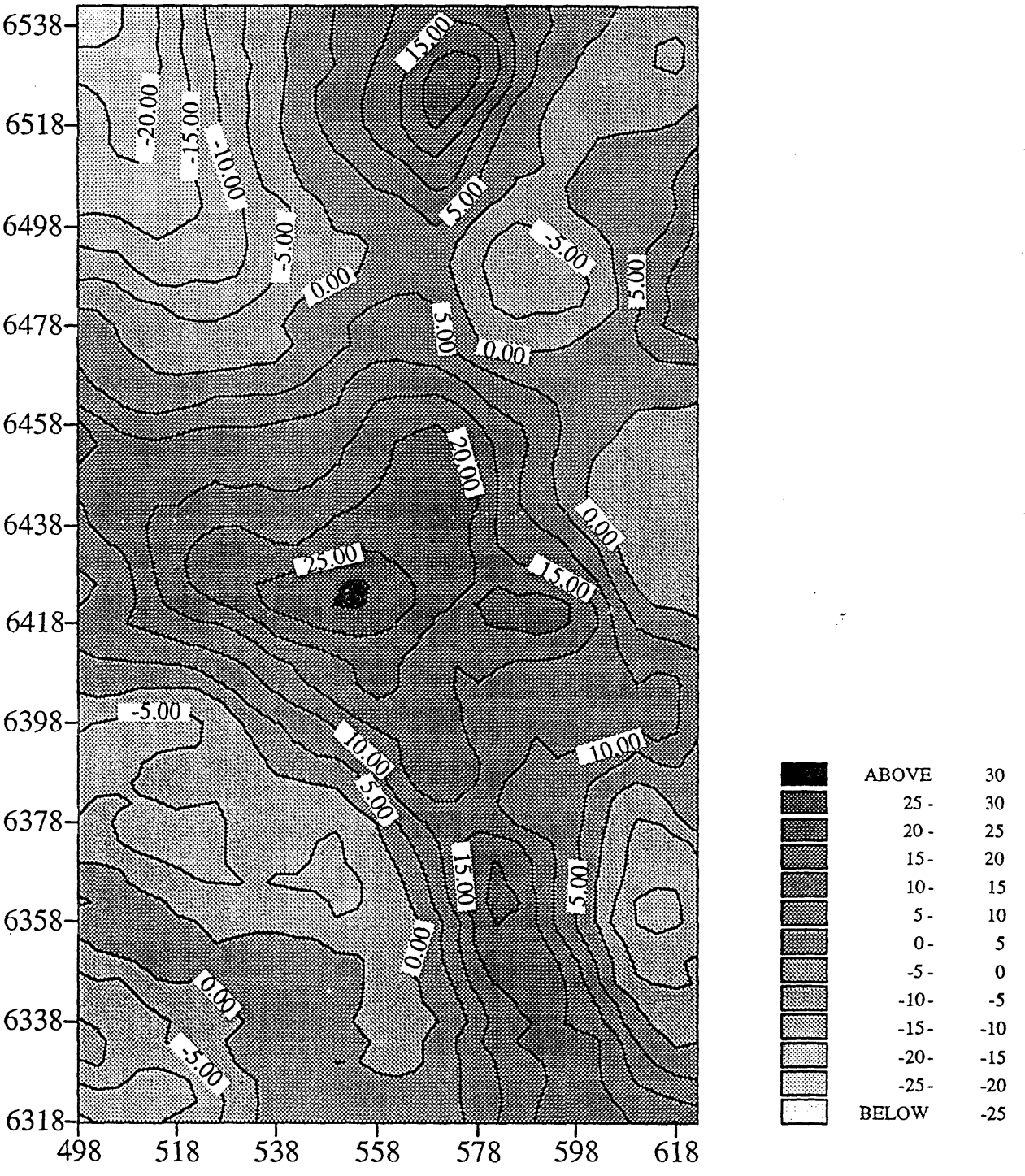


FIGURE 7.4 The 'observed' Bouguer anomaly data for the study area (mGals).

The question now arises as to whether or not a lithospheric plate with a value for T_e of less than 5 km can support the loads implied by the gravity models. Turcotte and Schubert (1982) demonstrate that the degree to which a lithospheric plate of finite elastic thickness can support a periodic load by flexure is a function of that load's wavelength. Figure 7.5 (after Turcotte and Schubert, 1982) shows the relationship between the degree of compensation, C, and the non-dimensional wavelength of the load.

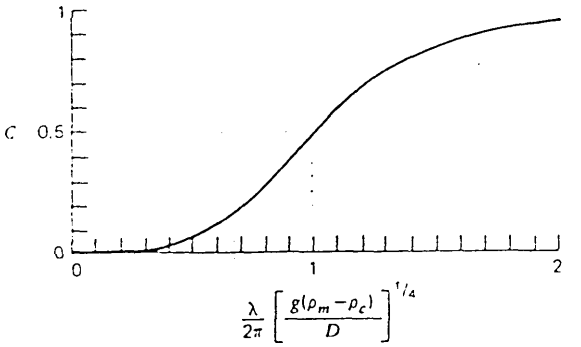


FIGURE 7.5

$$C = \frac{(\rho_m - \rho_c)}{\rho_m - \rho_c + \frac{D}{g}\left[\frac{2\Pi}{\lambda}\right]^4}$$

ρ_m = Density of the mantle (3250 kg m^{-3})

ρ_c = Density of the crust (2750 kg m^{-3})

g = Acceleration due to gravity (9.78 m s^{-2})

λ = Wavelength of the load

D = Flexural rigidity of the plate which is defined by:

$$D = \frac{Eh^3}{12(1-\nu^2)}$$

Where:

E = Young's Modulus (70 GPa)

h = Elastic Thickness (5000 m)

ν = Poisson's Ratio (0.25)

Using the above parameters and the graph shown in figure 7.5 it can be shown that for a lithospheric plate with an elastic thickness of 5 km a periodic load is 50 % compensated (C = 0.5) if the wavelength of that load is approximately 125 km. Loads with a wavelength shorter than this are substantially supported by the rigidity of the lithosphere, larger wavelengths are only weakly supported.

The models derived in this study show an increase in the load across the basin of approximately 0.68 kbar however, the wavelength associated with the excess load is everywhere less than 125 km. It can therefore be concluded that a lithosphere with an elastic thickness of 5 km can support the loads implied by the gravity models by a combination of flexure and Airy-type isostasy.

7.2.2 Uniform Basement and Nature of the Moho.

The assumption of a uniform basement is essential to the gravity modelling philosophy outlined in chapter 3. In this research the basement is taken to be everything between the Base Cretaceous and the Moho. Pre-Cretaceous sediments were not included in the modelling since their thicknesses are unknown throughout the study area. As outlined in 6.4.2 the effect of including more low density sediments in the models would be to make the gravity Moho appear shallower than it does in any of the models presented in chapters 3 and 5. However, since the densities of such deep sediments will be relatively high and approaching that assumed for the basement their total gravitational effect will be relatively small. One of the main assumptions made in the gravity modelling process is that the crystalline basement is both laterally and vertically homogeneous. Holliger and Klemperer (1990) suggest that the only way to determine whether or not such large-scale density contrasts exist within the basement is to compare the interpretations of Moho depths from both gravity modelling and seismic data in the same area. The lack of good deep reflection or refraction seismic data from the study area makes this impossible. The only deep

seismic reflection profile crossing the study area is the BIRPS NSDP-85-05 line which crosses the Central Graben in the extreme south-east of the study area. Holliger and Klemperer (1990) present a 2D gravity interpretation along this line and do not report any significant contrasts between the depths to their gravity Moho and the interpreted reflection Moho. This would suggest that no significant density contrasts occur within the crystalline basement. However, the gravity modelling in this study results in a Moho which is locally up to 7 km. shallower than that of Holliger and Klemperer (1990). As outlined in 6.4.4 the 3D models used in this study are on a much smaller scale than the regional, basin-wide profiles of Holliger and Klemperer (1990) and therefore contain more detail and involve a better quality of fit between the observed and calculated fields. If these models are more accurate than those of Holliger and Klemperer (1990) then the difference between the gravity and reflection Moho needs to be explained.

The Moho as derived in the gravity modelling is defined by a sharp density contrast which is interpreted as being the crust-mantle boundary. The reflection Moho however, is usually defined as being the base of the highly reflective zone of the lower crust. Holliger and Klemperer (1989) point out that if the lower crust were to be either underplated or intruded by layers of basalt whose density approaches that of the upper-most mantle then the reflection Moho will appear deeper than that of the gravity Moho. It seems probable that underplating is most likely to occur where the crust is most thinned, thus it may explain the difference between the gravity and reflection Moho in the thinned crust of the Central Graben. In support of this idea, the results of modelling in the Central North Sea using the McKenzie and Bickle (1988) technique presented by Latin (1990) showed that melting might be expected in every region where the crustal stretching factor is greater than 2.5. Magmatism is not observed in the study area apart from in the Forties region however, much of the rift axis areas are characterised by Beta factors approaching or greater than 2.5. It is possible that much of the melt predicted by the Mckenzie and Bickle technique never reached the upper crustal levels and is present as deep-crustal intrusions or underplating.

7.2.3 Control of North Sea Rifts by Caledonian Basement Structures

The crystalline basement of the Central North Sea has undergone a very complex geological history. As seen from the magnetic data (chapter 4) the Caledonian orogeny imparted a very strong structural grain to many parts of the study area. It seems possible that re-activation of these ancient structural discontinuities may have influenced the development of the younger rift system. In the study area the Caledonian trend is dominantly NE - SW or ENE - WSW. Johnson and Dingwall (1981) report that re-activated Caledonian faults in the Witch Ground and Buchan Grabens facilitated much of the stress release involved in the mid-Jurassic to early-Cretaceous rifting event. They also point out that the 'triple-junction' area almost forms a termination for a north-east extension of the Highland Boundary Fault and that the Highland Boundary Fault itself marks the southern edge of the Caledonian stabilised zone.

Frost et al (1981) in a study of the ages and lithologies of crystalline basement sampled from deep wells note that there is a distinct difference between the basement north and south of the fault. To the north they report the basement as consisting of high-grade metamorphic rock which was originally metamorphosed in the Pre-Cambrian. To the south the basement consists of low-grade Caledonian metamorphic rock. The Highland Boundary Fault lineament may therefore control the southern extent of extension in the Buchan and Witch Ground Grabens. Johnson and Dingwall (1981), point out that the South Viking Graben is bound to the west by the shallow basement of the Fladen Ground Spur which is largely made up of Devonian strata with a thin Mesozoic cover and thicker Tertiary sediments. To the east the basement is also shallow but wells drilled on the Norwegian shelf reveal a Pre-Cambrian basement marking the westward extent of the Baltic Shield. The Viking Graben may therefore have developed along the basement discontinuity marking the junction of these zones. Frost (1977) and Frost et al (1981) believe that in the Central and Southern North Sea the Caledonian has a NW - SE grain (see figure 4 of Ziegler, 1981) which may have strongly influenced the development of the Central Graben.

It is not within the scope of this research to produce a working model for the geological history of the North Sea rifts (for detailed studies see Ziegler and Van Hoorn, 1990 and Gibbs (1990)). However, it is interesting to speculate on whether the zones of maximum crustal thinning defined in this study are related to ancient basement discontinuities. In many areas of the models defining gravity Moho topography the topographical gradient is seen to be very steep (eg. the North Central Graben). It seems possible that if ancient crustal discontinuities existed in the area prior to the onset of rifting then during an extensional event stress will tend to concentrate along such weaknesses thus influencing the location of the rift axes.

7.2.4 Further Work

The potential field modelling techniques outlined in this research have provided useful information about the deep-crustal structure of the Central North Sea in the absence of any good quality deep seismic data. A major critique of the method could be that no pre-Cretaceous sediments were taken into account during the modelling. If the data were available (perhaps from commercial sources) it would be useful to re-model the area to include sediments down to say, the Base-Zechstein. A second improvement would be to use a tighter grid spacing in the grids defining the depths to each of the near-surface layers. This would improve the resolution over major faults in the area.

The study area used in this research is relatively small in comparison with the regional basin-wide gravity profiles presented by Holliger and Klemperer (1989, 1990) and Zervos (1987). There is no reason why, given the time and data, that 3D gravity models such as those presented in this study could not be produced on the same regional scale. Deep seismic refraction and reflection lines would provide useful controls to constrain the models at several points, something which was not really possible in this study.

REFERENCES

Anderton, R., Bridges, P.H., Leeder, M.R. and Sellwood, B.W. (1979). A Dynamic Stratigraphy of the British Isles: A Study in Crustal Evolution. London, George, Allen and Unwin.

Andreason, G.E., and Zietz, I. (1969), Magnetic fields for a 4 x 6 prismatic model. U.S. Geological Survey - Professional paper 666.

Andrews, I.J., and Brown, S. (1987). Stratigraphic evolution of the Jurassic, Moray Firth. In Petroleum Geology of North West Europe, (Eds., J. Brooks and K. Glennie), Graham and Trotman, London. 785-795

Baranov, V. (1957). A new method for the interpretation of aeromagnetic maps: pseudo gravimetric anomalies. Geophysics, **22**, 359-383

Barton, P. (1986). The relationship between seismic velocity and density in the continental crust - a useful constraint?. Geophysical Journal of the Royal Astronomical Society., **87**, 195-208

Barton, P., and Wood, R. (1984). Tectonic evolution of the North Sea Basin: crustal stretching and subsidence. Geophysical Journal of the Royal Astronomical Society, **79**, 987-1922

Beach, A. (1986). Some comments on sedimentary basin development in the northern North Sea. Scottish Journal of Geology, **22**, 1-20

Beach, A., Bird, T., and Gibbs, A. (1987). Extensional tectonics and crustal structure: deep seismic reflection data from the northern North Sea Viking Graben. In Continental Extensional Tectonics (Eds. M.P. Coward, J.F. Dewey, and P.L. Hancock), Geological Society of London Special Publication, **28**, 467-476

Behrendt, J.C., and Grim, M.S. (1985). Structure of the U.S. Atlantic continental margin from derivative and filtered maps of the magnetic field. In The Utility of Regional Gravity and Magnetic Maps. (Ed., W.J. Hinze) Society of Exploration Geophysics. p 325

Boccaletti, M., Horvarth, F., Loddo, M., Mongelli, F., and Stegena, L. (1976). The Tyrrhenian and Pannonian Basins: a comparison of two Mediterranean interarc basins. Tectonophysics, **35**, 45.

Briggs, I.C. (1974). Machine contouring using minimum curvature. Geophysics, **39**, No. 1, 39-48.

Buck, W.R., Martinez, F., Steckler, M.S., and Cochran, J.R. (1988). Thermal consequences of lithospheric extension: pure and simple. Tectonics, **7**, 213-234

Christie, P.A.F., and Sclater, J.G. (1980). An extensional origin for the Buchan and Witchground Grabens. Nature, **283**, 729-32

Condon, P.J. (1988). Seismic Stratigraphy and Distribution of Palaeogene Sediments West and East of Shetland. Unpublished Ph.D. thesis, University of Edinburgh.

Day, G.A., Cooper, B.A., Anderson, C., Burgers, W.F.J., Ronnevik, H.C., and Schoneich, H. (1981). Regional seismic structure maps of the North Sea. In Petroleum Geology of the Continental Shelf of North-West Europe, (Eds. L.V. Illing and G.D Hobson) pp 76-84, Institute of Petroleum, London.

Dixon, J.E., Fitton, J.G., and Frost, R.T.C. (1981). The tectonic significance of post-Carboniferous igneous activity in the North Sea Basin. In Petroleum Geology of the Continental Shelf of North-West Europe, (Eds. L.V. Illing and G.D Hobson) pp 121-37, Institute of Petroleum, London.

Dods, S.D., Tesky, D.J. and Hood, P.J. (1985). The new series of 1:1 000 000 scale magnetic anomaly maps of the Geological Survey of Canada: compilation techniques and interpretation. In The Utility of Regional Gravity and Magnetic Maps. (Ed., W.J. Hinze) Society of Exploration Geophysics.

Donato, J.A., and Tulley, M.C. (1981). A regional interpretation of North Sea Gravity Data. In Petroleum Geology of the Continental Shelf of North-West Europe, (Eds. L.V. Illing and G.D Hobson) pp 65-75, Institute of Petroleum, London.

Fall, H.G. (1980). The Petrology and Geochemistry of Jurassic Igneous Rocks from the Northern North Sea. Unpublished Ph.D. thesis. University of Sheffield.

Fall, H.G., Gibb, F.G.F., and Kanaris-Sotiriou, R. (1982). Jurassic volcanic rocks of the northern North Sea. Journal of the Geological Society of London, **139**, 277-92

Fichler, C., and Hospers, J. (1990). Deep crustal structure of the northern North North Sea Viking Graben: results from deep reflection seismic and gravity data. Tectonophysics, **178**, 241-254.

Frost, R.T.C, and Fitch, F.J., and Miller, J.A. (1981). The age and nature of the crystalline basement of the North Sea Basin. In Petroleum Geology of the Continental Shelf of North-West Europe, (Eds. L.V. Illing and G.D Hobson) pp 43-57, Institute of Petroleum, London.

Gibbs, A.D. (1987). Deep seismic profiles in the northern North Sea. In Petroleum Geology of North-West Europe (Eds. J. Brooks and K.W. Glennie). pp 1025-28, Graham and Trotman, London.

Gibbs, A.D. (1990). Extension of the North Sea basins. In Extensional Tectonics and Stratigraphy of the North Atlantic Margins (Eds. A.J. Tankard and H.R. Balkwill) American Association of Petroleum Geologists, Memoir **46**, 81-93

Glennie, K.A. (1984). Introduction to the Petroleum Geology of the North Sea. Oxford, Blackwell Scientific Publications.

Glennie, K.A. (1986). Development of N.W. Europe's Southern Permian gas basin. In Habitat of Palaeozoic gas in N.W. Europe (Eds. J. Brooks, J.C. Goff and B. Vav Hoorn) Geological Society Special Publication **23**, 3-22

Gunn, P.J. (1975). Linear Transforms of Gravity and Magnetic Fields. Geophysical Prospecting, **23**, 300-312.

Harker, S.D., Gustav, S.H., and Riley, L.A. (1987). Triassic to Cenomanian stratigraphy of the Witch Ground Graben. In Petroleum Geology of North West Europe, (Eds., J. Brooks and K. Glennie), Graham and Trotman, London. 808-818

Harland, R.K., Cox, A.v., Llewellyn, P.B., Pickton, C.A., Smith, A.G., and Walters, R. (1982). A Geological Time Scale. Cambridge University Press, p. 131

Hellinger, S.J., and Sclater, J.G. (1983). Some comments on two-layer extensional models for the evolution of sedimentary basins. Journal of Geophysical Research, **88**, 8251-69

Hellinger, S.J., Sclater, J.G., and Giltner, J. (1989) Mid-Jurassic through mid-Cretaceous extension in the Central Graben of the North Sea - part 1: estimates from subsidence., Basin Research, **1**, 191-200

Hildenbrandt, G.G., and Kuchs, P.P. (1985) Model of the geothermal system in south-western South Dakota from gravity and magnetic studies. In The Utility of Regional Gravity and Magnetic Maps. (Ed., W.J. Hinze) Society of Exploration Geophysics. p 233

Holliger, K., and Klemperer, S.L. (1989). A comparison of the Moho interpreted from gravity data and from deep seismic reflection data in the northern North Sea. Geophysical Journal of the Royal Astronomical Society, **97**, 247-258.

Holliger, K., and Klemperer, S.I. (1990). Gravity and deep seismic reflection profiles across the North Sea rifts. In Tectonic evolution of the North Sea Rifts (Eds. D.J. Blundell and A. Gibbs), Oxford University Press, in press.

Hood, P.J., McGrath, P.H., and Taskey, D.J. (1985). Evolution of Geological Survey of Canada magnetic anomaly maps: a Canadian Perspective. In The Utility of Regional Gravity and Magnetic Maps. (Ed., W.J. Hinze) Society of Exploration Geophysics. p 62

Hospers, J., Finnstrom, E.G., and Rathore, J.S. (1985). A regional gravity study of the Northern North Sea (52 - 56° N.). Geophysical Prospecting, **33**, 543-566

Howitt, F., Aston, E.R., and Jacque, M. (1975). The occurrence of Jurassic volcanics in the North Sea. In Petroleum and Continental Shelf of North West Europe, Volume 1: Geology., (Ed., A.W. Woodland), pp 379-88, Applied Science Publishers Ltd., Barking, Essex.

Jarvis, G.T., and McKenzie D.P. (1980). Sedimentary basin formation with finite extension rates. Earth and Planetary Science Letters, **48**, 42-52

Johnson, R.J., and Dingwall, R.G. (1981). The Caledonides: their influence on the stratigraphy of the north-west European continental shelf. In Petroleum Geology of the Continental Shelf of North-West Europe, (Eds. L.V. Illing and G.D Hobson) pp 43-57, Institute of Petroleum, London.

Klemperer, S.L. (1988) Crustal thinning and nature of extension in the northern North Sea from deep seismic reflection profiling. Tectonics, **7**, 803-21

Latin, D.M. (1990). The Relationship Between Extension And Magmatism In The North Sea Basin. Unpublished Ph.D. thesis, Edinburgh University.

Latin, D., and White, N. (1990). Generating melt by extension of the lithosphere: pure shear vs simple shear. Geology, **18**, 327-331

Latin, D.M., Dixon, J.E., and Fitton, J.G. (1990a). Rift-related magmatism in the North Sea basin. In Tectonic evolution of the North Sea Rifts (Eds. D.J. Blundell and A. Gibbs), Oxford University Press, in press.

Latin, D.M., Dixon, J.E., Fitton, J.G., and White, N. (1990b). Mesozoic magmatic activity in the North Sea basin: implications for stretching history. in Tectonic Movements Responsible for Britain's Oil and Gas Reserves, (Eds. R.F.P. Hardman and J.R.V. Brooks) Geological Society of London Special Publication, in press.

Livermore, R.A., and Smith, A.G. (1985). Some boundary conditions for the evolution of the Mediterranean region. In Geological Evolution of the Mediterranean Basin. (Eds., D.J. Stanley and F. Wezel) pp. 83-98, Springer-Verlag, New York.

McKenzie, D.P., (1978). Some remarks on the development of sedimentary basins. Earth and Planetary Science Letters, **40**, 25-32

McKenzie, D.P., and Bickle, M.J. (1988). The volume and composition of melt generated by extension of the lithosphere. Journal of Petrology, **29**, 625-29

Morgan, W.J. (1981). Hot spot tracks and the opening of the Atlantic and Indian Oceans. In The Sea. **7**, (Ed. C. Emiliani) pp. 443-487. John Wiley and Sons, New York.

Parasnis, D.S. (1962). Principles of Applied Geophysics (4th. Ed). Chapman and Hall.

Paterson, N.R., and Reeves, C.V., (1985). The Applications of gravity and magnetic surveys: the state of the art in 1985. Geophysics, **50**, No. 12, 2558-2594

Pegrum, R.M. (1984). The extension of the Tornquist zone in the Norwegian North Sea. Norsk Geologisk Tidsskrift, **64**, 39-68

Plouff, D. (1975). Derivation of formulas and Fortran programs to compute gravity anomalies of prisms. Report No. USGS-GD-75-015, National Technical Information Service, U.S. Dept. of Commerce.

Ritchie, J.D., Swallow, J.L., Mitchell, J.G., and Morton, A.C. (1988). Jurassic ages from intrusives and extrusives within the Forties igneous province. Scottish Journal of Geology, **24**, 81-88

Rowley, D.B. and Sahagian, D. (1986). Depth-dependent stretching: A different approach. Geology, **14**, 32-35

Royden, L., and Keen, C.E. (1980). Rifting process and thermal evolution of the continental margin of eastern Canada determined from subsidence curves. Earth and Planetary Science Letters, **51**, 345-61

Sclater, J.G., and Christie, P.A.F. (1980). Continental stretching: An explanation of the post mid-Cretaceous subsidence of the Central North Sea Basin. Journal of Geophysical Research, **85**, 3711-39.

Sclater, J.G., and Shorey, M.D. (1989) Mid-Jurassic through mid-Cretaceous extension in the Central Graben of the North Sea - Part 2: estimates from faulting observed on a seismic reflection line. Basin Research, **1**, 201-215

Sclater, J.G., Royden, L., Horvarth, F., Burchfiel, B.C., Semken, S., and Stegna, L. (1980) The formation of intra Carpathian Basins as determined from subsidence data. Earth and Planetary Science Letters, **51**, 139-62

Steckler, M.S., and Watts, A.B. (1978). Subsidence of the Atlantic-type continental margin off New York. Earth and Planetary Science Letters, **41**, 1-13

Solli, M. (1976) En seismik skorpeuderokelse Norges-Shetland. Unpublished Ph.D. thesis, Uninversity of Bergen.

Spector, A. and Grant, F.S. (1970). Statistical models for interpreting aeromagnetic data. Geophysics, **35**, 293-302.

Swain, C.J. (1976) A Fortran IV program for interpolating irregulary spaced data using the difference equations for minimum curvature. Computers and Geosciences, **1**, 231-240.

Talwani, M., and Ewing, M. (1960). Rapid computation of gravitational attraction of three-dimensional bodies of arbitrary shape. Geophyics, **25**, No.1, 203-225.

Telford, W.M., Geldart, L.P., Sheriff, R.E. and Keys, D.A. (1976). Applied Geophysics. Chapters 2 and 3. Cambridge University Press.

Tulley, M.C., and Donato, J.A. (1985). 1:1 000 000 northern North Sea Bouguer anomaly gravity map. British Geological Survey report **16**, No. 6.

Turcotte, D.L., and Schubert, G. (1982). Geodynamics: applications of continuum physics to geological problems. John Wiley and Sons, New York.

Upton, B.G.J., (1988). History of Tertiary igneous activity in the N Atlantic borderlands. In Early Tertiary Volcanism and the Opening of the North Atlantic., (Eds., A.C. Morton and L.M. Parson), Geological Society of London Special Publication No. **39**, 429-453

Vacquire, V., Steenland, N.C., Henderson, R.G. and Zietz, I. (1951). Interpretation of aeromagnetic maps. Geological Society of America, Memoir **47**.

Voorhoeve, H., and Houseman, G. (1988). The thermal evolution of lithosphere extending on a low-angle detachment. Basin Research, **1**, 1-9

Watts, A.B., and Thorne, J. (1984). Tectonics, global changes in sea-level and their relationship to stratigraphic sequences at the U.S. Atlantic continental margin. Marine and Petroleum Geology, **1**, 319-339

Wernicke, B. (1981). Low angle noraml faults in the Basin and Range Province: Nappe tectonics in an extending orogen. Nature, **291**, 645-648

Wernicke, B. (1985). Uniform sense simple shear of the continental lithosphere. Canadian Journal of Earth Sciences, **22**, 108-25

White, N.J. (1988). Extension and Subsidence of the Continental Lithosphere. Unpublished Ph.D. thesis, Cambridge University.

White, N.J. (1989). The nature of lithospheric extension in the North Sea. Geology, **17**, 111-114

White, N. and McKenzie, D.P. (1988). Formation of the 'steer's head' geometry of sedimentary basins by differential stretching of the crust and mantle. Geology, **16**, 250-53

White, R.S. and McKenzie, D.P. (1989). Magmatism at rift zones: The generation of volcanic continental margins and flood basalts. Journal of Geophysical Research, **94**, 7685-7729.

Wood, R., and Barton, P. (1983). Crustal thinning and subsidence in the North Sea. Nature, **302**, 134-36.

Woodhall, D., and Knox, R.W. (1979). Mesozoic volcanism in the northern North Sea and adjacent areas. Bulletin of the geological Survey of Great Britain, **70**, 34-56

Yielding, G. (1990) Footwall uplift associated with late Jurassic normal faulting in the northern North Sea. Journal of the Geological Society of London, **147**, 219-222

Zervos, F.A. (1986). Geophysical Investigation of Sedimentary Basin Development: Viking Graben, North Sea. Unpublished Ph.D. thesis, Edinburgh University.

Zervos, F.A. (1987). A compilation and regional interpretation of the northern North Sea gravity map. In Continental Extensional Tectonics (Eds. M.P. Coward, J.F. Dewey, and P.L. Hancock), Geological Society of London Special Publication, **28**, pp 477-493

Ziegler, P.A. (1981). Evolution of sedimentary basins in north-west Europe. In In Petroleum Geology of the Continental Shelf of North-West Europe, (Eds. L.V. Illing and G.D Hobson) pp 3-39, Institute of Petroleum, London.

Ziegler, P.A. (1982). Geological atlas of western and central Europe. Shell Internationale Maatschappij B.V., the Hague.

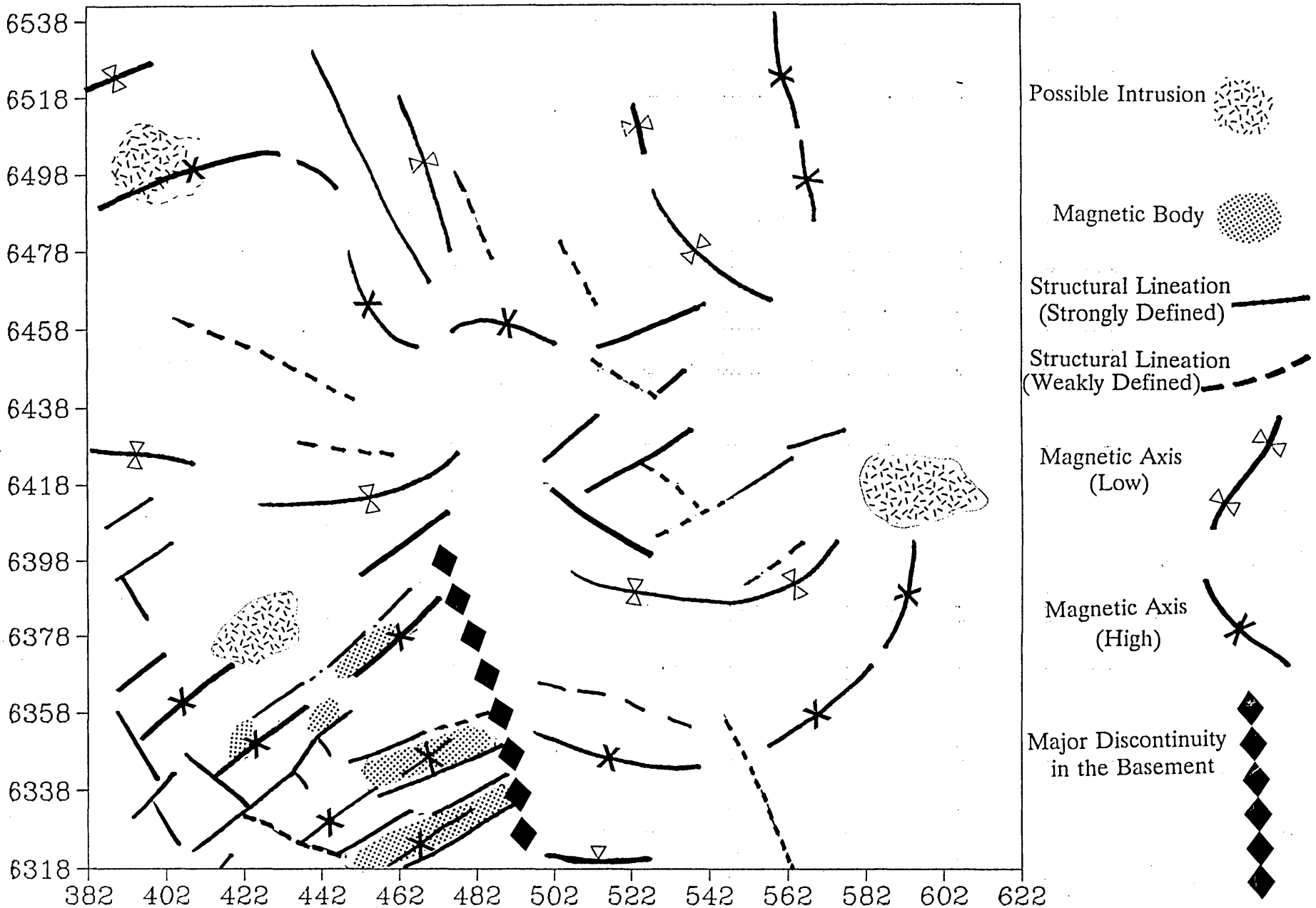
Ziegler, P.A. (1983). Crustal thinning and subsidence in the North Sea. Nature, **304**, 561

Ziegler, P.A. (1988). Evolution of the Arctic-North Atlantic rift system. American Association of Petroleum Geologists, Memoir 43, 198p.

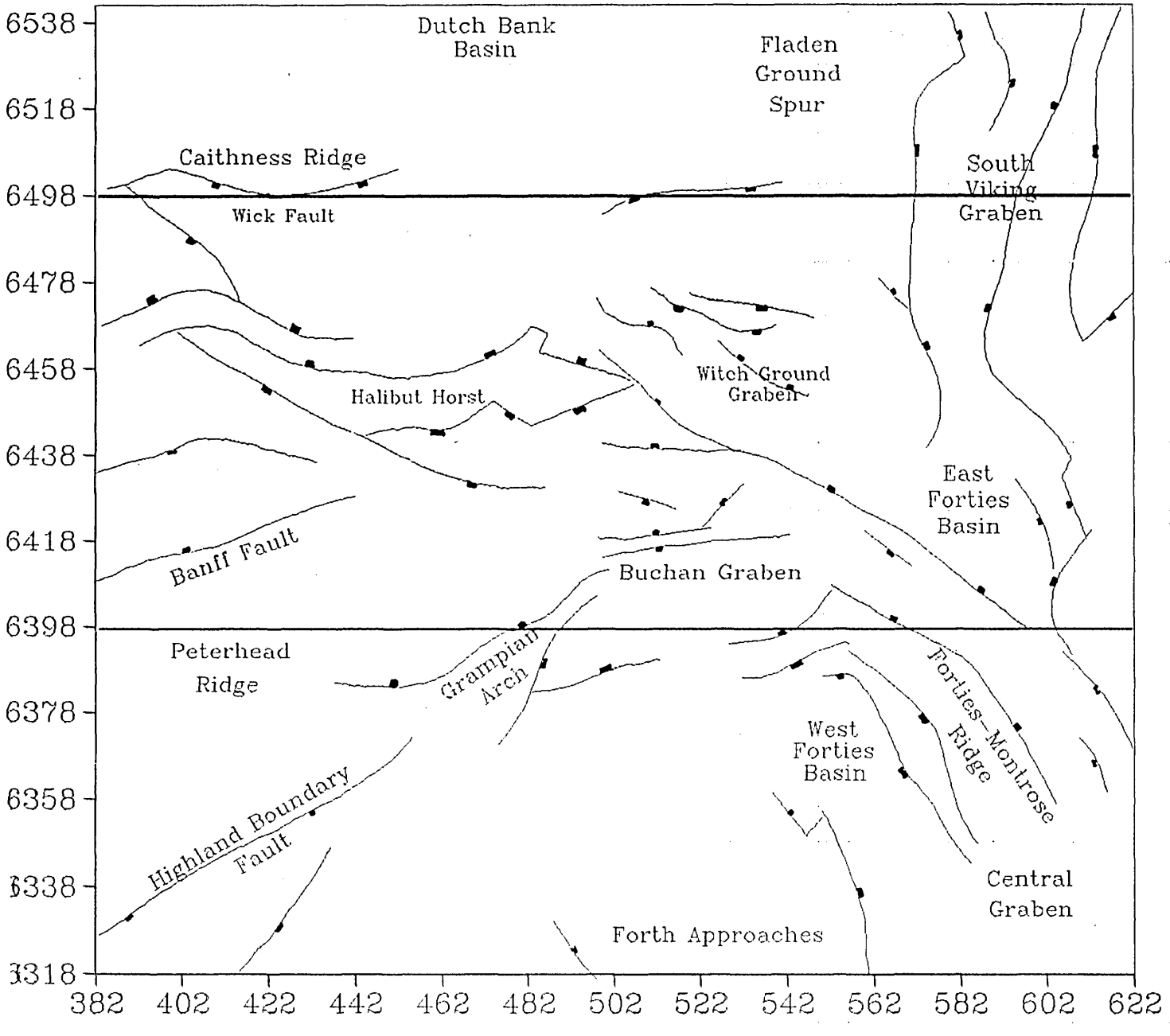
Ziegler, P.A. and Louwerens, C. (1979). Tectonics of the North Sea. In The Quaternary History of the North Sea. (Eds. E. Oele et al.) Acta University Uppsala, Symposium, University Uppsala, Annum Quingentesimum Celebrantis, 7-22

Ziegler, P.A. and Van Hoorn, B. (1990). Evolution of the North Sea rift system. In Extensional Tectonics and Stratigraphy of the North Atlantic Margins (Eds. A.J. Tankard and H.R. Balkwill) American Association of Petroleum Geologists, Memoir **46**, 471-500

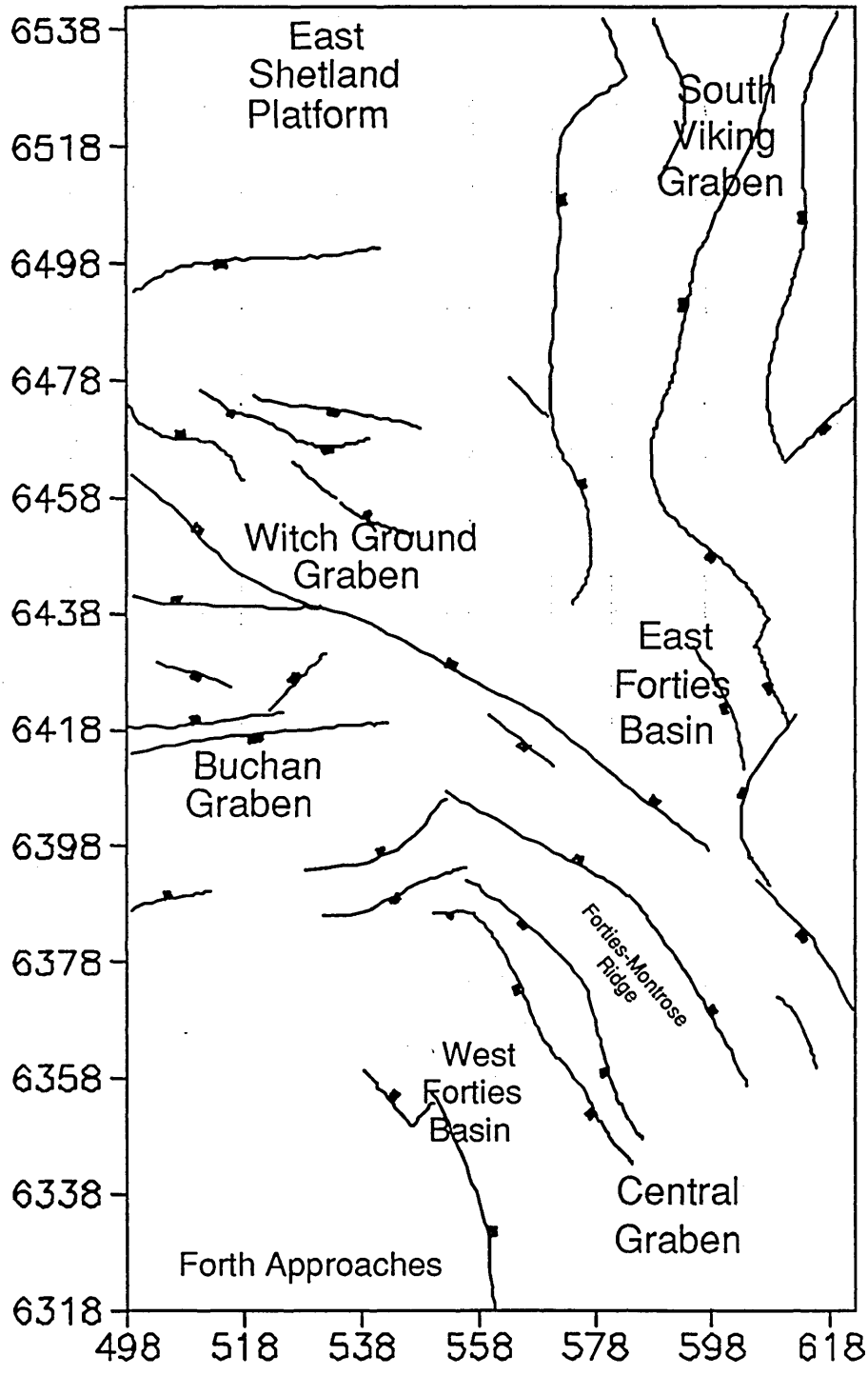
MAGNETIC INTERPRETATION OVERLAY 1



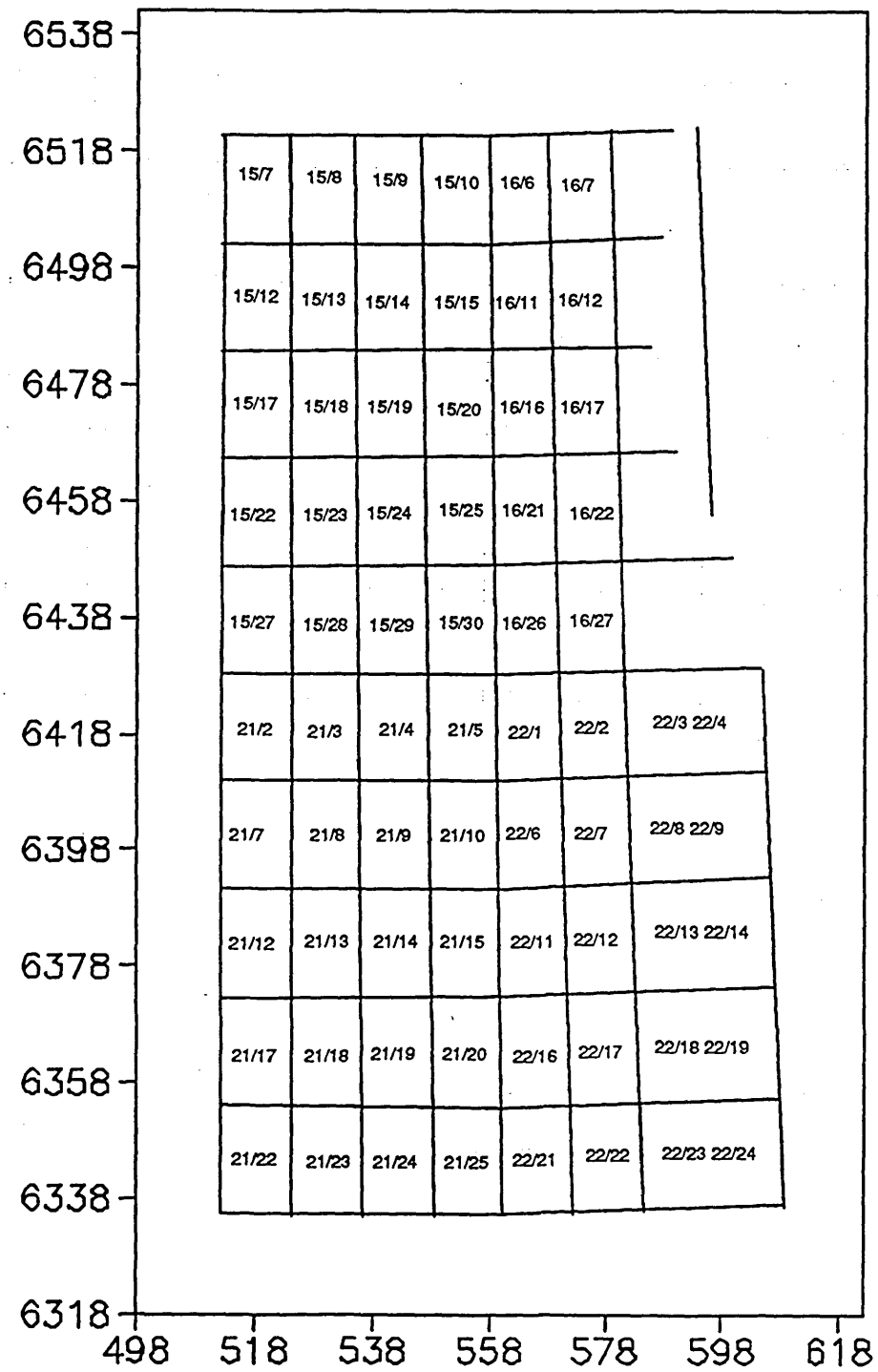
STRUCTURAL OVERLAY 1



STRUCTURAL OVERLAY 2

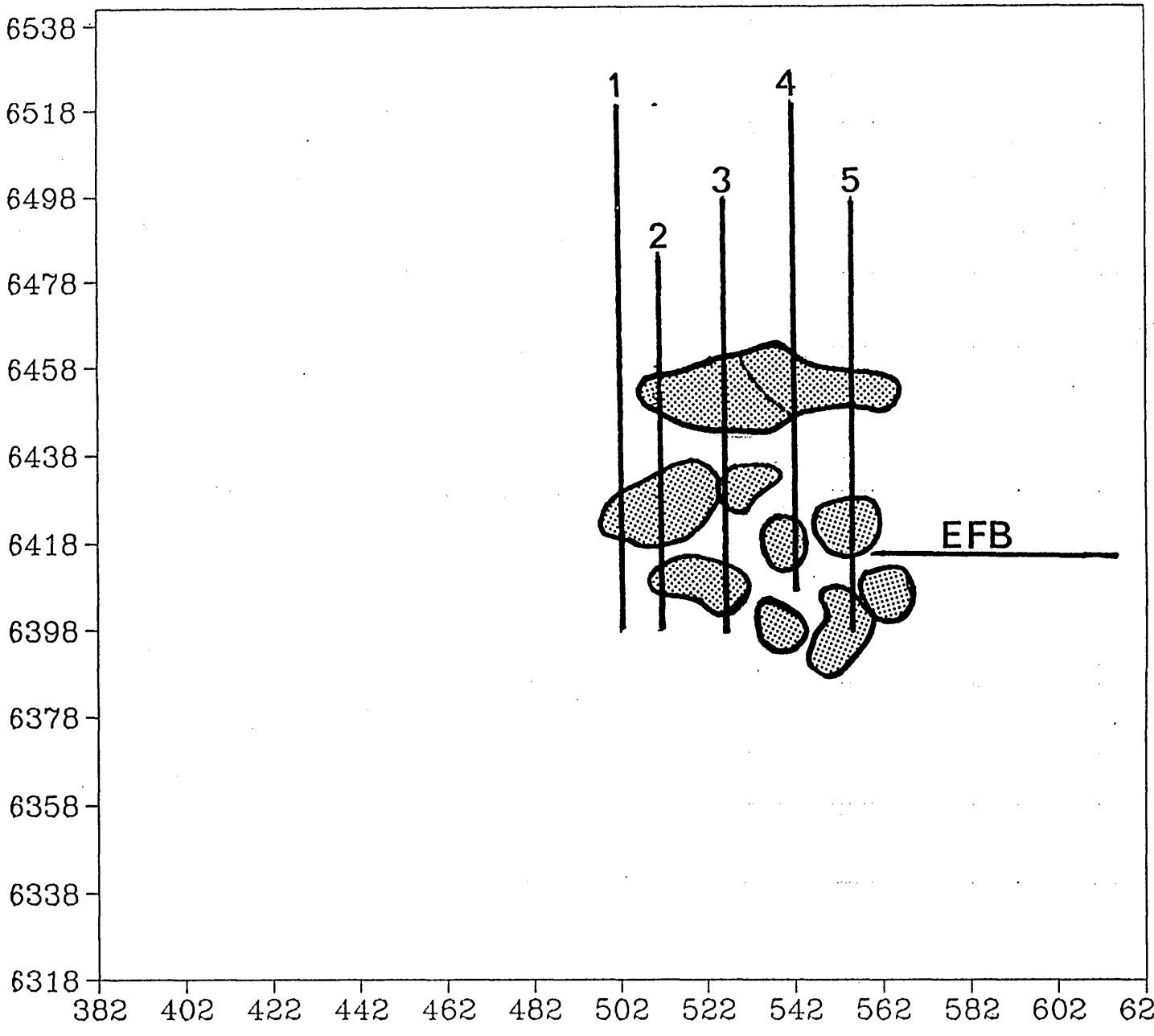


NORTH SEA LICENSE BLOCKS



MAGNETIC INTERPETATION OVERLAY 2

(PROFILES IN FORTIES AREA)



Magnetic Body
(Defined by 2VD Map)

EFB = East Forties Basin

BETA FACTORS (After Latin 1990)

